

Computational Modeling of Biomechanical Phenomena - Remodeling, Growth and Reorientation -

vom Fachbereich Maschinenbau und Verfahrenstechnik
der Technischen Universität Kaiserslautern
zur Verleihung des akademischen Grades

Doktor-Ingenieur (Dr.-Ing.)

genehmigte Dissertation

von

Dipl.-Ing. Grieta Himpel
aus Aachen

Hauptreferent:	Prof. Dr.-Ing. P. Steinmann
Korreferenten:	Prof. Dr.-Ing. E. Kuhl Prof. Dr.-Ing. J. Schröder
Vorsitzender:	Prof. Dr.-Ing. M. Maier
Dekan:	Prof. Dr.-Ing. J. C. Aurich

Tag der Einreichung: 19. September 2007
Tag der mündl. Prüfung: 12. Dezember 2007

Kaiserslautern, Januar 2008

D 386

Vorwort

Die vorliegende Arbeit entstand während meiner Tätigkeit als wissenschaftliche Mitarbeiterin am Lehrstuhl für Technische Mechanik (LTM) der Technischen Universität Kaiserslautern.

Ich bedanke mich ganz herzlich bei Herrn Professor Paul Steinmann dafür, daß er mir die Realisierung dieser Arbeit ermöglicht hat. Seine konsequente wissenschaftliche Förderung und Motivation sowie die eingeräumten Freiräume führten zu einer konstruktiven und angenehmen Arbeitsatmosphäre.

Besonders bedanken möchte ich mich auch bei Frau Professor Ellen Kuhl und Herrn Professor Andreas Menzel für die intensive wissenschaftliche Betreuung, die wesentlich zum Gelingen dieser Arbeit beigetragen hat, und ihr großes Interesse auch über ihre Zeit am LTM hinaus. Ich bedanke mich bei Herrn Professor Paul Steinmann für die Übernahme des Hauptreferats und bei Frau Professor Ellen Kuhl und Herrn Professor Jörg Schröder für die Übernahme des Korreferats und für die zügige Begutachtung der Arbeit.

Meine Grundlagenausbildung auf den Gebieten der Mechanik und numerischen Methoden verdanke ich Herrn Professor Miehe, der damit mein Interesse an diesen Themengebieten geweckt hat. Mein besonderer Dank gilt auch Nikolas Apel, der mich für die Kontinuumsmechanik begeistert und mir den Anstoß für diese Promotion gegeben hat.

Ich bedanke mich bei allen Kollegen am LTM für das angenehme und freundliche Arbeitsklima und die Hilfsbereitschaft. Ganz besonders bedanke ich mich bei Frau Jeblick, Herrn Barth und Natalia Konratieva für ihre Unterstützung bei allen Aufgaben des universitären Lebens. Ein besonderer Dank für anregende Diskussionen geht an Julia Mergheim, Gunnar Possart und Ralf Denzer. Für ihre Hilfe bei rechnerischen Fragestellungen bedanke ich mich bei Ralf Denzer, Gunnar Possart und Patrick Schmitt.

Außerdem bedanke ich mich bei Mark Harris für das Korrekturlesen der Arbeit.

Vor allem jedoch danke ich meinen Eltern, die mir durch meine gute Ausbildung diese Promotion ermöglicht haben, und Ingo für seine Unterstützung und Geduld sowie den starken Rückhalt den er mir während meiner Arbeit am Lehrstuhl gegeben hat.

Kaiserslautern, Januar 2008

Grieta Himpel

Zusammenfassung

Ziel der vorliegenden Arbeit ist die numerische Implementierung biologisch relevanter Phänomene. Wie anhand zahlreicher Beispiele gezeigt werden kann, paßt sich (lebendes) biologisches Gewebe in der Regel seiner Belastung an. Eine Art der Anpassung ist beispielsweise die Optimierung der Masse. Die Masse eines Körpers wird sowohl durch die Dichte als auch durch das Volumen des betreffenden Materials bestimmt. Deshalb wird in dieser Arbeit unterschieden zwischen *Umbau* (remodeling) im Sinne reiner Dichteänderung bei konstantem Volumen und *Wachstum* (growth) im Sinne reiner Volumenänderung bei konstanter Dichte.

Wie bereits im 19. Jahrhundert von VON MEYER [139], CULMANN [25], ROUX [117] und WOLFF [142] untersucht wurde, hängt beispielsweise die Knochendichte von der mechanischen Belastung ab. Dabei führen größere Spannungen zu einer Erhöhung der Dichte, während Unterbelastung, zum Beispiel infolge langer Bettlägerigkeit oder Schwerelosigkeit im Weltall, zu einer Abnahme der Knochendichte führen kann. Während Umbauvorgänge im gesunden Körper zu einer Optimierung der Masse führen, sind sie bei Implantateinsätzen häufig von Nachteil. Da das Implantat in der Regel eine höhere Steifigkeit als der zu ersetzende Knochen besitzt, übernimmt es einen größeren Anteil an der Lastabtragung, als der Knochen im natürlichen Zustand. Infolgedessen bildet sich der Knochen, der das Implantat umgibt, zurück, was zu einer Lockerung der Prothese führt. Derartige Umbauvorgänge werden in der Mechanik üblicherweise auf konstitutiver Ebene formuliert, beispielsweise durch Wichtung der freien Energiefunktion mit der Dichte, wie von HARRIGAN & HAMILTON [46] vorgeschlagen und von CARTER & HAYES [16] experimentell unterlegt wurde. Mögliche anisotrope Materialeigenschaften werden analog zu reiner Elastizität über die freie Energie realisiert. Wenngleich dieser Ansatz auch für große Verzerrungen geeignet ist, wird er aufgrund biologischer Motive meist eher für harte Gewebe wie beispielsweise Knochen verwendet, welche kleinen Verzerrungen ausgesetzt sind.

In weichen Geweben, wie Muskeln, Sehnen, Bändern oder Knorpelgeweben führt eine steigende mechanische Belastung in der Regel zu einer Volumenzunahme, also Wachstum. Ein offensichtliches Beispiel hierfür sind Muskeln, welche infolge stärkerer Belastung wachsen, sich bei geringerem Training jedoch zurückbilden. Während dies beim sportlichen Muskelaufbau gewünscht ist, kann Wachstum jedoch auch zu einer krankhaften Hypertrophie des Herzens oder zu Verdickungen der Arterienwände nach einer Stent-Implantation führen. Kontinuumsmechanisch läßt sich ein derartiges Wachstum auf kinematischer Ebene einführen. Basierend auf den Ideen von

SKALAK U.A. [124] und RODRIGUEZ, HOGER & MCCULLOCH [116] wird die totale Deformation hierfür multiplikativ in zwei Anteile zerlegt: einen reinen Wachstumsanteil und einen rein elastischen Anteil. Eine analoge Zerlegung wurde erstmals von LEE [90] eingeführt, um finite Deformationen im Rahmen der Elastoplastizität zu beschreiben. Die Beschreibung des Wachstums erfolgt damit über einen zweistufigen Wachstums-Deformationstensor. Um anisotropes Wachstum zu implementieren, muß dieser entsprechend definiert werden. Anisotropie wird in biologischen Geweben häufig durch Faserverstärkung hervorgerufen, charakterisiert durch eine oder mehrere Faserrichtungen. Im Rahmen dieser Arbeit beschränken wir uns auf Materialien mit einer ausgezeichneten Faserrichtung, also transversal isotrope Materialien. Der transversal isotrope Wachstums-Deformationstensor wird im wesentlichen durch zwei Kennzahlen beschrieben. Diese werden als Verzerrungsgrade parallel und orthogonal zur Faserrichtung bezeichnet.

Eine weitere Art der Anpassung anisotroper Gewebe an äußere Belastungen kann durch *Umorientierung* (reorientation) der inneren Ausrichtung erfolgen. Dies kann beispielsweise im menschlichen Femurkopf beobachtet werden, in dem die Knochenbälkchen derart orientiert sind, daß sie der täglich auftretenden Belastung mit einem Optimum an Masse standhalten. Auch in weichem Gewebe wie der Arterienwand oder Muskelgewebe richten sich die Kollagen- oder Muskelfasern entlang der Belastungsrichtungen aus. Ändert sich die Belastung, zum Beispiel infolge einer Stent-Implantation, so paßt sich das Material durch Umorientierung der Fasern den geänderten Randbedingungen an. Für transversal isotrope Materialien kann dieser Prozess durch eine Rotation der ausgezeichneten Richtung beschrieben werden. Wie von MENZEL [99] vorgeschlagen, schließen wir dabei Verdrillung aus. Wodurch die Umorientierung gesteuert wird, ist bis heute nicht eindeutig erforscht. Aus mathematischer Sicht läßt sich eine Umorientierung entlang Hauptverzerrungen motivieren. Wie VIANELLO [136] gezeigt hat, erreicht die freie Energie einen stationären Zustand, wenn die Spannungen und Verzerrungen koaxial sind. Für transversale Isotropie ist dies der Fall, wenn die Faserrichtung parallel zu einer der Hauptverzerrungsrichtungen zeigt. Aus biologischer Sicht jedoch läßt sich, abhängig vom Material, sowohl eine verzerrungs- als auch eine spannungsgetriebene Umorientierung motivieren, weshalb in der vorliegenden Arbeit diese beiden Fälle betrachtet werden.

Die drei Aspekte Umbau, Wachstum und Umorientierung werden zunächst in einer umfassenden kontinuumsmechanischen Materialformulierung zusammengefaßt. Dies umschließt die Beschreibung der Kinematik, der Bilanzgleichungen und des Materialgesetzes. Wie bereits erwähnt, erfolgt dabei die Modellierung von Wachstum auf kinematischer Ebene durch eine Zerlegung der totalen Deformation in einen wachstumsbeschreibenden und einen elastischen Anteil. Dies beinhaltet die Einführung einer im allgemeinen inkompatiblen Zwischenkonfiguration. Die materielle Konfiguration wird durch den Wachstums-Deformationstensor auf die Zwischenkonfiguration abgebildet. Die Abbildung der Zwischenkonfiguration auf die räumliche Konfiguration

erfolgt mittels des elastischen Deformationstensors. Um bei der Formulierung der Bilanzgleichungen Masseänderungen, also Änderungen der Dichte und des Volumens, zu ermöglichen, wird eine Massequelle eingeführt. Ein Massefluß wird im Rahmen dieser Arbeit nicht berücksichtigt. Die Massequelle entspricht der Änderung der materiellen Dichte über die Zeit. Die Änderung der Dichte hat ebenfalls einen Einfluß auf die freie Energie und damit auf die Materialgleichungen. Wie oben erwähnt, wird die Dichteänderung über einer Wichtung der freien Energiefunktion mit der Dichte realisiert. Die Beschreibung des Umorientierungsprozesses erfolgt ebenfalls auf konstitutiver Ebene. Im Gegensatz zu sonst üblichen Formulierungen für transversale Isotropie wird hier eine zeitliche Änderung der charakteristischen Richtung zugelassen. Um die konkreten Änderungen von Dichte, Volumen und Faserrichtung zu beschreiben, werden interne Variablen eingeführt. Dies sind die Dichte, die Verzerrungsgrade und die Faserrichtung. Die Evolutionsgleichungen dieser internen Variablen müssen zusätzlich zur freien Energiefunktion materialabhängig definiert werden.

Hauptaspekt dieser Arbeit ist die Implementierung der oben diskutierten Effekte. Dafür werden die Konstitutivgleichungen für die internen Variablen so gewählt, daß Umbau, Wachstum und Umorientierung in jeweils reiner Form beschrieben werden. Infolgedessen ergeben sich drei Kapitel mit jeweils gleicher Gliederung. Zunächst werden die Evolutionsgleichungen für die internen Variablen entsprechend gewählt. Dies bedeutet für eine reine Dichteänderung, daß die Faserrichtung und die Verzerrungsgrade konstant sind. Infolgedessen wird die totale Deformation vollständig durch den elastischen Deformationstensor beschrieben und die Zwischenkonfiguration kann vernachlässigt werden. Die Dichteänderung ist gleich der Massequelle, welche definiert werden muß. Entsprechend wird zur Beschreibung reinen Wachstums, eine Dichteänderung von der materiellen Konfiguration zur Zwischenkonfiguration ausgeschlossen. Daraus folgt, daß die Massequelle eindeutig durch den Wachstums-Deformationstensor beschrieben wird. Dieser ergibt sich aus Definition der beiden Verzerrungsgrade. Die Faserrichtung ist ebenfalls konstant. Reine Umorientierung bei konstanter Masse fordert, daß die Massequelle verschwindet und die Zwischenkonfiguration gleich der materiellen Konfiguration ist. Basierend auf Starrkörperbewegungen, läßt sich zeigen, daß die Umorientierung einer Rotation der Fasern entspricht. Analog zu Annahmen in der Schalentheorie schließen wir hierbei Verdrillungen aus. Es wird sowohl eine Orientierung entlang der Hauptverzerrungen als auch eine Orientierung entlang der Hauptspannungen betrachtet.

Die Implementierung erfolgt mit Hilfe finiter Elemente und gliedert sich in zwei Teile: eine lokale Berechnung der internen Variablen sowie die Bestimmung des globalen Tangentenmoduls. Um die Dichte sowie die Verzerrungsgrade aus deren Evolutionsgleichungen zu bestimmen, verwenden wir ein implizites Euler-Backward-Verfahren. Die aktuelle Faserrichtung wird dahingegen mit einem impliziten exponentiellen Verfahren berechnet. Die sich daraus ergebenden nichtlinearen Gleichungen werden mit Hilfe einer lokalen Newton-Iteration gelöst. Die entsprechenden Gleichungen werden

dazu ebenso wie der globale Tangentenmodul vollständig linearisiert. Zur Bestimmung des Tangentenmoduls wird dabei die Ableitung der internen Variablen nach den Verzerrungen benötigt. Da jedoch nur die Evolutionsgleichungen der internen Variablen definiert sind, werden die gesuchten Ableitungen anhand der Ableitungen der Residuen innerhalb der jeweiligen impliziten Verfahren bestimmt. Die Lösungs-Algorithmen sind für alle drei Aspekte tabellarisch angegeben. Zur Veranschaulichung der implementierten Aspekte werden verschiedene numerische Beispiele betrachtet.

Contents

1	Introduction	1
2	Governing equations	5
2.1	Kinematics	5
2.2	Balance equations	8
2.2.1	Stresses and heat flux	9
2.2.2	Master balance law	11
2.2.3	Balance of mass	12
2.2.4	Balance of linear momentum	13
2.2.5	Balance of angular momentum	14
2.2.6	Balance of internal energy	15
2.2.7	Balance of entropy	15
2.3	General constitutive equations	17
2.3.1	Principles for the construction of constitutive equations	17
2.3.2	Transversely isotropic elasticity	18
2.4	Different biomechanical effects	22
3	Remodeling	25
3.1	Introduction	25
3.2	Constitutive equations	26
3.3	Implementation	28
3.3.1	Incremental update of the density field	28
3.3.2	Incremental tangent modulus	29
3.4	Numerical examples	32
3.4.1	Simple tension	32
3.4.2	Human femur	35
3.4.3	Three-dimensional cylindrical tube	39
3.5	Discussion	42
4	Growth	45
4.1	Introduction	45
4.2	Constitutive equations	46
4.3	Implementation	49
4.3.1	Incremental update of the stretch ratios	49

4.3.2	Incremental tangent modulus	52
4.4	Numerical examples	53
4.4.1	Simple tension	55
4.4.2	Three-dimensional cylindrical tube	59
4.5	Discussion	65
5	Reorientation	67
5.1	Introduction	67
5.2	Constitutive equations	69
5.2.1	Transversely isotropic hyper-elasticity	69
5.2.2	Evolution of a line element	70
5.2.3	Kinematics-based reorientation	71
5.3	Implementation	75
5.3.1	Incremental update of the characteristic direction	75
5.3.2	Incremental tangent modulus	78
5.4	Numerical examples	82
5.4.1	Uniaxial stress and uniaxial tension	82
5.4.2	Strip under tension	90
5.4.3	Tube under inside radial displacement load	96
5.5	Discussion	97
6	Discussion	101
6.1	Conclusion	101
6.2	Future work	104
A	Notation	105
B	Some matrix identities	107
B.1	Matrix determinant lemma	107
B.2	Sherman-Morrison formula	107
C	Derivatives	109
C.1	Exponent of a skew symmetric tensor	109
C.2	Eigenvectors and eigenvalues	109
C.3	Invariants	111
	Bibliography	112
	List of figures	123
	List of tables	125

1 Introduction

The main concern of this contribution is the computational modeling of biomechanically relevant phenomena. To minimize resource requirements, living biomaterials commonly adapt to changing demands. One way to do so is the optimization of mass. For the modeling of biomaterials with changing mass, we distinguish between two different approaches: the coupling of mass changes and deformations at the constitutive level and at the kinematic level. Mass change at the constitutive level is typically realized by weighting the free energy function with respect to the density field, as experimentally motivated by CARTER & HAYES [16] and computationally realized by HARRIGAN & HAMILTON [46]. Such an ansatz enables the simulation of changes in density while the overall volume remains unaffected. In this contribution we call this effect *remodeling*. Although in principle applicable for small and large strains, this approach is typically adopted for hard tissues, e.g. bone, which usually undergo small strain deformations. Remodeling in anisotropic materials is realized by choosing an appropriate anisotropic free energy function.

Within the kinematic coupling, a changing mass is characterized through a multiplicative decomposition of the deformation gradient into a growth part and an elastic part, as first introduced in the context of plasticity by LEE [90]. In this formulation, which we will refer to as *growth* in the following, mass changes are attributed to changes in volume while the material density remains constant. This approach has classically been applied to model soft tissues undergoing large strains, e.g. the arterial wall. The first contribution including this ansatz is the work by RODRIGUEZ, HOGER & MCCULLOCH [116]. To model anisotropic growth, an appropriate anisotropic growth deformation tensor has to be formulated. In this contribution we restrict ourselves to transversely isotropic growth, i.e., growth characterized by one preferred direction. On that account, we define a transversely isotropic growth deformation tensor determined by two variables, namely the stretch ratios parallel and perpendicular to the characteristic direction.

Another method of material optimization is the adaption of the inner structure of a material to its loading conditions. In anisotropic materials this can be realized by a suitable orientation of the material directions. For example, the trabeculae in the human femur head are oriented such that they can carry the daily loads with an optimum mass. Such a behavior can also be observed in soft tissues. For instance, the fibers of muscles and the collagen fibers in the arterial wall are oriented along the loading directions to carry a maximum of mechanical load. If the overall loading conditions change, for instance during a balloon angioplasty or a stent implantation, the material orienta-

tion readapts, which we call *reorientation*. The anisotropy type in biomaterials is often characterized by fiber reinforcement. A particular subclass of tissues, which includes muscles, tendons and ligaments, is featured by one family of fibers. More complex microstructures, such as arterial walls, show two fiber families, which do not necessarily have to be perpendicular. Within this contribution we confine ourselves to the first case, i.e., transversely isotropic materials indicated by one characteristic direction. The reorientation of the fiber direction in biomaterials is commonly smooth and continuous. For transverse isotropy it can be described by a rotation of the characteristic direction. Analogous to the theory of shells, we additionally exclude drilling rotations, see also MENZEL [99]. However, the driving force for these reorientation processes is still under discussion. Mathematical considerations promote strain driven reorientations. As discussed, for instance, in VIANELLO [137], the free energy reaches a critical state for coaxial stresses and strains. For transverse isotropy, it can be shown that this can be achieved if the characteristic direction is aligned with a principal strain direction. From a biological point of view, depending on the kind of material (i.e. bone, muscle tissue, cartilage tissue, etc.), both strains and stresses can be suggested as stimuli for reorientation. Thus, within this contribution both approaches are investigated. In contrast to previous works, in which remodeling, growth and reorientation are discussed separately, the present work provides a framework comprising all of the three mentioned effects at once. This admits a direct comparison how and on which level the individual phenomenon is introduced into the material model, and which influence it has on the material behavior. For a uniform description of the phenomenological quantities an internal variable approach is chosen. Moreover, we particularly focus on the algorithmic implementation of the three effects, each on its own, into a finite element framework. The nonlinear equations on the local and the global level are solved by means of the Newton-Raphson scheme. Accordingly, the local update of the internal variables and the global update of the deformation field are consistently linearized yielding the corresponding tangent moduli. For an efficient implementation into a finite element code, unitized update algorithms are given. The fundamental characteristics of the effects are illustrated by means of some representative numerical simulations. Due to the unified framework, combinations of the individual effects are straightforward.

The present work is divided in four parts. In **chapter 2** the continuummechanical model containing the three effects *remodeling*, *growth* and *reorientation* is discussed. This indicates the general description of the kinematics, the balance equations and the constitutive equations. To enable the declaration of growth, the multiplicative split of the total deformation gradient into a growth part and an elastic part is established on the kinematic level. This causes the introduction of a generally incompatible intermediate configuration. For transverse isotropy, the growth part can be completely defined by two stretch ratios. Within the determination of the balance equations in terms of open systems, a mass source is introduced to allow mass changes. On the constitutive

level, the free energy function is weighted by a relative density, to describe remodeling. Further on, transverse isotropy is described by a characteristic direction specified by a vector. Due to reorientation this vector may rotate during the deformation. To define the particular material behavior more detailed specifications for the evolution of the stretch ratios, the density and the characteristic direction must be made.

Thus, first we consider pure remodeling signifying pure density changes in **chapter 3**. For this purpose, the general equations of chapter 2 are adapted to the considered effect. Consequently, the intermediate configuration may be neglected and the characteristic direction is constant. Since, the evolution of the density is equal to the mass source, due to mass balance, a definition of this quantity is required. Afterwards, we focus on the numerical implementation of the material model. This includes a consistent linearization of the density evolution equation by means of an implicit Euler backward scheme as well as the development of the incremental tangent modulus within the context of finite elements. Finally, essential features of the model will be illustrated by means of representative numerical examples.

Analogously, in **chapter 4** the general equations are adapted to growth in the sense of pure volume changes. Accordingly, the density and the characteristic direction are constant. This implies that the weighting of the free energy vanishes and the mass source is constituted by evolution of the same stretch ratios which define the growth deformation tensor. Thus, the growth process is clearly described by definition of the evolution of the stretch ratios. Next, we concentrate on the numerical implementation of the constitutive framework for growth. For the algorithmic treatment of the stretch ratio evolution and the computation of the incremental tangent modulus within a finite element setting we use an implicit Euler backward scheme. Concluding, the theory of growth is discussed by means of numerical examples.

Chapter 5 is dedicated to the modeling of pure reorientation with constant mass. Hence, the mass source is equal to zero, and the intermediate configuration can be neglected. To describe the reorientation process, an evolution equation for the characteristic direction must be defined. Based on the rigid body motion of a line element, the evolution results in a pure rotation of the characteristic direction. In this regard, as an additional restriction, we preset an avoidance of drilling rotations, analogous to considerations in the theory of shells. Further on, both an alignment along the principal strains as well as an alignment along principal stresses is considered. For the algorithmic implementation of the reorientation process into a finite element framework, an implicit exponential update of the characteristic direction is applied by using the Rodriguez formula to express the exponential term. The resulting nonlinear equations within a Newton-Raphson scheme are solved by consistent linearizations on the local and the global level. Concluding, we discuss the material model by means of numerical examples.

In **chapter 6** we close the work with a short conclusion and an outlook on possible future work.

2 Governing equations

To set the stage and illustrate the used notation, this chapter is dedicated to an introduction to continuum mechanics. For a more detailed overview of nonlinear continuum mechanics the reader is referred to the works of TRUESDELL & NOLL [133], CHADWICK [17] and MARSDEN & HUGHES [95] as well as to the more recent textbooks of OGDEN [106], BAŞAR & WEICHERT [8], HAUPT [49] and HOLZAPFEL [55]. The first section is addressed to finite kinematics. In the second section, to complete the set of material-independent equations, the balance equations for open systems are discussed. In the third section we consider the general aspects concerning the material dependent constitutive equations. Finally the terms remodeling, growth and reorientation are described and assigned to different biological effects.

2.1 Kinematics

In this section we discuss the kinematics of finite deformations and growth. Knowledge of the kinematics is required to describe the material-independent response of the body to mechanical loads.

For this, it is useful to consider two configurations: the material configuration \mathcal{B}_0 at time t_0 and the spatial configuration \mathcal{B}_t at time t . Let $\mathbf{X} \in \mathcal{B}_0$ denote the placement of a particle of the body B in the material configuration and $\mathbf{x} \in \mathcal{B}_t$ the corresponding placement in the spatial configuration. Both configurations are uniquely linked by the nonlinear point map

$$\mathbf{x} = \boldsymbol{\varphi}(\mathbf{X}, t) : \quad \mathcal{B}_0 \rightarrow \mathcal{B}_t. \quad (2.1)$$

The tangent map from the material tangent space $T_{\mathbf{X}}\mathcal{B}_0$ to the spatial tangent space $T_{\mathbf{x}}\mathcal{B}_t$ is defined by the deformation gradient

$$\mathbf{F} := \nabla_{\mathbf{X}}\boldsymbol{\varphi}(\mathbf{X}, t) : \quad T_{\mathbf{X}}\mathcal{B}_0 \rightarrow T_{\mathbf{x}}\mathcal{B}_t \quad (2.2)$$

with the Jacobian $J := \det \mathbf{F} > 0$. The cofactor of the deformation gradient $\text{cof } \mathbf{F} = J\mathbf{F}^{-t}$ maps a material area element $d\mathbf{A}$ to a spatial area element

$$\mathbf{n} \, da = d\mathbf{a} = J\mathbf{F}^{-t} \cdot d\mathbf{A} = J\mathbf{F}^{-t} \cdot \mathbf{N} \, dA. \quad (2.3)$$

Since the Jacobian constitutes a scalar value, \mathbf{F}^{-t} denotes the normal map from the

material cotangent space $T_{\mathbf{x}}^*\mathcal{B}_0$ to the spatial cotangent space $T_{\mathbf{x}}^*\mathcal{B}_t$

$$\mathbf{F}^{-t} : T_{\mathbf{x}}^*\mathcal{B}_0 \rightarrow T_{\mathbf{x}}^*\mathcal{B}_t . \quad (2.4)$$

Describing mass changes in elastic materials, the deformation of the body can be decomposed into two parts: a growth part and an elastic part. As schematically depicted in figure 2.1 by means of two quadratic elements, each particle of the body grows or alternatively degrades independently in the growth process. The pure growth part

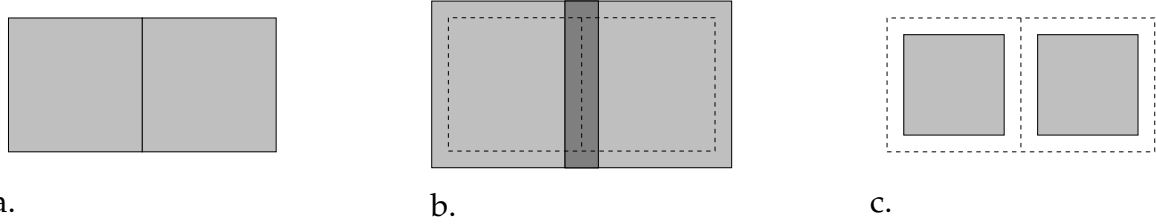


Figure 2.1: Each element of the body grows or degrades in the growth process. Thus, the pure growth part of the deformation results in a generally incompatible configuration. (a) Two elements in the undeformed configuration. (b) Pure growth of the elements causes self-penetration. (c) Pure resorption of the elements causes voids.

of the deformation results in a generally incompatible intermediate configuration $\widehat{\mathcal{B}}_0$. Hence, an additional elastic deformation is needed to ensure compatibility of the total deformation. This phenomenon is illustrated in the work of RODRIGUEZ, HOGER & MCCULLOCH [116] by a growing ventricle. Herein pure growth in tangential direction of the ventricle causes self-penetration, and pure resorption causes voids which must be compensated by an elastic deformation. Accordingly, the authors introduced a multiplicative split of the deformation gradient

$$\boxed{\mathbf{F} = \mathbf{F}_e \cdot \mathbf{F}_g} \quad (2.5)$$

into a growth deformation tensor \mathbf{F}_g and an elastic deformation tensor \mathbf{F}_e , as illustrated in figure 2.2. Remark that the elastic part of the deformation tensor contains both the elastic deformations to satisfy compatibility and the deformations due to elastic stresses, see also SKALAK ET AL. [125]. In the theory of elastoplasticity an analogous split was first introduced by LEE [90]. Later on it has been applied to several material models. A comparison of constitutive theories based on a multiplicative split of the deformation gradient is given by LUBARDA [92]. Analogous to the total deformation, the deformation tensors \mathbf{F}_g and \mathbf{F}_e characterize the following tangent and normal maps

$$\mathbf{F}_g : T_{\mathbf{x}}\mathcal{B}_0 \rightarrow T_{\widehat{\mathbf{x}}}\widehat{\mathcal{B}}_0 , \quad \mathbf{F}_e : T_{\widehat{\mathbf{x}}}\widehat{\mathcal{B}}_0 \rightarrow T_{\mathbf{x}}\mathcal{B}_t , \quad (2.6)$$

$$\mathbf{F}_g^{-t} : T_{\widehat{\mathbf{x}}}^*\widehat{\mathcal{B}}_0 \rightarrow T_{\mathbf{x}}^*\mathcal{B}_0 , \quad \mathbf{F}_e^{-t} : T_{\widehat{\mathbf{x}}}^*\widehat{\mathcal{B}}_0 \rightarrow T_{\mathbf{x}}^*\mathcal{B}_t . \quad (2.7)$$

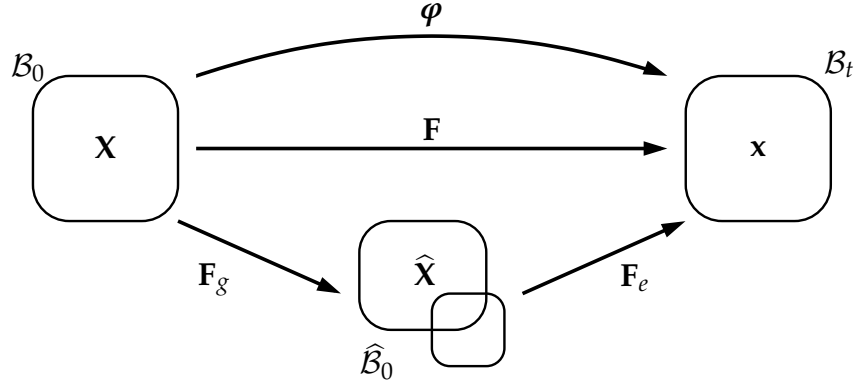


Figure 2.2: Multiplicative split of the total deformation gradient \mathbf{F} into a growth deformation tensor \mathbf{F}_g and an elastic deformation tensor \mathbf{F}_e . The intermediate configuration $\hat{\mathcal{B}}_0$ may be incompatible.

The corresponding Jacobians

$$J = \det \mathbf{F} > 0, \quad J_g = \det \mathbf{F}_g > 0, \quad J_e = \det \mathbf{F}_e > 0 \quad (2.8)$$

transform a volume element into the well-known form

$$dv = J dV = J_e d\hat{V}, \quad d\hat{V} = J_g dV, \quad (2.9)$$

with dV , $d\hat{V}$ and dv denoting a volume element in the material, intermediate and spatial configurations, respectively.

Further on, the metric tensors \mathbf{G} in the material configuration, $\hat{\mathbf{G}}$ in the intermediate configuration and \mathbf{g} in the spatial configuration are introduced, relating the tangent and cotangent spaces

$$\mathbf{G} : T_{\mathbf{X}}\mathcal{B}_0 \rightarrow T_{\mathbf{X}}^*\mathcal{B}_0, \quad \hat{\mathbf{G}} : T_{\hat{\mathbf{X}}}\hat{\mathcal{B}}_0 \rightarrow T_{\hat{\mathbf{X}}}^*\hat{\mathcal{B}}_0, \quad \mathbf{g} : T_{\mathbf{x}}\mathcal{B}_t \rightarrow T_{\mathbf{x}}^*\mathcal{B}_t. \quad (2.10)$$

With this we define the Cauchy-Green deformation measures

$$\boxed{\mathbf{C} := \mathbf{F}^t \cdot \mathbf{g} \cdot \mathbf{F}, \quad \hat{\mathbf{C}} := \mathbf{F}_e^t \cdot \mathbf{g} \cdot \mathbf{F}_e, \quad \mathbf{b} := \mathbf{F} \cdot \mathbf{G}^{-1} \cdot \mathbf{F}^t} \quad (2.11)$$

in the material, intermediate and spatial configurations, respectively. Analogous to illustrations in APEL [4] in the context of elastoplasticity, the correlations between the metric tensors and the deformation tensors are visualized in figure 2.3.

In the following the abbreviation $\{\dot{\bullet}\} = \partial_t\{\bullet\}|_{\mathbf{X}}$ denotes the material time derivative of a quantity $\{\bullet\}$ at fixed material placement \mathbf{X} . Thus, to describe the temporal evolution of the spatial line element with respect to the spatial line element itself

$$d\dot{\mathbf{x}} = \frac{\partial \dot{\mathbf{x}}}{\partial \mathbf{x}} \cdot d\mathbf{x} = \nabla_{\mathbf{x}} \mathbf{v} \cdot d\mathbf{x}, \quad (2.12)$$

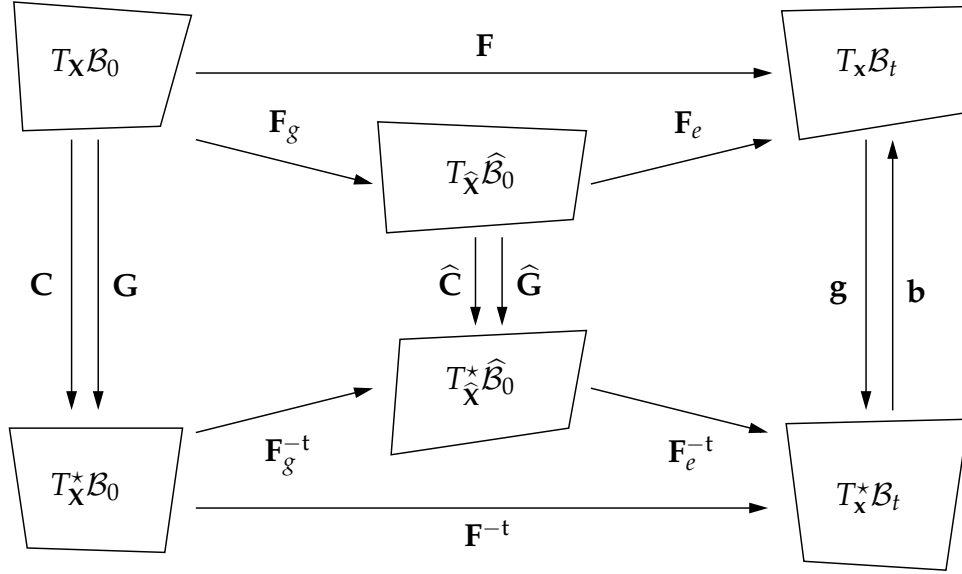


Figure 2.3: Visualization of the metric tensors and the deformation tensors between the tangent space and the cotangent space in the material configuration, the intermediate configuration and the spatial configuration.

the spatial velocity gradient can be introduced as

$$\mathbf{l} := \nabla_{\mathbf{x}} \mathbf{v} = \dot{\mathbf{F}} \cdot \mathbf{F}^{-1}, \quad (2.13)$$

wherein $\mathbf{v} = \dot{\mathbf{x}}$ characterizes the spatial velocity. The pull-back of the spatial velocity gradient in equation (2.13) to the intermediate configuration

$$\hat{\mathbf{L}} := \mathbf{F}_e^{-1} \cdot \mathbf{l} \cdot \mathbf{F}_e = \hat{\mathbf{L}}_e + \hat{\mathbf{L}}_g, \quad (2.14)$$

can be additively split into the growth velocity gradient and the elastic velocity gradient

$$\hat{\mathbf{L}}_g := \dot{\mathbf{F}}_g \cdot \mathbf{F}_g^{-1} \quad \text{and} \quad \hat{\mathbf{L}}_e := \mathbf{F}_e^{-1} \cdot \dot{\mathbf{F}}_e, \quad (2.15)$$

respectively.

2.2 Balance equations

To constitute the physical basis of continuum mechanics, the balance equations for open systems are discussed in this section. One fundamental assumption of the theory of closed systems in classical mechanics is that mass is constant over time. Since biomaterials, such as bone or soft tissue, undergo the continuous processes of growth, remodeling and morphogenesis, this assumption is not applicable to biomechanical problems. Thus, the theory of open systems has to be applied in this work. For fur-

ther aspects concerning this theory, the reader is referred to the articles of EPSTEIN & MAUGIN [33,34] and KUHLE & STEINMANN [80] as well as to the works of HIMPEL [50] and KUHLE [74]. Since the balance equations have to apply for each material point, we consider a cut-out part of the body. First, the action of the cut-off part of the body on the considered part is discussed. Afterwards the postulation of conservation laws yields the balance equations, of which, in this context, we concentrate on the balance of mass, of linear and angular momentum and of entropy in the context of continuum thermodynamics.

2.2.1 Stresses and heat flux

As depicted in figure 2.4 we cut out a part \mathcal{P}_t of the body \mathcal{B}_t . The mechanical effect of the cut-off part is represented by the stress vector \mathbf{t} onto the surface $\partial\mathcal{P}_t$. The Cauchy

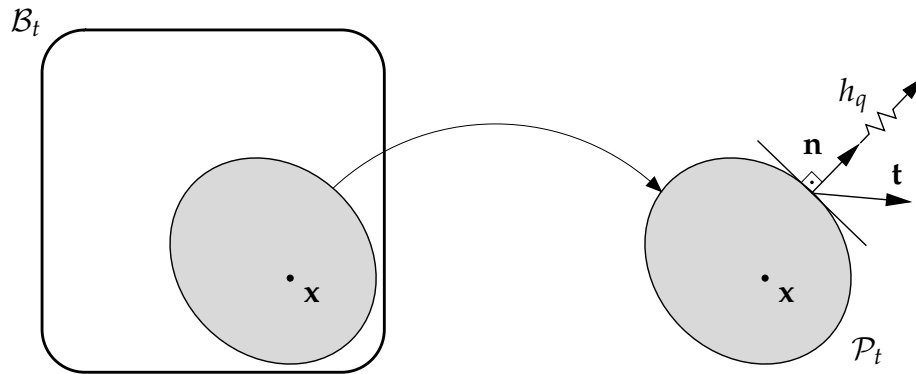


Figure 2.4: Isolated part \mathcal{P}_t of the body \mathcal{B}_t in the spatial configuration. The mechanical and thermal impact on the surface of the cut-out part are represented by the stress vector \mathbf{t} and the heat out-flux h_q . Mass flux should be neglected.

theorem

$$\mathbf{t}(\mathbf{x}, t, \mathbf{n}) = \boldsymbol{\sigma}(\mathbf{x}, t) \cdot \mathbf{n} \quad (2.16)$$

gives the relation between the stress vector \mathbf{t} and the Cauchy stresses $\boldsymbol{\sigma}$. Since the Cauchy stresses relate the current forces to the current area element they are also called *true stresses*. Multiplication of the Cauchy stresses with the Jacobian yields the Kirchhoff stresses

$$\boldsymbol{\tau} = J\boldsymbol{\sigma} . \quad (2.17)$$

The Cauchy stress tensor and the Kirchhoff stress tensor are mappings from the cotangent space $T_{\mathcal{X}}^*\mathcal{B}_t$ to the tangent space $T_{\mathcal{X}}\mathcal{B}_t$ in the spatial configuration. The relation of the current forces to the undeformed area element is given by the first Piola-Kirchhoff stresses

$$\mathbf{P} = J\boldsymbol{\sigma} \cdot \mathbf{F}^{-t} = \boldsymbol{\tau} \cdot \mathbf{F}^{-t} . \quad (2.18)$$

The first Piola-Kirchhoff stress tensor is a mapping from the material cotangent space $T_X^*\mathcal{B}_0$ to the spatial tangent space $T_x\mathcal{B}_x$. The pull-back of the Kirchhoff stress tensor defines the second Piola-Kirchhoff stresses in the material and in the intermediate configuration

$$\mathbf{S} = \mathbf{F}^{-1} \cdot \boldsymbol{\tau} \cdot \mathbf{F}^{-t} \quad \text{and} \quad \widehat{\mathbf{S}} = \mathbf{F}_e^{-1} \cdot \boldsymbol{\tau} \cdot \mathbf{F}_e^{-t} = \mathbf{F}_g \cdot \mathbf{S} \cdot \mathbf{F}^t, \quad (2.19)$$

respectively. Furthermore, in the following explanations we use the Mandel stresses

$$\widehat{\mathbf{M}} := \widehat{\mathbf{C}} \cdot \widehat{\mathbf{S}} \quad (2.20)$$

in the intermediate configuration, which are work conjugated to the growth velocity gradient $\widehat{\mathbf{L}}_g$. The introduced stresses and their work conjugated quantities are visualized in figure 2.5.

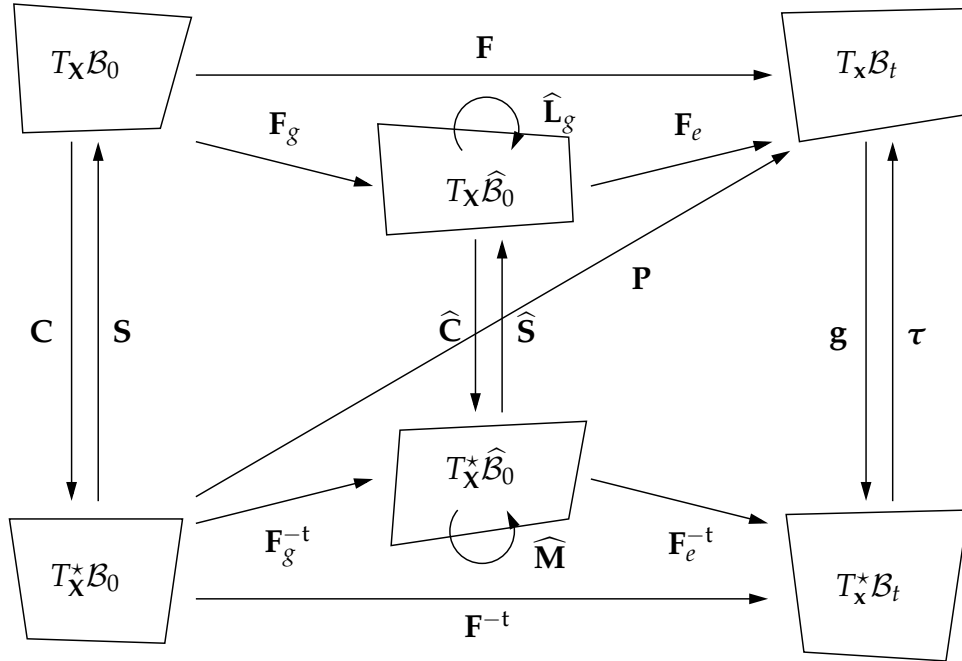


Figure 2.5: Visualization of the stress tensors and the work conjugated deformation tensors. \mathbf{S} and $\widehat{\mathbf{S}}$ denote the Piola-Kirchhoff stresses in the material and in the intermediate configuration. $\boldsymbol{\tau}$ characterizes the Kirchhoff stress tensor.

The heat out-flux through the surface $\partial\mathcal{P}_t$ is denoted by h_q . In analogy to the Cauchy-theorem in equation (2.16) we assume

$$h_q(\mathbf{x}, t, \mathbf{n}) = \mathbf{q}(\mathbf{x}, t) \cdot \mathbf{n}, \quad (2.21)$$

with the spatial heat flux vector \mathbf{q} .

2.2.2 Master balance law

Since each balance law has the same structure, we initially formulate a master balance law, see also MIEHE [101], which afterwards is adapted to the different physical quantities. The temporal change of the balanced quantity \mathcal{Q} of a body consists of an accretion due to a source \mathcal{S} inside the body and an influx \mathcal{F} through its surface as well as a production \mathcal{P} inside the body

$$\frac{d}{dt}\mathcal{Q} = \mathcal{S} + \mathcal{F} + \mathcal{P}. \quad (2.22)$$

If the production \mathcal{P} is equal to zero, \mathcal{Q} is a conserved quantity. Reformulation of the master balance law in integral form in the spatial setting yields

$$\frac{d}{dt} \int_{\mathcal{P}_t} \mathfrak{q} \, dv = \int_{\mathcal{P}_t} \mathfrak{s} \, dv + \int_{\partial\mathcal{P}_t} \mathfrak{f} \cdot \mathbf{n} \, da + \int_{\mathcal{P}_t} \mathfrak{p} \, dv, \quad (2.23)$$

with the balanced quantity \mathfrak{q} per unit volume, the source \mathfrak{s} and the production \mathfrak{p} inside \mathcal{P}_t and the influx \mathfrak{f} through the surface $\partial\mathcal{P}_t$ as depicted in figure 2.6. The volume

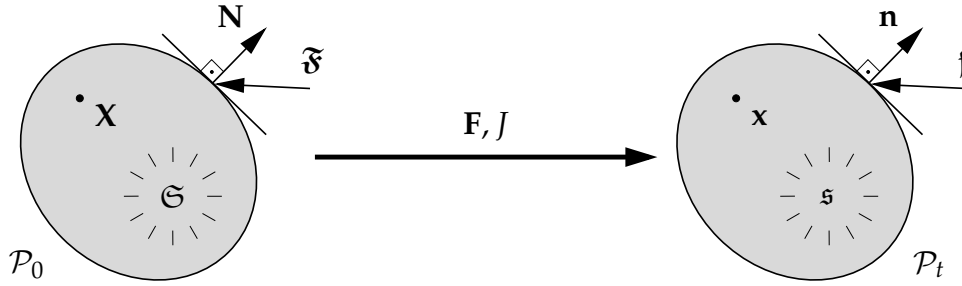


Figure 2.6: The balanced quantity $\mathcal{Q}, \mathfrak{q}$ changes in time due to a source $\mathcal{S}, \mathfrak{s}$, an influx $\mathcal{F}, \mathfrak{f}$ and a production $\mathcal{P}, \mathfrak{p}$.

and surface integrals have to coincide in the material and spatial configuration

$$\int_{\mathcal{P}_t} \{v\} \, dv = \int_{\mathcal{P}_0} \{V\} \, dV \quad \text{and} \quad \int_{\partial\mathcal{P}_t} \{a\} \, da = \int_{\partial\mathcal{P}_0} \{A\} \, dA, \quad (2.24)$$

so that, using equations (2.9) and (2.3) and the localization theorem, the transformation of the volume and surface quantities between the material and spatial setting is given by

$$\{V\} = J\{v\} \quad \text{and} \quad \{A\} = J\{a\}\mathbf{F}^{-t}. \quad (2.25)$$

Thus, the material formulation of equation (2.23) becomes

$$\frac{d}{dt} \int_{\mathcal{P}_0} \mathcal{Q} \, dV = \int_{\mathcal{P}_0} \mathcal{S} \, dV + \int_{\partial\mathcal{P}_0} \mathcal{F} \cdot \mathbf{N} \, dA + \int_{\mathcal{P}_0} \mathcal{P} \, dV, \quad (2.26)$$

with the balanced quantity \mathcal{Q} , the source \mathcal{S} and the production \mathcal{P} inside \mathcal{P}_0 and the influx \mathcal{F} through the surface $\partial\mathcal{P}_0$. With the Gauss integral theorem and the localization

theorem, the material local master balance law reads as

$$\dot{\mathcal{Q}} = \mathcal{G} + \text{DIV } \mathfrak{F} + \mathfrak{P}. \quad (2.27)$$

2.2.3 Balance of mass

A key difference between the theory of open systems and the theory of closed systems is the balance of mass. In contrast to the theory of closed systems, the mass is not assumed to be constant for open systems. We consider a mass source \mathcal{R}_0 per unit volume inside the part of the body \mathcal{P}_0 . A mass flux through the surface $\partial\mathcal{P}_0$ is neglected in this work. An extension to materials including a mass flux is described in the contributions of EPSTEIN & MAUGIN [33,34], KUHL, MENZEL & STEINMANN [78] and KUHL & STEINMANN [80,81]. The initial density of a part of the body \mathcal{P}_0 is denoted by ρ_0 , so that the initial mass element becomes

$$dM = \rho_0 dV. \quad (2.28)$$

Consequently, the grown mass element dm consists of the initial mass element and a term taking into account the accretion of mass by the mass source during the time interval $[t_0, t]$

$$dm = dM + \int_{t_0}^t \mathcal{R}_0 d\tau dV. \quad (2.29)$$

Since mass changing terms are entirely determined in the material configuration, see figure 2.7, the grown mass element can be described on the basis of the quantities in

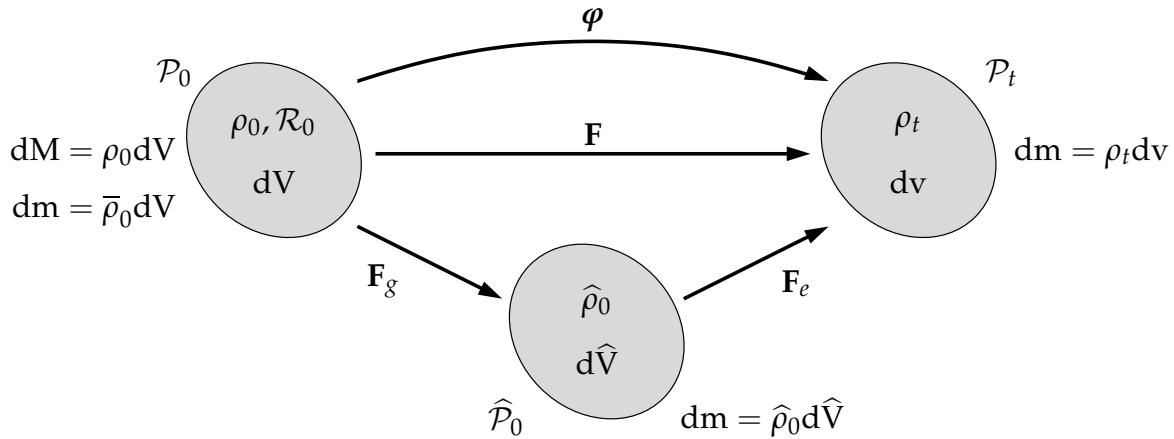


Figure 2.7: The grown mass element dm consists of the initial mass element dM and a term which accounts for the mass source $\mathcal{R}_0 t$. Mass changing terms are entirely determined in the material configuration.

the different configurations as

$$dm = \bar{\rho}_0 dV = \hat{\rho}_0 d\hat{V} = \rho_t dv. \quad (2.30)$$

In this the (grown) material density is defined as

$$\boxed{\bar{\rho}_0 := \rho_0 + \int_{t_0}^t \mathcal{R}_0 d\tau} \quad (2.31)$$

and $\hat{\rho}_0$ and ρ_t denote the density in the intermediate and spatial configuration, respectively. Thus, the density expressions transform via Jacobians inversely to the volume transformations in (2.9), namely

$$\hat{\rho}_0 = J_e \rho_t \quad \text{and} \quad \bar{\rho}_0 = J \rho_t = J_g \hat{\rho}_0, \quad (2.32)$$

see also equation (2.25)₁. The time derivative of (2.31) yields the local balance of mass in the material configuration

$$\boxed{\dot{\bar{\rho}}_0 = \mathcal{R}_0.} \quad (2.33)$$

This can also be derived from the local master balance law (2.27) with

$$\Omega^{(\text{mass})} = \bar{\rho}_0, \quad \mathfrak{S}^{(\text{mass})} = \mathcal{R}_0, \quad \mathfrak{F}^{(\text{mass})} = \mathbf{0}, \quad \mathfrak{P}^{(\text{mass})} = 0. \quad (2.34)$$

Insertion of the density transformation in (2.32)₃ and the definition of the growth velocity gradient in (2.15)₂ into the local balance of mass in the material configuration (2.33) yields the local balance of mass in the intermediate configuration

$$\hat{\rho}_0 = J_g^{-1} \mathcal{R}_0 - \hat{\rho}_0 \text{tr} \hat{\mathbf{L}}_g, \quad (2.35)$$

in which $\dot{J}_g = \partial_{\mathbf{F}_g} J_g : \dot{\mathbf{F}}_g = J_g \mathbf{F}_g^{-t} : \dot{\mathbf{F}}_g = J_g \text{tr} \hat{\mathbf{L}}_g$.

2.2.4 Balance of linear momentum

The balance of linear momentum is equivalent to the second axiom of Newton, which states that the temporal change of linear momentum of a body is equal to the sum of applied forces. The linear momentum is defined as the product of mass and velocity

$$\mathbf{I}_{\mathcal{P}_t} := \int_{\mathcal{P}_t} \mathbf{v} dm = \int_{\mathcal{P}_t} \rho_t \mathbf{v} dv, \quad (2.36)$$

from which we conclude that the balanced quantity in equation (2.23) is $\mathfrak{q}^{(\text{lm})} = \rho_t \mathbf{v}$. Transformation via equation (2.25) yields $\Omega^{(\text{lm})} = \bar{\rho}_0 \mathbf{v}$. The remaining terms in equation (2.27) can also be identified as

$$\Omega^{(\text{lm})} = \bar{\rho}_0 \mathbf{v}, \quad \mathfrak{S}^{(\text{lm})} = \bar{\rho}_0 \mathbf{b}_0 + \mathcal{R}_0 \mathbf{v}, \quad \mathfrak{F}^{(\text{lm})} = \mathbf{P}, \quad \mathfrak{P}^{(\text{lm})} = \mathbf{0}, \quad (2.37)$$

in which \mathbf{b}_0 denotes the body acceleration and $\mathcal{R}_0\mathbf{v}$ is the force per unit volume resulting from the mass accretion due to the mass source. Insertion of equations (2.37) in equation (2.27) yields

$$\dot{\bar{\rho}}_0\mathbf{v} + \bar{\rho}_0\dot{\mathbf{v}} = \bar{\rho}_0\mathbf{b}_0 + \mathcal{R}_0\mathbf{v} + \text{DIV } \mathbf{P} . \quad (2.38)$$

Combining this equation with the local balance of mass (2.33) yields the local balance of linear momentum in the material configuration

$$\boxed{\bar{\rho}_0\dot{\mathbf{v}} = \bar{\rho}_0\mathbf{b}_0 + \text{DIV } \mathbf{P} .} \quad (2.39)$$

2.2.5 Balance of angular momentum

In accordance with the balance of linear momentum, the balance of angular momentum states that the temporal change of angular momentum of a body is equal to the sum of the applied torques. The angular momentum is defined as the cross product of the position vector and the linear momentum vector

$$\mathbf{D}_0 := \int_{\mathcal{P}_t} \mathbf{x} \times \mathbf{v}\rho_t dV . \quad (2.40)$$

Thus, analogous to the derivation of the balance of linear momentum, the quantities in the local master balance law (2.27) can be identified as

$$\begin{aligned} \mathcal{Q}^{(\text{am})} &= \mathbf{x} \times \mathbf{v}\bar{\rho}_0 , & \mathcal{S}^{(\text{am})} &= \mathbf{x} \times \mathbf{b}_0\bar{\rho}_0 + \mathbf{x} \times \mathbf{v}\mathcal{R}_0 , \\ \mathcal{F}^{(\text{am})} &= \mathbf{x} \times \mathbf{P} , & \mathcal{P}^{(\text{am})} &= \mathbf{0} . \end{aligned} \quad (2.41)$$

Herein the outer product of a vector and a second-order tensor yields a second-order tensor and is defined as $\mathbf{a} \times \mathbf{B} = \varepsilon_{ijk}a_iB_{jl}$, with ε denoting the third-order permutation tensor. Insertion of equations (2.41) into the local master balance law (2.27) yields

$$\mathbf{x} \times \mathbf{v}\dot{\bar{\rho}}_0 + \mathbf{x} \times \dot{\mathbf{v}}\bar{\rho}_0 = \mathbf{x} \times \mathbf{b}_0\bar{\rho}_0 + \mathbf{x} \times \mathbf{v}\mathcal{R}_0 + \nabla_{\mathbf{X}}\mathbf{x} \times \mathbf{P} + \mathbf{x} \times \text{DIV } \mathbf{P} , \quad (2.42)$$

wherein the vector product of two second-order tensors is defined as $\mathbf{A} \times \mathbf{B} = \varepsilon_{ijk}A_{il}B_{jl}$. Thus, with $\nabla_{\mathbf{X}}\mathbf{x} \times \mathbf{P} = \mathbf{F} \times \mathbf{P} = \varepsilon : (\mathbf{F} \cdot \mathbf{P}^t) = 2 \text{ax}(\mathbf{P} \cdot \mathbf{F}^t)$, see DE BOER [26], and $\text{ax}(\mathbf{A})$ denoting the axial vector of the second-order tensor \mathbf{A} , equation (2.42) can be reformulated as

$$\mathbf{x} \times \mathbf{v}(\dot{\bar{\rho}}_0 - \mathcal{R}_0) + \mathbf{x} \times (\bar{\rho}_0\dot{\mathbf{v}} - \bar{\rho}_0\mathbf{b}_0 - \text{DIV } \mathbf{P}) - 2 \text{ax}(\mathbf{P} \cdot \mathbf{F}^t) = \mathbf{0} . \quad (2.43)$$

Insertion of the balance of mass (2.33) and the balance of linear momentum (2.39) finally yields that the axial vector of the tensor $\mathbf{P} \cdot \mathbf{F}^t$ must be zero, which means that the tensor itself must be symmetric. With the definitions of the Piola-Kirchhoff stress tensors in equations (2.18) and (2.19) we identify that the Cauchy stresses and the second

Piola-Kirchhoff stresses must be symmetric

$$\boxed{\boldsymbol{\sigma} = \boldsymbol{\sigma}^t, \quad \mathbf{S} = \mathbf{S}^t.} \quad (2.44)$$

2.2.6 Balance of internal energy

The balance of internal energy, also denoted as first law of thermodynamics, states that the temporal change of internal energy equals the sum of internal mechanical and thermal power. The internal energy is defined as

$$E_{\mathcal{P}_t} := \int_{\mathcal{P}_t} \rho_t e \, dv, \quad (2.45)$$

with e denoting the internal energy per unit mass. The internal mechanical power results from the mass source. The thermal power is caused by a heat source q per unit mass and the heat out-flux $\mathbf{Q} = J\mathbf{q} \cdot \mathbf{F}^{-t}$, see also equations (2.21) and (2.25)₂. In addition, the stresses acting on the part of the body produce internal mechanical power. Thus, the quantities in equation (2.27) are

$$\begin{aligned} \mathcal{Q}^{(\text{energy})} &= \bar{\rho}_0 e, & \mathcal{S}^{(\text{energy})} &= \mathcal{R}_0 e + \bar{\rho}_0 q, \\ \mathfrak{F}^{(\text{energy})} &= -\mathbf{Q}, & \mathfrak{P}^{(\text{energy})} &= \frac{1}{2} \mathbf{S} : \dot{\mathbf{C}} \end{aligned} \quad (2.46)$$

for the balance of internal energy. Analogous to the above mentioned operations and using equations (2.27) and (2.33) the material local balance of internal energy becomes

$$\boxed{\bar{\rho}_0 \dot{e} = \bar{\rho}_0 q - \text{DIV } \mathbf{Q} + \frac{1}{2} \mathbf{S} : \dot{\mathbf{C}}.} \quad (2.47)$$

2.2.7 Balance of entropy

Entropy was introduced by the German physicist CLAUSIUS in the mid-19th-century to describe the direction of thermodynamical processes. It can be expressed as

$$H_{\mathcal{P}_t} := \int_{\mathcal{P}_t} \rho_t h \, dv, \quad (2.48)$$

with the specific entropy per unit mass h . The second law of thermodynamics requires that the entropy production, defined as the difference between the rate of entropy and the entropy power

$$\wp^{\text{entropy}} = \frac{d}{dt} \mathcal{Q}^{\text{entropy}} - [\mathcal{S}^{\text{entropy}} + \mathfrak{F}^{\text{entropy}}] \geq 0, \quad (2.49)$$

has to be greater than or equal to zero, see also equation (2.22). Analogous to the previous treatments, the entropy power includes a source part and a flux part. As discussed in GARIKIPATI ET AL. [41], to satisfy thermodynamical consistency, chemical or thermal processes must be included in remodeling procedures that stiffen the material. Thus, to take into account the increase of entropy due to non-mechanical components, we consider an extra entropy source \mathcal{S} in addition to the standard entropy power. Furthermore, the entropy production is defined as

$$\Gamma_{\mathcal{P}_t} := \int_{\mathcal{P}_t} \rho_t \gamma \, dv, \quad (2.50)$$

with the entropy production per unit mass γ . Thus, we can identify

$$\begin{aligned} \mathfrak{Q}^{(\text{entropy})} &= \bar{\rho}_0 h, & \mathfrak{S}^{(\text{entropy})} &= \mathcal{R}_0 h + \bar{\rho}_0 \frac{1}{\theta} q + \bar{\rho}_0 \mathcal{S}, \\ \mathfrak{F}^{(\text{entropy})} &= -\frac{1}{\theta} \mathbf{Q}, & \mathfrak{P}^{(\text{entropy})} &= \bar{\rho}_0 \gamma \end{aligned} \quad (2.51)$$

in the master balance law (2.27), so that with the balance of mass (2.33), the entropy inequality (2.49) becomes

$$\bar{\rho}_0 \gamma = \bar{\rho}_0 \dot{h} - \bar{\rho}_0 \frac{1}{\theta} q - \bar{\rho}_0 \mathcal{S} + \text{DIV} \left(\frac{1}{\theta} \mathbf{Q} \right). \quad (2.52)$$

To obtain the dissipation inequality, this equation has to be multiplied with the absolute temperature $\theta > 0$. Beyond this, insertion of the internal energy balance (2.47) yields

$$\bar{\rho}_0 \mathcal{D} = \frac{1}{2} \mathbf{S} : \dot{\mathbf{C}} - \bar{\rho}_0 \theta \dot{h} - \bar{\rho}_0 \dot{e} - \frac{1}{\theta} \mathbf{Q} \cdot \nabla_x \theta - \bar{\rho}_0 \theta \mathcal{S}, \quad (2.53)$$

wherein the local dissipation per unit mass is defined as $\mathcal{D} := \theta \gamma$. Finally, with the Legendre transformation $\psi = e - \theta h$, where ψ is the free energy per unit mass, the material dissipation inequality becomes

$$\boxed{\bar{\rho}_0 \mathcal{D} := \frac{1}{2} \mathbf{S} : \dot{\mathbf{C}} - \bar{\rho}_0 \dot{\psi} - \theta \bar{\rho}_0 \mathcal{S} \geq 0} \quad (2.54)$$

for the isothermal case .

Remark 2.1 (Open systems versus closed systems) In contrast to the approach of e.g. EPSTEIN & MAUGIN [33,34], in this contribution the balance equations for momentum and energy do not contain any open system-specific terms. Analogous to the derivations in KUHL & STEINMANN [81,82], they are identical to those for closed systems. ■

2.3 General constitutive equations

Constitutive equations have to be defined in order to take into account the characteristic material response. The content of this work is the modeling of remodeling, growth and reorientation in transversely isotropic elastic materials. Thus, to specify the elastic part of material behavior, a free energy function ψ has to be defined. To describe the form of mass changes, a further constitutive equation, for example for the mass source \mathcal{R}_0 , must be provided. Moreover, to indicate other non-elastic material behavior, i.e., fiber reorientations, we apply the concept of internal variables. Additionally to this concept, the constitutive equations have to satisfy some more fundamental principles, which are discussed first. Afterwards the constitutive equations themselves are specified.

2.3.1 Principles for the construction of constitutive equations

Besides the concept of internal variables, the two most important principles for the construction of material equations are the principle of material objectivity and the principle of material symmetry. Thus, in the following we concentrate on these three principles. For a more detailed overview about all principles see TRUESDELL & NOLL [133] and HAUPT [49].

2.3.1.1 Principle of material objectivity

The principle of material objectivity states that the constitutive equations are invariant with respect to the observer. Since this expression is rather cumbersome to evaluate, commonly another equivalent version of this principle is used that requires invariance with respect to superposed rigid body motions, $\boldsymbol{\varphi}^+ = \mathbf{c} + \mathbf{Q} \cdot \boldsymbol{\varphi}$. In terms of the free energy function, this means that the free energy has to stay constant for a rotated object

$$\psi(\mathbf{F}^+) = \psi(\mathbf{F}) \quad \text{with } \mathbf{F}^+ = \mathbf{Q} \cdot \mathbf{F} \quad \forall \mathbf{Q} \in \mathcal{SO}(3), \quad (2.55)$$

with $\mathcal{SO}(3)$ denoting the special orthogonal group, i.e., $\det \mathbf{Q} = 1 \wedge \mathbf{Q}^t \cdot \mathbf{Q} = \mathbf{1}$. To obtain a constitutive equation satisfying the principle of material objectivity a priori, the dependency of the free energy function on the deformation gradient is commonly realized by a dependency on the right Cauchy-Green tensor

$$\psi(\mathbf{C}^+) = \psi(\mathbf{C}) \quad \text{with } \mathbf{C}^+ = (\mathbf{F}^t \cdot \mathbf{Q}^t) \cdot \mathbf{g} \cdot (\mathbf{Q} \cdot \mathbf{F}) = \mathbf{C} \quad \forall \mathbf{Q} \in \mathcal{SO}(3). \quad (2.56)$$

2.3.1.2 Principle of material symmetry

It is obvious that the material behavior as well as the stored free energy of anisotropic materials depend on the orientation of the material with respect to the deformation state. An easy example is fiber reinforced materials with one characteristic fiber direction under unidirectional tension. It is evident that the material behavior as well as the

stored free energy differ, depending on whether the fibers are aligned parallel or perpendicular to the loading direction. To describe specific anisotropic material behavior, a symmetry group $\mathcal{G} \subset \mathcal{O}(3)$ has to be defined, with $\mathcal{O}(3)$ denoting the orthogonal group, i.e., $\det \mathbf{Q} = \pm 1 \wedge \mathbf{Q}^t \cdot \mathbf{Q} = \mathbf{1}$. A symmetry group consists of those transformations among which the constitutive equations are invariant. Thus, for the free energy function in equation (2.56) the symmetry group is determined by

$$\mathcal{G} := \{ \mathbf{Q} \in \mathcal{O}(3) | \psi(\mathbf{C}) = \psi(\mathbf{Q} \cdot \mathbf{C} \cdot \mathbf{Q}^t) \} . \quad (2.57)$$

2.3.1.3 Concept of internal variables

To describe history-dependent deformations, internal variables are introduced. For instance, the density $\bar{\rho}_0$ can be used to model density changes. The evolution of the internal variables is given by additional equations. The concept of internal variables states that the current deformation state of dissipative materials, described by the free energy function

$$\psi = \psi(\mathbf{F}, \mathcal{I}) , \quad (2.58)$$

depends on a set of internal variables \mathcal{I} in addition to the deformation gradient \mathbf{F} .

2.3.2 Transversely isotropic elasticity

For the representation of transverse isotropy, it is common practice to introduce the characteristic direction \mathbf{n}^A in the material configuration or, rather, the sign-independent structural tensor \mathbf{A} . In this work, following MENZEL [97], the characteristic direction is assumed to be a non-constant, reorienting unit vector

$$\mathbf{A} = \mathbf{n}^A \otimes \mathbf{n}^A \quad \text{with} \quad \mathbf{n}^A \cdot \mathbf{n}^A = 1 \quad \text{and} \quad \mathbf{n}^A \neq \text{const.} , \quad (2.59)$$

which is introduced as an internal variable, see section 2.3.1.3. It describes, for instance, the fiber direction in a fiber-reinforced material or the collagen fibers in the arterial wall. Following the notation of Schönflies, see BORCHARDT-OTT [14], the transverse isotropic symmetry group is denoted by $D_{\infty h} := \{ \mathbf{Q} \in \mathcal{O}(3) | \mathbf{Q} \cdot \mathbf{A} \cdot \mathbf{Q}^t = \mathbf{A} \}$.

Following LUBARDA & HOGER [93], we assume that the characteristic direction is identical in the material configuration and in the intermediate configuration. Thus, \mathbf{n}^A has to be a principal direction of the growth deformation tensor, namely

$$\mathbf{F}_g \cdot \mathbf{n}^A = \eta \mathbf{n}^A , \quad (2.60)$$

wherein η describes the stretch ratio during the growth process parallel to the characteristic direction. Consequently, with ϑ indicating the stretch ratio orthogonal to the

characteristic direction, the growth deformation tensor can be represented by

$$\mathbf{F}_g = \vartheta \mathbf{1} + [\eta - \vartheta] \mathbf{n}^A \otimes \mathbf{n}^A . \quad (2.61)$$

The stretch ratios η and ϑ are internal variables. The related Jacobian is $J_g = \eta\vartheta^2$, see appendix B.1.

We assume an a priori objective free energy per unit volume $\psi_0 = \bar{\rho}_0 \psi$ depending on the right Cauchy Green tensor in the intermediate configuration $\hat{\mathbf{C}}$ and a set of internal variables \mathcal{I}

$$\psi_0 = \psi_0(\hat{\mathbf{C}}, \mathcal{I}) , \quad (2.62)$$

see equations (2.58) and (2.56). From equations (2.11) and (2.5) or respectively from figure 2.3 we can identify

$$\hat{\mathbf{C}} = \mathbf{F}_g^{-t} \cdot \mathbf{C} \cdot \mathbf{F}_g^{-1} . \quad (2.63)$$

Thus, the dependence of the free energy function on the internal variables η , ϑ and \mathbf{n}^A is already ensured by the dependence on $\hat{\mathbf{C}}$. As described in section 2.2.3 the density can change due to a mass source \mathcal{R}_0 . To include this in the constitutive setting, we introduce the density in the intermediate configuration $\hat{\rho}_0$ as an internal variable. As suggested in HARRIGAN & HAMILTON [46] and motivated by experimental observations described in CARTER & HAYES [16], the dependence of the free energy on the density is realized by weighting the free energy function by the relative density $[\hat{\rho}_0/\rho_0]^n$

$$\psi_0 = \left[\frac{\hat{\rho}_0}{\rho_0} \right]^n \psi_0^e(\hat{\mathbf{C}}) . \quad (2.64)$$

The exponent n and the initial density ρ_0 are material constants with n varying from 1 to 3.5 according to the porosity of the material, see KUHL & STEINMANN [81]. Summing up, we consider four internal variables: the density $\hat{\rho}_0$, the stretch ratios η and ϑ , and the characteristic direction \mathbf{n}^A . The appropriate evolution equations have to be specified depending on the material behavior.

Following the principle of material symmetry (2.57), an exclusive dependence of ψ_0^e on $\hat{\mathbf{C}}$ would lead to an anisotropic free energy function, i.e., for transverse isotropy

$$\psi_0^e(\hat{\mathbf{C}}) = \psi_0^e(\mathbf{Q} \cdot \hat{\mathbf{C}} \cdot \mathbf{Q}^t) \quad \forall \quad \mathbf{Q} \in D_{\infty h} . \quad (2.65)$$

For an isotropic representation of anisotropic tensor functions, based on the works of LOKHIN & SEDOV [91] and BOEHLER [13], we extend the tensor function isotropically by means of structural tensors. This leads to the isotropic representation of the free

energy function for transverse isotropy

$$\psi_0^e(\widehat{\mathbf{C}}, \mathbf{A}) = \psi_0^e(\mathbf{Q} \cdot \widehat{\mathbf{C}} \cdot \mathbf{Q}^t, \mathbf{Q} \cdot \mathbf{A} \cdot \mathbf{Q}^t) \quad \forall \mathbf{Q} \in \mathcal{O}(3), \quad (2.66)$$

with \mathbf{Q} now being allowed to be any member of the orthogonal group $\mathcal{O}(3)$. The dependency on the right Cauchy-Green tensor and the structural tensor is typically realized by invariants, for instance the basic invariants of \mathbf{C} and the mixed invariants of \mathbf{C} and \mathbf{A}

$$I_{i=1,2,3} = \text{tr}(\mathbf{C}^i) \quad \text{and} \quad I_{i=4,5} = \text{tr}(\mathbf{C}^{i-3} \cdot \mathbf{A}), \quad (2.67)$$

respectively, see for instance SPENCER [127], SCHRÖDER [118] and APEL [4]. For a dependence on the right Cauchy-Green tensor in the intermediate configuration, we choose the appropriate invariants of $\widehat{\mathbf{C}}$ and \mathbf{A}

$$\widehat{I}_{i=1,2,3} = \text{tr}(\widehat{\mathbf{C}}^i) \quad \text{and} \quad \widehat{I}_{i=4,5} = \text{tr}(\widehat{\mathbf{C}}^{i-3} \cdot \mathbf{A}). \quad (2.68)$$

Summing up, the material free energy per unit mass (2.66) is described by

$$\boxed{\psi = \frac{1}{\bar{\rho}_0} \psi_0 \quad \text{with} \quad \psi_0 = \left[\frac{\widehat{\rho}_0}{\rho_0} \right]^n \psi_0^e(\widehat{\mathbf{C}}, \mathbf{A}) = \left[\frac{\widehat{\rho}_0}{\rho_0} \right]^n \psi_0^e(\widehat{I}_1, \widehat{I}_2, \widehat{I}_3, \widehat{I}_4, \widehat{I}_5).} \quad (2.69)$$

By application of the chain rule

$$\begin{aligned} \dot{\psi} &= \frac{\partial \psi}{\partial \widehat{\mathbf{C}}} : \frac{\partial \widehat{\mathbf{C}}}{\partial \mathbf{C}} : \dot{\mathbf{C}} + \frac{\partial \psi}{\partial \widehat{\mathbf{C}}} : \frac{\partial \widehat{\mathbf{C}}}{\partial \mathbf{F}_g} : \dot{\mathbf{F}}_g + \frac{\partial \psi}{\partial \bar{\rho}_0} \frac{\partial \bar{\rho}_0}{\partial \mathbf{F}_g} : \dot{\mathbf{F}}_g \\ &\quad + \frac{\partial \psi}{\partial \bar{\rho}_0} \frac{\partial \bar{\rho}_0}{\partial \widehat{\rho}_0} \dot{\widehat{\rho}}_0 + \frac{\partial \psi}{\partial \widehat{\rho}_0} \dot{\widehat{\rho}}_0 + \frac{\partial \psi}{\partial \mathbf{A}} : \dot{\mathbf{A}} \end{aligned} \quad (2.70)$$

and insertion of equations (2.63) and (2.32), the time derivative of the free energy per unit mass becomes

$$\begin{aligned} \dot{\psi} &= \frac{1}{\bar{\rho}_0} \left[\left[\mathbf{F}_g^{-1} \cdot \frac{\partial \psi_0}{\partial \widehat{\mathbf{C}}} \cdot \mathbf{F}_g^{-t} \right] : \dot{\mathbf{C}} - \left[2\widehat{\mathbf{C}} \cdot \frac{\partial \psi_0}{\partial \widehat{\mathbf{C}}} + \psi_0 \mathbf{1} \right] : \left[\dot{\mathbf{F}}_g \cdot \mathbf{F}_g^{-1} \right] \right. \\ &\quad \left. - \left[\frac{1}{\widehat{\rho}_0} \psi_0 - \frac{\partial \psi_0}{\partial \widehat{\rho}_0} \right] \dot{\widehat{\rho}}_0 + \frac{\partial \psi_0}{\partial \mathbf{A}} : \dot{\mathbf{A}} \right]. \end{aligned} \quad (2.71)$$

With this and the Clausius-Planck inequality (2.54), we obtain the definition of the second Piola-Kirchhoff stresses in the material configuration

$$\boxed{\mathbf{S} := 2\mathbf{F}_g^{-1} \cdot \frac{\partial \psi_0}{\partial \widehat{\mathbf{C}}} \cdot \mathbf{F}_g^{-t} = 2 \frac{\partial \psi_0}{\partial \mathbf{C}}} \quad (2.72)$$

by the standard argumentation of rational mechanics. Accordingly, the push-forward of the second Piola-Kirchhoff stresses to the intermediate configuration follows as

$$\widehat{\mathbf{S}} = 2 \frac{\partial \psi_0}{\partial \widehat{\mathbf{C}}}, \quad (2.73)$$

see also equation (2.19). Hence, with equations (2.20) and (2.15) the reduced dissipation inequality becomes

$$\boxed{\bar{\rho}_0 \mathcal{D}^{red} = [\widehat{\mathbf{M}} + \psi_0 \mathbf{1}] : \widehat{\mathbf{L}}_g + \left[\frac{1}{\widehat{\rho}_0} \psi_0 - \frac{\partial \psi_0}{\partial \widehat{\rho}_0} \right] \dot{\widehat{\rho}}_0 - \frac{\partial \psi_0}{\partial \mathbf{A}} : \dot{\mathbf{A}} - \theta \bar{\rho}_0 \mathcal{S} \geq 0,} \quad (2.74)$$

which also points out the energetic conjugation of the Mandel stresses $\widehat{\mathbf{M}}$ and the growth velocity gradient $\widehat{\mathbf{L}}_g$.

Insertion of the invariant-based version of the free energy function (2.69) into the general definition of the second Piola-Kirchhoff stresses (2.73) and (2.72) and application of the chain rule yields the Piola-Kirchhoff stresses

$$\widehat{\mathbf{S}} = 2 \sum_{i=1}^5 \frac{\partial \psi_0}{\partial \widehat{I}_i} \frac{\partial \widehat{I}_i}{\partial \widehat{\mathbf{C}}} = \widehat{\Phi}_1 \mathbf{1} + \widehat{\Phi}_2 \widehat{\mathbf{C}} + \widehat{\Phi}_3 \widehat{\mathbf{C}}^2 + \widehat{\Phi}_4 \mathbf{A} + 2 \widehat{\Phi}_5 [\widehat{\mathbf{C}} \cdot \mathbf{A}]^{sym} \quad (2.75)$$

and

$$\begin{aligned} \mathbf{S} &= 2 \mathbf{F}_g^{-1} \cdot \left[\sum_{i=1}^5 \frac{\partial \psi_0}{\partial \widehat{I}_i} \frac{\partial \widehat{I}_i}{\partial \widehat{\mathbf{C}}} \right] \cdot \mathbf{F}_g^{-t} \\ &= 2 \sum_{i=1}^5 \frac{\partial \psi_0}{\partial I_i} \frac{\partial I_i}{\partial \mathbf{C}} = \Phi_1 \mathbf{1} + \Phi_2 \mathbf{C} + \Phi_3 \mathbf{C}^2 + \Phi_4 \mathbf{A} + 2 \Phi_5 [\mathbf{C} \cdot \mathbf{A}]^{sym} \end{aligned} \quad (2.76)$$

depending on the scalar values $\widehat{\Phi}_i = 2 \partial \psi_0 / \partial \widehat{I}_i$ and $\Phi_i = 2 \partial \psi_0 / \partial I_i$ and the derivatives of the invariants with respect to the right Cauchy-Green tensors as depicted in appendix C.3.

Remark 2.2 (Isotropic mass growth in transversely isotropic elasticity) For isotropic volumetric mass growth, the stretch ratios must be identical in each direction, i.e., $\eta \equiv \vartheta$. Thus, the growth deformation tensor in equation (2.61) reduces to $\mathbf{F}_g^{iso} = \vartheta \mathbf{1}$, and the related Jacobian is $J_g^{iso} = \vartheta^3$. However, the dependence on the internal variable \mathbf{n}^A is ensured via the isotropic extension of the free energy by means of the structural tensor \mathbf{A} , see equations (2.66) and (2.69). ■

2.4 Different biomechanical effects

In his review article about functional adaption of biomaterials, TABER [129] differentiates between growth, remodeling and morphogenesis. In his nomenclature, growth signifies mass changes through cell divisions (hyperplasia), cell enlargements (hypertrophy), secretion of extracellular matrix (ECM) or accretion on external or internal surfaces. Negative growth is called atrophy. He denotes remodeling as changes of material properties such as strength, density or the internal structure in his nomenclature. Lastly, he describes morphogenesis as shape change, for example the generation of an animal's form by cell division, cell motion and cell death.

The mass is composed of the volume and the density. Thus, as depicted in figure 2.8, one can distinguish between three cases inducing a mass change. First, the volume is

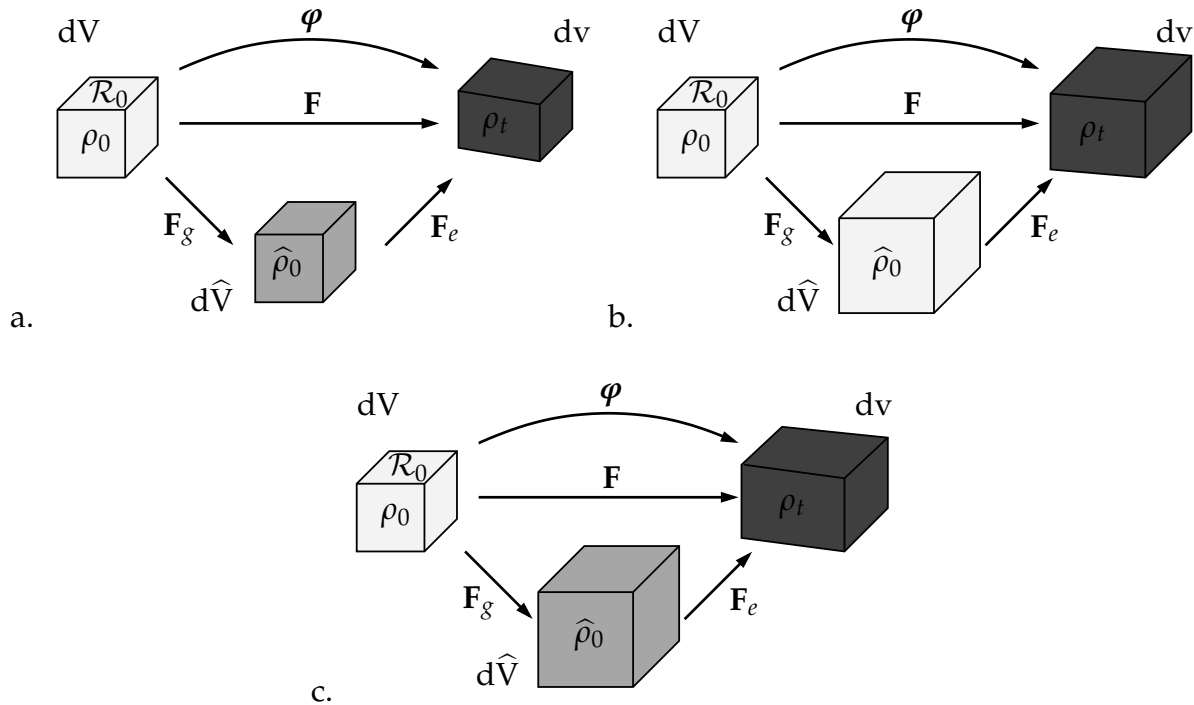


Figure 2.8: Mass changes can occur due to different effects. (a) If the volume is preserved, i.e., $d\hat{V} = dV$, the density must change to induce a mass change. This effect is denoted by remodeling. (b) For density preservation, i.e., $\hat{\rho}_0 = \rho_0$, the volume has to change, which is denoted as growth. (c) A combination of volume and density changes is described by a combination of growth and remodeling.

kept constant, so for a mass change, the density must change. Second, the density is kept constant, such that the volume must change. Third, the density and the volume can change. As mentioned in section 2.1 mass growth takes part in the deformation via the growth deformation tensor F_g . Thus, changes of density or volume denote changes from the initial state to the intermediate configuration. In figure 2.8 different densities are characterized by different colors and volume changes are depicted by varying sizes of the volume element. In order to avoid confusion, in the present work growth should denote pure changes of the volume, whereas density changes fall in the

category of remodeling. Also, reorientation of the characteristic direction implicates a change of the internal structure, which is characterized by TABER as remodeling. Thus, to get around mix-ups, in the following remodeling refers to density changes whereas alterations of the characteristic direction are denoted as reorientation. Summing up, we consider three biomechanically relevant effects, namely

- *remodeling*, as related in the following to pure density changes,
- *growth*, denoting pure volume changes, and
- *reorientation* of the characteristic direction.

In the past, remodeling has successfully been applied to simulate porous biomaterials such as hard tissues, see e.g. VAN RIETBERGEN ET AL. [135]. However, for soft tissues, these models seem less appropriate since the addition of new material has a direct impact on the volume of the tissue, see for instance HUMPHREY [63]. Reorientation processes can occur both in hard and soft tissues. As depicted in WOLFF [142] and HUISKES ET AL. [61], the trabecular orientation in bones adapts to external loadings. Appropriate behavior can be observed in soft tissues, wherein the anisotropic behavior is induced, for instance, by cell orientations or collagen fibers, see SHERRATT ET AL. [123] and DRIESSEN ET AL. [31]. As a matter of course, combinations of remodeling, growth and reorientation are conceivable as well.

A detailed description of the three aforementioned biological effects is given in the following chapters. We follow the same structure for each effect: Firstly, an introduction is given describing the particular effect, its relevance in biomechanics and its historical background. Afterwards, the constitutive equations determined in the present chapter are applied to the individual effect, and necessary evolution equations are determined. In the third part, we concentrate on the numerical implementation of the constitutive framework. Finally, each model is studied by numerical examples.

3 Remodeling

3.1 Introduction

By the end of the 19th century prestigious scientists, such as VON MEYER [139], CULMANN [25], ROUX [117] and WOLFF [142], ascertained that the density of bone depends on mechanical impact. Describing this effect, the concept of functional adaption was introduced by ROUX in the 1880s. According to this, the internal structure of bone adapts to the mechanical loads applied in terms of the body weight and the musculoskeletal system, see for instance PAUWELS [108, 109]. Hence, higher stresses induce densification of the bone and lower stresses cause a lightening of the structure. Ossifications of connection points of muscles and tendons are also an effect of functional adaption. For instance, the trochanter major is developed from constant tension of the gluteal muscles, see e.g. TITTEL [132]. Whereas in the healthy body this mechanism provides an optimized utilization of material, in replacement surgeries it induces a loosening of prostheses. Since the stiffness of a prosthesis is generally much higher than that of the surrounding bone, the stresses are primarily carried by the prosthesis. Thus, the mechanical impact on the bone is less than in the healthy situation, which causes atrophy of bone and, thus, a loosening of the prosthesis., see e.g. HUISKES ET AL. [62], WENG [140] and KUHL & BALLE [75]. Another example for bone density adaption in the negative sense is bedridden patients or astronauts in zero gravity. As a consequence of less load impact than in the normal, healthy situation, these people are often afflicted with osteoporosis. In most publications this adaption of hard tissues to external loads by densification is called growth. As aforementioned, to avoid a mix-up with volume growth, in this work it is signified by *remodeling*.

The first continuum model in this regard has been examined by COWIN & HEGEDUS [23], who permitted density changes based on a mass source. In the last decades this model, which is embedded into the thermodynamics of open systems, has been elaborated further. EPSTEIN & MAUGIN [33] introduced a mass flux in their considerations in addition to the mass source. Due to the way the flux terms are introduced in the balance principles, the resulting equations are different from those for closed systems. In contrast to this, with the assumptions made by KUHL, MENZEL & STEINMANN [78] and KUHL & STEINMANN [79, 81, 83], the allowance of a mass flux changes the balance of mass, but leaves the other balance equations unchanged compared to the closed systems theory. In these as well as in further publications, e.g. of ORR ET AL. [107], BEAUPRÉ, ORR & CARTER [11, 10], HARRIGAN & HAMILTON [46, 47], CARTER & HAYES [16], KRSTIN, NACKENHORST & LAMMERING [73], HIMPEL [50]

and MENZEL [97], an exchange of the balanced quantities of the considered part of the body with the surrounding material is permitted.

Contrary to this approach, the theory of porous media does not allow any exchange of mass, momentum, energy and entropy of the considered part with the circumjacent material. Due to this theory, the balanced quantities of the whole mixture are constant but may change between individual constituents of the mixture, see for instance CARTER & HAYES [16], DE BOER [27], STEEB & DIEBELS [128] and RICKEN, SCHWARZ & BLUHM [115].

In this chapter, we consider remodeling within the continuum approach based on the equations derived in chapter 2. Therefore, in the next section the constitutive equations determined in section 2.3 are applied to remodeling. Afterwards we concentrate on the numerical implementation of the constitutive theory into a finite element code. This includes the algorithmic treatment of the density evolution as well as the computation of the incremental tangent modulus. Finally, the theory is discussed by means of numerical examples.

3.2 Constitutive equations

In this section the constitutive equations, as derived in section 2.3, are adapted to remodeling. As aforementioned, within this work remodeling denotes density changes under volume preservation from the initial state to the intermediate configuration, viz $d\hat{V} = dV = \text{const}$, as depicted in figure 2.8.a. The characteristic direction is assumed to be constant. From equations (2.9) and (2.61) one can easily read that, for remodeling, the Jacobian related to \mathbf{F}_g becomes $J_g = \eta\vartheta^2 = 1$, see also appendix B.1. Accordingly, with equation (2.32) the material density is identical to the density in the intermediate configuration, i.e., $\bar{\rho}_0 = \hat{\rho}_0$. The simplest way to satisfy this requirement is to assume that $\vartheta = 1$. In this case the growth deformation gradient and the elastic deformation gradient become

$$\boxed{\mathbf{F}_g = \vartheta \mathbf{1} + \left[\frac{1}{\vartheta^2} - \vartheta \right] \mathbf{n}^A \otimes \mathbf{n}^A = \mathbf{1} \quad \text{and} \quad \mathbf{F}_e = \mathbf{F} \quad \text{with} \quad \vartheta := 1,} \quad (3.1)$$

respectively. Hence, for remodeling with the aforesaid special choice of the stretch ratios, the intermediate configuration coincides with the material configuration. The intermediate configuration is thus dispensable. Since, in this particular case, changes in mass follow exclusively from changes in density, they are entirely described by the mass balance equation (2.33) or by the constitutive specification of the mass source.

Following HARRIGAN & HAMILTON [46,47], the mass source is defined as

$$\mathcal{R}_0 := k_\rho \left[\begin{array}{c} \left[\frac{\bar{\rho}_0}{\rho_0} \right]^{-m} \\ \psi_0 - \psi_0^* \end{array} \right], \quad (3.2)$$

with the stress stimulus attractor ψ_0^* indicating the point where the density rate becomes zero, see BEAUPRÉ, ORR & CARTER [11]. For numerical stability the exponent m must be greater than the exponent n in the free energy function, see also KUHL, MENZEL & STEINMANN [78]. The coefficient k_ρ governs the rate of density adaption. With the above mentioned conditions, the material free energy per unit mass (2.69) becomes

$$\psi = \frac{1}{\bar{\rho}_0} \psi_0 = \frac{1}{\bar{\rho}_0} \left[\frac{\bar{\rho}_0}{\rho_0} \right]^n \psi_0^e(\mathbf{C}, \mathbf{A}). \quad (3.3)$$

Insertion into the definition of the second Piola-Kirchhoff stresses (2.72) yields

$$\mathbf{S} = \left[\frac{\bar{\rho}_0}{\rho_0} \right]^n 2 \frac{\partial \psi_0^e}{\partial \mathbf{C}} = \left[\frac{\bar{\rho}_0}{\rho_0} \right]^n \mathbf{S}^e. \quad (3.4)$$

Thus, the stresses follow the same structure as the free energy; they are a combination of the density-independent elastic stresses \mathbf{S}^e weighted by the relative density $[\bar{\rho}_0/\rho_0]^n$. A formulation of the last two equations analogous to that of equations (2.69) and (2.76) (i.e., depending on the invariants) is possible. Remark that, due to the definition of the growth tensor (3.1), the intermediate configuration and the material configuration coincide. Consequently, the invariants in equations (2.67) and (2.68) as well as the stresses in equations (2.72) and (2.73) are identical. Since the growth deformation tensor (3.1) is constant, the growth velocity gradient (2.15)₁ vanishes. Also, with the assumption of a constant fiber direction, the evolution in time of the structural tensor disappears. Hence, the first and third parts of the reduced dissipation inequality (2.74) can be omitted. With the identity $\hat{\rho}_0 = \bar{\rho}_0$, the derivative of the free energy with respect to the density $\hat{\rho}_0$ is equal to the derivative with respect to $\bar{\rho}_0$, namely

$$\frac{\partial \psi_0}{\partial \hat{\rho}_0} = \frac{\partial \psi_0}{\partial \bar{\rho}_0} = n \left[\frac{\bar{\rho}_0}{\rho_0} \right]^{n-1} \frac{1}{\rho_0} \psi_0^e = n\psi. \quad (3.5)$$

Consequently, in the context of remodeling, the reduced dissipation inequality (2.74) can be rewritten in terms of remodeling as

$$\bar{\rho}_0 \mathcal{D}^{red} = [1 - n] \psi \dot{\bar{\rho}}_0 - \theta \bar{\rho}_0 \mathcal{S} \geq 0. \quad (3.6)$$

Solving for the extra entropy term and inserting the mass balance equation (2.33) and the definition of the mass source (3.2) finally yields

$$\mathcal{S} \leq \frac{1}{\theta \bar{\rho}_0} [1 - n] \psi k_\rho \left[\left[\frac{\bar{\rho}_0}{\rho_0} \right]^{-m} \psi_0 - \psi_0^* \right]. \quad (3.7)$$

Remark 3.1 (Isotropic remodeling) With the aforesaid choice of the stretch ratios as $\vartheta \equiv \eta \equiv 1$, remodeling is introduced isotropically a priori. Thus, the above mentioned equations apply to isotropic remodeling as well. Nonetheless, the elastic behavior can be assumed to be isotropic as well as anisotropic by choice of an appropriate elastic free energy function ψ_0^e in equation (3.3). ■

3.3 Implementation

In this section we concentrate on the numerical implementation of the discussed constitutive theory for remodeling. Since, in this work, mass accretion is exclusively introduced by a mass source, we can apply standard finite element techniques based on an internal variable formulation describing density changes. In contrast to this, if an additional mass flux is assumed, density changes must be incorporated into the finite element formulation via an additional nodal degree of freedom, namely the density $\bar{\rho}_0$. Within this so-called node-based approach, the density field is determined by linearization of the balance of mass, see for instance KUHL, MENZEL & STEINMANN [78]. Since the stretch ratios as well as the characteristic direction are constant, the only remaining internal variable is the density $\bar{\rho}_0$. Thus, in the previous section the update of the density field is considered first. Afterwards, the incremental tangent modulus at the spatial time step is developed.

3.3.1 Incremental update of the density field

The evolution of the density is described by the material mass balance (2.33) combined with the definition of the mass source (3.2) as

$$\dot{\bar{\rho}}_0 = k_\rho \left[\left[\frac{\bar{\rho}_0}{\rho_0} \right]^{-m} \psi_0 - \psi_0^* \right]. \quad (3.8)$$

To obtain the density at the spatial time step, we apply an implicit Euler backward scheme

$$\bar{\rho}_{0n+1} = \bar{\rho}_{0n} + \dot{\bar{\rho}}_{0n+1} \Delta t, \quad (3.9)$$

with the index n denoting the time increment. The related residual

$$r_\rho = -\bar{\rho}_{0n+1} + \bar{\rho}_{0n} + \dot{\bar{\rho}}_{0n+1} \Delta t = 0 \quad (3.10)$$

must vanish at the solution point. This nonlinear equation can be solved by application of a Newton iteration scheme. For this, we expand equation (3.10) in Taylor series at $\bar{\rho}_0$

$$r_\rho^{k+1} = r_\rho^k + \frac{\partial r_\rho^k}{\partial \bar{\rho}_{0n+1}} \Delta \bar{\rho}_0 = 0. \quad (3.11)$$

For the sake of readability the indices $n + 1$ and k are neglected in the following. Thus, the combination of equations (3.10) and (3.11) can be rewritten as

$$r_\rho^{k+1} = r_\rho + \left[-1 + \frac{\partial \dot{\bar{\rho}}_0}{\partial \bar{\rho}_0} \Delta t \right] \Delta \bar{\rho}_0 = 0 \quad (3.12)$$

and solved for the increment

$$\Delta \bar{\rho}_0 = \left[1 - \frac{\partial \dot{\bar{\rho}}_0}{\partial \bar{\rho}_0} \Delta t \right]^{-1} r_\rho. \quad (3.13)$$

The derivative of the density evolution with respect to the density itself arises from equations (3.2) and (3.3) as

$$\frac{\partial \dot{\bar{\rho}}_0}{\partial \bar{\rho}_0} = k_\rho [n - m] \left[\frac{\bar{\rho}_0}{\rho_0} \right]^{n-m-1} \frac{1}{\rho_0} \psi_0^e = k_\rho [n - m] \left[\frac{\bar{\rho}_0}{\rho_0} \right]^{-m} \psi. \quad (3.14)$$

Finally, we obtain the algorithmic update of the density

$$\bar{\rho}_0^{k+1} = \bar{\rho}_0^k + \Delta \bar{\rho}_0, \quad (3.15)$$

which has to be applied until a convergence criterion is reached.

3.3.2 Incremental tangent modulus

With the density and the strains at hand, the stresses can be derived, see equation (3.4). Based on the definition of the stresses (2.72), the relation between the incremental stresses and the incremental strains results in

$$\Delta \mathbf{S} = \mathbb{C} : \frac{1}{2} \Delta \mathbf{C} \quad (3.16)$$

with the incremental tangent modulus \mathbb{C} describing the change of stresses with respect to the change of strains

$$\mathbb{C} = 2 \frac{\partial \mathbf{S}}{\partial \mathbf{C}} + 2 \frac{\partial \mathbf{S}}{\partial \bar{\rho}_0} \otimes \frac{\partial \bar{\rho}_0}{\partial \mathbf{C}}. \quad (3.17)$$

Analogous to equation (3.4), the first part of equation (3.17) can be identified as the elastic tangent modulus \mathbb{C}^e weighted by the relative density $[\bar{\rho}_0/\rho_0]^n$

$$2 \frac{\partial \mathbf{S}}{\partial \mathbf{C}} = 2 \left[\frac{\bar{\rho}_0}{\rho_0} \right]^n \frac{\partial \mathbf{S}^e}{\partial \mathbf{C}} = 4 \left[\frac{\bar{\rho}_0}{\rho_0} \right]^n \frac{\partial^2 \psi_0^e}{\partial \mathbf{C} \partial \mathbf{C}} = \left[\frac{\bar{\rho}_0}{\rho_0} \right]^n \mathbb{C}^e. \quad (3.18)$$

Corresponding to equations (2.69) and (2.76), the elastic tangent modulus can alternatively be represented depending on the invariants

$$\mathbb{C}^e = 4 \sum_{i=1}^5 \left[\sum_{j=1}^5 \left[\frac{\partial^2 \psi_0^e}{\partial I_i \partial I_j} \frac{\partial I_i}{\partial \mathbf{C}} \otimes \frac{\partial I_j}{\partial \mathbf{C}} \right] + \frac{\partial \psi_0^e}{\partial I_i} \frac{\partial^2 I_i}{\partial \mathbf{C} \partial \mathbf{C}} \right]. \quad (3.19)$$

The second part of equation (3.17) can be derived from equation (3.4) as

$$2 \frac{\partial \mathbf{S}}{\partial \bar{\rho}_0} = 2n \frac{1}{\bar{\rho}_0} \left[\frac{\bar{\rho}_0}{\rho_0} \right]^n \mathbf{S}^e. \quad (3.20)$$

Since solely the evolution of the density $\bar{\rho}_0$ is known, but not the density itself, the third part of equation (3.17) cannot be computed as directly as the others. To determine this derivative, the residual of $\bar{\rho}_0$ in an Euler backward scheme as depicted in equation (3.10) must be differentiated with respect to the right Cauchy-Green tensor

$$\frac{\partial r_\rho}{\partial \mathbf{C}} = -\frac{\partial \bar{\rho}_0}{\partial \mathbf{C}} + \left[\frac{\partial \dot{\bar{\rho}}_0}{\partial \mathbf{C}} + \frac{\partial \dot{\bar{\rho}}_0}{\partial \bar{\rho}_0} \frac{\partial \bar{\rho}_0}{\partial \mathbf{C}} \right] \Delta t = \mathbf{0}. \quad (3.21)$$

Solving this equation for the derivative in demand yields

$$\frac{\partial \bar{\rho}_0}{\partial \mathbf{C}} = \left[1 - \frac{\partial \dot{\bar{\rho}}_0}{\partial \bar{\rho}_0} \Delta t \right]^{-1} \frac{\partial \dot{\bar{\rho}}_0}{\partial \mathbf{C}} \Delta t, \quad (3.22)$$

wherein, with equations (3.8), (2.72) and (3.4), the derivative of the density evolution with respect to the Cauchy-Green tensor is

$$\frac{\partial \dot{\bar{\rho}}_0}{\partial \mathbf{C}} = k_\rho \left[\frac{\bar{\rho}_0}{\rho_0} \right]^{-m} \frac{\partial \psi_0}{\partial \mathbf{C}} = \frac{1}{2} k_\rho \left[\frac{\bar{\rho}_0}{\rho_0} \right]^{n-m} \mathbf{S}^e. \quad (3.23)$$

The derivative of the density evolution with respect to the density itself is already depicted in equation (3.14). Recapitulatory, the tangent modulus reads as

$$\mathbb{C} = \left[\frac{\bar{\rho}_0}{\rho_0} \right]^n \mathbb{C}^e + nk_\rho \frac{1}{\bar{\rho}_0} \left[\frac{\bar{\rho}_0}{\rho_0} \right]^{2n-m} \left[1 - \frac{\partial \dot{\bar{\rho}}_0}{\partial \bar{\rho}_0} \Delta t \right]^{-1} \Delta t \mathbf{S}^e \otimes \mathbf{S}^e. \quad (3.24)$$

A summary of the complete algorithm is given in table 3.1.

history data: internal variable $\bar{\rho}_0$

1. set initial values

$$\bar{\rho}_0 = \bar{\rho}_{0n}$$

2. compute density independent quantities

$$\psi_0^e(\mathbf{C}), \quad \mathbf{S}^e = 2 \frac{\partial \psi_0^e}{\partial \mathbf{C}}, \quad \mathbb{C}^e = 4 \frac{\partial^2 \psi_0^e}{\partial \mathbf{C} \partial \mathbf{C}}$$

3. local Newton iteration

- a. compute residual

$$r_\rho = -\bar{\rho}_0 + \bar{\rho}_{0n} + k_\rho \left[\left[\frac{\bar{\rho}_0}{\rho_0} \right]^{n-m} \psi_0^e - \psi_0^* \right] \Delta t$$

- b. compute incremental update

$$\Delta \bar{\rho}_0 = \left[1 - \frac{\partial \dot{\bar{\rho}}_0}{\partial \bar{\rho}_0} \Delta t \right]^{-1} r_\rho \quad \text{with} \quad \frac{\partial \dot{\bar{\rho}}_0}{\partial \bar{\rho}_0} = k_\rho [n - m] \frac{1}{\bar{\rho}_0} \left[\frac{\bar{\rho}_0}{\rho_0} \right]^{n-m} \psi_0^e$$

- c. update

$$\bar{\rho}_0 \leftarrow \bar{\rho}_0 + \Delta \bar{\rho}_0$$

- d. check tolerance

IF $\|r_\rho\| < \text{tol}$ GOTO 4

ELSE GOTO 3.a

4. compute stresses and moduli

$$\mathbf{S} = \left[\frac{\bar{\rho}_0}{\rho_0} \right]^n \mathbf{S}^e$$

$$\mathbb{C} = \left[\frac{\bar{\rho}_0}{\rho_0} \right]^n \mathbb{C}^e + nk_\rho \frac{1}{\bar{\rho}_0} \left[\frac{\bar{\rho}_0}{\rho_0} \right]^{2n-m} \left[1 - \frac{\partial \dot{\bar{\rho}}_0}{\partial \bar{\rho}_0} \Delta t \right]^{-1} \Delta t \mathbf{S}^e \otimes \mathbf{S}^e$$

Table 3.1: Algorithmic update scheme for remodeling

3.4 Numerical examples

In this section the presented constitutive specifications for remodeling are discussed by means of numerical examples. As mentioned above, constitutive equations for the free energy and for the mass source must be specified. We choose an isotropic free energy density of Neo-Hooke-type expanded by a transversely isotropic part

$$\psi_0 = \psi_0^{iso} + \psi_0^{ti} \quad \text{with} \quad \begin{cases} \psi_0^{iso} &= \frac{\lambda}{2} \ln^2 J + \frac{\mu}{2} [I_1 - 3 - 2 \ln J] \\ \psi_0^{ti} &= \frac{\alpha}{2} [I_4 - 1]^2 \end{cases} \quad (3.25)$$

depending on the invariants $I_1 = \text{tr} \mathbf{C}$, $J = \det \mathbf{C}$ and $I_4 = \text{tr}(\mathbf{C} \cdot \mathbf{A})$. The Jacobian can be represented by means of the basic invariants (2.68) as $J = \frac{1}{6} I_1^3 - \frac{1}{2} I_1 I_2 + \frac{1}{3} I_3$. Convexity related issues are not in the focus of this work - the reader is referred to the contribution by SCHRÖDER & NEFF [119] for detailed background information. The mass source for remodeling is indicated by equation (3.2).

3.4.1 Simple tension

To demonstrate the basic features of the presented material model, we first consider a stepwise increasing loading of an isotropic cube, see figures 3.1 and 3.2.a. Several

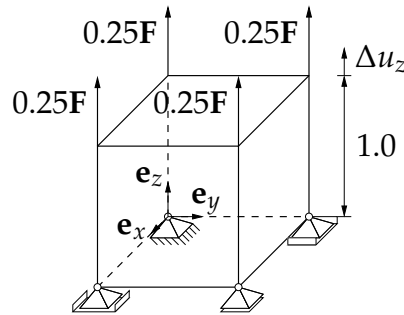


Figure 3.1: Loads and boundary conditions in the simple tension test.

studies have been conducted to identify the elastic material parameters of bone. Considering solely the human femur, the results span between extreme values, depending on the part of the bone, the age and condition of the proband, the experimental design and many other factors, see for instance EVANS [36], KNAUSS [71] and ABÉ, HAYASHI & SATO [1]. Herein, oriented by the contribution of NACKENHORST [105], the elastic parameters are the elasticity modulus $E = 2000\text{N/mm}^2$ and the Poisson's ratio $\nu = 0.3$, corresponding to the Lamé constant $\lambda = 1153846\text{N/mm}^2$ and the shear modulus $\mu = 769.231\text{N/mm}^2$. In order to describe isotropic response, the anisotropy parameter in equation (3.25) must be $\alpha = 0$. Unless otherwise stated, the remodeling parameters are chosen as $\rho_0 = 1.2\text{g/cm}^3$, $\psi_0^* = 0.01\text{N/mm}^2$, $n = 2$, $m = 3$ and

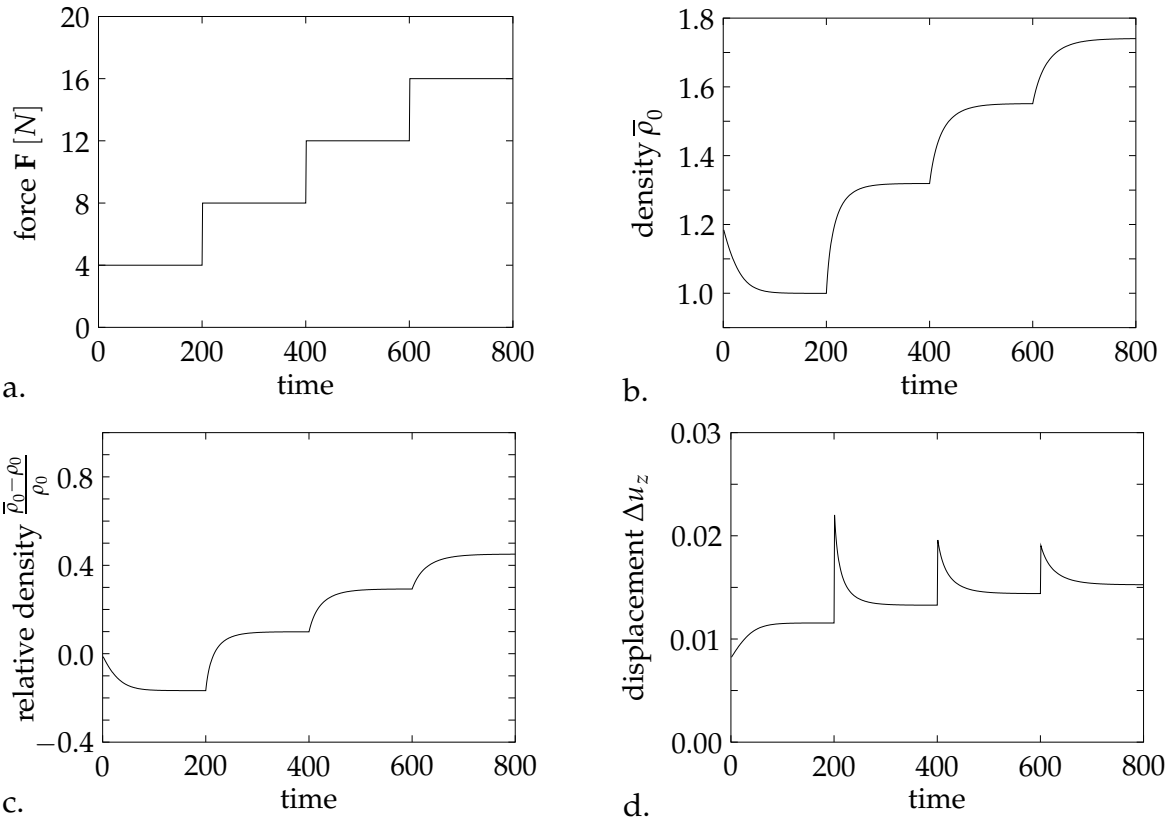


Figure 3.2: Isotropic simple tension test on a remodeling cube. (a) A stepwise increasing force is applied. (b) The density converges time-dependent to the biological equilibrium. (c) Negative relative densities denote a decrease of density. For positive values the material density is higher than the initial density. (d) The deformation reaches a peak value at the beginning of each load step. It converges to the biological equilibrium inversely to the density.

$k_\rho = 1.0$. The time step is $\Delta t = 1.0$. As one can see in figure 3.2.b, the density $\bar{\rho}_0$ does not change instantaneously, even though the force is applied at once; rather, it converges progressively, time-dependent on the so-called biological equilibrium. The biological equilibrium is defined as the state where the deformations and the internal variable describing the mass changes, i.e., here the density, remain constant for a constant load. With the chosen parameters, the density decreases in the first load step and increases in the following steps. The relative change of density with respect to the initial density ρ_0 is shown in figure 3.2.c. In this figure negative values characterize a decrease of density, and positive values characterize an increase in density. In figure 3.2.d the displacement of the upper boundary of the cube in the z -direction is depicted. At the beginning of each load step where the density has not reached the final value to compensate the load, the displacement and, thus, also the strain reach peak values. Then, with increasing density, but constant loading force, the strain decreases until the biological equilibrium is reached. For a decreasing density, the deformation is lower at the beginning of the load step. Over the load step, the density decreases, the material gets weaker and, therefore, the displacement rises.

In the following the sensitivity of the material behavior with respect to the material

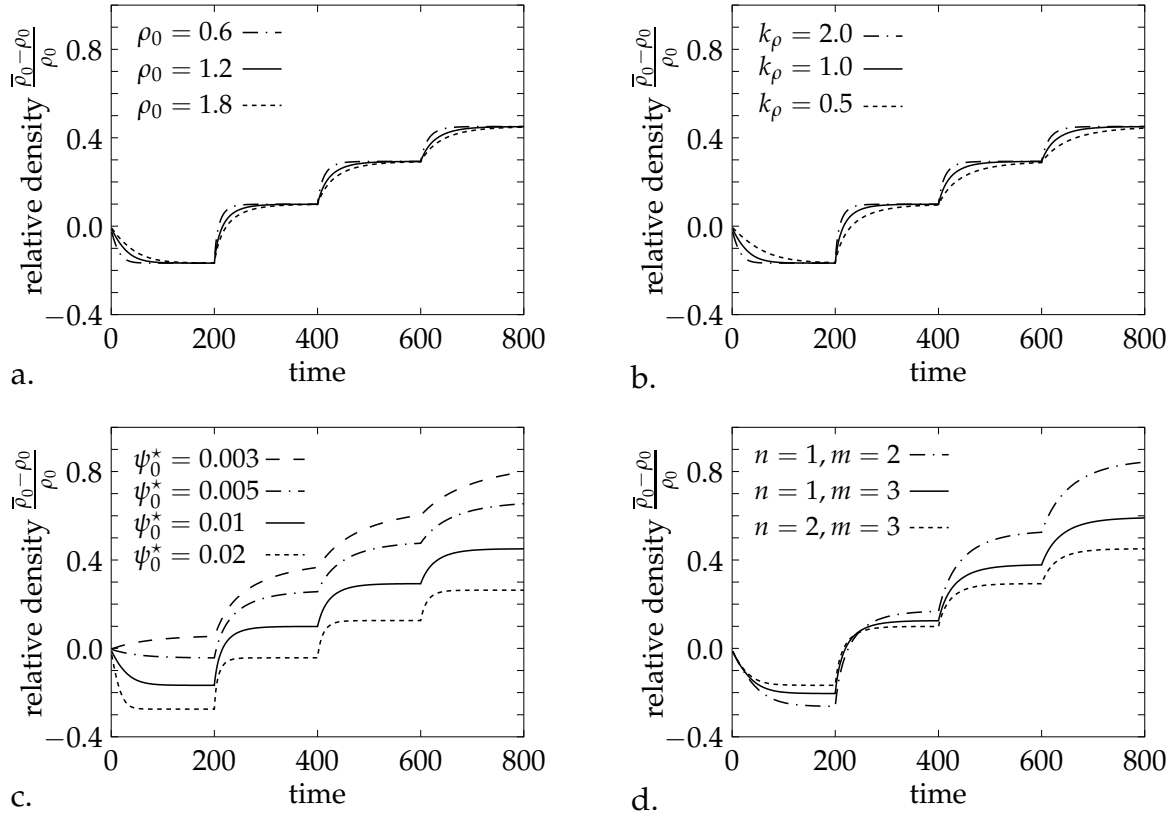


Figure 3.3: Variation of the materials parameters in the simple tension test. (a) The initial density ρ_0 has no influence on the final relative density. (b) The parameter k_ρ governs the rate of convergence. (c & d) The stimulus attractor ψ_0^* and the exponents n and m control the level of the final relative density and the convergence rate.

parameters has been studied. As one can see in figure 3.3.a, the final relative density does not depend on the initial density, but only the rate of convergence. Hence, the final material density $\bar{\rho}_0$ is proportional to initial density ρ_0 . The same can be shown by a combination of equations (2.33), (3.2) and (3.3). Since the evolution of density must be zero at biological equilibrium, we obtain

$$\left[\frac{\bar{\rho}_0}{\rho_0} \right]^{n-m} \psi_0^e - \psi_0^* = 0 \quad \Rightarrow \quad \frac{\bar{\rho}_0}{\rho_0} = \left[\frac{\psi_0^*}{\psi_0^e} \right]^{\frac{1}{n-m}}. \quad (3.26)$$

Equivalent observations have been made by BALLE [9] by means of computations of the human femur. As introduced in the constitutive definition of the mass source (3.2), the parameter k_ρ governs the rate of convergence, see figure 3.3.b. For increasing values of k_ρ the rate of convergence increases, too. In figure 3.3.c the sensitivity of the evolution of the relative density with respect to the stimulus attractor ψ_0^* is depicted. This parameter influences whether the density increases or decreases, how much it changes and how fast its evolution converges. The lower the parameter ψ_0^* is, the less the density decreases. Depending on the other material parameters, there exists a threshold for ψ_0^* , beneath which the density increases. Moreover, for smaller values of ψ_0^* , the

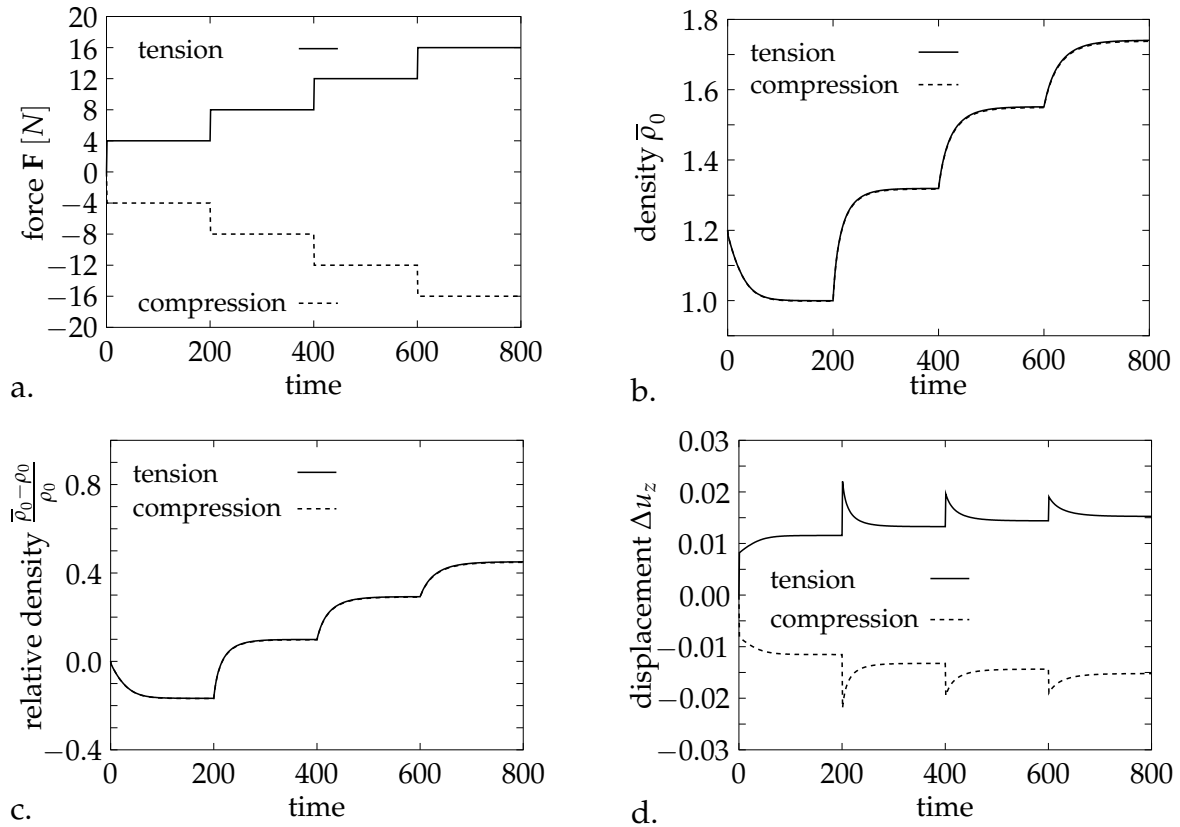


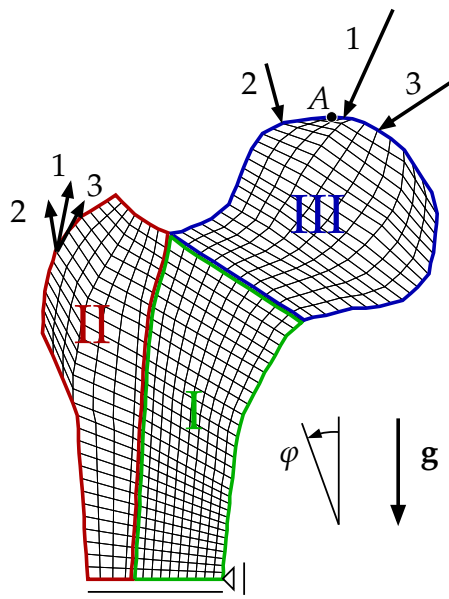
Figure 3.4: With the chosen constitutive equations for remodeling, the density changes depend solely on the magnitude of stresses, but not on the sign. The apparent linear elastic behavior is caused by the application of small deformations.

convergence rate is smaller. The exponential parameters n and m also govern the level of the density as well as the rate of convergence, see figure 3.3.d.

Further on, we compare the material behavior for tension and compression. Since we applied small deformations in this case, the elastic behaviour is more or less linear, see figure 3.4. The remodeling part of the material does not notice whether we apply tension or compression. Density changes are solely influenced by the magnitudes of the stresses (not by the sign).

3.4.2 Human femur

In this section, as a classical representative example for hard tissue biomechanics, we consider a human femur in the two-dimensional setting as depicted in figure 3.5. Indeed, mechanically relevant effects resulting from the three-dimensional setting of the femur, see for instance WENG [140] and references cited therein, are neglected within this model. However, an extension to more realistic models is straightforward. As described in CARTER & BEAUPRÉ [15], three typical loading situations can be identified. Load case 1 characterizes the midstance phase of gait and load cases 2 and 3 stand for the extreme range of abduction and adduction, respectively. To simulate a daily loading situation, we apply the three load cases at once. Additionally, the weight



load case	1	2	3
zone II			
value	2317 N	1158 N	1548 N
direction	-24°	15°	-56°
zone III			
value	703 N	351 N	468 N
direction	-28°	8°	-35°
zones I, II & III			
body force (g)	$60 \frac{\text{N}}{\text{mm}^3}$		

Figure 3.5: Loads and boundary conditions of the human femur model.

of the femur is indicated by a constant body force of $60\text{N}/\text{mm}^3$. All loads are constant during the whole simulation.

At first isotropic material behavior is considered with the same elastic material parameters as for the simple tension test in section 3.4.1, namely $E = 2000\text{N}/\text{mm}^2$ and $\nu = 0.3$. The material parameters describing remodeling are $\rho_0 = 0.8\text{g}/\text{cm}^3$, $\psi_0^* = 0.001\text{N}/\text{mm}^2$, $n = 2$, $m = 3$ and $k_\rho = 10.0$. The time step is $\Delta t = 1.0$. The evolution of the relative density is depicted in figure 3.6. We started with a homogeneous density distribution. Due to the load, an inhomogeneous density change occurs. The loads applied to the head of the femur (zone III) are transmitted directly to the medial zone of the femur shaft. The loads applied to the trochanter major (upper zone II) are transmitted to the lateral zone of the femur shaft. The medial zone of the femur neck, the inner zone of the femur shaft and the zone above the trochanter major are more or less unloaded. Consequently in the latter regions a decrease of density is observable, whereas in the medial femur shaft the density increases. Such a density distribution corresponds to the observed density distribution; for instance, in x-ray photographs of the femur as depicted in the pertinent literature, see also figure 3.7.c. Moreover, it can be seen that the density change occurs faster at the beginning of the simulation and converges with time to the biological equilibrium state. The material density after 200 time steps averaged over the total model is $\bar{\rho}_0^{aver} = 0.613\text{g}/\text{cm}^3$.

For the description of bone, one fundamentally distinguishes between cortical and cancellous bone. With respect to the femur, cortical bone can be found in the shaft of the femur, whilst the femur head consists of cancellous bone. Cortical bone con-

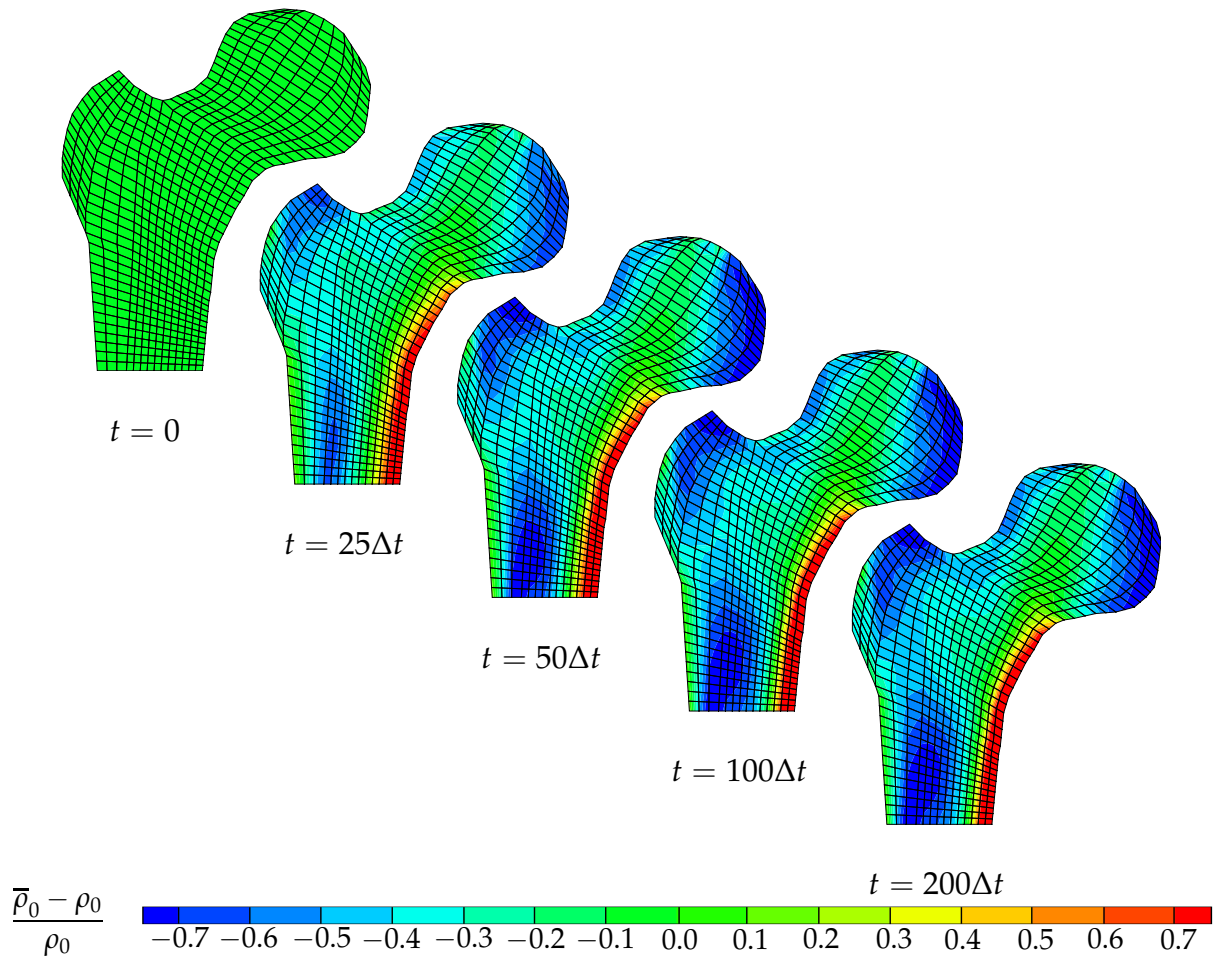


Figure 3.6: Evolution of the relative density in the isotropic human femur model. The averaged density after 200 time steps is $\bar{\rho}_0^{aver} = 0.613\text{g/cm}^3$.

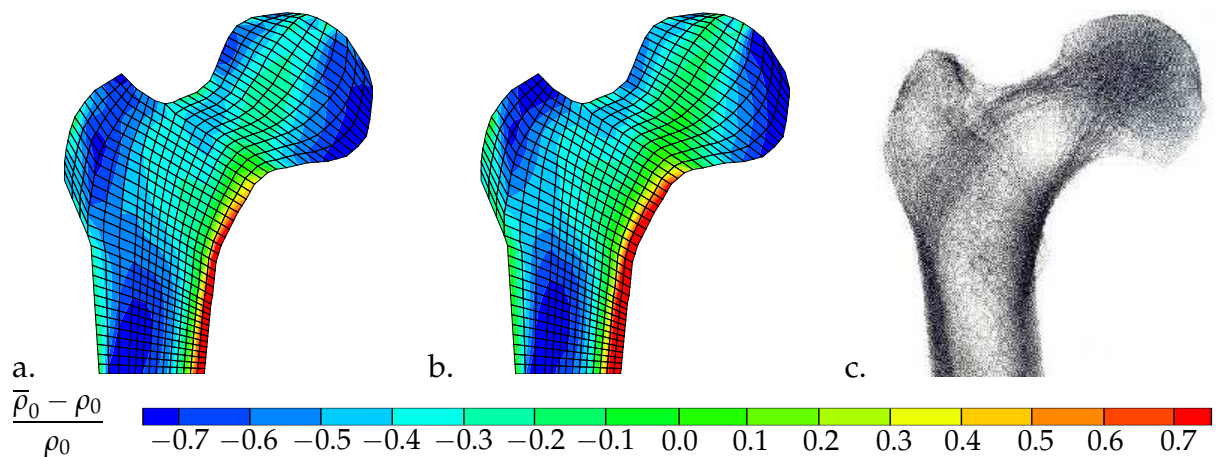


Figure 3.7: Relative density after 200 time steps in the transversely isotropic human femur model. The characteristic direction is (a) parallel and (b) orthogonal to the roughly estimated principal stress directions in the femur or respectively to the directions of the trabeculae. The averaged densities after 200 time steps are (a) $\bar{\rho}_{0a}^{aver} = 0.529\text{g/cm}^3$ and (b) $\bar{\rho}_{0b}^{aver} = 0.597\text{g/cm}^3$. (c) X-ray photograph of the human femur (from PAUWELS [109]).

inc	global it.	global residual	inc	global iteration	local iteration	local residual
1	0	3.39302E+00	1	4	1	1.58356811E-02
1	1	1.42429E+00	1	4	2	1.73325865E-06
1	2	1.84432E-01	1	4	3	2.16321915E-14
1	3	4.81581E-03	1	5	1	1.58356811E-02
1	4	4.11976E-06	1	5	2	1.73325865E-06
1	5	8.07694E-11	1	5	3	2.16044969E-14
2	0	5.44681E-01	2	0	1	1.57498618E-02
2	1	2.72397E-02	2	0	2	1.82247474E-06
2	2	9.56304E-05	2	0	3	2.54364333E-14
2	3	1.16423E-09	2	1	1	1.56943757E-02
3	0	3.63937E-01	2	1	2	1.83287907E-06
3	1	8.82386E-03	2	1	3	2.59958418E-14
3	2	9.00925E-06				
3	3	8.54772E-11				

global convergence local convergence

Table 3.2: Quadratic convergence on the global and on the local level for remodeling

sists of a more or less compact material with a transversely isotropic structure, see for instance REILLY & BURSTEIN [113]. In contrast to this, cancellous bone has a porous trabecular structure. As described by e.g. GARDEN [39], in the femur the trabeculae form a complex three-dimensional structure. At the end of the 19th century VON MEYER [139] and WOLFF [141] already supposed a mechanical interrelation between the form of the trabeculae in the femur head and the applied mechanical loads. This idea has later on been resumed by PAUWELS [108, 109], COWIN [21] and FUNG [38] among others, who stated that the trabeculae are aligned with the principal stress directions. In the model considered here, the structure of the cancellous bone is in a second computation approximated by transverse isotropy. However, an extension to more complex types of anisotropy is straightforward. The material parameters are the same as in the isotropic femur, but with an anisotropy parameter $\alpha = 1000\text{N}/\text{mm}^2$. Based on a rough estimate of the maximum principal stress directions depicted by PAUWELS [109], the angles describing the characteristic directions in the subdomains I, II and III, see figure 3.5, are chosen as $\varphi_{\text{I}}^{\text{a}} = -10^\circ$, $\varphi_{\text{II}}^{\text{a}} = -15^\circ$ and $\varphi_{\text{III}}^{\text{a}} = -20^\circ$, respectively. For comparison, the same transversely isotropic material is assumed in a third computation but with characteristic directions orthogonal to those mentioned above, i.e., $\varphi_{\text{I}}^{\text{b}} = 80^\circ$, $\varphi_{\text{II}}^{\text{b}} = 75^\circ$ and $\varphi_{\text{III}}^{\text{b}} = 70^\circ$. The relative density distribution for both transversely isotropic cases is depicted in figure 3.7. As one can easily observe, the density absorption is higher for the parallel case (a) than for the orthogonal case (b). The same

can be observed by comparison of the averaged material density. For the characteristic direction being more or less parallel to the maximum principal stress direction the averaged density is lower than for the orthogonal characteristic directions, namely $\bar{\rho}_{0a}^{aver} = 0.529\text{g/cm}^3 < 0.597\text{g/cm}^3 = \bar{\rho}_{0b}^{aver}$. Moreover, comparison with an x-ray photograph, as exemplarily depicted in figure 3.7.c, shows that the density distribution corresponds to reality much better in figure 3.7.a than in the other figures. Particularly the region of low density within the femoral neck can be reproduced. Presumably, the simulations get more realistic for a more precise alignment of the characteristic directions with the maximum principal stress direction.

Further on, the computation converges quadratically on both the global and the local levels, as exemplarily depicted in table 3.2. The left table shows the global convergence for the first three loading steps. In the right table the local convergence in point A is depicted for the four global iterations marked gray in the left tabular. A similar convergence can be observed in the other loading steps.

3.4.3 Three-dimensional cylindrical tube

In this section we consider a homogeneous as well as an inhomogeneous deformation of a tube, in order to examine the material behavior in three dimensions and for comparison with the later discussed effect of growth. The tube can be understood as a stylization of an artery, which is a classical example for soft tissue mechanics. For the homogeneous deformation, the tube is constantly stretched in the axial direction to one and a half times the initial length. The discretization, loads and boundary conditions are depicted in figure 3.8. At first we consider isotropic material behavior with

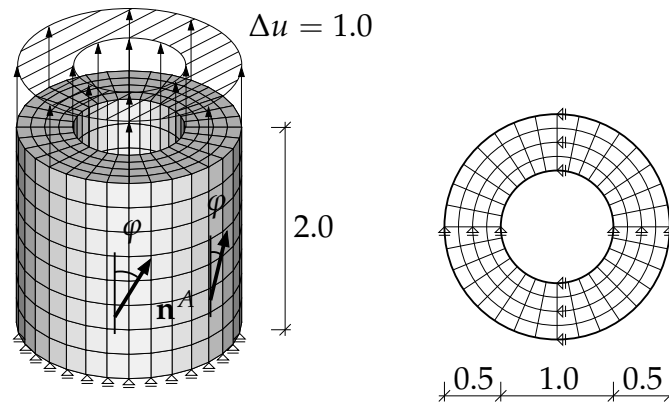


Figure 3.8: Loads and boundary conditions for the homogeneously deformed tube.

the elastic parameters $E = 3\text{N/mm}^2$ and $\nu = 0.45$, or respectively $\lambda = 9.310\text{N/mm}^2$ and $\mu = 1.034\text{N/mm}^2$ as well as the parameters $\rho_0 = 1.0\text{g/cm}^3$, $\psi_0^* = 0.1\text{N/mm}^2$, $n = 2$, $m = 3$ and $k_\rho = 1.0$ for remodeling. At first, in order to model isotropy, the anisotropy parameter is $\alpha = 0$. For the time step we choose $\Delta t = 0.1$. The deformation of the tube and the evolution of the relative density are depicted in figure 3.9.

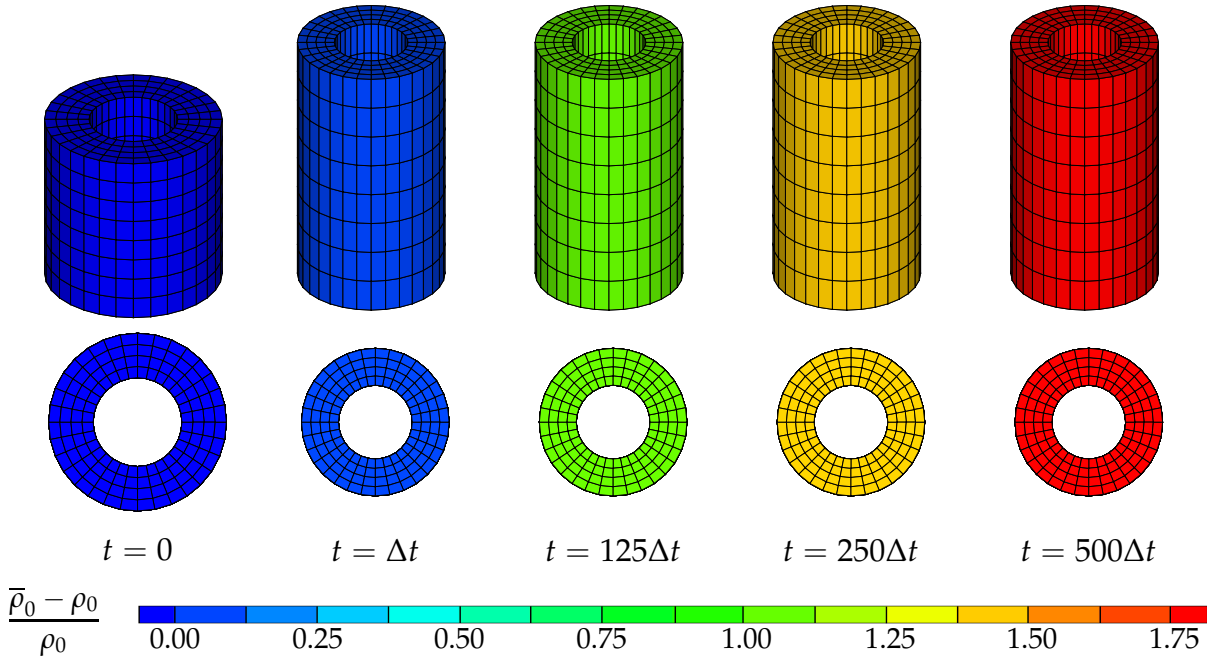


Figure 3.9: Deformation and density evolution of the isotropic tube under tension.

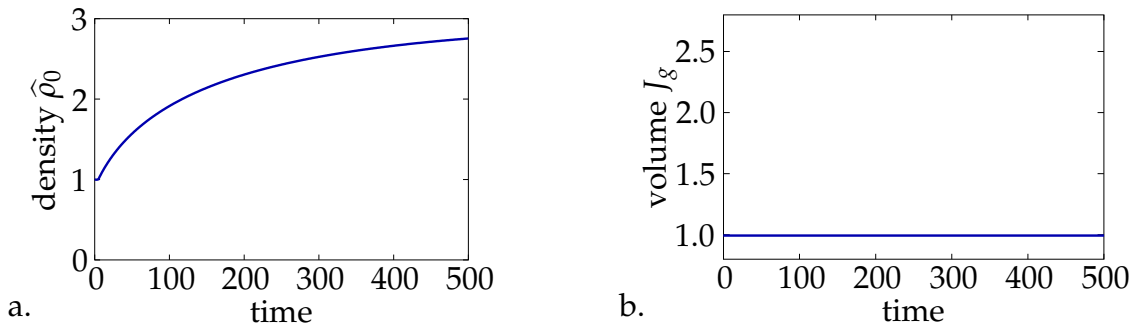


Figure 3.10: Isotropic tube under tension. (a) The evolution of the density $\bar{\rho}_0 \equiv \hat{\rho}_0$ converges to the biological equilibrium state. (b) For remodeling volume preservation from the initial state to the intermediate configuration is prescribed, i.e., $J_g \equiv 1$.

Herein we observe that in the first loading step, due to the elongation, the tube contracts in the radial direction, as expected for almost incompressible elastic materials. The stretch is then held constant for 500 time steps within which the density of the tube increases whilst the deformation stays constant. Moreover, it is observable that the impact of remodeling is more or less the same for the first 125 time steps as for the following 375 time steps. This underlines the effect that the density relaxes to a biological equilibrium state, which can also be seen in figure 3.10.a. In this figure the material density of the tube is plotted over time. Recall that, due to the constitutive assumptions made for remodeling, see section 3.2, the material configuration and the intermediate configuration coincide. Thus, the material density and the intermediate density are equivalent, namely $\bar{\rho}_0 \equiv \hat{\rho}_0$. In figure 3.10.b the evolution of the growth deformation gradient is depicted. Since remodeling is defined as volume preservation

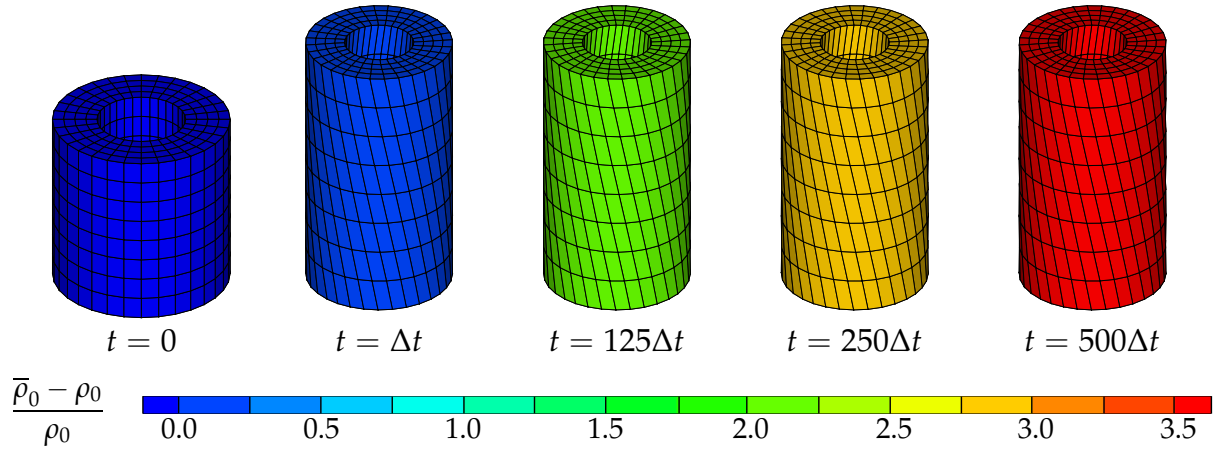


Figure 3.11: Deformation and density evolution of the transversely isotropic tube under tension.

from the material to the intermediate configuration, it holds that $J_g \equiv 1$. Nonetheless, due to elastic deformations, the volume in the spatial configuration generally is not constant, i.e., $J \equiv J_e \neq \text{const.}$

For the examination of transversely isotropic material behavior, we choose the same material parameters as for the isotropic tube, but with a Poisson's ratio $\nu = 0.4$ and an anisotropy parameter $\alpha = 1.0\text{N/mm}^2$. The characteristic direction is arranged in the tangential plane as depicted in figure 3.8, the inclination angle is $\varphi = 30^\circ$. Figure 3.11 shows the deformation and the evolution of the relative density for several time steps. Analogous to the isotropic example, we observe a contraction of the tube in the first loading step. Additionally the tube rotates due to the higher stiffness of the fibers as we would expect for a standard purely elastic transversely isotropic material. If we keep the stretch constant, the density again increases and converges to a biological equilibrium.

Next, we consider an inhomogeneous deformation of a tube. The discretization, loads and boundary conditions are depicted in figure 3.12. The upper and lower

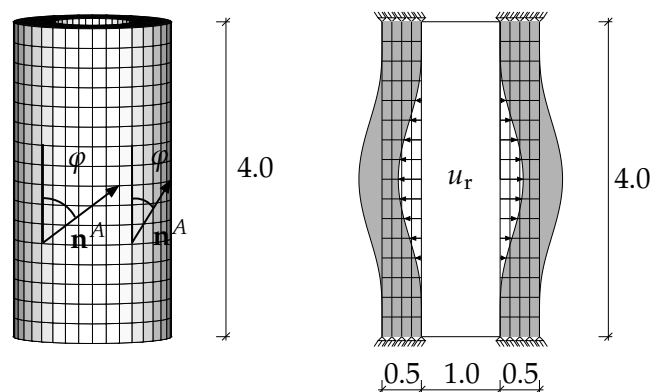


Figure 3.12: Loads and boundary conditions for the inhomogeneously deformed tube.

boundaries of the tube are fixed in space. We apply a constant sinusoidal displacement load in the radial direction at the inside of the tube. The maximum displacement in the middle of the tube is $u_r^{max} = 0.3$. The material parameters for isotropy and for transverse isotropy are identical to those for the tube under tension. Only the convergence parameter for transverse isotropy is set to $k_\rho = 2.0$. The characteristic direction is again arranged in the tangential plane but with an inclination angle of $\varphi = 60^\circ$. The deformation of the tube as well as the relative evolution of the density are depicted in figures 3.13 and 3.14 for isotropy and transverse isotropy, respectively. Again, at the first load step we observe standard elastic material behavior, both for isotropy and transverse isotropy. In the latter case, due to the stiffer characteristic direction, the tube twists itself and the mesh forms an s-shape. The inside radial displacement load is then held constant for 1000 time steps. Because of the resulting high stresses on the inside middle part of the tube, the density in this area increases for both simulations. Vice versa, since the outer upper and lower parts are less loaded, the density decreases in these regions. Again, the density converges to a biological equilibrium state. As a result of the changing density, the stresses change too, so that the non-fixed points of the tube deform slightly further during the relaxation process, which can especially be seen at the outer boundary of the upper and lower parts of the tube.

3.5 Discussion

This chapter is dedicated to the discussion a transversely isotropic version of the remodeling model as proposed by HARRIGAN & HAMILTON [46] and, amongst others, implemented by KUHLE, MENZEL & STEINMANN [78]. We refer to remodeling as changes in density under volume preservation from the initial to the intermediate configuration. In contrast to the discussions in HIMPEL [50], within this work the material model is integrated into the generalized framework for remodeling, growth and reorientation. By an adequate choice of constitutive equations the effects of growth and reorientation are excluded, so that the exclusive impact of remodeling can be considered. The embedding into the generalized framework allows a comparison with pure growth with respect to the computational formulation, the numerical implementation and the overall material behavior. Moreover, within this framework combinations with growth and reorientations are straightforward. In contrast to the implementations discussed in MENZEL [97], we consistently linearized the appropriate nonlinear equations. Thus, with the choice of convenient material parameters, we reached quadratic convergence both on the local and the global level. The material model is solely defined for physically suitable parameters, more precisely, that is a positive density. Thus, for an unsuitable choice of material parameters, i.e., such that the density becomes negative during the solution process, convergence is not provided. To prevent such a sensitivity to the choice of material parameters, it seems reasonable to include adequate penalty functions in the material model.

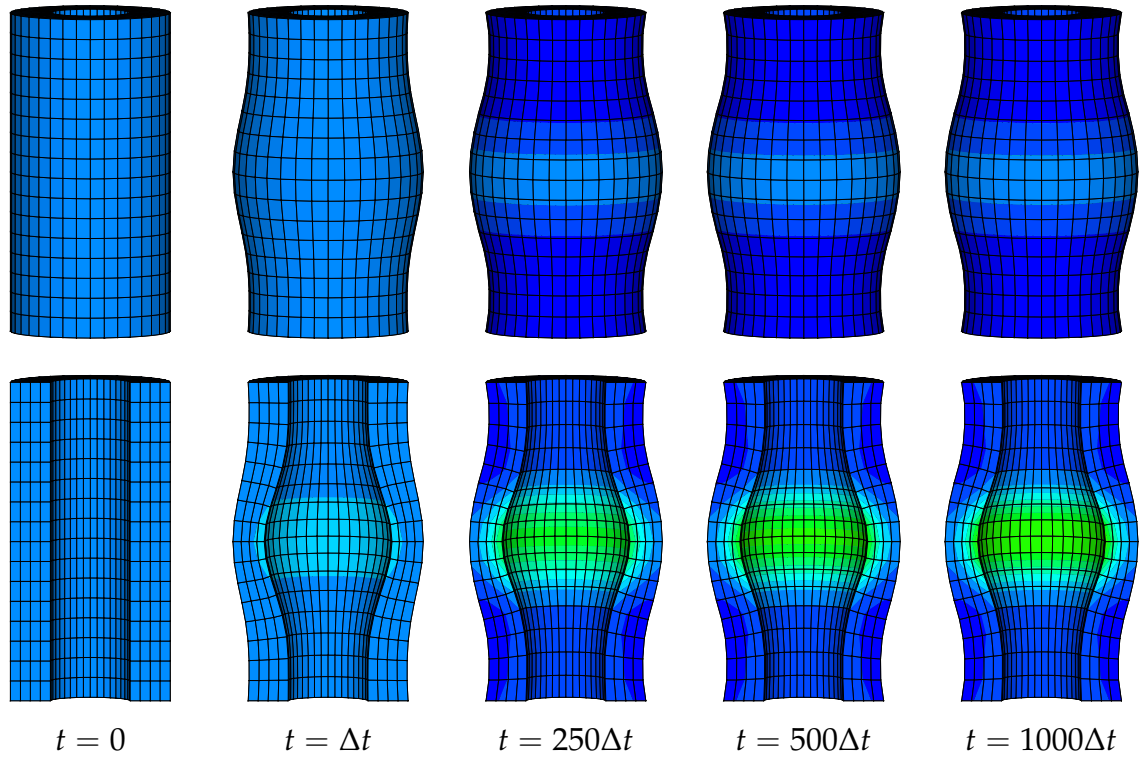


Figure 3.13: Deformation and density evolution in the isotropic tube under inside displacement load.

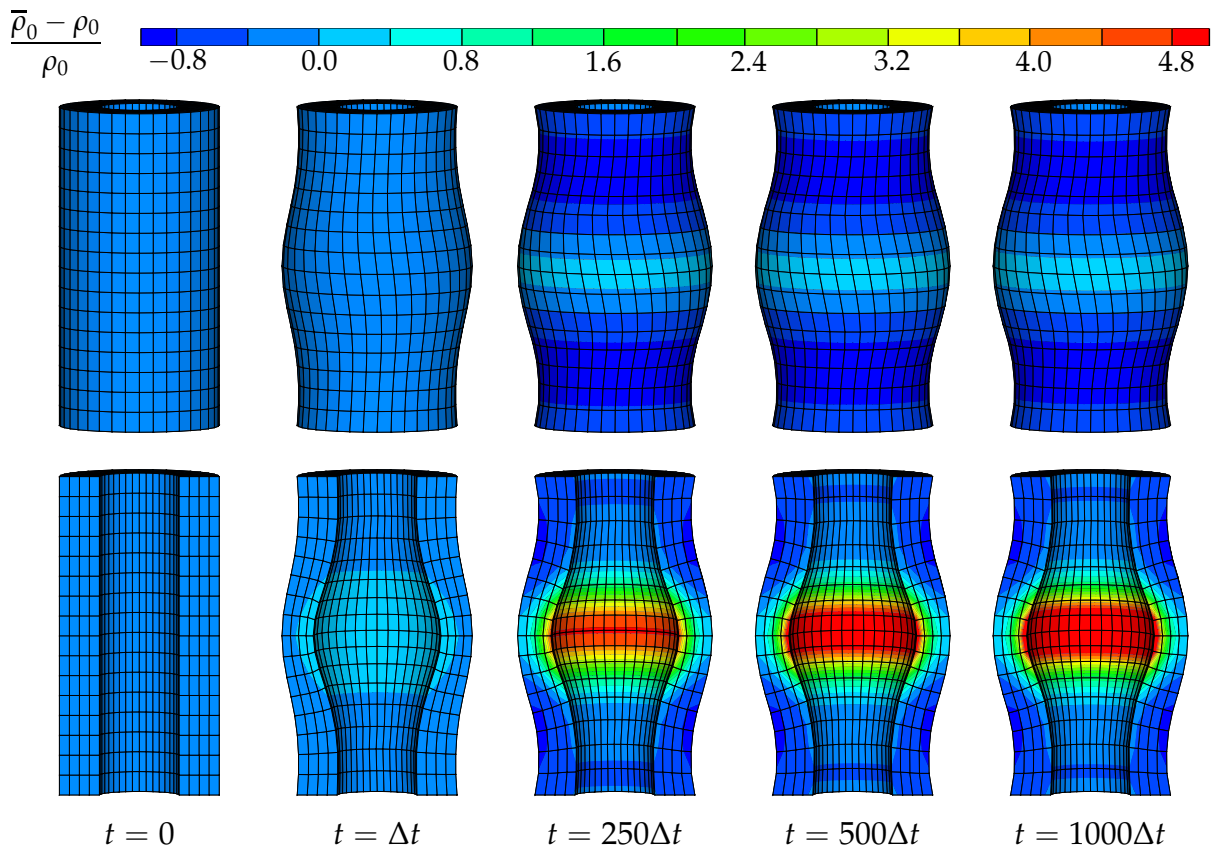


Figure 3.14: Deformation and density evolution of the transversely isotropic tube under inside displacement load.

4 Growth

4.1 Introduction

In medical sense, growth is defined as accretion of mass. This definition has also been used by TABER [129] in his comprehensive review paper. He particularly distinguished between volumetric growth and surface growth. Another form of mass accretion is density growth (in this work denoted by remodeling) which has already been discussed in chapter 3. As mentioned in section 2.4, to avoid ambiguity, in this work *growth* should signify volumetric growth under density preservation. Negative growth is called atrophy. Surface growth is not considered herein. One of the most evident cases of volumetric growth can be observed in muscles. Everybody knows that muscles grow or reduce in response to loading. But also in other biological soft tissues, such as tendons, ligaments or cartilage tissue, mechanically induced growth can be observed. In pathological sense this effect can be detected by wall thickening of the hypertrophic heart or by restenosis of the arterial wall after stent implantation. On the cell level this means that in response to overloadings the number and volume of cells increase, see for instance RICHTER & KELLNER [114], ANVERSA ET AL. [3] and HU ET AL. [59] as well as the excellent textbooks of FUNG [38,37] and HUMPHREY [63].

In the context of continuum mechanics, one of the first contributions attended to growth was published by SKALAK ET AL. [124]. Based on their ideas, RODRIGUES, HOGER & MCCULLOCH [116] introduced the multiplicative split of the deformation gradient for the description of finite growth. This framework enables the modeling of changes in volume, and is commonly used for soft tissues undergoing large strain deformations. Further elaborations can be found in the contributions of TABER & EGGERS [130], CHEN & HOGER [18], AMBROSI & MOLLICA [2] and GARIKIPATI ET AL. [40]. Computational aspects concerning this theory are discussed in the papers of TABER & PERUCCHIO [131], KLISCH, VAN DYKE & HOGER [70], HIMPEL ET AL. [52], MAAS [94] and KUHL ET AL. [77] for isotropic growth as well as in the works of IMATANI & MAUGIN [66], RAO, HUMPHREY & RAJAGOPAL [112], HIMPEL ET AL. [51], MENZEL [99] for transversely isotropic growth and MENZEL [98] for orthotropic growth. For a comprehensive review about biomechanical growth the reader is referred to the paper of HUMPHREY & RAJAGOPAL [65] as well as to the book of HUMPHREY & DELANGE [64]. As discussed in section 2.1, within the multiplicative split the deformation is decomposed into a growth part and an elastic part. Since the growth part results in a generally incompatible configuration, elastic deformations are necessary to ensure compatibility. In this way residual stresses develop in the speci-

men. The existence of residual stresses is particularly obvious at the arterial wall. Since the arterial ring in the unloaded configuration is residually stressed, it springs open if cut radially, as extensively described in VAISHNAV & VOSSOUGH [134], HOLZAPFEL, GASSER & OGDEN [57] and HOLZAPFEL [56]. In this work, residual stresses are not discussed. For more details about this topic we refer to JOHNSON & HOGER [68], SKALAK ET AL. [125] and HOGER [54]. In addition to these deformations providing compatibility, elastic deformations resulting from elastic stresses can occur.

The present chapter is mainly based on the recent work of LUBARDA & HOGER [93]. In particular we focus on the representation of a density preserving material with transverse isotropy. As a main contribution of this work, we discuss the algorithmic setup of the advocated material model. The organization of the present chapter is similar to that in chapter 3. First, the constitutive equations determined in section 2.3 are applied to growth. Second, the numerical implementation of the constitutive theory into a finite element code is discussed. Analogous to the previous chapter this comprises the algorithmic evolution of the internal variables as well as the computation of the incremental tangent modulus. At last, the basic features of the model are illustrated by means of representative numerical examples.

4.2 Constitutive equations

In this section the constitutive equations for the free energy and the mass source, as discussed in chapter 2, are adapted to growth. Analogous to the definition of density changes under volume preservation as described in section 3.2, volume changes under density preservation are introduced from the initial state to the intermediate configuration, viz, $\hat{\rho}_0 = \rho_0 = \text{const}$, as depicted in figure 2.8. Again, the characteristic direction is assumed to be constant. Insertion of a constant density, i.e., $\hat{\rho}_0 = 0$, into the local balance of mass (2.35) in the intermediate configuration yields the mass source

$$\mathcal{R}_0 = J_g \hat{\rho}_0 \text{tr } \hat{\mathbf{L}}_g = J_g \rho_0 \text{tr } \hat{\mathbf{L}}_g . \quad (4.1)$$

The growth velocity gradient $\hat{\mathbf{L}}_g$ is the product of the evolution of the growth deformation tensor (2.61) and its inverse, see equation (2.15). The evolution of \mathbf{F}_g in time can easily be determined as

$$\dot{\mathbf{F}}_g = \dot{\vartheta} \mathbf{1} + [\dot{\eta} - \dot{\vartheta}] \mathbf{n}^A \otimes \mathbf{n}^A . \quad (4.2)$$

Its inverse

$$\mathbf{F}_g^{-1} = \frac{1}{\vartheta} \mathbf{1} + \left[\frac{1}{\eta} - \frac{1}{\vartheta} \right] \mathbf{n}^A \otimes \mathbf{n}^A \quad (4.3)$$

can be computed by application of the Sherman-Morrison formula, see appendix B.2. Thus, the growth velocity gradient becomes

$$\widehat{\mathbf{L}}_g = \dot{\mathbf{F}}_g \cdot \mathbf{F}_g^{-1} = \frac{\dot{\vartheta}}{\vartheta} \mathbf{1} + \left[\frac{\dot{\eta}}{\eta} - \frac{\dot{\vartheta}}{\vartheta} \right] \mathbf{n}^A \otimes \mathbf{n}^A. \quad (4.4)$$

Its trace is

$$\text{tr } \widehat{\mathbf{L}}_g = 2 \frac{\dot{\vartheta}}{\vartheta} + \frac{\dot{\eta}}{\eta}. \quad (4.5)$$

The determinant of the growth velocity gradient $J_g = \eta \vartheta^2$ can be derived by means of the matrix determinant lemma as described in appendix B.1. Consequently, reformulation of equation (4.1)

$$\mathcal{R}_0 = \eta \vartheta^2 \rho_0 \left[\frac{\dot{\eta}}{\eta} + 2 \frac{\dot{\vartheta}}{\vartheta} \right] \quad (4.6)$$

shows that the mass source and, thus, the evolution of the density is clearly driven by the evolution of the stretch ratios. In LUBARDA & HOGER [93], the evolution of the stretch ratios is assumed to depend on the stretch ratios themselves and the second Piola-Kirchhoff stresses (2.19). As can be read from the reduced dissipation inequality (2.74), the Mandel stresses (2.20) are work conjugated to the growth velocity gradient. Consequently, we prefer a dependence of the evolution of the stretch ratios

$$\dot{\vartheta} = f_\vartheta(\eta, \vartheta, \widehat{M}_i) \quad \text{and} \quad \dot{\eta} = f_\eta(\eta, \vartheta, \widehat{M}_i) \quad (4.7)$$

on the stretch ratios themselves and, via the invariant-type scalars

$$\widehat{M}_{i=1,2,3} = \text{tr}(\widehat{\mathbf{M}}^i) \quad \text{and} \quad \widehat{M}_{i=4,5} = \text{tr}(\widehat{\mathbf{M}}^{i-3} \cdot \mathbf{A}), \quad (4.8)$$

on the Mandel stresses $\widehat{\mathbf{M}}$, see also equation (2.68) and the explanations in MENZEL [99]. Conceptually speaking, $\text{tr } \widehat{\mathbf{M}}$ equals $\text{tr } \boldsymbol{\tau}$, see equation (2.17), which takes the interpretation as a representative scalar of the volumetric stress contribution. In analogy to the representations of LUBARDA & HOGER [93], we adopt a linear dependence of the evolution of the stretch ratios on the components of $\widehat{\mathbf{M}}$

$$\boxed{\dot{\vartheta} := k_\vartheta(\vartheta) \left[\widehat{M}_4 - \nu_\vartheta \left[\widehat{M}_1 - \widehat{M}_4 \right] \right] \quad \text{and} \quad \dot{\eta} := k_\eta(\eta) \left[\widehat{M}_4 - \nu_\eta \left[\widehat{M}_1 - \widehat{M}_4 \right] \right]} \quad (4.9)$$

with the coefficients k_η and k_ϑ preventing unlimited growth, namely

$$\boxed{
 \begin{aligned}
 k_\vartheta(\vartheta) &:= \begin{cases} k_\vartheta^+ \left[\frac{\vartheta^+ - \vartheta}{\vartheta^+ - 1} \right]^{m_\vartheta^+} & \text{for } [1 + \nu_\vartheta] \widehat{M}_4 > \nu_\vartheta \widehat{M}_1, \\ k_\vartheta^- \left[\frac{\vartheta - \vartheta^-}{1 - \vartheta^-} \right]^{m_\vartheta^-} & \text{for } [1 + \nu_\vartheta] \widehat{M}_4 < \nu_\vartheta \widehat{M}_1, \end{cases} \\
 k_\eta(\eta) &:= \begin{cases} k_\eta^+ \left[\frac{\eta^+ - \eta}{\eta^+ - 1} \right]^{m_\eta^+} & \text{for } [1 + \nu_\eta] \widehat{M}_4 > \nu_\eta \widehat{M}_1, \\ k_\eta^- \left[\frac{\eta - \eta^-}{1 - \eta^-} \right]^{m_\eta^-} & \text{for } [1 + \nu_\eta] \widehat{M}_4 < \nu_\eta \widehat{M}_1. \end{cases}
 \end{aligned}
 } \tag{4.10}$$

The parameters $\vartheta^+, \eta^+ > 1$ and $\vartheta^-, \eta^- < 1$ denote the limiting values of the stretch ratios that can be reached by growth and atrophy, respectively. The parameters $k_{\vartheta/\eta}^\pm$, $m_{\vartheta/\eta}^\pm$ and $\nu_{\vartheta/\eta}$ are additional material parameters. Due to the above described assumptions of density preservation, the material free energy per unit mass (2.69)

$$\psi = \frac{1}{\rho_0} \psi_0 = \frac{1}{\rho_0} \psi_0^e(\widehat{\mathbf{C}}, \mathbf{A}) \tag{4.11}$$

is equivalent to the standard format for an elastic free energy function described in terms of the intermediate configuration. Consequently, the second Piola-Kirchhoff stresses in the material configuration (2.72) and in the intermediate configuration (2.73) become

$$\mathbf{S} = 2 \frac{\partial \psi_0^e}{\partial \mathbf{C}} \quad \text{and} \quad \widehat{\mathbf{S}} = 2 \frac{\partial \psi_0^e}{\partial \widehat{\mathbf{C}}}, \tag{4.12}$$

respectively. Again, a formulation depending on the invariants (2.67) and (2.68) is also possible, analogous to that in equations (2.69), (2.76) and (2.75). Since the density in the intermediate configuration $\widehat{\rho}_0$ and the characteristic direction \mathbf{n}^A are constant, the second and third parts in equation (2.74) vanish, and the reduced dissipation inequality abridges for growth to

$$\overline{\rho}_0 \mathcal{D}^{red} = [\widehat{\mathbf{M}} + \psi_0 \mathbf{1}] : \widehat{\mathbf{L}}_g - \theta \overline{\rho}_0 \mathcal{S} \geq 0. \tag{4.13}$$

Solving for the extra entropy term and inserting the growth velocity gradient (4.4) finally yields

$$\mathcal{S} \leq \frac{1}{\theta \overline{\rho}_0} \left[\frac{\dot{\vartheta}}{\vartheta} \widehat{M}_1 + \left[\frac{\dot{\eta}}{\eta} - \frac{\dot{\vartheta}}{\vartheta} \right] \widehat{M}_4 + \left[\frac{\dot{\eta}}{\eta} + 2 \frac{\dot{\vartheta}}{\vartheta} \right] \psi_0 \right]. \tag{4.14}$$

Remark 4.1 (Isotropic growth) As already mentioned in remark 2.2 for isotropic volumetric growth, the stretch ratios are identical in each direction, i.e., $\eta \equiv \vartheta$. Accordingly, the material parameters in equations (4.9) and (4.10) are also identical in each direction, namely $\eta^\pm \equiv \vartheta^\pm$, $k_\eta^\pm \equiv k_\vartheta^\pm$ and $m_\eta^\pm \equiv m_\vartheta^\pm$. Furthermore, to achieve independence in the characteristic direction, we choose $\nu_\eta \equiv \nu_\vartheta \equiv -1$. Hence, for isotropic growth, the evolution of the stretch ratio reduces to

$$\dot{\vartheta} = k_\vartheta(\vartheta) \operatorname{tr} \widehat{\mathbf{M}}, \quad (4.15)$$

with the coefficient

$$k_\vartheta(\vartheta) := \begin{cases} k_\vartheta^+ \left[\frac{\vartheta^+ - \vartheta}{\vartheta^+ - 1} \right]^{m_\vartheta^+} & \text{for } \operatorname{tr} \widehat{\mathbf{M}} > 0 \\ k_\vartheta^- \left[\frac{\vartheta - \vartheta^-}{1 - \vartheta^-} \right]^{m_\vartheta^-} & \text{for } \operatorname{tr} \widehat{\mathbf{M}} < 0 \end{cases} \quad (4.16)$$

differentiating between tension and compression. These assumptions correspond to those of LUBARDA & HOGER [93]. ■

4.3 Implementation

In this section we concentrate on the numerical implementation of the discussed constitutive theory for growth. Analogous to the implementation of remodeling in section 3.3, we apply standard finite element techniques based on an internal variable formulation for the stretch ratios. Again, the implementation is split in two parts: the update of the internal variables and the computation of the incremental tangent modulus.

4.3.1 Incremental update of the stretch ratios

For a more concise description, in the following the stretch ratios and modifications of them are combined in vectors

$$\boldsymbol{\vartheta} = \begin{bmatrix} \vartheta \\ \eta \end{bmatrix}, \quad \dot{\boldsymbol{\vartheta}} = \begin{bmatrix} \dot{\vartheta} \\ \dot{\eta} \end{bmatrix}, \quad \Delta \boldsymbol{\vartheta} = \begin{bmatrix} \Delta \vartheta \\ \Delta \eta \end{bmatrix}, \quad \mathbf{r}_\vartheta = \begin{bmatrix} r_\vartheta \\ r_\eta \end{bmatrix}. \quad (4.17)$$

In this, r_ϑ and r_η are residuals in an Euler backward scheme as described later. Consequently, the evolution of the stretch ratios (4.9) can be rewritten as

$$\dot{\boldsymbol{\vartheta}} = \begin{bmatrix} k_\vartheta(\vartheta) \left[\widehat{M}_4 - \nu_\vartheta \left[\widehat{M}_1 - \widehat{M}_4 \right] \right] \\ k_\eta(\eta) \left[\widehat{M}_4 - \nu_\eta \left[\widehat{M}_1 - \widehat{M}_4 \right] \right] \end{bmatrix} \quad (4.18)$$

with the coefficients k_ϑ and k_η as depicted in equation (4.10) and the invariant-type scalars comprising the dependence on the Mandel stresses (4.8). Analogous to the implementation of remodeling, we use an implicit Euler backward scheme to compute the internal variable at the spatial time step

$$\vartheta_{n+1} = \vartheta_n + \dot{\vartheta}_{n+1} \Delta t, \quad (4.19)$$

with the index n for the time increment. The residual

$$\mathbf{r}_\vartheta = -\vartheta_{n+1} + \vartheta_n + \dot{\vartheta}_{n+1} \Delta t = \mathbf{0} \quad (4.20)$$

has to vanish in the solution point. To solve this equation by means of a Newton method, we reformulate it in terms of Taylor series at ϑ

$$\mathbf{r}_\vartheta^{k+1} = \mathbf{r}_\vartheta + \frac{\partial \mathbf{r}_\vartheta}{\partial \vartheta} \cdot \Delta \vartheta = \mathbf{0} \quad (4.21)$$

and solve it for the increment

$$\Delta \vartheta = - \left[\frac{\partial \mathbf{r}_\vartheta}{\partial \vartheta} \right]^{-1} \cdot \mathbf{r}_\vartheta. \quad (4.22)$$

In this, for the sake of readability, we already neglected the indices $n+1$ and k , compare with equations (3.11) and (3.12). The Jacobian matrix of the residual vector $\mathbf{r}_\vartheta(\vartheta)$ is

$$\frac{\partial \mathbf{r}_\vartheta}{\partial \vartheta} = \begin{bmatrix} \frac{\partial r_\vartheta}{\partial \vartheta} & \frac{\partial r_\vartheta}{\partial \eta} \\ \frac{\partial r_\eta}{\partial \vartheta} & \frac{\partial r_\eta}{\partial \eta} \end{bmatrix} = \begin{bmatrix} -1 + \frac{\partial \dot{\vartheta}}{\partial \vartheta} \Delta t & \frac{\partial \dot{\vartheta}}{\partial \eta} \Delta t \\ \frac{\partial \dot{\eta}}{\partial \vartheta} \Delta t & -1 + \frac{\partial \dot{\eta}}{\partial \eta} \Delta t \end{bmatrix}, \quad (4.23)$$

with the derivatives of the evolution of the stretch ratios with respect to the stretch ratios themselves

$$\begin{aligned} \frac{\partial \dot{\vartheta}}{\partial \vartheta} &= k_\vartheta \left[\frac{\partial \widehat{M}_4}{\partial \vartheta} - \nu_\vartheta \left[\frac{\partial \widehat{M}_1}{\partial \vartheta} - \frac{\partial \widehat{M}_4}{\partial \vartheta} \right] \right] + \frac{\partial k_\vartheta}{\partial \vartheta} \left[\widehat{M}_4 - \nu_\vartheta \left[\widehat{M}_1 - \widehat{M}_4 \right] \right], \\ \frac{\partial \dot{\eta}}{\partial \eta} &= k_\eta \left[\frac{\partial \widehat{M}_4}{\partial \eta} - \nu_\eta \left[\frac{\partial \widehat{M}_1}{\partial \eta} - \frac{\partial \widehat{M}_4}{\partial \eta} \right] \right] + \frac{\partial k_\eta}{\partial \eta} \left[\widehat{M}_4 - \nu_\eta \left[\widehat{M}_1 - \widehat{M}_4 \right] \right], \\ \frac{\partial \dot{\vartheta}}{\partial \eta} &= k_\vartheta \left[\frac{\partial \widehat{M}_4}{\partial \eta} - \nu_\vartheta \left[\frac{\partial \widehat{M}_1}{\partial \eta} - \frac{\partial \widehat{M}_4}{\partial \eta} \right] \right], \\ \frac{\partial \dot{\eta}}{\partial \vartheta} &= k_\eta \left[\frac{\partial \widehat{M}_4}{\partial \vartheta} - \nu_\eta \left[\frac{\partial \widehat{M}_1}{\partial \vartheta} - \frac{\partial \widehat{M}_4}{\partial \vartheta} \right] \right], \end{aligned} \quad (4.24)$$

resulting directly from equation (4.18). In this, the partial derivatives of $\widehat{M}_1 = \text{tr } \widehat{\mathbf{M}}$ and $\widehat{M}_4 = \text{tr}(\widehat{\mathbf{M}} \cdot \mathbf{A})$ with respect to the stretch ratios are

$$\begin{aligned}
\frac{\partial \widehat{M}_1}{\partial \vartheta} &= \frac{1}{\vartheta} \left[-2\widehat{M}_1 + 2\widehat{M}_4 - \widehat{\mathbf{C}} : \widehat{\mathbf{C}}^e : [\widehat{\mathbf{C}} - \widehat{\mathbf{C}} \cdot \mathbf{A}] \right] , \\
\frac{\partial \widehat{M}_4}{\partial \vartheta} &= \frac{1}{\vartheta} \left[-\widehat{M}_4 + \widehat{I}_4 \widehat{S}_4 - [\widehat{\mathbf{C}} \cdot \mathbf{A}] : \widehat{\mathbf{C}}^e : [\widehat{\mathbf{C}} - \widehat{\mathbf{C}} \cdot \mathbf{A}] \right] , \\
\frac{\partial \widehat{M}_1}{\partial \eta} &= \frac{1}{\eta} \left[-2\widehat{M}_4 - \widehat{\mathbf{C}} : \widehat{\mathbf{C}}^e : [\widehat{\mathbf{C}} \cdot \mathbf{A}] \right] , \\
\frac{\partial \widehat{M}_4}{\partial \eta} &= \frac{1}{\eta} \left[-\widehat{M}_4 - \widehat{I}_4 \widehat{S}_4 - [\widehat{\mathbf{C}} \cdot \mathbf{A}] : \widehat{\mathbf{C}}^e : [\widehat{\mathbf{C}} \cdot \mathbf{A}] \right] ,
\end{aligned} \tag{4.25}$$

with the invariant-type scalars as described in equations (2.68) and (4.8) and, analogously,

$$\widehat{S}_4 = \text{tr}(\widehat{\mathbf{S}} \cdot \mathbf{A}). \tag{4.26}$$

The elastic tangent modulus in the intermediate configuration is defined as

$$\widehat{\mathbf{C}}^e := 4 \frac{\partial^2 \psi_0^e}{\partial \widehat{\mathbf{C}}^2} = 2 \frac{\partial \widehat{\mathbf{S}}}{\partial \widehat{\mathbf{C}}}. \tag{4.27}$$

Recall from equation (4.10) that we distinguished between stress ratios that are parallel and those that are orthogonal to the characteristic direction. Correspondingly, concerning the derivatives of the coefficients k_ϑ and k_η with respect to the stretch ratios

$$\begin{aligned}
\frac{\partial k_\vartheta}{\partial \vartheta} &:= \begin{cases} \frac{m_\vartheta^+}{\vartheta - \vartheta^+} k_\vartheta(\vartheta) & \text{for } [1 + \nu_\vartheta] \widehat{M}_4 > \nu_\vartheta \widehat{M}_1 , \\ \frac{m_\vartheta^-}{\vartheta - \vartheta^-} k_\vartheta(\vartheta) & \text{for } [1 + \nu_\vartheta] \widehat{M}_4 < \nu_\vartheta \widehat{M}_1 , \end{cases} \\
\frac{\partial k_\eta}{\partial \eta} &:= \begin{cases} \frac{m_\eta^+}{\eta - \eta^+} k_\eta(\eta) & \text{for } [1 + \nu_\eta] \widehat{M}_4 > \nu_\eta \widehat{M}_1 , \\ \frac{m_\eta^-}{\eta - \eta^-} k_\eta(\eta) & \text{for } [1 + \nu_\eta] \widehat{M}_4 < \nu_\eta \widehat{M}_1 , \end{cases}
\end{aligned} \tag{4.28}$$

we distinguish between different stretch ratios, too. Combining equations (4.22) to (4.28), we finally get the algorithmic update for the stretch ratios

$$\vartheta^{k+1} = \vartheta^k + \Delta \vartheta , \tag{4.29}$$

analogous to that for the density in case of remodeling (3.15).

4.3.2 Incremental tangent modulus

Since the material model is formulated with respect to the intermediate configuration, the corresponding tangent modulus is considered in terms of stresses and strains in the intermediate configuration, i.e., the second Piola-Kirchhoff stresses $\widehat{\mathbf{S}}$ and the elastic Cauchy-Green tensor $\widehat{\mathbf{C}}$. By application of the chain rule we obtain the incremental elastic-growth tangent modulus in the intermediate configuration at the spatial time step

$$\widehat{\mathbf{C}} = 2 \frac{\partial \widehat{\mathbf{S}}}{\partial \widehat{\mathbf{C}}} + 2 \frac{\partial \widehat{\mathbf{S}}}{\partial \vartheta} \cdot \frac{\partial \vartheta}{\partial \widehat{\mathbf{C}}}. \quad (4.30)$$

The partial derivative of the stresses with respect to the strains is already defined in equation (4.27) as the elastic tangent modulus in the intermediate configuration. Analogous to remodeling (3.19), it can alternatively be represented depending on the invariants

$$\widehat{\mathbf{C}}^e = 4 \sum_{i=1}^5 \left[\sum_{j=1}^5 \left[\frac{\partial^2 \psi_0^e}{\partial \widehat{I}_i \partial \widehat{I}_j} \frac{\partial \widehat{I}_i}{\partial \widehat{\mathbf{C}}} \otimes \frac{\partial \widehat{I}_j}{\partial \widehat{\mathbf{C}}} \right] + \frac{\partial \psi_0^e}{\partial \widehat{I}_i} \frac{\partial^2 \widehat{I}_i}{\partial \widehat{\mathbf{C}} \partial \widehat{\mathbf{C}}} \right]. \quad (4.31)$$

In order to determine the second part of equation (4.30), we apply the chain rule

$$2 \frac{\partial \widehat{\mathbf{S}}}{\partial \vartheta} = 2 \frac{\partial \widehat{\mathbf{S}}}{\partial \widehat{\mathbf{C}}} : \frac{\partial \widehat{\mathbf{C}}}{\partial \mathbf{F}_g} : \frac{\partial \mathbf{F}_g}{\partial \vartheta}. \quad (4.32)$$

In this equation, the first derivative on the right side is the elastic tangent modulus (4.27). From equations (2.63) and (2.61), the remaining two derivatives can be determined as

$$\begin{aligned} \frac{\partial \widehat{\mathbf{C}}}{\partial \mathbf{F}_g} &= -\frac{1}{2} \left[\widehat{\mathbf{C}} \otimes \mathbf{F}_g^{-1} + \widehat{\mathbf{C}} \underline{\otimes} \mathbf{F}_g^{-1} + \mathbf{F}_g^{-1} \overline{\otimes} \widehat{\mathbf{C}} + \mathbf{F}_g^{-1} \underline{\otimes} \widehat{\mathbf{C}} \right], \\ \frac{\partial \mathbf{F}_g}{\partial \vartheta} &= \mathbf{1} - \mathbf{n}^A \otimes \mathbf{n}^A \quad \text{and} \quad \frac{\partial \mathbf{F}_g}{\partial \eta} = \mathbf{n}^A \otimes \mathbf{n}^A, \end{aligned} \quad (4.33)$$

with the definition of the varied dyadic products as defined in appendix A. Summarizing, with the benefit of the minor symmetry of the elastic tangent modulus, see e.g. HOLZAPFEL [55], the derivatives of the stresses with respect to the stretch ratios are

$$2 \frac{\partial \widehat{\mathbf{S}}}{\partial \vartheta} = -\frac{2}{\vartheta} \widehat{\mathbf{C}}^e : \left[\widehat{\mathbf{C}} - \widehat{\mathbf{C}} \cdot \mathbf{A} \right] \quad \text{and} \quad 2 \frac{\partial \widehat{\mathbf{S}}}{\partial \eta} = -\frac{2}{\eta} \widehat{\mathbf{C}}^e : \left[\widehat{\mathbf{C}} \cdot \mathbf{A} \right]. \quad (4.34)$$

Computing the third part of equation (4.30) is not straightforward because the actual stretch ratios are unknown. Rather, only their evolution is known, and analogous to the expressions in section 3.3.2, we differentiate the residual of ϑ in an Euler backward

scheme (4.20) with respect to the Cauchy-Green tensor $\widehat{\mathbf{C}}$

$$\frac{\partial \mathbf{r}_\vartheta}{\partial \widehat{\mathbf{C}}} = -\frac{\partial \vartheta}{\partial \widehat{\mathbf{C}}} + \left[\frac{\partial \dot{\vartheta}}{\partial \widehat{\mathbf{C}}} + \frac{\partial \dot{\vartheta}}{\partial \vartheta} \cdot \frac{\partial \vartheta}{\partial \widehat{\mathbf{C}}} \right] \Delta t = \mathbf{0}. \quad (4.35)$$

Solving this equation for the derivative in demand yields

$$\frac{\partial \vartheta}{\partial \widehat{\mathbf{C}}} = - \left[-\mathbf{1} + \frac{\partial \dot{\vartheta}}{\partial \vartheta} \Delta t \right]^{-1} \cdot \frac{\partial \dot{\vartheta}}{\partial \widehat{\mathbf{C}}} \Delta t = - \left[\frac{\partial \mathbf{r}_\vartheta}{\partial \vartheta} \right]^{-1} \cdot \frac{\partial \dot{\vartheta}}{\partial \widehat{\mathbf{C}}} \Delta t \quad (4.36)$$

with the Jacobian matrix of \mathbf{r}_ϑ and the corresponding derivatives as depicted in equations (4.23) to (4.28). The derivative of $\dot{\vartheta}$ with respect to $\widehat{\mathbf{C}}$ in (4.36) can directly be determined as

$$\begin{aligned} \frac{\partial \dot{\vartheta}}{\partial \widehat{\mathbf{C}}} &= k_\vartheta(\vartheta) \left[\frac{\partial \widehat{M}_4}{\partial \widehat{\mathbf{C}}} - \nu_\vartheta \left[\frac{\partial \widehat{M}_1}{\partial \widehat{\mathbf{C}}} - \frac{\partial \widehat{M}_4}{\partial \widehat{\mathbf{C}}} \right] \right], \\ \frac{\partial \dot{\eta}}{\partial \widehat{\mathbf{C}}} &= k_\eta(\eta) \left[\frac{\partial \widehat{M}_4}{\partial \widehat{\mathbf{C}}} - \nu_\eta \left[\frac{\partial \widehat{M}_1}{\partial \widehat{\mathbf{C}}} - \frac{\partial \widehat{M}_4}{\partial \widehat{\mathbf{C}}} \right] \right], \end{aligned} \quad (4.37)$$

with

$$\frac{\partial \widehat{M}_1}{\partial \widehat{\mathbf{C}}} = \widehat{\mathbf{S}} + \frac{1}{2} \widehat{\mathbf{C}} : \widehat{\mathbf{C}}^e \quad \text{and} \quad \frac{\partial \widehat{M}_4}{\partial \widehat{\mathbf{C}}} = \left[\widehat{\mathbf{S}} \cdot \mathbf{A} \right]^{sym} + \frac{1}{2} \left[\widehat{\mathbf{C}} \cdot \mathbf{A} \right] : \widehat{\mathbf{C}}^e. \quad (4.38)$$

Summarizing, the asymmetric tangent modulus reads

$$\widehat{\mathbf{C}} = \widehat{\mathbf{C}}^e - \widehat{\mathbf{C}}^e : \frac{\partial \widehat{\mathbf{C}}}{\partial \vartheta} \cdot \left[\frac{\partial \mathbf{r}_\vartheta}{\partial \vartheta} \right]^{-1} \cdot \frac{\partial \dot{\vartheta}}{\partial \widehat{\mathbf{C}}} \Delta t. \quad (4.39)$$

A summary of the complete algorithm within the implementation of growth into a finite element program is depicted in table 4.1.

4.4 Numerical examples

For the elaboration of the material behavior, we choose a free energy density of Neo-Hooke type

$$\psi_0 = \psi_0^{iso} + \psi_0^{ti} \quad \text{with} \quad \begin{cases} \psi_0^{iso} &= \frac{\lambda}{2} \ln^2 J + \frac{\mu}{2} \left[\widehat{I}_1 - 3 - 2 \ln J \right] \\ \psi_0^{ti} &= \frac{\alpha}{2} \left[\widehat{I}_4 - 1 \right]^2 \end{cases} \quad (4.40)$$

depending on the invariants $\widehat{I}_1 = \text{tr} \widehat{\mathbf{C}}$, $J = \det \widehat{\mathbf{C}} = \frac{1}{6} \widehat{I}_1^3 - \frac{1}{2} \widehat{I}_1 \widehat{I}_2 + \frac{1}{3} \widehat{I}_3$ and $\widehat{I}_4 = \text{tr}(\widehat{\mathbf{C}} \cdot \mathbf{A})$. The mass source in case of growth is clearly described by the stretch ratios and their

history data: internal variables ϑ ; η

1. set initial values

$$\vartheta = \vartheta_n; \quad \eta = \eta_n; \quad \mathbf{F}_e = \mathbf{F} \cdot \mathbf{F}_g^{-1} = \frac{1}{\vartheta} \mathbf{F} + \left[\frac{1}{\eta} - \frac{1}{\vartheta} \right] \mathbf{F} \cdot \mathbf{A}; \quad \widehat{\mathbf{C}} = \mathbf{F}_e^t \cdot \mathbf{F}_e;$$

$$\widehat{\mathbf{S}} = \frac{\partial \psi_0^e}{\partial \widehat{\mathbf{C}}}; \quad \widehat{\mathbf{M}} = \widehat{\mathbf{C}} \cdot \widehat{\mathbf{S}}; \quad \widehat{M}_1 = \text{tr} \widehat{\mathbf{M}}; \quad \widehat{M}_4 = \text{tr}(\widehat{\mathbf{M}} \cdot \mathbf{A})$$

2. check loading

IF $[1 + \nu_\vartheta] \widehat{M}_4 > \nu_\vartheta \widehat{M}_1$ THEN

IF $[1 + \nu_\eta] \widehat{M}_4 > \nu_\eta \widehat{M}_1$ THEN

$$\text{apply } k_\vartheta(\vartheta) = k_\vartheta^+ \left[\frac{\vartheta^+ - \vartheta}{\vartheta^+ - 1} \right]^{m_\vartheta^+}; \quad \frac{\partial k_\vartheta}{\partial \vartheta} = \frac{m_\vartheta^+}{\vartheta - \vartheta^+} k_\vartheta(\vartheta)$$

$$k_\eta(\eta) = k_\eta^+ \left[\frac{\eta^+ - \eta}{\eta^+ - 1} \right]^{m_\eta^+}; \quad \frac{\partial k_\eta}{\partial \eta} = \frac{m_\eta^+}{\eta - \eta^+} k_\eta(\eta)$$

ELSE

$$\text{apply } k_\vartheta(\vartheta) = k_\vartheta^+ \left[\frac{\vartheta^+ - \vartheta}{\vartheta^+ - 1} \right]^{m_\vartheta^+}; \quad \frac{\partial k_\vartheta}{\partial \vartheta} = \frac{m_\vartheta^+}{\vartheta - \vartheta^+} k_\vartheta(\vartheta)$$

$$k_\eta(\eta) = k_\eta^- \left[\frac{\eta - \eta^-}{1 - \eta^-} \right]^{m_\eta^-}; \quad \frac{\partial k_\eta}{\partial \eta} = \frac{m_\eta^-}{\eta - \eta^-} k_\eta(\eta)$$

ENDIF

ELSE

IF $[1 + \nu_\eta] \widehat{M}_4 > \nu_\eta \widehat{M}_1$ THEN

$$\text{apply } k_\vartheta(\vartheta) = k_\vartheta^+ \left[\frac{\vartheta - \vartheta^-}{1 - \vartheta^-} \right]^{m_\vartheta^-}; \quad \frac{\partial k_\vartheta}{\partial \vartheta} = \frac{m_\vartheta^-}{\vartheta - \vartheta^-} k_\vartheta(\vartheta)$$

$$k_\eta(\eta) = k_\eta^+ \left[\frac{\eta^+ - \eta}{\eta^+ - 1} \right]^{m_\eta^+}; \quad \frac{\partial k_\eta}{\partial \eta} = \frac{m_\eta^+}{\eta - \eta^+} k_\eta(\eta)$$

ELSEIF $[1 + \nu_\eta] \widehat{M}_4 < \nu_\eta \widehat{M}_1$ THEN

$$\text{apply } k_\vartheta(\vartheta) = k_\vartheta^+ \left[\frac{\vartheta - \vartheta^-}{1 - \vartheta^-} \right]^{m_\vartheta^-}; \quad \frac{\partial k_\vartheta}{\partial \vartheta} = \frac{m_\vartheta^-}{\vartheta - \vartheta^-} k_\vartheta(\vartheta)$$

$$k_\eta(\eta) = k_\eta^- \left[\frac{\eta - \eta^-}{1 - \eta^-} \right]^{m_\eta^-}; \quad \frac{\partial k_\eta}{\partial \eta} = \frac{m_\eta^-}{\eta - \eta^-} k_\eta(\eta)$$

ELSE

$$\widehat{\mathbf{C}} = \widehat{\mathbf{C}}^e \quad \text{EXIT}$$

ENDIF

ENDIF

Table 4.1: Algorithmic update scheme for growth (part 1)

<p>3. local Newton iteration</p> <p>a. compute residual</p> $\mathbf{r}_\vartheta = -\vartheta + \vartheta_n + \dot{\vartheta} \Delta t$ <p>b. compute incremental update</p> $\Delta\vartheta = - \left[\frac{\partial \mathbf{r}_\vartheta}{\partial \vartheta} \right]^{-1} \cdot \mathbf{r}_\vartheta \quad \text{with} \quad \frac{\partial \mathbf{r}_\vartheta}{\partial \vartheta} = \begin{bmatrix} -1 + \frac{\partial \dot{\vartheta}}{\partial \vartheta} \Delta t & \frac{\partial \dot{\vartheta}}{\partial \eta} \Delta t \\ \frac{\partial \dot{\eta}}{\partial \vartheta} \Delta t & -1 + \frac{\partial \dot{\eta}}{\partial \eta} \Delta t \end{bmatrix}$ <p>c. update</p> $\vartheta \leftarrow \vartheta + \Delta\vartheta$ $\mathbf{F}_e = \frac{1}{\vartheta} \mathbf{F} + [\eta - \vartheta] \mathbf{F} \cdot \mathbf{A}; \quad \widehat{\mathbf{C}} = \mathbf{F}_e^t \cdot \mathbf{F}_e;$ $\widehat{\mathbf{S}} = \frac{\partial \psi_0^e}{\partial \widehat{\mathbf{C}}}; \quad \widehat{\mathbf{M}} = \widehat{\mathbf{C}} \cdot \widehat{\mathbf{S}}; \quad \widehat{M}_1 = \text{tr} \widehat{\mathbf{M}}; \quad \widehat{M}_4 = \text{tr}(\widehat{\mathbf{M}} \cdot \mathbf{A})$ <p>d. check tolerance</p> <p>IF $\ \mathbf{r}_\vartheta\ < \text{tol}$ GOTO 4</p> <p>ELSE GOTO 3.a</p> <p>4. compute moduli and density</p> $\widehat{\mathbf{C}} = \widehat{\mathbf{C}}^e - \widehat{\mathbf{C}}^e : \frac{\partial \widehat{\mathbf{C}}}{\partial \vartheta} \cdot \left[\frac{\partial \mathbf{r}_\vartheta}{\partial \vartheta} \right]^{-1} \cdot \frac{\partial \vartheta}{\partial \widehat{\mathbf{C}}} \Delta t$ $\bar{\rho}_0 = \eta \vartheta^2 \rho_0$

Table 4.1: Algorithmic update scheme for growth (part 2)

evolution, see equation (4.6). The initial stretch ratios are $\vartheta|_{t=0} = \eta|_{t=0} = 1.0$ for all computations.

4.4.1 Simple tension

At first, we consider the behavior of the material model at a stepwise increasing elongation of an isotropic cube as depicted in figures 4.1 and 4.2.a. Naturally, the material parameters for soft tissues are as difficult to measure as those for hard tissues, see section 3.4.1. To get a first sense of the material model, we choose the elastic parameters $E = 1\text{N/mm}^2$ and $\nu = 0.3$, corresponding to $\lambda = 0.577\text{N/mm}^2$ and $\mu = 0.385\text{N/mm}^2$. The initial density is $\rho_0 = 1\text{g/cm}^3$. In order to describe isotropy, see remark 4.1, the material parameters are identical in each direction and $\nu_\eta \equiv \nu_\vartheta \equiv -1$. Further on,

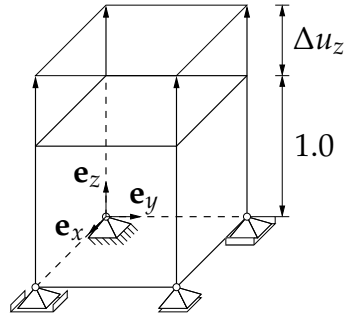


Figure 4.1: Loads and boundary conditions in the simple tension test.

the anisotropy parameter in equation (4.40) must be $\alpha = 0$. Unless otherwise stated, the limiting values of the stretch ratio are $\vartheta^+ = 1.3$ for growth and $\vartheta^- = 0.7$ for atrophy, and the remaining material parameters in equation (4.10) or alternatively equation (4.16) are $k_\vartheta^+ = 1.0$, $k_\vartheta^- = 1.0$, $m_\vartheta^+ = 2.0$ and $m_\vartheta^- = 2.0$. For the time step we choose $\Delta t = 1.0$. As one can see in figure 4.2.b, the stretch ratio ϑ increases at every elongation step until the limiting value ϑ^+ is reached. For $\vartheta = \vartheta^+$, the evolution of the stretch ratio stops, i.e., $\dot{\vartheta} = 0$, see equations (4.9) and (4.10) or alternatively equations (4.15) and (4.16). Moreover, although the stretch is applied at once, the stretch ratio does

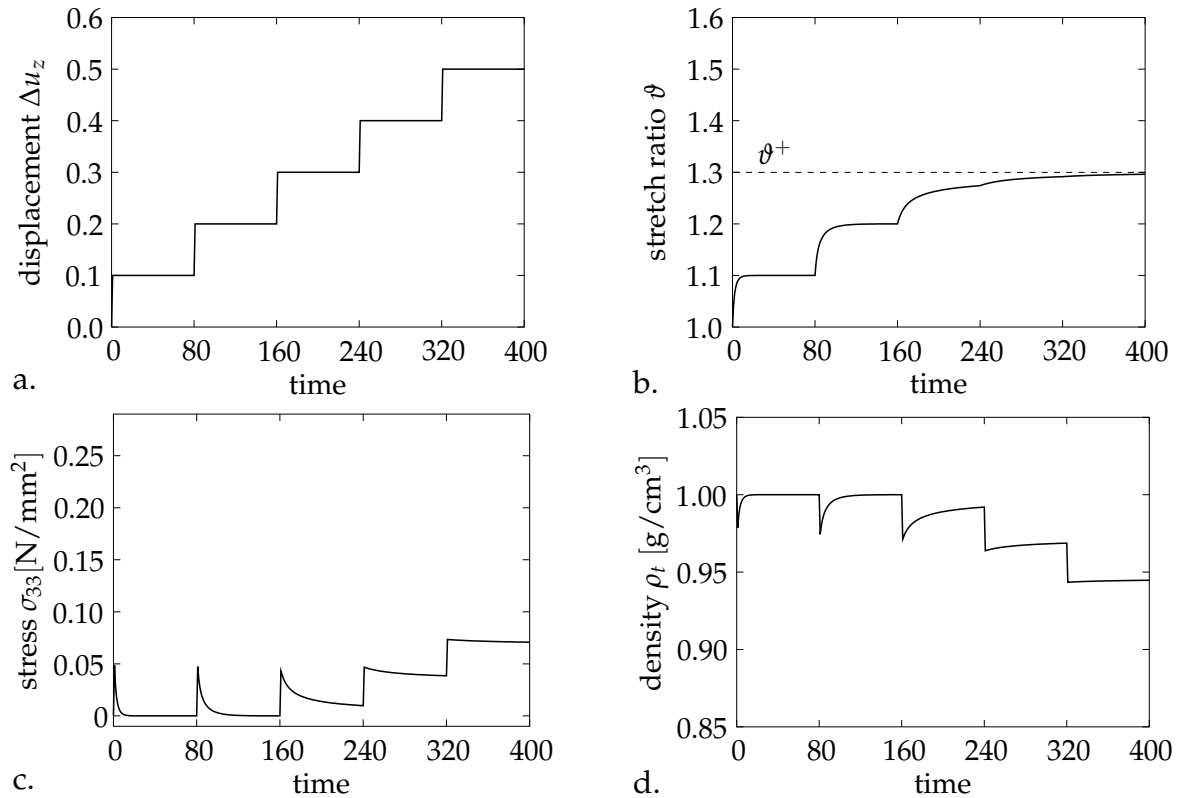


Figure 4.2: Isotropic simple tension test on a growing cube. (a) An incrementally increasing stretch is applied. (b) The stretch ratio converges time-dependently to the biological equilibrium. (c) The stresses vanish in the biological equilibrium state as long as $\vartheta < \vartheta^+$. (d) The density in the biological equilibrium state does not change as long as $\vartheta < \vartheta^+$.

not increase outright; rather, it converges progressively and time-dependently to the biological equilibrium. Analogous to remodeling, the biological equilibrium is defined as the state where the stretch ratio remains constant, and thus, neither the density nor the stresses in the considered specimen change unless an additional load is applied. As we can identify from equations (4.15) and (4.16), the trace of the Mandel stresses must vanish in the biological equilibrium state until the limiting stretch ratio is not reached, viz, $\vartheta \neq \vartheta^+$. This effect can be observed in figure 4.2.c, which displays the evolution of the normal stresses in the stretch direction. Due to the boundary conditions, the normal stresses in the other directions are zero. With equation (2.32)₂ and the determinant for isotropic growth $J_g = \vartheta^3$, the spatial density becomes $\rho_t = J^{-1}\vartheta^3\rho_0$. Its evolution is depicted in figure 4.2.d. Obviously, as long as the limiting value of the stretch ratio is not reached, the density relaxes to its initial value. Variation of the lim-

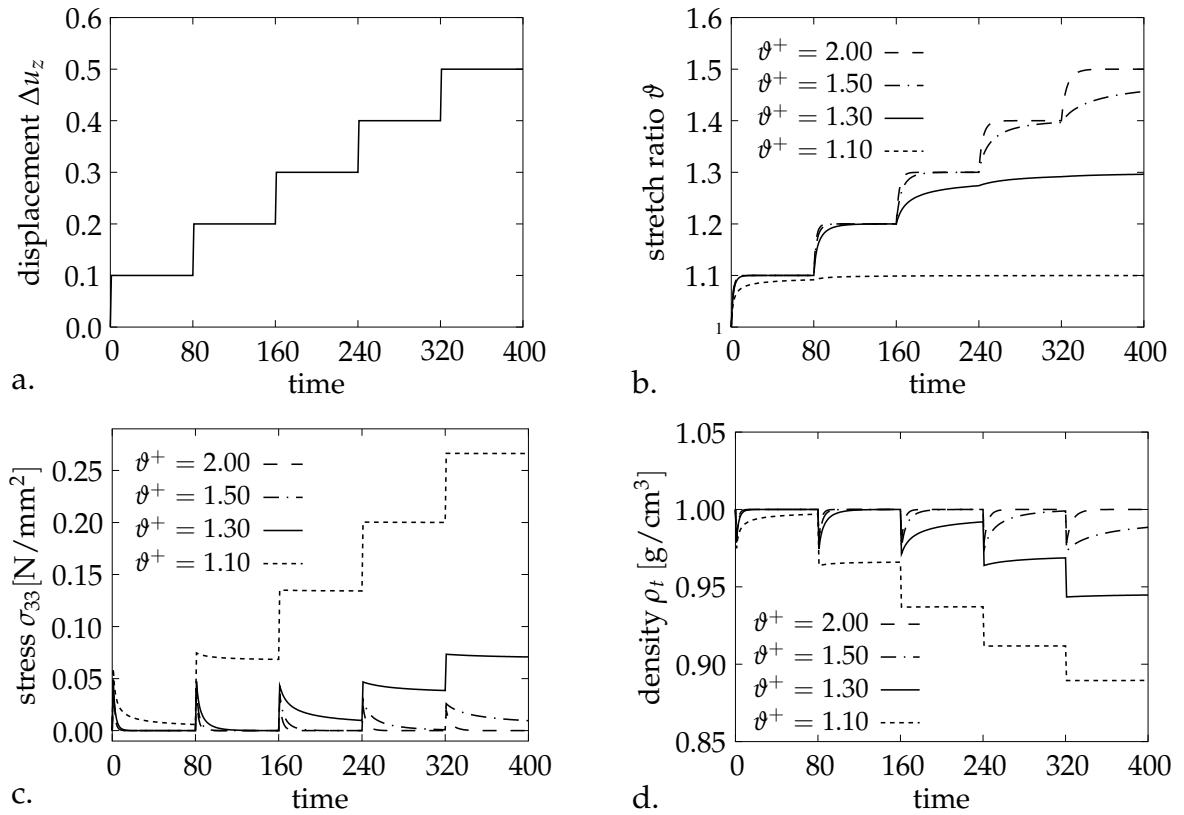


Figure 4.3: Variation of the limiting stretch ratio ϑ^+ in the simple tension test. The stretch ratio increases until the limiting value is reached. If the limiting value of the stretch ratio is reached the material behavior is purely elastic.

iting stretch ratio ϑ^+ , see figure 4.3, underlines the fact that this parameter limits the effect of growth. Practically speaking, as long as the material can grow, i.e., $\vartheta < \vartheta^+$, the overall stretch in the biological equilibrium is completely compensated by growth. Consequently, the density relaxes to the initial density and the stresses in the biological equilibrium are zero. Once the limit of growth is reached, i.e., $\vartheta = \vartheta^+$, the stretch can no longer be compensated by growth but is a purely elastic deformation. Hence, the stresses are no longer equal to zero and the density changes. In figure 4.4 the sensi-

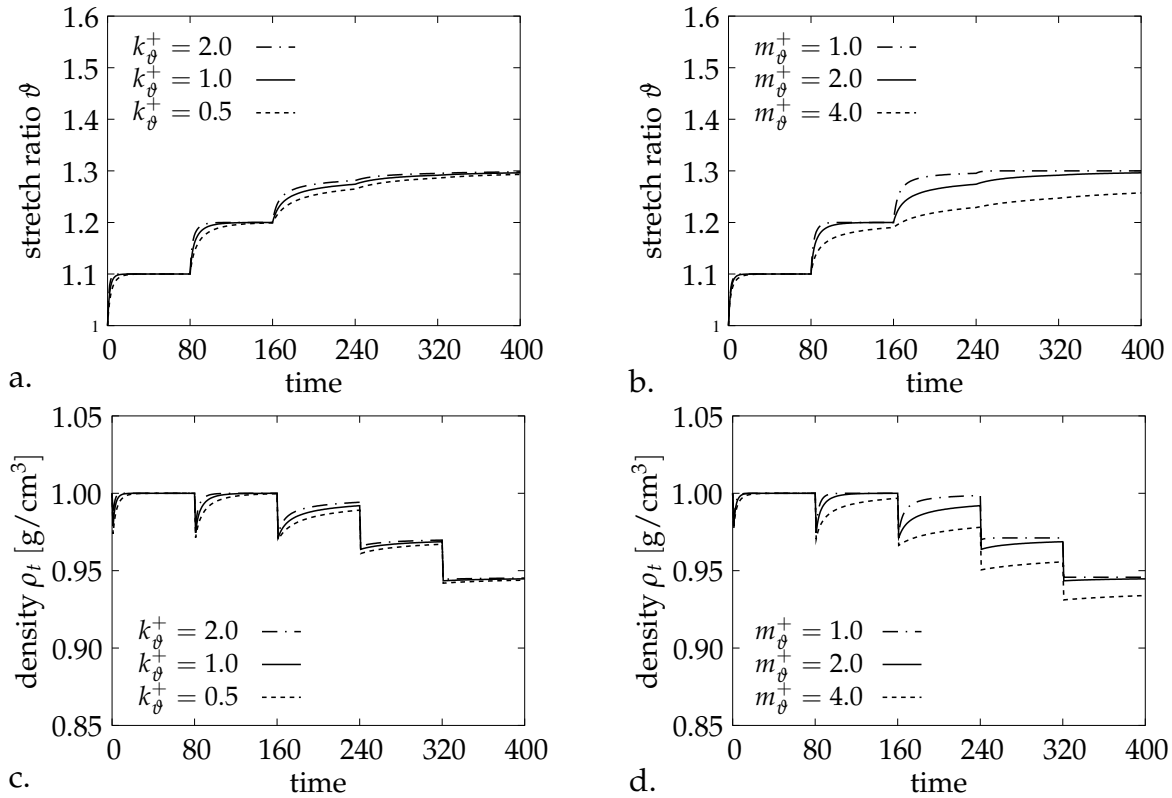


Figure 4.4: Variation of the material parameters k_ϕ^+ and m_ϕ^+ in the simple tension test. They influence the relaxation time, but not the final state at biological equilibrium.

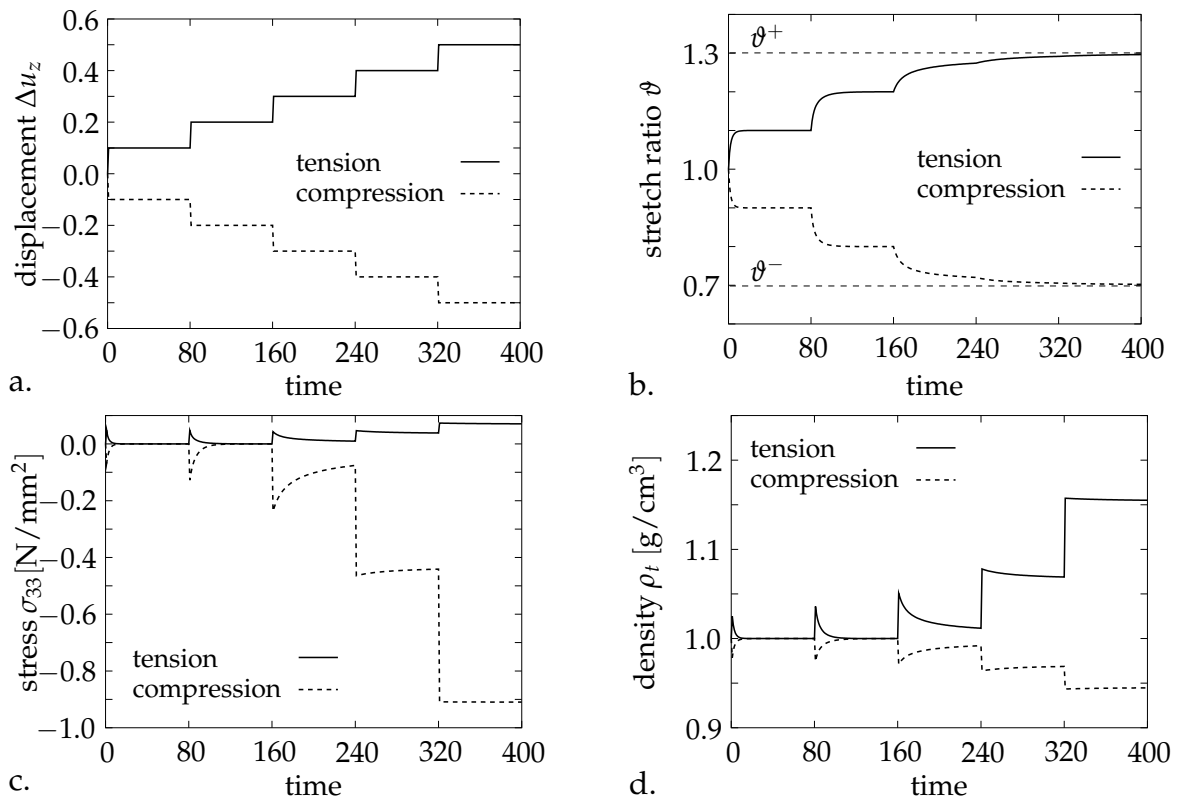


Figure 4.5: The material distinguishes between tension and compression. In case of tension the material grows, and in case of compression the material decreases.

tivity of the material behavior with respect to the material parameters k_{ϑ}^+ and m_{ϑ}^+ is illustrated. Obviously, a variation of these parameters influences the relaxation time but not the final state at biological equilibrium. For higher values of k_{ϑ}^{\pm} , the evolution of the stretch ratio in equations (4.15) and (4.16) increases. Since $(\vartheta^+ - \vartheta)/(\vartheta^+ - 1)$ and $(\vartheta - \vartheta^-)/(1 - \vartheta^-)$ are always smaller than one, the evolution of the stretch ratio increases for smaller values of m_{ϑ}^{\pm} . Hence, the attainment of biological equilibrium is more rapid for high values of k_{ϑ}^{\pm} and small values of m_{ϑ}^{\pm} .

Next, we compare the material behavior for tension and compression. The applied loading and the results are depicted in figure 4.5. In contrast to the model considered for remodeling, in this growth-model we distinguish between tension and compression. Consequently, for compression the material atrophies depending on the parameters ϑ^- , k_{ϑ}^- and m_{ϑ}^- . Analogous to growth, atrophy does not occur instantaneously, but relaxes time-dependently to the biological equilibrium.

4.4.2 Three-dimensional cylindrical tube

In this section, the material model is applied to a cylindrical tube, analogous to section 3.4.3. Again, we start with a homogeneous deformation in terms of a constant axial elongation of the tube to one and a half times the initial length, see figure 4.6. For com-

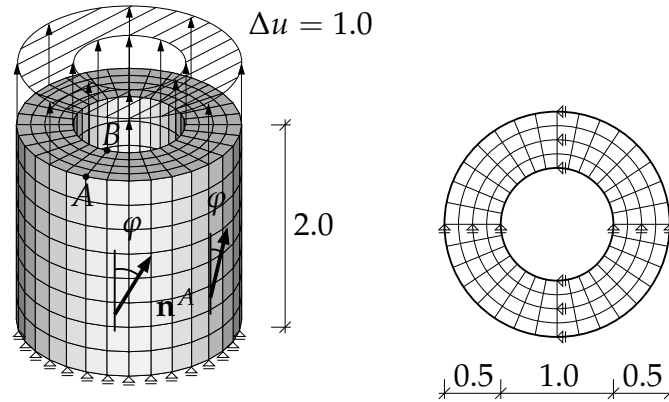


Figure 4.6: Loads and boundary conditions for the homogeneously deformed tube.

parison with remodeling, we first consider isotropic material behavior with the elastic material parameters $E = 3\text{N/mm}^2$ and $\nu = 0.45$, corresponding to $\lambda = 9.310\text{N/mm}^2$ and $\mu = 1.034\text{N/mm}^2$. The initial material density is $\rho_0 = 1.0\text{g/cm}^3$, and the material parameters describing growth are $\vartheta^+ = 1.3$, $\vartheta^- = 0.7$, $k_{\vartheta}^+ = k_{\vartheta}^- = 0.01$ and $m_{\vartheta}^+ = m_{\vartheta}^- = 2.0$. Again, to describe isotropy, the material parameters are identical in each direction, the parameter determining the stress ratio in the biological equilibrium is $\nu_{\vartheta} \equiv \nu_{\gamma} \equiv -1$, and the elastic anisotropy parameter is $\alpha = 0$, see remark 4.1. The time iteration has been executed with time steps $\Delta t = 0.1$. The deformation of the tube and the evolution of the stretch ratio are depicted in figure 4.7. In the first loading step, the cross section of the tube decreases due to the classical Poisson effect. The

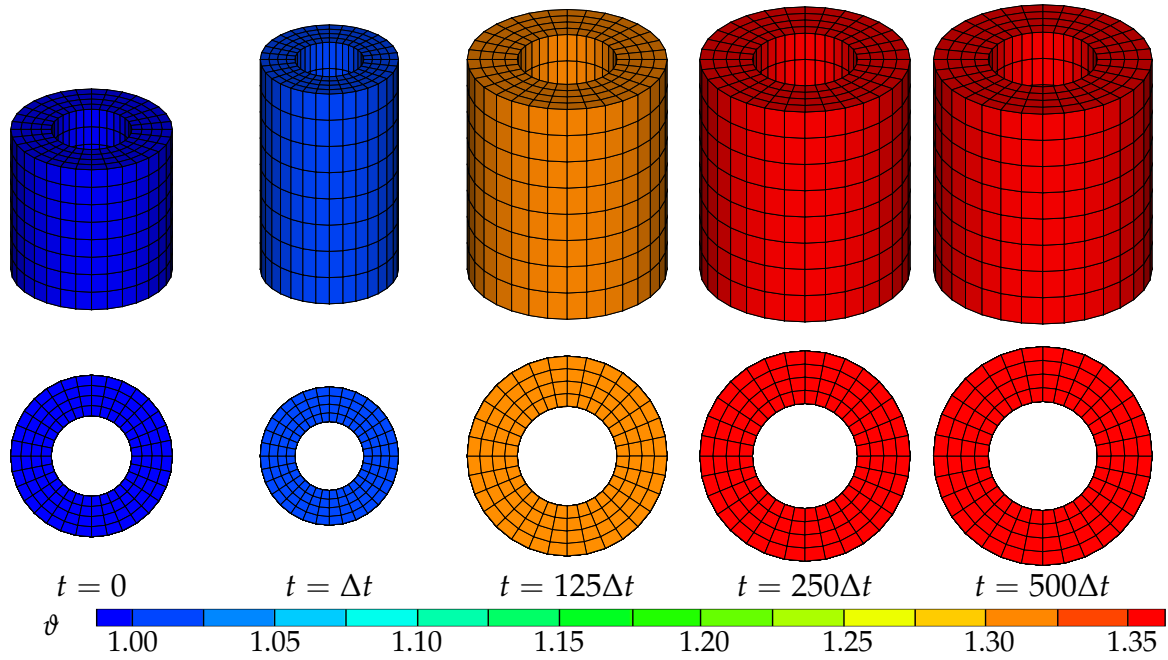


Figure 4.7: Deformation and evolution of the stretch ratio of the isotropic tube under tension.

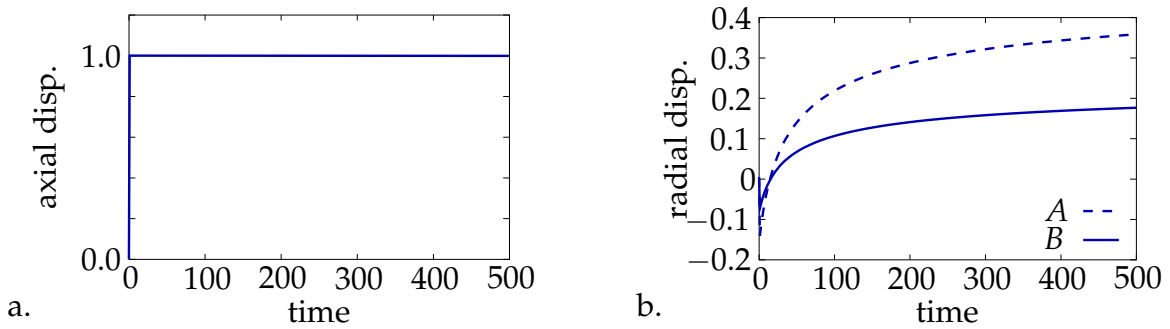


Figure 4.8: (a) Axial and (b) radial displacement of the points A at the outer boundary of the tube and B at the inner boundary of the tube.

applied stretch is then held constant for 500 time steps within which the tube grows. Consequently, both the diameter and the thickness of the tube increase, which can also be seen in figure 4.8. In this, the radial displacement of the two points A and B , see figure 4.6, are plotted over time. Moreover, it is observable that the impact of growth is larger for the first 250 time steps compared to the second period. This reflects that the stretch ratio relaxes to a biological equilibrium, which can also be seen in figure 4.9. In figure 4.9.b the change of volume, characterized by the determinant of the growth deformation gradient $J_g^{iso} = \vartheta^3$, is plotted over time. In figure 4.9.a the evolution of the density is depicted. Since growth is defined as density preservation from the initial state to the intermediate configuration, the density $\hat{\rho}_0$ stays constant. Comparison with the appropriate diagrams for remodeling in figure 3.10 once more accentuates the different assumptions made for remodeling and growth.

For the discussion of transversely isotropic growth, the elastic material parameters are

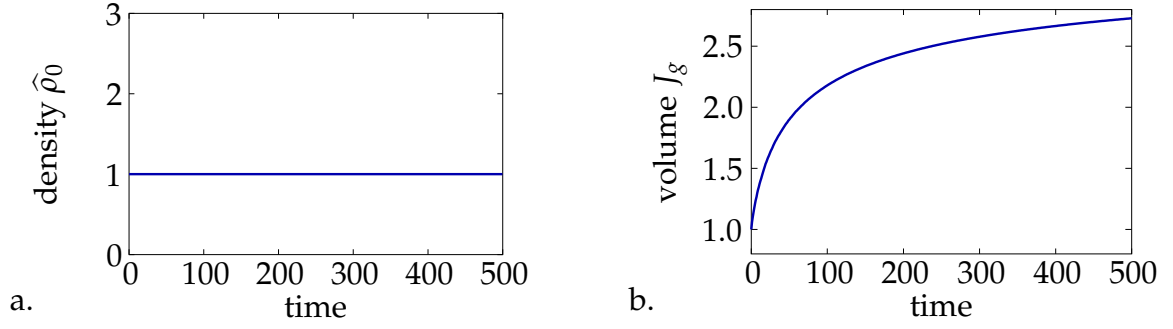


Figure 4.9: Isotropic tube under tension. (a) For growth, density preservation from the initial state to the intermediate configuration is prescribed, i.e., $\hat{\rho}_0 \equiv \rho_0 = \text{const.}$ (b) The volume growth, characterized by J_g , converges to a biological equilibrium.

$E = 3\text{N/mm}^2$, $\nu = 0.4$ and $\alpha = 1\text{N/mm}^2$. First, the characteristic direction \mathbf{n}^A is set parallel to the axial direction of the tube. We compare two cases: in one case, the limiting stretch ratio in fiber direction is higher, i.e., $\eta^+ > \vartheta^+$; in the other case it is vice versa, i.e., $\eta^+ < \vartheta^+$. Due to the boundary conditions and loads, the limiting parameters for atrophy are not used here, but in the next example. Concretely, we applied the parameters $\vartheta^+ = 1.3$, $\vartheta^- = 0.7$, $\eta^+ = 1.8$, $\eta^- = 0.2$, $k_{\vartheta/\eta}^\pm = 0.01$, $m_{\vartheta/\eta}^\pm = 2.0$ and $\nu_{\vartheta/\eta} = 0.5$ for the first case and swapped the values for the second case. The time step is $\Delta t = 0.1$. Figure 4.10.a shows the deformation and the evolution of the stretch ratios η and ϑ after 500 time steps. For $\eta^+ > \vartheta^+$, growth parallel to \mathbf{n}^A , i.e., in the axial di-

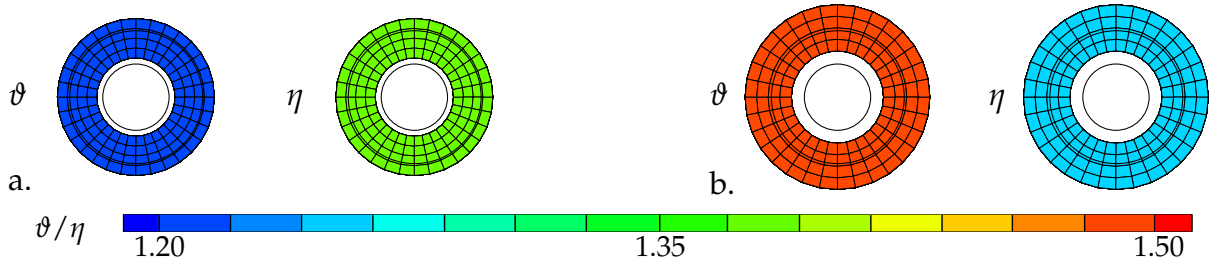


Figure 4.10: Deformation and evolution of the stretch ratios of the transversely isotropic tube with axial characteristic direction and variation of the limiting stretch ratios: (a) $\eta^+ > \vartheta^+$ (b) $\eta^+ < \vartheta^+$.

rection, is higher than growth orthogonal to \mathbf{n}^A and vice versa. Thus, for $\eta^+ > \vartheta^+$ (a), the stress is primarily compensated in the axial direction, whereas for $\eta^+ < \vartheta^+$ (b), it is compensated by growth orthogonal to the axial direction. Consequently, the increase of the diameter of the tube in (b) is greater than that in (a).

Second, we examine the impact of the orientation of the characteristic direction \mathbf{n}^A . The material parameters are identical to those of the previous example with $\eta^+ > \vartheta^+$, but $\nu_{\vartheta/\eta} = 1$. In figure 4.11 the deformations and evolution of stretch ratios are depicted after 500 time steps for \mathbf{n}^A in the axial, radial and circumferential directions. Due to the axial stretching of the tube, the stresses in the axial direction are larger than in the radial and circumferential directions. This takes the interpretation that, for an axial characteristic direction \mathbf{n}^A , the stresses parallel to \mathbf{n}^A are higher than those orthogonal to \mathbf{n}^A . Consequently, the tube grows, which can be observed by an in-

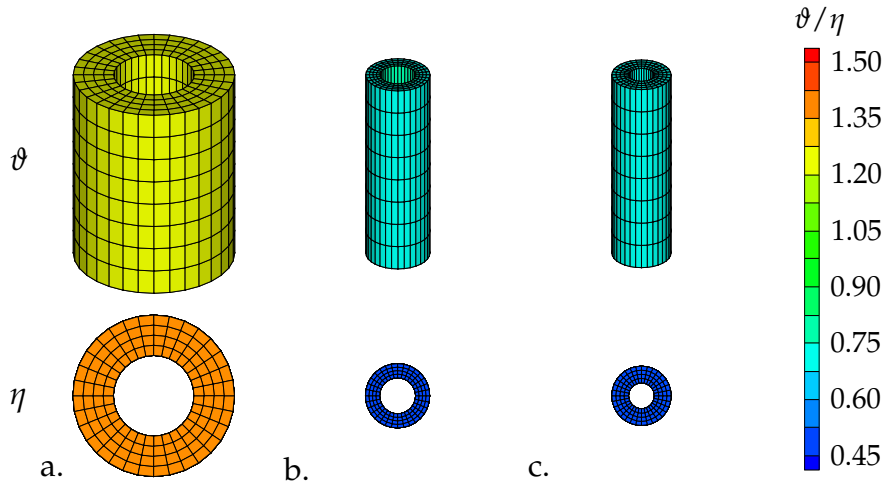


Figure 4.11: Deformation and evolution of the stretch ratios of the transversely isotropic tube with $\eta^+ > \vartheta^+$ and (a) axial, (b) radial and (c) circumferential characteristic direction.

creasing diameter of the tube. For both a radial and a circumferential orientation of the characteristic direction, the stresses parallel to \mathbf{n}^A are smaller than those orthogonal to \mathbf{n}^A , which induces mass reduction, see equation (4.10). Since we chose $\vartheta^- > \eta^-$, the mass resorption parallel to \mathbf{n}^A is higher than that which is orthogonal to \mathbf{n}^A . Hence the wall thickness of the tube becomes thinner with a radial orientation of the characteristic direction than with a circumferential orientation, but in the latter case the diameter is less.

Third, we consider a transversely isotropic tube, in which the characteristic direction is arranged in the tangential plane with an inclination angle $\varphi = 30^\circ$, see figure 4.6. The material parameters describing growth are $\vartheta^+ = 1.5$, $\vartheta^- = 0.6$, $\eta^+ = 2.5$, $\eta^- = 0.4$, $k_{\vartheta/\eta}^\pm = 0.1$, $m_{\vartheta/\eta}^\pm = 2.0$ and $\nu_{\vartheta/\eta} = 0.5$. The deformation of the tube and the evolution of the stretch ratios are depicted in figure 4.12. We observe that the tube rotates at the first loading step due to transversely isotropic elasticity, see also figure 3.11. If we keep the stretch constant, the material continues to grow. Since $\eta^+ > \vartheta^+$, the growth in the fiber direction is higher than in the direction orthogonal to \mathbf{n}^A . Consequently, the tube rotates opposite to the previous rotation until a biological equilibrium is reached.

Next, as an inhomogeneous deformation, a sinusoidal displacement load is applied radially to a cylindrical tube. The discretization, loads and boundary conditions, are depicted in figure 4.13. We consider isotropic and transversely isotropic material behavior. For isotropy, the elastic material parameters are $E = 3\text{N/mm}^2$, $\nu = 0.45$ and, implicitly, $\alpha = 0$. The growth parameters are $\vartheta^+ = 1.5$, $\vartheta^- = 0.5$, $k_\vartheta^\pm = 1.0$ and $m_\vartheta^\pm = 2.0$. The time step is $\Delta t = 0.1$. The deformation and the evolution of the stretch ratio are depicted in figure 4.14. Again, in the first loading step, we observe standard elastic material behavior, comparable with that for remodeling in figure 3.13. The displacement load is then held constant for 400 time steps. It is observable that, due to the stretch of the outside layer, the material grows in the middle of the tube. At the upper

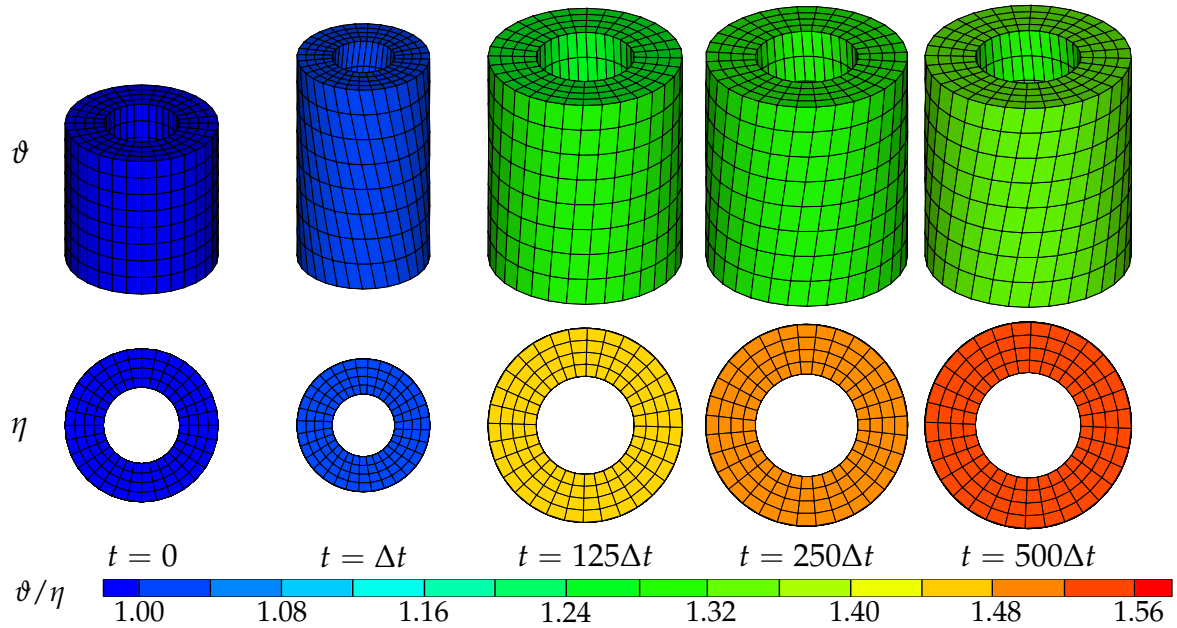


Figure 4.12: Deformation and stretch ratios of the transversely isotropic tube under tension with inclined characteristic direction.

and lower boundary, due to compression, atrophy is observed.

For transverse isotropy, we set $E = 3\text{N/mm}^2$, $\nu = 0.4$ and $\alpha = 2.0\text{N/mm}^2$ as well as $\vartheta^+ = 1.3$, $\vartheta^- = 0.7$, $\eta^+ = 1.1$, $\eta^- = 0.9$, $k_{\vartheta/\eta}^{\pm} = 0.1$, $m_{\vartheta/\eta}^{\pm} = 1.0$ and $\nu_{\vartheta/\eta} = 0.5$. The time step is $\Delta t = 0.1$. The characteristic direction is arranged in the tangential plane. The inclination angle is $\varphi = 60^\circ$. Figure 4.15 shows the deformation and the evolution of the stretch ratios for the transversely isotropic simulation. Again, in the first loading step, we observe standard elastic material behavior analogous to that in figure 3.14. Due to the stiffer fiber direction, the mesh forms an s-shape. The displacement load is then held constant for 400 time steps. Again, since $\eta^+ > \vartheta^+$, the tube rotates opposite to the previous rotation, until biological equilibrium is reached. The convergence in

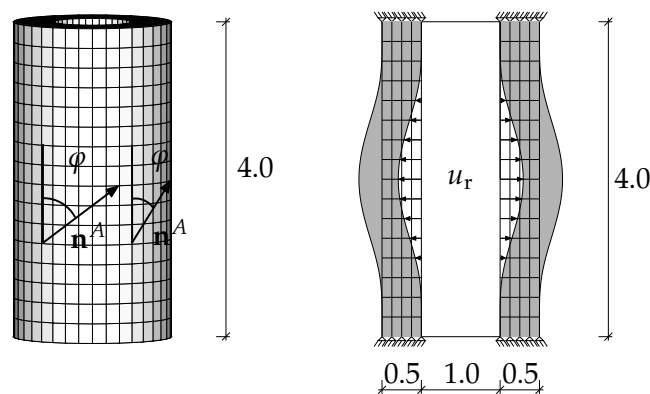


Figure 4.13: Loads and boundary conditions for the inhomogeneously deformed tube.

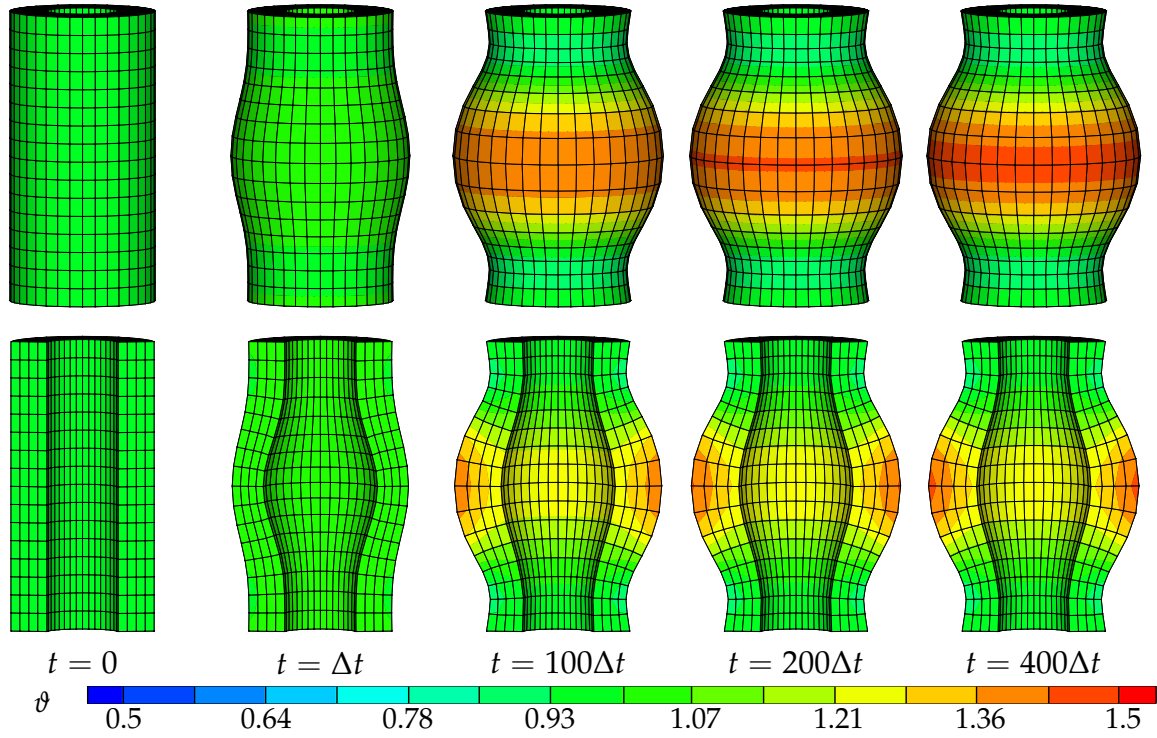


Figure 4.14: Deformation and evolution of the stretch ratio in the isotropic tube under inside displacement load.

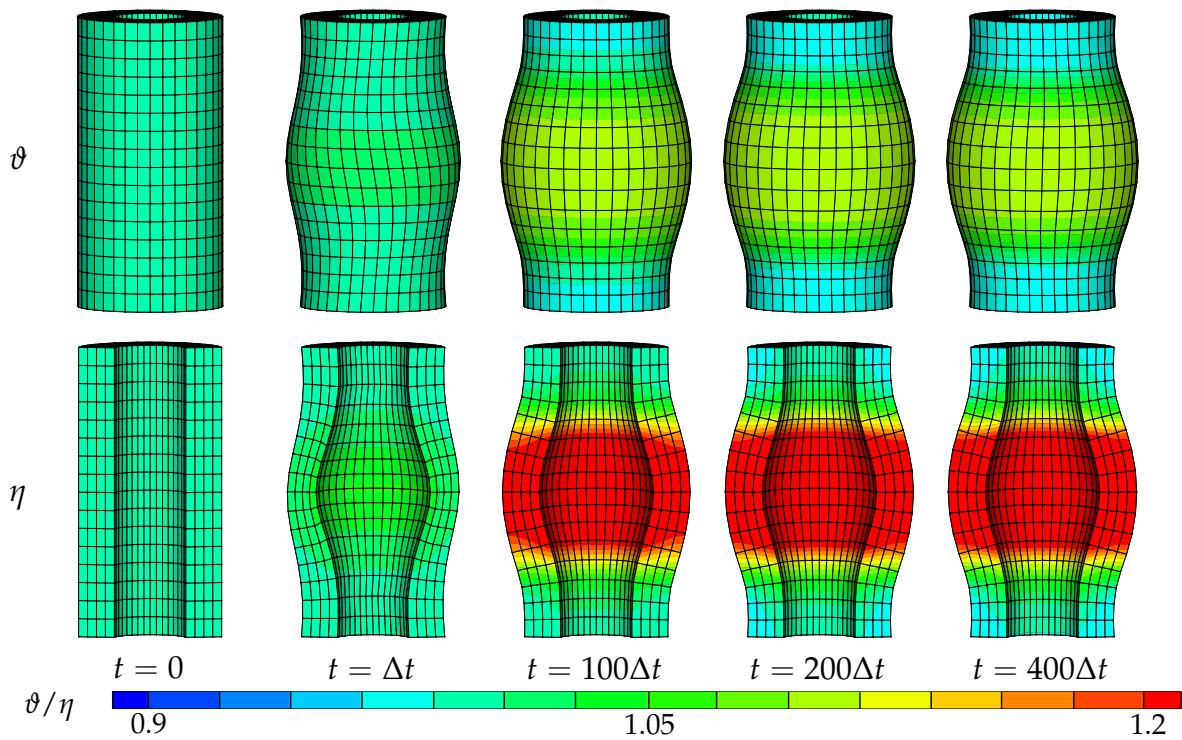


Figure 4.15: Deformation and evolution of the stretch ratios in the transversely isotropic tube under inside displacement load.

this computation is exemplarily presented in table 4.2. The left table shows the global convergence for the first three loading steps. The right table presents the local convergence at a point in the outside layer of the fixed boundary. In this, we restrict ourselves to the four global iterations marked gray in the left table. In the other loading steps a similar convergence can be observed.

inc	global it.	global residual
1	0	3.81838E+00
1	1	4.81407E-01
1	2	7.96106E-02
1	3	3.76890E-03
1	4	2.41756E-05
1	5	8.37675E-07
1	6	4.05621E-08
2	0	1.31136E-01
2	1	6.10783E-03
2	2	3.66436E-05
2	3	7.93160E-08
3	0	1.02786E-01
3	1	3.01562E-03
3	2	1.05575E-05
3	3	1.94190E-08

global convergence

inc	global iteration	local iteration	local residual
1	5	1	4.22238357E-03
1	5	2	1.02127676E-05
1	5	3	3.16276656E-11
1	6	1	4.22238360E-03
1	6	2	1.02127678E-05
1	6	3	3.16274348E-11
2	0	1	3.79211345E-03
2	0	2	8.18197077E-06
2	0	3	2.03398043E-11
2	1	1	3.76516164E-03
2	1	2	8.06820837E-06
2	1	3	1.97668511E-11

local convergence

Table 4.2: Quadratic convergence on the global and on the local level for growth

4.5 Discussion

Content of this chapter is the discussion of transversely isotropic growth as proposed by LUBARDA & HOGER [93]. With growth we denote pure volume changes under density preservation from the initial to the intermediate configuration. For transversely isotropic growth, changes in volume are characterized through two stretch ratios which are treated as internal variables. In contrast to LUBARDA & HOGER [93], we assume the stretch ratios to be driven by the Mandel stresses $\text{tr } \widehat{\mathbf{M}}$ rather than by the elastic Piola-Kirchhoff stresses $\text{tr } \widehat{\mathbf{S}}$. The pure growth model is embedded into the comprehensive framework of chapter 2 by an adequate choice of constitutive equations. This provides an easy comparison with remodeling as well as combinations with remodeling and reorientation. The main feature of this work is the numerical im-

plementation of the model by consistent linearizations of the appropriate nonlinear equations. Consequently, quadratic convergence can be achieved both on the local and the global level. Compared to the remodeling model in chapter 3, within constraints the growth model is insensitive to the choice of material parameters. With the demonstrated algorithmic update scheme an implementation into any finite element program is straightforward. Thus, with appropriate data processing tools to generate patient specific models from computer tomography data, the model seems useful during stent implantations or for an better understanding and prevention of hypertrophy, amongst others.

5 Reorientation

5.1 Introduction

Transversely isotropic materials, i.e., materials with one characteristic direction, can not only be found in biomechanics, but in various fields of our daily life. In many cases the characteristic direction is fixed in the matrix material, but particularly in living materials the characteristic direction can change due to changes in their environment. These changes can be either smooth and continuous, as for instance in biological materials, or discontinuous, as in piezoelectric materials. In biological soft tissues such as muscle tissue, cartilage tissue or our skin, the fibers, described by the characteristic directions, adapt their orientations to their mechanical loading environment. Also in hard tissues, reorientation can be observed, for instance, of the trabeculae in cancellous bone. So far, it is not clearly investigated, which are the driving forces for the reorientation process in biomaterials. Some authors advocate principal strains being the biological stimulus in soft tissues, see for instance DRIESSEN ET AL. [28, 29, 31, 32], KUHLE ET AL. [76], MENZEL [97] and HIMPEL [53]. In HARITON ET AL. [45] stresses are chosen to drive the reorientation process. Besides biomaterials, reorienting transverse isotropy can, amongst others, be observed in liquid crystals, i.e., liquids with a crystalline structure. The physical condition of these materials is between the solid and the fluid phase. As common in transversely isotropic materials, the characteristic direction of a liquid crystal is described by a position-dependent director. The most common application of liquid crystals are liquid crystal displays (LCDs), but they are also a central component of biological systems such as myelin, DNS, protein and cell membranes. Further, liquid crystals can be found in polymers, thermometers, pressure sensors and so forth. For a broad outline of liquid crystals the reader is referred to the book of COLLINGS [19]. Driving forces for the reorientation process in liquid crystalline materials, amongst others, are contact with other materials, electric or magnetic fields, see ERICKSEN [35]. To give another example on anisotropic reorienting materials, recall that piezo-ceramics can be poled by displacements or electric fields, so that the polarization direction characterizes transversely isotropic material behavior. A distinction is drawn between two fundamentally different piezoelectric effects: the direct one and the inverse one. The direct piezoelectric effect characterizes charging of the material caused by applied stresses as, for instance, used in sensors. In actuators, the inverse piezoelectric effect is exploited, which means that an applied electric field induces mechanical strains. For a general survey on piezoelectric materials we refer to KAMLAH [69] and SMITH [126]. Due to mechanical or electrical loading, switching of

the polarization direction may be induced, where a difference is made between ferroelastic switching and ferroelectric switching. Ferroelastic switching refers to reorientation of domains under purely mechanical loading and ferroelectric switching refers to reorientation under electric loading, see e.g. SCHRÖDER & ROMANOWSKI [120] and AROCKIARAJAN ET AL. [5,6,7] and references cited therein. Furthermore, reorientation phenomena can be observed in various polycrystalline materials, of which metals are a classical example. Apart from texture evolution, for instance, related to the constitutive behavior within the individual grain, such grains might themselves reorient according to the overall loading conditions. In this regard, a thermodynamically consistent and stress-driven framework has, among others, been proposed by JOHANSSON, MENZEL & RUNESSON [67]. For a general survey the reader is referred to the contributions in KOCKS, TOMÉ & WENK [72]. As a last example, simulations including reorienting characteristic directions can be used in context of optimization problems for composites, for instance, reinforced concrete in civil engineering or carbon fiber reinforced materials in motor sports, yachting, aircraft or wind engine construction, see e.g. PEDERSEN [110]. For optimization problems typically principal stresses or strains are assumed as driving forces.

It can be shown that for anisotropic elasticity the free energy reaches a critical state for coaxial stresses and strains, see VIANELLO [136, 137] and SGARRA & VIANELLO [121]. Stresses and strains are coaxial if the characteristic direction is aligned with the principal strain direction. This confirms the assumption of reorientation along the maximum principal strain direction. Also from the biological point of view, it is conceivable that principal strains are the mechanical stimulus for reorientation. For example, PAUWELS [108] predicted that tensile strains affect the orientation of collagen fibers, since they can just carry traction. In the context of hard tissues, COWIN [20], among others, also supposed that strains provoke the orientation of the trabecular bone. On the other hand, PAUWELS [108], based on the stress trajectories, stated that the trabeculae are oriented along the principal stresses. In terms of soft tissues, HARTON ET AL. [45] assumed that the orientation of the collagen fibers in the arterial wall is driven by principal stresses. They refer to the fact that the fiber orientation varies through the thickness of the wall analogous to the stress distribution, see HOLZAPFEL, STADLER & SCHULZE-BAUER [58]. Moreover, the Langer's cleavage lines are oriented along the maximum principal stress directions of our skin. The Langer's cleavage lines are the lines, along which a surgery cut should be made, to obtain a fine scar, see LANGER [84, 86, 87, 88, 89, 85]. All in all, it is safe to say that the orientation of anisotropy in biomaterials is often geared to mechanical stimuli, such as strains or stresses. Thus, in this chapter, we consider both reorientation along principal strains and reorientation along principal stresses, and compare them against each other. At this, to monitor solely the reorientation effects, we restrict ourselves to hyper-elastic formats for the stress tensor. Again, the major intention is the derivation of a robust and efficient algorithmic formulation and its consistent linearization within a finite

element framework. In this context, as an additional material property, we assume a rotation of the characteristic direction, whereat drilling rotations are excluded. Even though we will restrict ourselves to studying a specific constitutive model, the general algorithmic formulation can be applied to a wide range of applications. To be specific, the consistent linearization related to a reorienting fiber direction embedded in an iterative finite element context will be useful for various types of adaptive materials as indicated above.

The chapter is organized analogous to the two latter ones. First, the constitutive equations derived in chapter 2 are adjusted to reorientation. Then, we consistently linearise the material model, including an algorithmic update scheme for the characteristic direction and the incremental tangent modulus. Finally the material model is discussed by means of numerical examples. Again, the material behavior will be demonstrated by a simple tension test before we apply the theory to a homogeneous and an inhomogeneous boundary value problem.

5.2 Constitutive equations

In this section the essential equations describing the reorientation process are determined. First, the assumptions made in chapter 2 are fitted to hyper-elasticity. Then, for the determination of the characteristic direction, we start with the description of the evolution in time of a line element according to a rigid body motion. Following, this is adapted the evolution of the characteristic direction.

5.2.1 Transversely isotropic hyper-elasticity

As mentioned above, for the sake of directness, we restrict ourselves to reorientation in hyper-elastic materials. Consequently, no mass changes are considered, which includes that both the density and the volume are constant, viz $\hat{\rho}_0 = \rho_0 = \text{const}$ and $d\hat{V} = dV = \text{const}$. Per definition, for zero mass increase the mass source

$$\mathcal{R}_0 = 0 \tag{5.1}$$

vanishes. Even if any proof of this condition is redundant, conformance with the determinations in chapter 2 can be shown as follows. From equations (2.9) and (2.61) one can read that, for volume preservation from the material to intermediate configuration, the Jacobian related to \mathbf{F}_g becomes $J_g = \eta\vartheta^2 = 1$, compare also with section 3.2. Thus, the stretch ratios are related to each other as $\eta = 1/\vartheta^2$ and the trace of the growth velocity gradient (4.5) becomes $\text{tr} \hat{\mathbf{L}}_g = 0$. Insertion of this and the precondition of density conservation, i.e., $\hat{\rho}_0 = 0$, into the local balance of mass (2.35), directly yields equation (5.1). Further on, from equation (2.32) we can read that the material density is equal to the initial density, i.e., $\bar{\rho}_0 = \hat{\rho}_0 = \rho_0$. Analogous to the specifications in

section 3.2, we define $\vartheta := 1$, so that the intermediate configuration coincides with the material configuration and, consequently, is dispensable. Thus, the free energy function (2.69)

$$\psi = \frac{1}{\rho_0} \psi_0 = \frac{1}{\rho_0} \psi_0^e(\mathbf{C}, \mathbf{A}) \quad (5.2)$$

and the consequential second Piola-Kirchhoff stresses (2.72)

$$\mathbf{S} = 2 \frac{\partial \psi_0^e}{\partial \mathbf{C}} \quad (5.3)$$

are identical to the standard elastic formats. As a matter of course, the latter two expressions can again be reformulated in terms of invariants, see equations (2.67), (2.69) and (2.72). Due to the above mentioned preconditions, the reduced dissipation inequality (2.74) results in

$$\mathcal{D}_0^{red} = -\frac{\partial \psi_0}{\partial \mathbf{A}} : \dot{\mathbf{A}} - \theta \rho_0 \mathcal{S} \geq 0 \quad (5.4)$$

and the extra entropy term becomes

$$\mathcal{S} \leq -\frac{1}{\theta \rho_0} \frac{\partial \psi_0}{\partial \mathbf{A}} : \dot{\mathbf{A}} . \quad (5.5)$$

5.2.2 Evolution of a line element

The characteristic direction in transversely isotropic materials is described by a unit vector \mathbf{n}^A , which means that any elongation of \mathbf{n}^A is inadmissible. Thus, to specify its evolution, we start with the description of the evolution in time of a line element in regard to a rigid body motion.

Recall that every second-order tensor $\mathbf{T} = \mathbf{T}^{sym} + \mathbf{T}^{skw}$ can uniquely be decomposed into a symmetric part $\mathbf{T}^{sym} = \text{sym}(\mathbf{T}) = \frac{1}{2} [\mathbf{T} + \mathbf{T}^t]$ and a skew symmetric part $\mathbf{T}^{skw} = \text{skew}(\mathbf{T}) = \frac{1}{2} [\mathbf{T} - \mathbf{T}^t]$. Since any skew symmetric tensor is completely characterized by three scalar values, it can also be described by its axial vector $\mathbf{t} = -\frac{1}{2} \mathbf{T}^{skw} : \boldsymbol{\varepsilon}$. The action of the skew tensor applied to any vector $\mathbf{a} \in \mathbb{R}^3$ is identical to the cross-product of the corresponding axial vector and \mathbf{a} , i.e., $\mathbf{T}^{skw} \cdot \mathbf{a} = \mathbf{t} \times \mathbf{a}$. The symmetric - skew symmetric decomposition of the spatial velocity gradient (2.13) yields

$$\mathbf{l} = \mathbf{d} + \mathbf{w} , \quad (5.6)$$

with the rate of deformation tensor and the spin tensor

$$\mathbf{d} = \text{sym}(\mathbf{l}) = \frac{1}{2} [\mathbf{l} + \mathbf{l}^t] \quad \text{and} \quad \mathbf{w} = \text{skew}(\mathbf{l}) = \frac{1}{2} [\mathbf{l} - \mathbf{l}^t] , \quad (5.7)$$

respectively. The spin tensor can also be represented by its axial vector $\boldsymbol{\omega}$ and describes the rate of rotation contained in the deformation map. For rigid body motions $\mathbf{x}(\mathbf{X}, t) = \mathbf{c}(t) + \mathbf{R}(t) \cdot \mathbf{X}$, where \mathbf{R} is the proper orthogonal rotation tensor, the spatial velocity gradient becomes

$$\mathbf{l} = \dot{\mathbf{R}} \cdot \mathbf{R}^t \quad \forall \quad \mathbf{R} \in \mathcal{SO}(3), \quad (5.8)$$

which is a skew symmetric tensor field. Thus, for a rigid body motion, the rate of deformation tensor vanishes and the spin tensor is equal to the spatial velocity gradient

$$\mathbf{d} = \mathbf{0} \quad \text{and} \quad \mathbf{w} = \mathbf{l} = \dot{\mathbf{R}} \cdot \mathbf{R}^t, \quad (5.9)$$

so that the variation of the line element (2.12) with respect to time reduces to a pure rotation

$$d\dot{\mathbf{x}} = \mathbf{w} \cdot d\mathbf{x} = \boldsymbol{\omega} \times d\mathbf{x}. \quad (5.10)$$

5.2.3 Kinematics-based reorientation

As mentioned above, the evolution of the characteristic direction \mathbf{n}^A may be discussed by means of a rigid body motion of \mathbf{n}^A , i.e., as a rotation about the axis $\boldsymbol{\omega}^A$, see figure 5.1.a. Thus, analogous to equation (5.10), the variation of the characteristic direc-

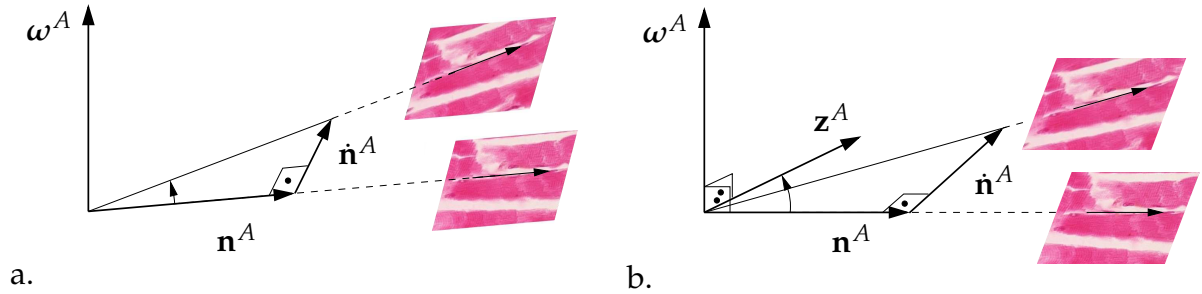


Figure 5.1: (a) The evolution of the characteristic direction amounts to a rotation of the characteristic direction \mathbf{n}^A with the angular velocity $\boldsymbol{\omega}^A$. (b) The characteristic direction \mathbf{n}^A rotates such that in the equilibrium state an alignment with a direction \mathbf{z}^A is achieved. To avoid drilling rotation, the angular velocity $\boldsymbol{\omega}^A$ must be perpendicular to the plane spanned by \mathbf{n}^A and \mathbf{z}^A .

tion in time becomes

$$\boxed{\dot{\mathbf{n}}^A = \boldsymbol{\omega}^A \times \mathbf{n}^A,} \quad (5.11)$$

which satisfies the orthogonality condition

$$\frac{d}{dt} (\mathbf{n}^A \cdot \mathbf{n}^A) = 0 \quad \Rightarrow \quad \dot{\mathbf{n}}^A \cdot \mathbf{n}^A = 0 \quad (5.12)$$

resulting from the constraint that \mathbf{n}^A is a unit vector. To specify the angular velocity ω^A in equation (5.11), for now, we assume an alignment of the characteristic direction \mathbf{n}^A with a direction \mathbf{z}^A . A more detailed description of this quantity depends on the driving force for the reorientation process and is specified later. Analogous to the theory of smooth shells, see for instance BETSCH, MENZEL & STEIN [12] and references cited therein, we exclude drilling rotations about the characteristic direction \mathbf{n}^A . Consequently, as depicted in figure 5.1.b, the angular velocity must be perpendicular to the plane spanned by \mathbf{n}^A and \mathbf{z}^A . This can be incorporated via

$$\boxed{\omega^A := \frac{\pi}{2t^*} \mathbf{n}^A \times \mathbf{z}^A,} \quad (5.13)$$

in which the material parameter $t^* > 0$ acts like a relaxation parameter, see also MENZEL [97]. For $t^* \rightarrow \infty$ one can easily observe from equation (5.13) that the evolution of the characteristic direction tends to zero, i.e., $\dot{\mathbf{n}}^A \rightarrow \mathbf{0}$, which means that the characteristic direction remains constant. Moreover, the closer the angle between two vectors the smaller the values that the norm of their cross-product takes. Accordingly, the norm of the angular velocity (5.13) takes high values for large differences between \mathbf{n}^A and \mathbf{z}^A and low values if the two vectors are almost aligned. The angular velocity is, thus, assumed to be higher at the beginning of the reorientation process than close to the final equilibrium state at the end of the reorientation process. The same observations can be made by insertion of equation (5.13) into equation (5.11), which yields

$$\dot{\mathbf{n}}^A = \frac{\pi}{2t^*} \left[\mathbf{1} - \mathbf{n}^A \otimes \mathbf{n}^A \right] \cdot \mathbf{z}^A. \quad (5.14)$$

From this, one can read that the evolution of the characteristic direction is the part of \mathbf{z}^A perpendicular to \mathbf{n}^A weighted by the constant scalar $\pi/(2t^*)$. Thus the reorientation occurs proportional to the sine of the angle between \mathbf{n}^A and \mathbf{z}^A , see figure 5.2.

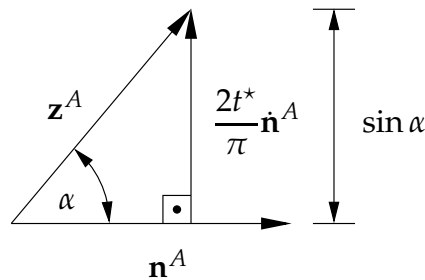


Figure 5.2: The magnitude of the evolution of the characteristic direction is proportional to the sine of the angle between \mathbf{n}^A and \mathbf{z}^A .

As mentioned in the introduction, we consider two different approaches concerning the impulsion of reorientation. First, elastic strains are set to drive the reorientation process. For linear and finite elasticity, it has been shown, that a critical state of the free energy can be reached if the strain and stress tensors are coaxial, see COWIN [22],

VIANELLO [136, 137] and SGARRA & VIANELLO [121, 122]. In isotropic materials this condition is a priori satisfied, however not in anisotropic materials. For the latter case, we consider the expression of the stresses in terms of invariants (2.76). From this, one can easily read that coaxiality of the structural tensor \mathbf{A} and the right Cauchy-Green tensor \mathbf{C} involves coaxiality of the Piola-Kirchhoff stresses \mathbf{S} and the right Cauchy-Green tensor \mathbf{C} . This can be achieved by aligning the characteristic direction \mathbf{n}^A with one of the principal directions of the right Cauchy-Green tensor. In this regard, we spectrally decompose the right Cauchy-Green tensor (2.11) such that we obtain

$$\mathbf{C} = \sum_{I=1}^3 \lambda_I^C \mathbf{n}_I^C \otimes \mathbf{n}_I^C, \quad (5.15)$$

with \mathbf{n}_I^C denoting the principal strain direction associated with the principal strain λ_I^C . In this contribution, we sort the principal strains such that the index I increases with increasing principal strain, so that it holds

$$\mathbf{n}_I^C \cdot \mathbf{n}_I^C = \delta_{IJ}, \quad \lambda_1^C \leq \lambda_2^C \leq \lambda_3^C. \quad (5.16)$$

Following the hypothesis of PAUWELS [108], we consider the maximum principle strain direction as one possible alignment-direction. On the other hand, as described in the introduction in section 5.1, from the biological point of view an alignment with the maximum principal stress directions makes sense. For this, the second Piola-Kirchhoff stresses (5.3) are decomposed

$$\mathbf{S} = \sum_{I=1}^3 \lambda_I^S \mathbf{n}_I^S \otimes \mathbf{n}_I^S, \quad (5.17)$$

analogous to the strains in equation (5.15), with the principal stress direction \mathbf{n}_I^S associated with the principal stress λ_I^S . Again, the principal stresses are arranged such that the index I increases with increasing principal stress. Thus, equivalent to equation (5.16), the same is true of the stresses, namely

$$\mathbf{n}_I^S \cdot \mathbf{n}_I^S = \delta_{IJ}, \quad \lambda_1^S \leq \lambda_2^S \leq \lambda_3^S. \quad (5.18)$$

For the sake of simplicity, we shall assume that the characteristic direction stays constant, i.e., $\dot{\mathbf{n}}^A = \mathbf{0}$, if there is no unique maximum principal stress or strain direction, i.e., $\lambda_1^{S/C} \leq \lambda_2^{S/C} = \lambda_3^{S/C}$, compare with the discussions in MENZEL [97]. Summariz-

ing, we examine the following two cases of reorientation

$$\begin{array}{ll}
 \text{(i)} & \mathbf{n}^A \rightsquigarrow \mathbf{z}^A = \mathbf{n}_3^C \quad \text{for } \lambda_1^C \leq \lambda_2^C < \lambda_3^C, \\
 & \mathbf{n}^A = \text{const} \quad \text{for } \lambda_1^C \leq \lambda_2^C = \lambda_3^C; \\
 \text{(ii)} & \mathbf{n}^A \rightsquigarrow \mathbf{z}^A = \mathbf{n}_3^S \quad \text{for } \lambda_1^S \leq \lambda_2^S < \lambda_3^S, \\
 & \mathbf{n}^A = \text{const} \quad \text{for } \lambda_1^S \leq \lambda_2^S = \lambda_3^S.
 \end{array} \tag{5.19}$$

Recall that the reorientation process solely depends on the angle between the characteristic direction \mathbf{n}^A and the alignment-direction \mathbf{z}^A . The magnitude of the strains or stresses, however, does not have any influence on the reorientation model applied here. For other strain based formulations of reorientation the reader is referred to IMATANI & MAUGIN [66], KUHLE ET AL. [76] and DRIESSEN ET AL. [28, 29, 31, 32] as well as to DRIESSEN ET AL. [30], in which the applied reorientation model is additionally assumed to depend on the magnitude of the principal strains. Concerning stress based reorientation see, for instance, HARITON ET AL. [45] and related discussions in MENZEL [97]. A stress-based reorientation model for elastoplasticity has been discussed in VINCENT, CALLOCH & MARQUIS [138] and JOHANSSON, MENZEL & RUNESSON [67]. For reorientation of microstructures in liquid crystals or piezoelectric materials a formulation driven by gradients of the electric or the magnetic fields seems to be more realistic from a physical point of view.

Remark 5.1 (Details on the reorientation process) The material behavior depends on the orientation but not on the direction of \mathbf{n}^A , see equations (2.59) and (2.69). Thus, the orientation of \mathbf{z}^A is changed to $-\mathbf{z}^A$, if the angle enclosed with the characteristic direction \mathbf{n}^A is obtuse. Accordingly, for reorientation along the maximum principal strains, equation (5.19.i) changes to

$$\begin{array}{ll}
 \mathbf{n}^A \rightsquigarrow \mathbf{z}^A = -\mathbf{n}_3^C & \text{for } \lambda_1^C \leq \lambda_2^C < \lambda_3^C, \\
 \mathbf{n}^A = \text{const} & \text{for } \lambda_1^C \leq \lambda_2^C = \lambda_3^C.
 \end{array} \tag{5.20}$$

For stress driven reorientation appropriate changes must be made. ■

Remark 5.2 (Alternative driving forces for the reorientation process) In regard to arterial walls, HOLZAPFEL, STADLER & SCHULZE-BAUER [58] hypothesized that the collagen fibers are aligned with the averaged direction of the two maximum principal stresses. This particularly makes sense for materials with two families of fibers, such as the arterial wall. For equal eigenvalues, specifications analogous to those in equa-

tion (5.19) are reasonable. Moreover, to model soft biological tissues, with soft fibers that do not carry any pressure, one may assume that \mathbf{n}^A stays constant, if all principal stresses or strains are compressive, i.e., $\lambda_3^{S/C} < 0$, or aligns with the maximum principal strain or stress direction, if tension occurs solely in this direction. Summarizing analogously to equation (5.19), following alternative formulations are, for example, conceivable

$$\begin{aligned}
\text{(iii) } \mathbf{n}^A \rightsquigarrow \mathbf{z}^A = \mathbf{n}^C & \quad \text{with } \mathbf{n}^C = \frac{\tilde{\mathbf{n}}^C}{\|\tilde{\mathbf{n}}^C\|} \text{ and } \tilde{\mathbf{n}}^C = \lambda_2^C \mathbf{n}_2^C + \lambda_3^C \mathbf{n}_3^C \\
& \quad \text{for } \lambda_1^C < \lambda_2^C \leq \lambda_3^C, \\
\mathbf{n}^A \rightsquigarrow \mathbf{z}^A = \mathbf{n}_3^C & \quad \text{for } \left[\lambda_2^C < 0 \wedge \lambda_3^C > 0 \right] \vee \lambda_1^C = \lambda_2^C < \lambda_3^C, \\
\mathbf{n}^A = \text{const} & \quad \text{for } \lambda_1^C = \lambda_2^C = \lambda_3^C \vee \lambda_3^C < 0; \\
\text{(iv) } \mathbf{n}^A \rightsquigarrow \mathbf{z}^A = \mathbf{n}^S & \quad \text{with } \mathbf{n}^S = \frac{\tilde{\mathbf{n}}^S}{\|\tilde{\mathbf{n}}^S\|} \text{ and } \tilde{\mathbf{n}}^S = \lambda_2^S \mathbf{n}_2^S + \lambda_3^S \mathbf{n}_3^S \\
& \quad \text{for } \lambda_1^S < \lambda_2^S \leq \lambda_3^S, \\
\mathbf{n}^A \rightsquigarrow \mathbf{z}^A = \mathbf{n}_3^S & \quad \text{for } \left[\lambda_2^S < 0 \wedge \lambda_3^S > 0 \right] \vee \lambda_1^S = \lambda_2^S < \lambda_3^S, \\
\mathbf{n}^A = \text{const} & \quad \text{for } \lambda_1^S = \lambda_2^S = \lambda_3^S \vee \lambda_3^S < 0.
\end{aligned} \tag{5.21}$$

■

5.3 Implementation

For the implementation into a finite element program, standard finite elements can be used with an internal variable formulation for the characteristic direction \mathbf{n}^A . Analogous to the latter two chapters, in the first part of this section we discuss the algorithmic update of the internal variable. In the second part the incremental tangent modulus is derived.

5.3.1 Incremental update of the characteristic direction

For the time integration of the evolution equation (5.11) an implicit Euler backward scheme $\mathbf{n}_{n+1}^A = \mathbf{n}_n^A + \dot{\mathbf{n}}_{n+1}^A \Delta t$ as discussed in HUGHES & WINGET [60] is conceivable. For such an update algorithm a post-processing normalization $\mathbf{n}_{n+1}^A \leftarrow \mathbf{n}_{n+1}^A / \|\mathbf{n}_{n+1}^A\|$ is necessary to ensure that the characteristic direction remains a unit vector.

In this work, however, a geometrically exact update is applied. The infinitesimal version of the Euler theorem indicates that the exponent $\exp(\hat{\omega}^A \Delta t) \in \mathcal{SO}(3)$ of the skew symmetric tensor $\hat{\omega}^A$ is a rotation about its axial vector ω^A by the angle $(\|\omega^A\| \Delta t)$, see

MARSDEN & RATIU [96] and GURTIN [44]. Thus, the implicit exponential map

$$\mathbf{n}_{n+1}^A = \exp(\hat{\omega}_{n+1}^A \Delta t) \cdot \mathbf{n}_n^A, \quad (5.22)$$

with the index n denoting the time increment, describes a rotation of the characteristic direction of the last time step \mathbf{n}_n^A about the current axis ω_{n+1}^A . Hence, the characteristic direction (5.22) remains a unit vector during the update procedure and a normalization is not necessary. The exponential expression in equation (5.22) can be rewritten by the Rodriguez formula

$$\exp(-\varepsilon \cdot \omega^A \Delta t) = \cos(\omega \Delta t) \mathbf{1} + [1 - \cos(\omega \Delta t)] \mathbf{n}^\omega \otimes \mathbf{n}^\omega + \sin(\omega \Delta t) \hat{\mathbf{n}}^\omega, \quad (5.23)$$

see MARSDEN & RATIU [96]. Herein $\omega = \|\omega^A\|$, $\mathbf{n}^\omega = \omega^A / \omega$ and $\hat{\mathbf{n}}^\omega = -\varepsilon \cdot \mathbf{n}^\omega$ are the norm of the angular velocity, the direction of the angular velocity and the corresponding skew symmetric tensor, respectively. The nonlinear residual equation related to equation (5.22)

$$\mathbf{r}_A = -\mathbf{n}_{n+1}^A + \exp(\hat{\omega}_{n+1}^A \Delta t) \cdot \mathbf{n}_n^A = \mathbf{0}, \quad (5.24)$$

can be solved by a Newton iteration scheme. Hence, equation (5.24) is expanded in linear Taylor series at \mathbf{n}^A

$$\mathbf{r}_A^{k+1} = \mathbf{r}_A^k + \frac{\partial \mathbf{r}_A^k}{\partial \mathbf{n}^A} \cdot \Delta \mathbf{n}^A = \mathbf{0}. \quad (5.25)$$

For the sake of readability, again, the indices $n+1$ and k are neglected in the following. Thus, by combining equation (5.24) with (5.25), it can be reformulated as

$$\mathbf{r}_A^{k+1} = \mathbf{r}_A - \Delta \mathbf{n}^A + \frac{\partial(\exp(\hat{\omega}^A \Delta t) \cdot \mathbf{n}_n^A)}{\partial \mathbf{n}^A} \cdot \Delta \mathbf{n}^A = \mathbf{0} \quad (5.26)$$

and solved for the increment

$$\Delta \mathbf{n}^A = \left[\mathbf{1} - \frac{\partial(\exp(\hat{\omega}^A \Delta t) \cdot \mathbf{n}_n^A)}{\partial \mathbf{n}^A} \right]^{-1} \cdot \mathbf{r}_A. \quad (5.27)$$

For the derivative of the exponential expression with respect to the characteristic direction we apply the chain rule

$$\frac{\partial \exp(\hat{\omega}^A \Delta t)}{\partial \mathbf{n}^A} = \frac{\partial \exp(\hat{\omega}^A \Delta t)}{\partial (\omega^A \Delta t)} \Delta t \cdot \frac{\partial \omega^A}{\partial \mathbf{n}^A}. \quad (5.28)$$

The derivative of the exponent of the skew symmetric tensor with respect to the according axial vector can be determined by means of Rodriguez' formula (5.23) as described in appendix C.1. The derivative of the angular velocity with respect to the characteris-

tic vector

$$\frac{\partial \boldsymbol{\omega}^A}{\partial \mathbf{n}^A} = \frac{\pi}{2t^*} \left[\boldsymbol{\varepsilon} \cdot \mathbf{z}^A - \left[\boldsymbol{\varepsilon} \cdot \mathbf{n}^A \right] \cdot \frac{\partial \mathbf{z}^A}{\partial \mathbf{n}^A} \right] \quad (5.29)$$

follows straightforwardly from the definition of the angular velocity (5.13). The derivative of the direction \mathbf{z}^A with respect to the characteristic direction \mathbf{n}^A depends on the type of reorientation as described in equation (5.19). Since the strains are constant within the local Newton iteration, the derivative $\partial \mathbf{z}^A / \partial \mathbf{n}^A$ is equal to zero for strain driven reorientation as described in equation (5.19.i). For reorientation along the principal stress direction, see equation (5.19.ii), the derivative can be computed by application of the chain rule. Summarizing, for the two cases in equation (5.19), the derivative in demand becomes

$$\begin{aligned} \text{(i)} \quad & \frac{\partial \mathbf{z}^A}{\partial \mathbf{n}^A} = \frac{\partial \mathbf{n}_3^C}{\partial \mathbf{n}^A} = \mathbf{0} ; \\ \text{(ii)} \quad & \frac{\partial \mathbf{z}^A}{\partial \mathbf{n}^A} = \frac{\partial \mathbf{n}_3^S}{\partial \mathbf{n}^A} = \frac{\partial \mathbf{n}_3^S}{\partial \mathbf{S}} : \frac{\partial \mathbf{S}}{\partial \mathbf{n}^A} . \end{aligned} \quad (5.30)$$

Unfortunately, the derivative of the eigenvector \mathbf{n}_I^S with respect to the corresponding tensor \mathbf{S} cannot be computed straightforwardly. Following MOSLER & MESCHKE [104], this contribution is derived from the derivative of the eigenvalue problem of \mathbf{S} and the derivative of the normalization condition of \mathbf{n}_I^S as described in appendix C.2. To compute the derivative of the stresses \mathbf{S} with respect to the characteristic direction \mathbf{n}^A , we introduce the fourth-order tangent modulus \mathbb{C}^n measuring the sensitivity of the stresses with respect to the structural tensor \mathbf{A} . By analogy to the elastic tangent modulus, see equations (3.19) and (5.38), we define

$$\mathbb{C}^n := 2 \frac{\partial \mathbf{S}}{\partial \mathbf{A}} = 4 \frac{\partial^2 \psi_0}{\partial \mathbf{C} \partial \mathbf{A}} = 4 \sum_{i=1}^5 \left[\sum_{j=4}^5 \left[\frac{\partial^2 \psi_0}{\partial I_i \partial I_j} \frac{\partial I_i}{\partial \mathbf{C}} \otimes \frac{\partial I_j}{\partial \mathbf{A}} \right] \right] + 4 \sum_{i=4}^5 \left[\frac{\partial \psi_0}{\partial I_i} \frac{\partial^2 I_i}{\partial \mathbf{C} \partial \mathbf{A}} \right], \quad (5.31)$$

in which the fact that the isotropic invariants $I_{i=1,2,3}$ do not depend on the structural tensor has already been considered. Thus, the missing derivative becomes

$$\frac{\partial \mathbf{S}}{\partial \mathbf{n}^A} = \frac{\partial \mathbf{S}}{\partial \mathbf{A}} : \frac{\partial \mathbf{A}}{\partial \mathbf{n}^A} = \frac{1}{2} \mathbb{C}^n : \frac{\partial \mathbf{A}}{\partial \mathbf{n}^A} = \mathbb{C}^n \cdot \mathbf{n}^A, \quad (5.32)$$

so that all terms in equation (5.30) are determined.

Reformulation of the evolution equation (5.11) in incremental manner yields the increment of the characteristic direction as

$$\Delta \mathbf{n}^A = \Delta \boldsymbol{\omega}^A \times \mathbf{n}^A \quad (5.33)$$

including the incremental angular velocity $\Delta \boldsymbol{\omega}^A = \boldsymbol{\omega}^{A^{k+1}} \Delta t - \boldsymbol{\omega}^{A^k} \Delta t$. Based on this

and excluding drilling rotations, the cross product of \mathbf{n}^A and $\Delta\mathbf{n}^A$

$$\mathbf{n}^A \times \Delta\mathbf{n}^A = \underbrace{[\mathbf{n}^A \cdot \mathbf{n}^A]}_{=1} \Delta\boldsymbol{\omega}^A - \underbrace{[\mathbf{n}^A \cdot \Delta\boldsymbol{\omega}^A]}_{=0} \mathbf{n}^A \quad (5.34)$$

yields the incremental angular velocity

$$\Delta\boldsymbol{\omega}^A = \mathbf{n}^A \times \Delta\mathbf{n}^A . \quad (5.35)$$

Thus, the updated characteristic direction becomes

$$\mathbf{n}^{A^{k+1}} = \exp(\Delta\hat{\boldsymbol{\omega}}^A) \cdot \mathbf{n}^A = \exp(-\boldsymbol{\varepsilon} \cdot [\mathbf{n}^A \times \Delta\mathbf{n}^A]) \cdot \mathbf{n}^A , \quad (5.36)$$

see also BETSCH, MENZEL & STEIN [12].

5.3.2 Incremental tangent modulus

Although both strain and stress driven reorientation algorithms have been discussed in the literature, so far none of the rotational update formulations have been linearized consistently. To benefit from the quadratic convergence properties of the Newton-Raphson scheme, we apply a consistent linearization of the rotational update which essentially relies on an exact linearization of the exponential update scheme. Analogous to the computations for remodeling and growth in equations (3.17) and (4.30), respectively, the incremental tangent modulus describing the elastic deformation including reorientation results as

$$\mathbb{C} = 2 \frac{\partial \mathbf{S}}{\partial \mathbf{C}} + 2 \frac{\partial \mathbf{S}}{\partial \mathbf{n}^A} \cdot \frac{\partial \mathbf{n}^A}{\partial \mathbf{C}} . \quad (5.37)$$

The first part of equation (5.37) can again be identified as the elastic tangent modulus

$$\mathbb{C}^e = 2 \frac{\partial \mathbf{S}}{\partial \mathbf{C}} = 4 \frac{\partial^2 \psi_0}{\partial \mathbf{C} \partial \mathbf{C}} , \quad (5.38)$$

see also equations (3.18) and (4.27). An alternative representation of this equation depending on the invariants follows identical to that for remodeling in equation (3.19). To compute the second part of equation (5.37), we introduced the tangent modulus \mathbb{C}^n , see equations (5.31) and (5.32).

Again, solely the evolution of the characteristic direction is given, but not the characteristic direction itself, so that the last part of equation (5.37) cannot be computed directly. To compute this derivative, we differentiate the residual of \mathbf{n}^A in the exponential update scheme (5.24) with respect to the right Cauchy-Green tensor

$$\frac{\partial \mathbf{r}_A}{\partial \mathbf{C}} = -\frac{\partial \mathbf{n}^A}{\partial \mathbf{C}} + \frac{\partial (\exp(\hat{\boldsymbol{\omega}}^A \Delta t) \cdot \mathbf{n}^A_n)}{\partial \mathbf{C}} + \frac{\partial (\exp(\hat{\boldsymbol{\omega}}^A \Delta t) \cdot \mathbf{n}^A_n)}{\partial \mathbf{n}^A} \cdot \frac{\partial \mathbf{n}^A}{\partial \mathbf{C}} = \mathbf{0} . \quad (5.39)$$

Solving this equation for the derivative in demand yields

$$\frac{\partial \mathbf{n}^A}{\partial \mathbf{C}} = \left[\mathbf{1} - \frac{\partial (\exp(\hat{\omega}^A \Delta t) \cdot \mathbf{n}^A_n)}{\partial \mathbf{n}^A} \right]^{-1} \cdot \frac{\partial (\exp(\hat{\omega}^A \Delta t) \cdot \mathbf{n}^A_n)}{\partial \mathbf{C}}. \quad (5.40)$$

In this, the inverse is identical to the inverse in equation (5.27). Analogous to equation (5.28), the derivative of the exponential expression with respect to the right Cauchy-Green tensor can be solved by application of the chain rule

$$\frac{\partial \exp(\hat{\omega}^A \Delta t)}{\partial \mathbf{C}} = \frac{\partial \exp(\hat{\omega}^A \Delta t)}{\partial (\omega^A \Delta t)} \Delta t \cdot \frac{\partial \omega^A}{\partial \mathbf{C}}. \quad (5.41)$$

The derivative of the exponent of the skew symmetric tensor with respect to its axial vector is identical to that in equation (5.28) and is described in appendix C.1. The derivative of the angular velocity with respect to the right Cauchy-Green tensor follows from equation (5.13) as

$$\frac{\partial \omega^A}{\partial \mathbf{C}} = -\frac{\pi}{2t^*} (\boldsymbol{\varepsilon} \cdot \mathbf{n}^A) \cdot \frac{\partial \mathbf{z}^A}{\partial \mathbf{C}} = \frac{\pi}{2t^*} \hat{\mathbf{n}}^A \cdot \frac{\partial \mathbf{z}^A}{\partial \mathbf{C}}. \quad (5.42)$$

Corresponding to equations (5.19) and (5.30), the derivative of the direction \mathbf{z}^A with respect to the strain tensor \mathbf{C} becomes

$$\begin{aligned} \text{(i)} \quad & \frac{\partial \mathbf{z}^A}{\partial \mathbf{C}} = \frac{\partial \mathbf{n}_3^C}{\partial \mathbf{C}}; \\ \text{(ii)} \quad & \frac{\partial \mathbf{z}^A}{\partial \mathbf{C}} = \frac{\partial \mathbf{n}_3^S}{\partial \mathbf{C}} = \frac{\partial \mathbf{n}_3^S}{\partial \mathbf{S}} : \frac{\partial \mathbf{S}}{\partial \mathbf{C}} = \frac{1}{2} \frac{\partial \mathbf{n}_3^S}{\partial \mathbf{S}} : \mathbb{C}^e. \end{aligned} \quad (5.43)$$

The derivatives of the eigenvectors \mathbf{n}_I^C or \mathbf{n}_I^S with respect to the corresponding tensors \mathbf{C} or \mathbf{S} , respectively, are described in appendix C.2. A summary of the complete algorithm is given in table 5.1.

Remark 5.3 (Details on the implementation of the reorientation process) If the angle enclosed with the characteristic direction \mathbf{n}^A is obtuse, the orientation of \mathbf{z}^A is changed to $-\mathbf{z}^A$, see remark 5.1. This implies that equations (5.30) and (5.43) must be adjusted accordingly. For example for reorientation along the maximum principal strains, equations (5.30.i) and (5.43.i) change to

$$\frac{\partial \mathbf{z}^A}{\partial \mathbf{n}^A} = \frac{\partial (-\mathbf{n}_3^C)}{\partial \mathbf{n}^A} = \mathbf{0} \quad \text{and} \quad \frac{\partial \mathbf{z}^A}{\partial \mathbf{C}} = \frac{\partial (-\mathbf{n}_3^C)}{\partial \mathbf{C}}, \quad (5.44)$$

respectively. For stress driven reorientation appropriate changes must be made. The derivative of the negative eigenvector with respect to the corresponding tensor is given in appendix C.2. ■

history data: internal variable $\mathbf{n}_n^A = [n_{n1}^A, n_{n2}^A, n_{n3}^A]^t$

1. set initial values

$$\mathbf{n}^A = \mathbf{n}_n^A, \quad \mathbf{A} = \mathbf{n}^A \otimes \mathbf{n}^A, \quad \mathbf{C} = \mathbf{F}^t \cdot \mathbf{F}, \quad \mathbf{S} = 2 \frac{\partial \psi_0}{\partial \mathbf{C}}$$

2. compute the principal strain and stress directions and eigenvalues

$$\mathbf{C} = \sum_{I=1}^3 \lambda_I^C \mathbf{n}_I^C \otimes \mathbf{n}_I^C \quad \text{with} \quad \lambda_1^C \leq \lambda_2^C \leq \lambda_3^C$$

$$\mathbf{S} = \sum_{I=1}^3 \lambda_I^S \mathbf{n}_I^S \otimes \mathbf{n}_I^S \quad \text{with} \quad \lambda_1^S \leq \lambda_2^S \leq \lambda_3^S$$

and set the alignment direction depending on stimulus for reorientation

- (i) IF $\lambda_2^C = \lambda_3^C$ THEN

$$\dot{\mathbf{n}}^A = \mathbf{0}, \quad \mathbf{C} = \mathbf{C}^e \quad \text{EXIT}$$

ELSE

$$\mathbf{z}^A = \mathbf{n}_3^C$$

ENDIF

- (ii) IF $\lambda_2^S = \lambda_3^S$ THEN

$$\dot{\mathbf{n}}^A = \mathbf{0}, \quad \mathbf{C} = \mathbf{C}^e \quad \text{EXIT}$$

ELSE

$$\mathbf{z}^A = \mathbf{n}_3^S$$

ENDIF

IF $\mathbf{n}^A \cdot \mathbf{z}^A < 0$ THEN $\mathbf{z}^A \mapsto -\mathbf{z}^A$ ENDIF

IF $\mathbf{n}^A \parallel \mathbf{z}^A$ THEN $\dot{\mathbf{n}}^A = \mathbf{0}, \mathbf{C} = \mathbf{C}^e$ EXIT

3. local Newton iteration

- a. compute residual

$$\mathbf{r}_A = -\mathbf{n}^A + \exp(\hat{\omega}^A \Delta t) \cdot \mathbf{n}_n^A$$

- b. compute incremental update

$$\Delta \mathbf{n}^A = \left[\mathbf{1} - \frac{\partial (\exp(\hat{\omega}^A \Delta t) \cdot \mathbf{n}_n^A)}{\partial \mathbf{n}^A} \right]^{-1} \cdot \mathbf{r}_A$$

Table 5.1: Algorithmic update scheme for reorientation (part 1)

<p>c. update</p> $\mathbf{n}^A \leftarrow \exp(-\varepsilon \cdot [\mathbf{n}^A \times \Delta \mathbf{n}^A]) \cdot \mathbf{n}^A$ $\mathbf{z}^A \leftarrow \begin{array}{l} \text{(i) no update for } \mathbf{z}^A \text{ necessary} \\ \text{(ii) } \mathbf{S} = 2 \frac{\partial \psi_0}{\partial \mathbf{C}} = \sum_{I=1}^3 \lambda_I^S \mathbf{n}_I^S \otimes \mathbf{n}_I^S \end{array}$ $\boldsymbol{\omega}^A = \frac{\pi}{2t^*} \mathbf{n}^A \times \mathbf{z}^A$ <p>d. check tolerance</p> <p>IF $\ \mathbf{r}_A\ < \text{tol}$ GOTO 4</p> <p>ELSE GOTO 3.a</p> <p>4. compute moduli</p> $\mathbb{C} = \mathbb{C}^e + 2 [\mathbb{C}^n \cdot \mathbf{n}^A] \cdot \left[\mathbf{1} - \frac{\partial(\exp(\hat{\boldsymbol{\omega}}^A \Delta t) \cdot \mathbf{n}^A_n)}{\partial \mathbf{n}^A} \right]^{-1} \cdot \frac{\partial(\exp(\hat{\boldsymbol{\omega}}^A \Delta t) \cdot \mathbf{n}^A_n)}{\partial \mathbf{C}}$ <p>with $\mathbb{C}^e = 4 \frac{\partial^2 \psi_0}{\partial \mathbf{C} \partial \mathbf{C}}$ and $\mathbb{C}^n = 4 \frac{\partial^2 \psi_0}{\partial \mathbf{C} \partial \mathbf{A}}$</p>
--

Table 5.1: Algorithmic update scheme for reorientation (part 2)

Remark 5.4 (Implementation of alternative driving forces) For the alternative driving forces as described in remark 5.2, the derivatives of the direction \mathbf{z}^A with respect to \mathbf{n}^A and \mathbf{C} become more complex. For this analogous to equations (5.30) and (5.43), we obtain

$$\begin{aligned} \text{(iii)} \quad \frac{\partial \mathbf{z}^A}{\partial \mathbf{n}^A} &= \frac{\partial \mathbf{n}^C}{\partial \mathbf{n}^A} = \mathbf{0}; \\ \text{(iv)} \quad \frac{\partial \mathbf{z}^A}{\partial \mathbf{n}^A} &= \frac{\partial \mathbf{n}^S}{\partial \mathbf{n}^A} = \frac{\mathbf{1} - \mathbf{n}^S \otimes \mathbf{n}^S}{\|\tilde{\mathbf{n}}^S\|} \cdot \sum_{I=2}^3 \left[\lambda_I^S \frac{\partial \mathbf{n}_I^S}{\partial \mathbf{S}} + \mathbf{n}_I^S \otimes \frac{\partial \lambda_I^S}{\partial \mathbf{S}} \right] : \frac{\partial \mathbf{S}}{\partial \mathbf{n}^A} \end{aligned} \quad (5.45)$$

and

$$\begin{aligned} \text{(iii)} \quad \frac{\partial \mathbf{z}^A}{\partial \mathbf{C}} &= \frac{\partial \mathbf{n}^C}{\partial \mathbf{C}} = \frac{\mathbf{1} - \mathbf{n}^C \otimes \mathbf{n}^C}{\|\tilde{\mathbf{n}}^C\|} \cdot \sum_{I=2}^3 \left[\lambda_I^C \frac{\partial \mathbf{n}_I^C}{\partial \mathbf{C}} + \mathbf{n}_I^C \otimes \frac{\partial \lambda_I^C}{\partial \mathbf{C}} \right]; \\ \text{(iv)} \quad \frac{\partial \mathbf{z}^A}{\partial \mathbf{C}} &= \frac{\partial \mathbf{n}^S}{\partial \mathbf{C}} = \frac{\mathbf{1} - \mathbf{n}^S \otimes \mathbf{n}^S}{\|\tilde{\mathbf{n}}^S\|} \cdot \sum_{I=2}^3 \left[\lambda_I^S \frac{\partial \mathbf{n}_I^S}{\partial \mathbf{S}} + \mathbf{n}_I^S \otimes \frac{\partial \lambda_I^S}{\partial \mathbf{S}} \right] : \frac{1}{2} \mathbb{C}^e, \end{aligned} \quad (5.46)$$

respectively. The additional derivatives of the eigenvalues λ_I^C or λ_I^S with respect to the corresponding tensor \mathbf{C} or \mathbf{S} , respectively, result from the same derivations as the derivatives of the eigenvectors as described in appendix C.2. \blacksquare

5.4 Numerical examples

For the discussion of the constitutive specifications, made within this chapter, by means of numerical examples, we choose the same free energy function as in the latter two chapters

$$\psi_0 = \psi_0^{iso} + \psi_0^{ti} \quad \text{with} \quad \begin{cases} \psi_0^{iso} &= \frac{\lambda}{2} \ln^2 J + \frac{\mu}{2} [I_1 - 3 - 2 \ln J] \\ \psi_0^{ti} &= \frac{\alpha}{2} [I_4 - 1]^2 \end{cases} \quad (5.47)$$

depending on the principal invariants $I_1 = \text{tr } \mathbf{C} = I_1$ and $J = \det \mathbf{C} = \frac{1}{6} I_1^3 - \frac{1}{2} I_1 I_2 + \frac{1}{3} I_3$ as well as the mixed invariant $I_4 = \text{tr}(\mathbf{C} \cdot \mathbf{A})$. Since for anisotropy the stresses and strains are generally not coaxial, we consider a uniaxial tension test additionally to the uniaxial stress test as described in section 3.4.1 and section 4.4.1. We compare a material with fixed fibers and a material including reorientation. Further on, for more complex boundary conditions, we consider a transversely isotropic strip under tension and a cylindrical tube under inside pressure-type loading, again comparing a material with a fixed characteristic direction with a material including reorientation of the characteristic direction.

5.4.1 Uniaxial stress and uniaxial tension

At first, we consider uniaxial stress by means of a transversely isotropic cube, with an elongation of the cube to one and a half of its original length in z -direction, as illustrated in figure 5.3.a. We compare a material with a fixed characteristic direction with a

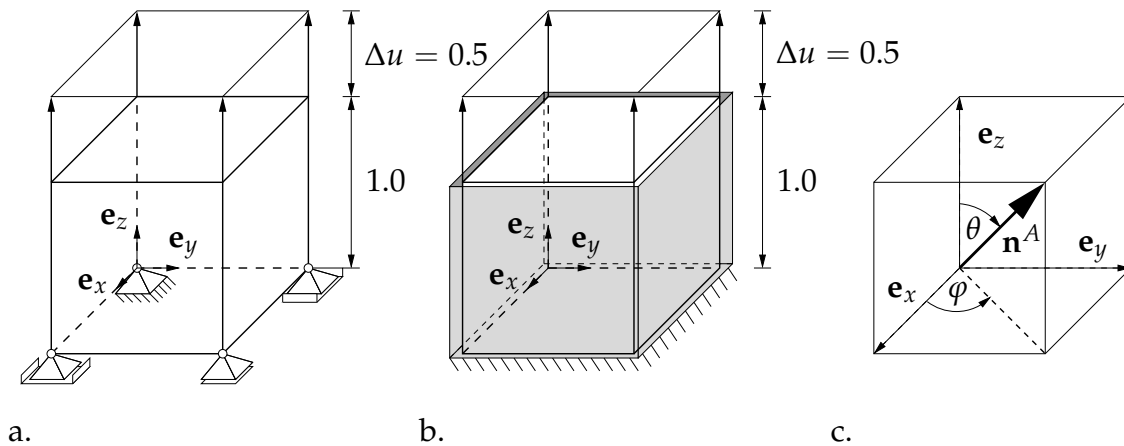


Figure 5.3: Loads and boundary conditions for (a) uniaxial stress and (b) uniaxial tension with (c) different orientations of the characteristic direction \mathbf{n}^A described by the angles θ and φ .

material including reorientation of the characteristic direction and different initial characteristic directions. The orientation of \mathbf{n}^A is, according to figure 5.3.c., described by the angles θ and φ . For the sake of clarity, the initial characteristic direction is arranged

in the y - z -plane, i.e., $\varphi = 90^\circ$, within this section. Further on, we compare strain and stress driven reorientation as described in equations (5.19.i) and (5.19.ii), respectively. The material parameters are the elasticity modulus $E = 15.0\text{N/mm}^2$ and the Poisson's ratio $\nu = 0.3$ related to the Lamé constant $\lambda = 8.654\text{N/mm}^2$ and the shear modulus $\mu = 5.769\text{N/mm}^2$ as well as the anisotropy parameter $\alpha = 5.0\text{N/mm}^2$. The relaxation time parameter t^* is assumed to be larger than the time step $\Delta t = 1.0 < t^*$, here we choose $t^* = 10.0$, $t^* = 100.0$ and $t^* = 200.0$.

At first, we consider a material with fixed fibers perpendicular to the loading direction, this means $\theta_0 = 90^\circ$. As expected for standard elasticity, the orientation of \mathbf{n}^A and the stresses do not change during the entire loading process, see figure 5.4. Due to the boundary conditions, all Cauchy stress components besides σ_{zz} are equal to zero.

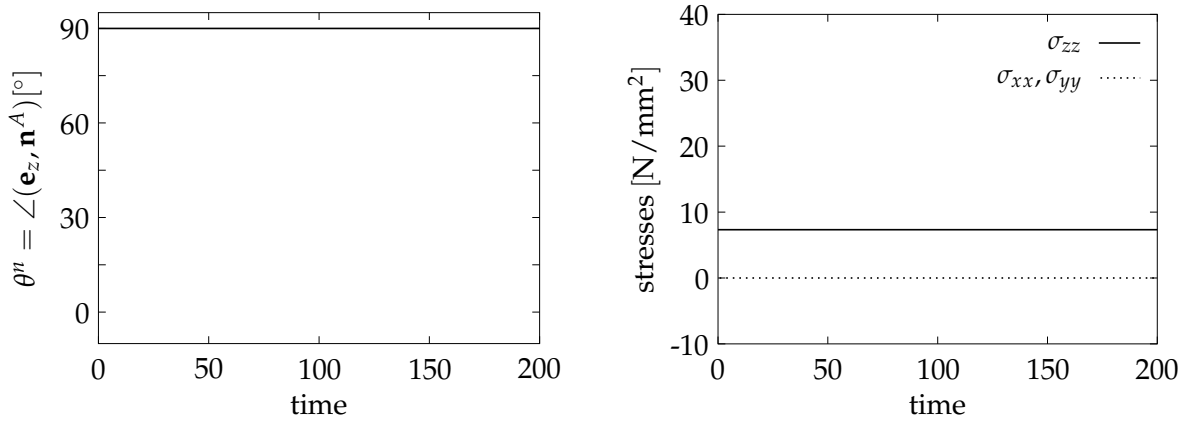


Figure 5.4: Results of the uniaxial stress test for a fixed characteristic direction \mathbf{n}^A perpendicular to the loading direction.

Next, we examine reorientation with the initial characteristic direction parallel to the loading direction, which means $\theta_0 = 0^\circ$. As one can read from figure 5.5, the characteristic direction also stays constant both for strain and stress driven reorientation, because the characteristic direction and the maximum principal stretch or strain direction are aligned ab initio. Consequently, the stress σ_{zz} is constant, too, but due to the stiffer characteristic direction at a higher level than in figure 5.4.

For reorientation with the initial characteristic direction perpendicular to the loading direction, i.e., $\theta_0 = 90^\circ$ one can read from figures 5.6 and 5.7 that the characteristic direction reorients gradually until it is aligned with the maximum principal strain or stress direction, respectively. Due to the boundary conditions, the characteristic direction as well as the principal strain and stress directions reorient in the y - z -plane, i.e., $\varphi^n \equiv \varphi^z \equiv 90^\circ$. Thus, the orientation of \mathbf{n}^A and \mathbf{z}^A is clearly described by the angles $\theta^n = \angle(\mathbf{e}_z, \mathbf{n}^A)$ and $\theta^z = \angle(\mathbf{e}_z, \mathbf{z}^A)$, respectively. Within this basic boundary value problem, the maximum principal directions at the beginning of the simulation and in the equilibrium state are aligned with the loading direction, both for strain and stress driven reorientation. As described in section 5.2.3, for both types it is observable that the reorientation process at the beginning proceeds faster than close to the final equilibrium state. For higher values of t^* the relaxation time is longer than for lower values of

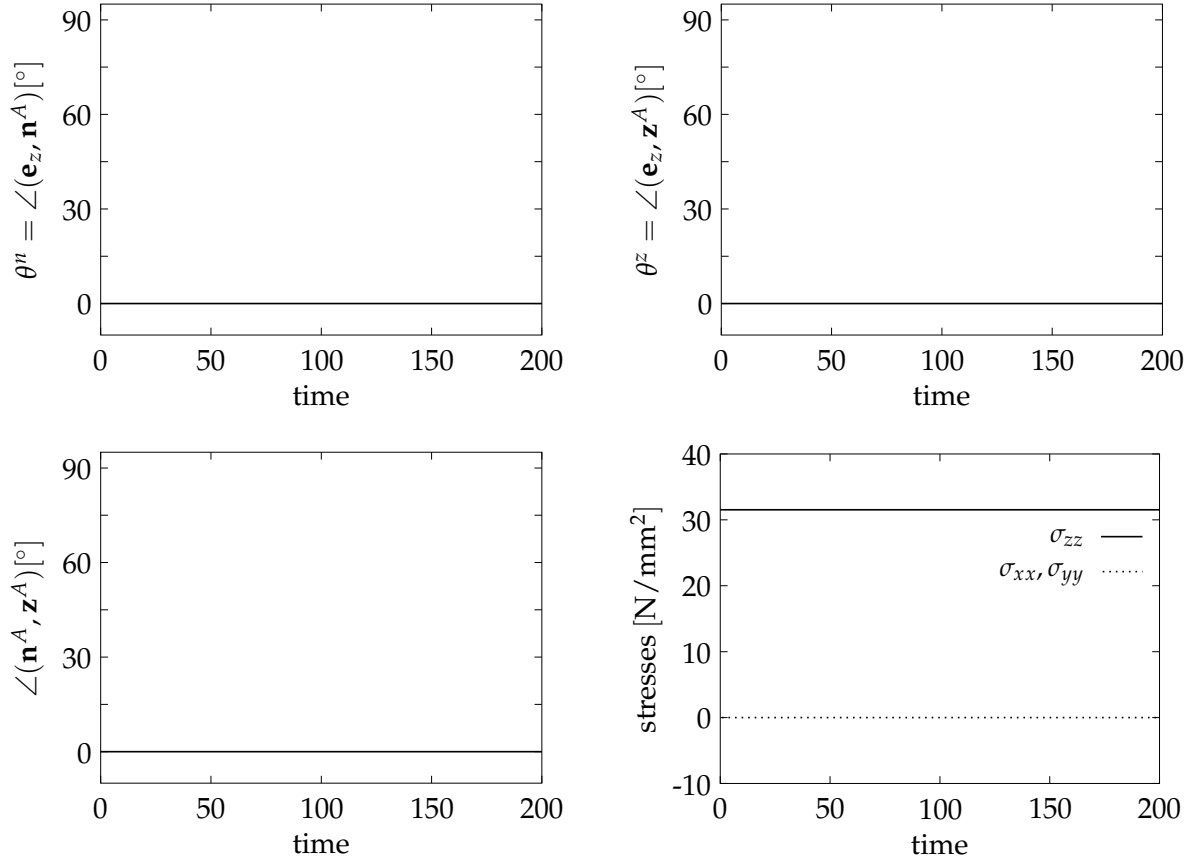


Figure 5.5: Results of the uniaxial stress test including reorientation with an initial direction \mathbf{n}^A parallel to the loading direction. Since the characteristic is initially aligned with the principal strain and stress direction, it stays constant both for strain and stress driven reorientation.

t^* . As aforementioned for $t^* \rightarrow \infty$ the evolution tends to zero, thus the fiber direction does not change. Furthermore, the normal stress in the loading direction starts with the same value as in figure 5.4 and changes, due to the reorientation and the alignment of the stiffer characteristic direction with the loading direction, until, in the final equilibrium state, the stresses are equal to that in figure 5.5. To elaborate whether the strains \mathbf{C} and stresses \mathbf{S} are coaxial, i.e., $\mathbf{C} \cdot \mathbf{S} = \mathbf{S} \cdot \mathbf{C}$, we introduce the scalar-valued quantity

$$\delta(\mathbf{C}, \mathbf{S}) = \frac{\|\mathbf{C} \cdot \mathbf{S} - \mathbf{S} \cdot \mathbf{C}\|}{\|\mathbf{C} \cdot \mathbf{S}\|}, \quad (5.48)$$

see also MENZEL [97]. With this, one can read from the corresponding graphs in figures 5.6 and 5.7 that the strains and stresses are coaxial and, consequently, the free energy is stationary in the final equilibrium state, for both types of reorientation. Since the fibers reorient such that the material stiffens, the energy increases to the final stationary state. Moreover, it is observable that a second state of coaxial strains and stresses appears for a minimum of free energy during the reorientation process. To compare strain and stress driven reorientation with each other, the results are combined in figure 5.8. At this, for the sake of clarity, we confine ourselves to simulations with $t^* = 10.0$. Since the variation of the maximum principal stress direction is higher than that of the maximum

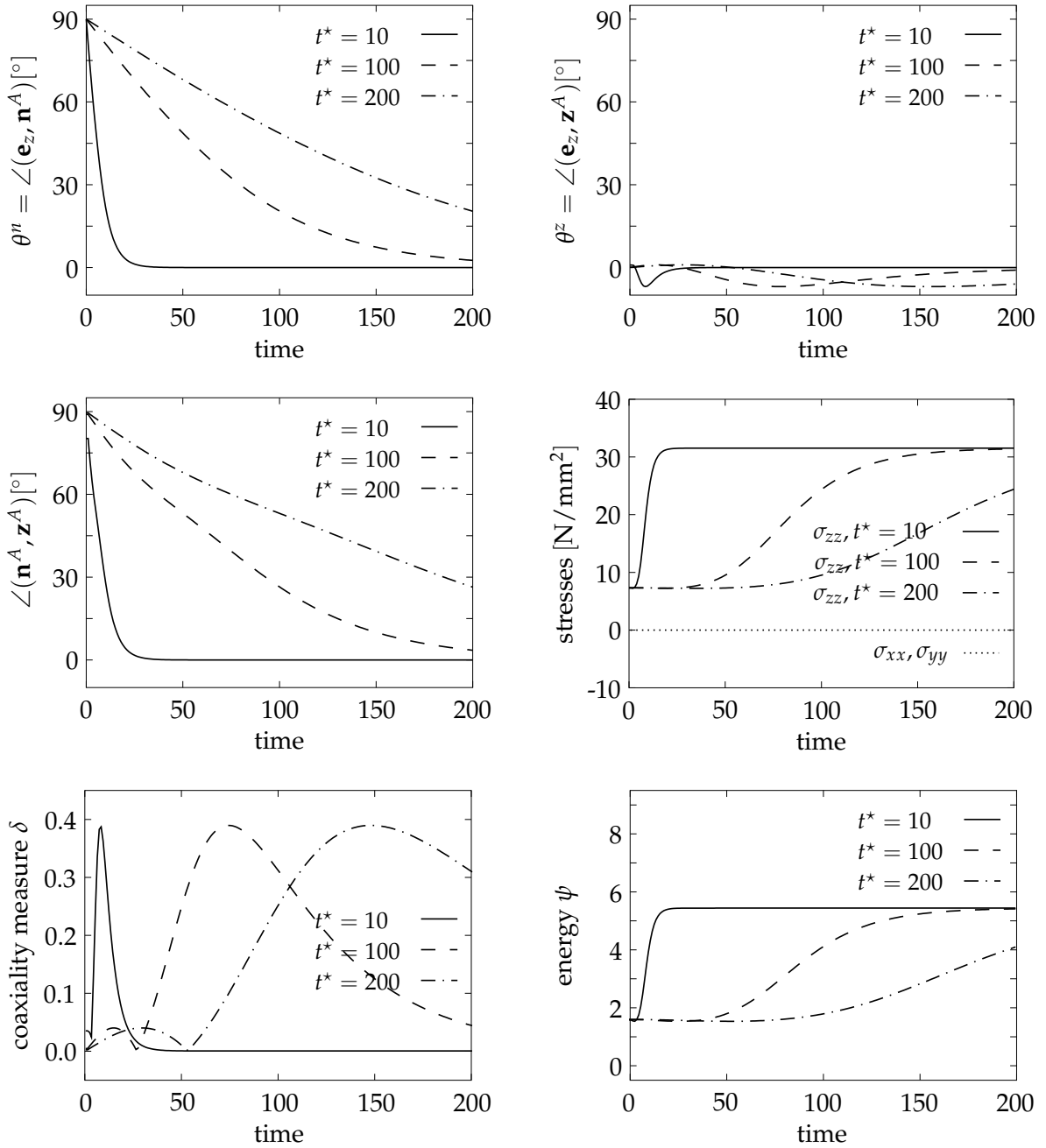


Figure 5.6: Results of the uniaxial stress test with reorientation along the maximum principal strain direction \mathbf{n}_3^C and the initial direction \mathbf{n}^A perpendicular to the loading direction.

principal strain direction, the convergence for reorientation along the principal stresses takes more time than for reorientation along the principal strains. Recall that due to the definition of the second Piola-Kirchhoff stresses (2.19), the maximum principal stress direction \mathbf{n}_3^S changes during the entire loading process, although the Cauchy stresses are uniaxial.

For a constant prescribed stretch direction we apply a uniaxial tension test as depicted in figure 5.3.B. At this, the x - and y - directions are completely fixed and we apply an elongation of the cube to one and a half of its original length in z -direction. Thus,

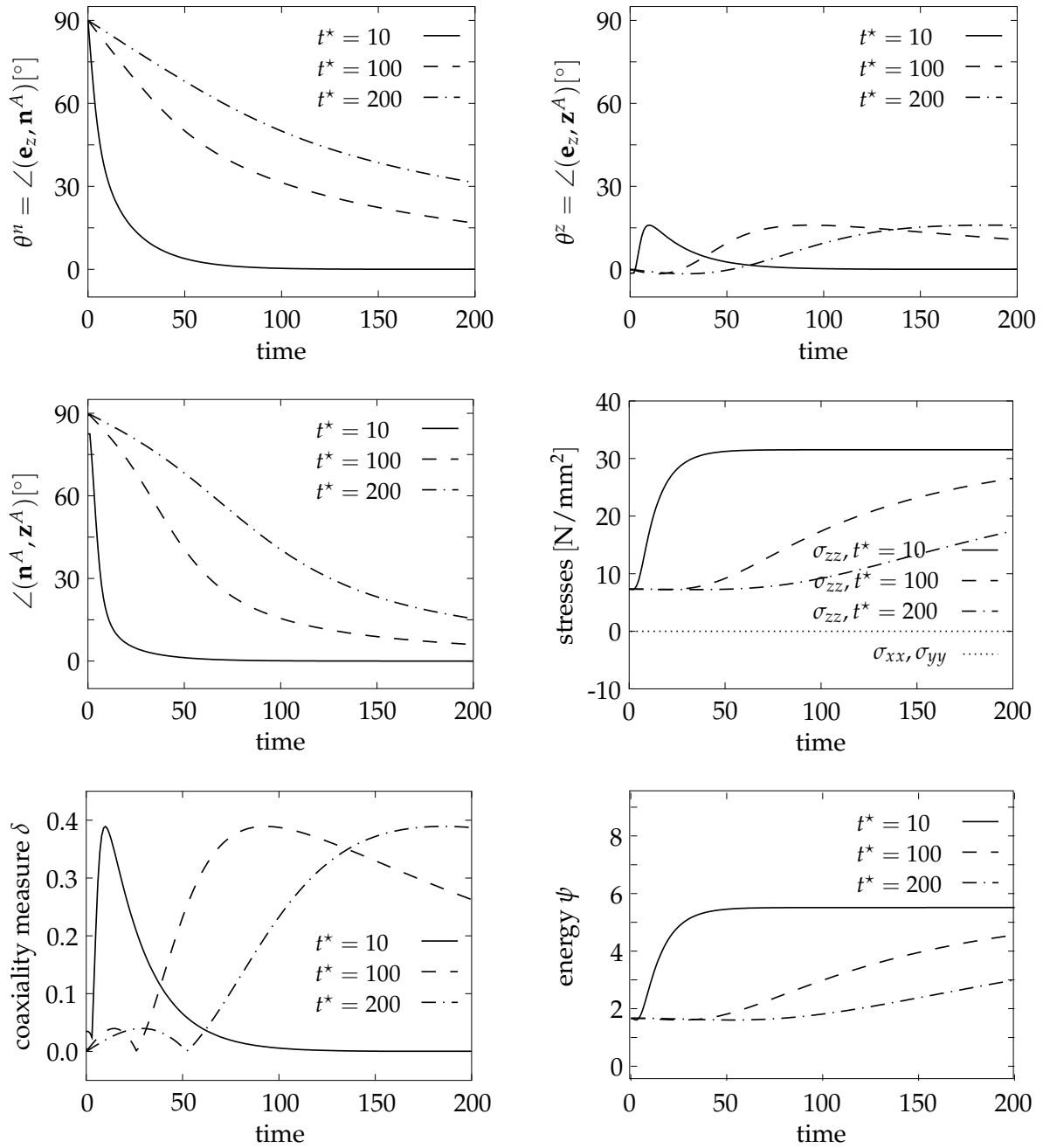


Figure 5.7: Results of the uniaxial stress test with reorientation along the maximum principal stress direction \mathbf{n}_3^S and the initial direction \mathbf{n}^A perpendicular to the loading direction.

the maximum principal stretch direction is prescribed in z -direction. We compare reorientation along the maximum principal strain direction with reorientation along the maximum principal stress direction for an initial characteristic direction perpendicular to the loading direction, i.e., $\theta = 90^\circ$, see figure 5.3.C. In figure 5.9 the results for the strain and stress driven reorientation are depicted for $t^* = 10.0$. As prescribed, the maximum principal strain direction is constant whereas the maximum principal stress direction changes during the reorientation process. Consequently, for reorientation along the principal stresses, it takes more time steps until the characteristic direction is

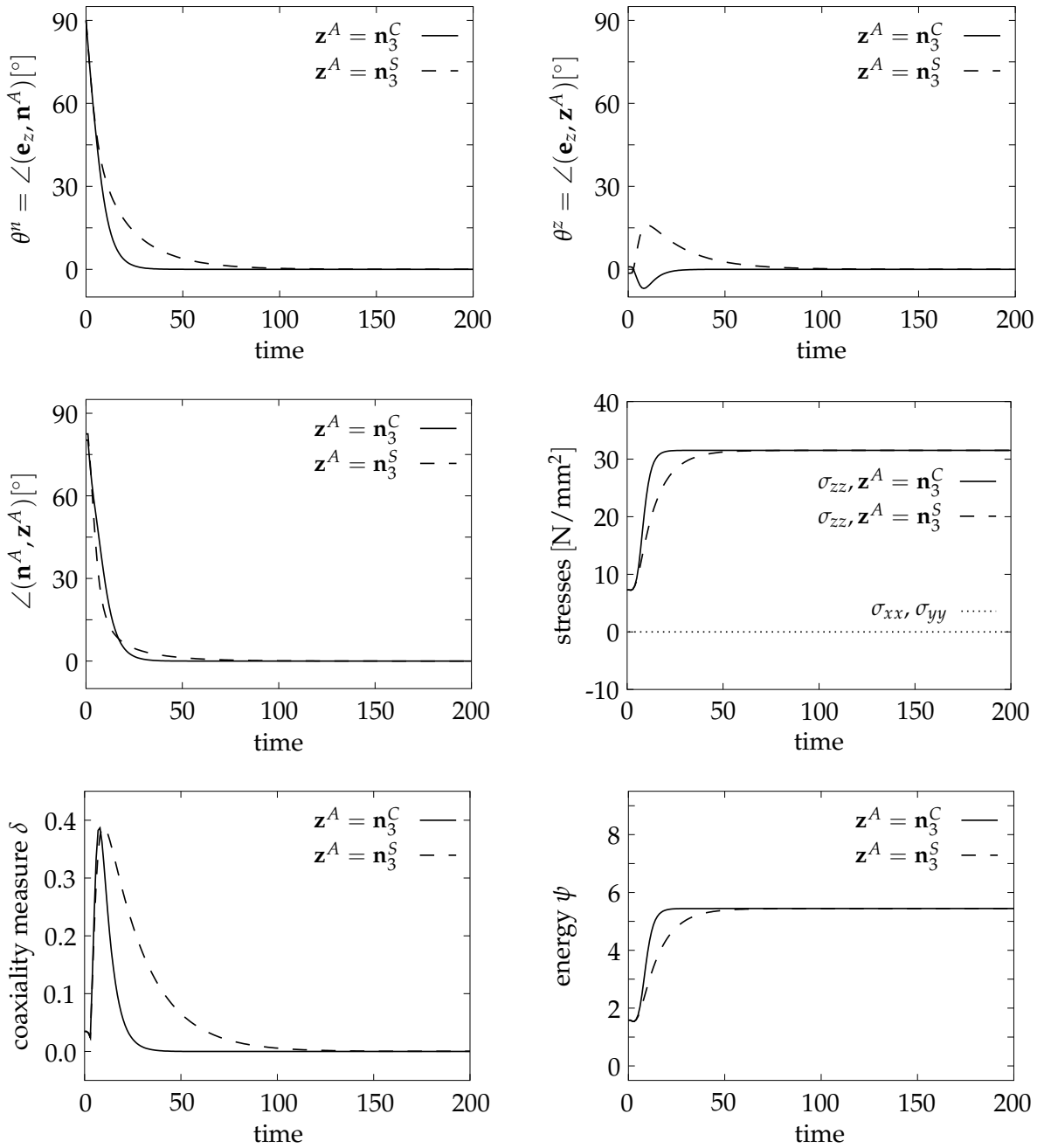


Figure 5.8: Results of the uniaxial stress test with an initial direction \mathbf{n}^A perpendicular to the loading direction. Comparison of reorientation along the maximum principal strain direction \mathbf{n}_3^C and reorientation along the maximum principal stress direction \mathbf{n}_3^S .

aligned with the principal direction than for reorientation along the principal strains. Again, the maximum principal strain and stress directions are parallel to the loading direction, at the beginning of the simulation and in the final equilibrium state. Moreover, one observes that the Cauchy stresses in the x - and y -directions are no longer equal to zero, and the stresses in the y -direction vary during the computation, until they are equal to those in x -direction, in the biological equilibrium. Since the stiffer fiber direction aligns with the z -direction, the corresponding normal stresses increase

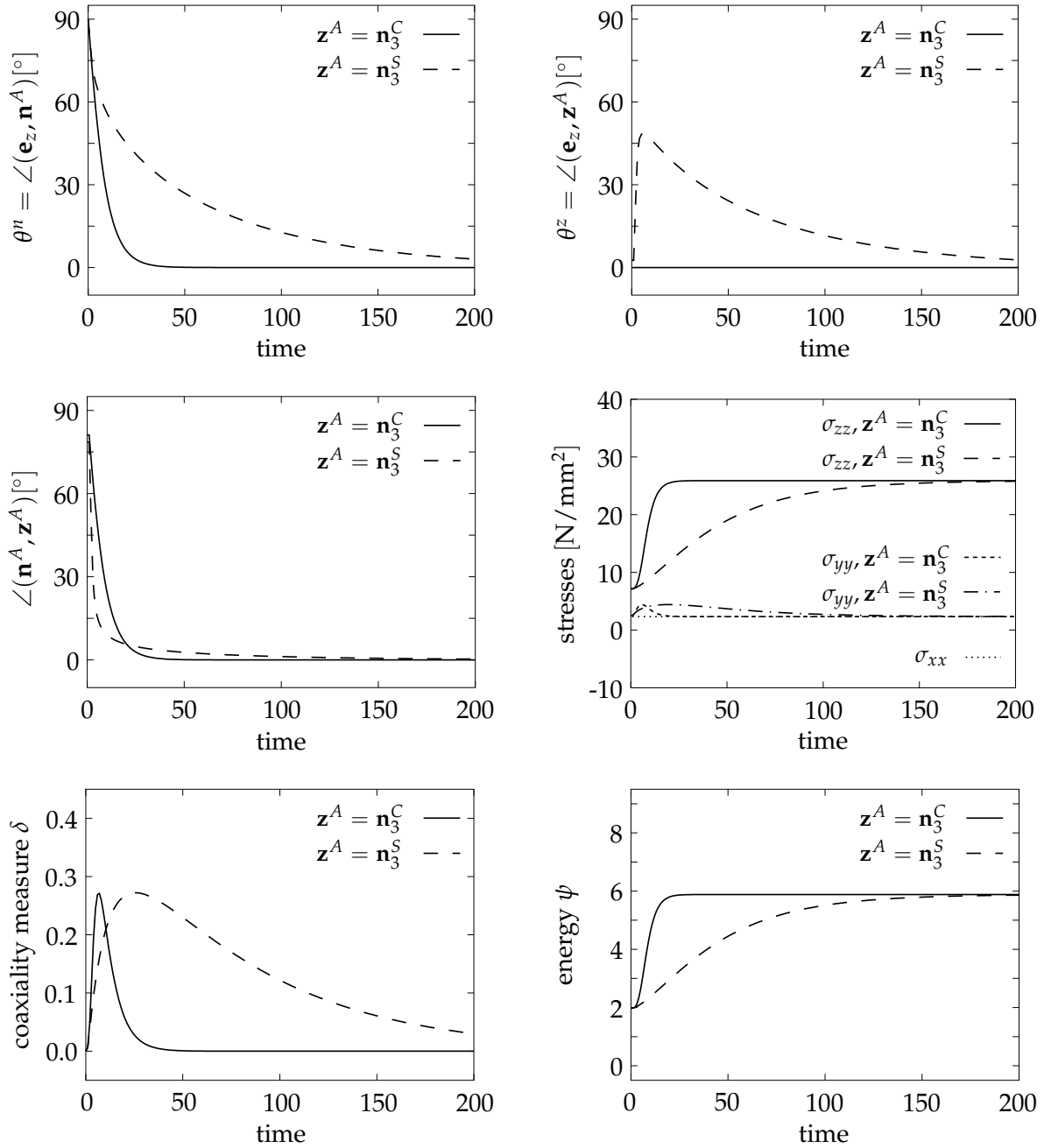


Figure 5.9: Results of the uniaxial tension test with an initial direction \mathbf{n}^A perpendicular to the loading direction. Comparison of reorientation along the maximum principal strain direction \mathbf{n}_3^C and reorientation along the maximum principal stress direction \mathbf{n}_3^S .

and reach a maximum value in the biological equilibrium state. For both types of reorientation, the strains and stresses are coaxial in the final equilibrium. The energy steadily increases to a stationary state in the final equilibrium state.

To consider an example in which the principal strain and stress directions differ at the beginning of the simulation, we choose an inclined orientation of the initial characteristic direction with $\theta_0 = 30^\circ$. The material parameters are identical to the previous ones but with a Poisson's ratio $\nu = 0.45$. For this, due to the boundary conditions

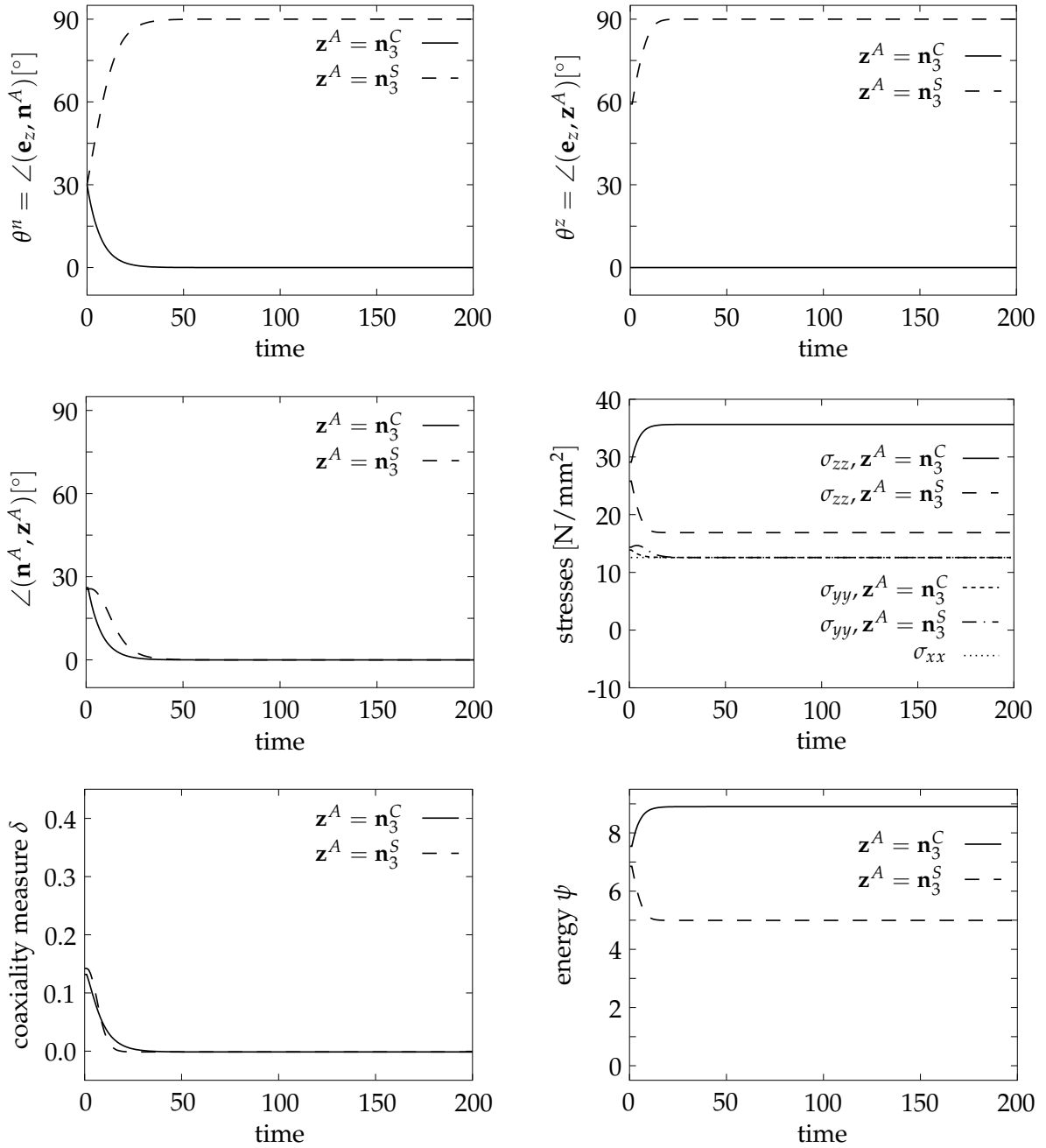


Figure 5.10: Results of the uniaxial tension test with an inclined initial direction \mathbf{n}^A . Comparison of reorientation along the maximum principal strain direction \mathbf{n}_3^C and reorientation along the maximum principal principal stress direction \mathbf{n}_3^S .

within the uniaxial tension test, the principal strain direction is, naturally, parallel to the loading direction. The principal stress direction lies in the y - z -plane and initially differs from the loading direction, see figure 5.10. For strain driven reorientation, one observes a reorientation of the characteristic direction until it is parallel to the loading direction. For stress driven reorientation, the characteristic direction aligns with the y -axis, which means perpendicular to the loading direction. However, in the final equilibrium state, the strains and stresses are coaxial both for an alignment with the

maximum principal strain direction and for an alignment with the maximum principal stress direction. Again, for strain driven reorientation, \mathbf{n}^A and \mathbf{z}^A are aligned faster than for stress driven reorientation. Again the normal stresses are constant in the x -direction and vary in the y - and z -directions. In the final equilibrium state $\sigma_{yy} = \sigma_{xx}$ for both types of reorientation. Since for strain driven reorientation the stiffer fiber is aligned with the z -direction, the corresponding stresses σ_{zz} are higher than for stress driven reorientation. Moreover, the free energy in the final equilibrium state is lower for an alignment with the maximum principal stress direction \mathbf{n}_3^S than for an alignment with the maximum principal strain direction \mathbf{n}_3^C .

5.4.2 Strip under tension

As a more complex example, a transversely isotropic strip either with fixed characteristic direction or including reorientation of the characteristic direction will be loaded by a constant displacement $\Delta u = 1.0$, as depicted in figure 5.11. The angle between the load-

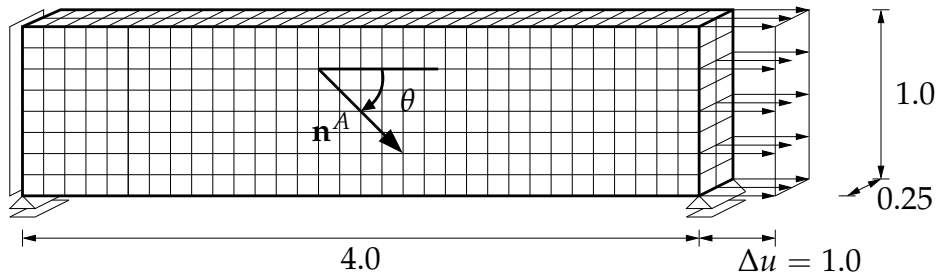


Figure 5.11: Discretization, loads and boundary conditions of the transversely isotropic strip. A displacement of $\Delta u = 1.0$ is applied to the left edge. The orientation of the characteristic direction is described by the angle θ .

ing direction and the initial characteristic direction is characterized as θ . For the material parameters we choose $E = 10.0\text{N/mm}^2$ and $\nu = 0.3$ related to $\lambda = 5.769\text{N/mm}^2$ and $\mu = 3.846\text{N/mm}^2$ as well as the anisotropy parameter $\alpha = 20.0\text{N/mm}^2$. The relaxation time parameter is $t_C^* = 10.0$ for strain driven reorientation and, because of the differences in convergence time, to $t_S^* = 5.0$ for stress driven reorientation. The time step is set to $\Delta t = 0.1$. At first, we again consider a material with fixed characteristic direction, the orientation is given with $\theta_0 = -45^\circ$. Figure 5.12 shows the deformation, the orientation of characteristic direction \mathbf{n}^A and the maximum principal directions \mathbf{n}_3^C and \mathbf{n}_3^S . In the contour plots the angle between \mathbf{n}^A and the maximum principal directions \mathbf{n}_3^C and \mathbf{n}_3^S as well as the coaxiality measure δ , see equation (5.48), are depicted. As expected for transverse isotropy, due to the stiffer characteristic direction, the initially rectangular strip deforms in an s-shape form. Since the characteristic direction is fixed, the deformation does not change during the constant displacement load.

Second, we consider strain and stress driven reorientation, again with $\theta_0 = -45^\circ$. As depicted in figure 5.13, the deformation in the first loading step is, as expected, identical to that for fixed fibers. In the following time steps, the characteristic directions

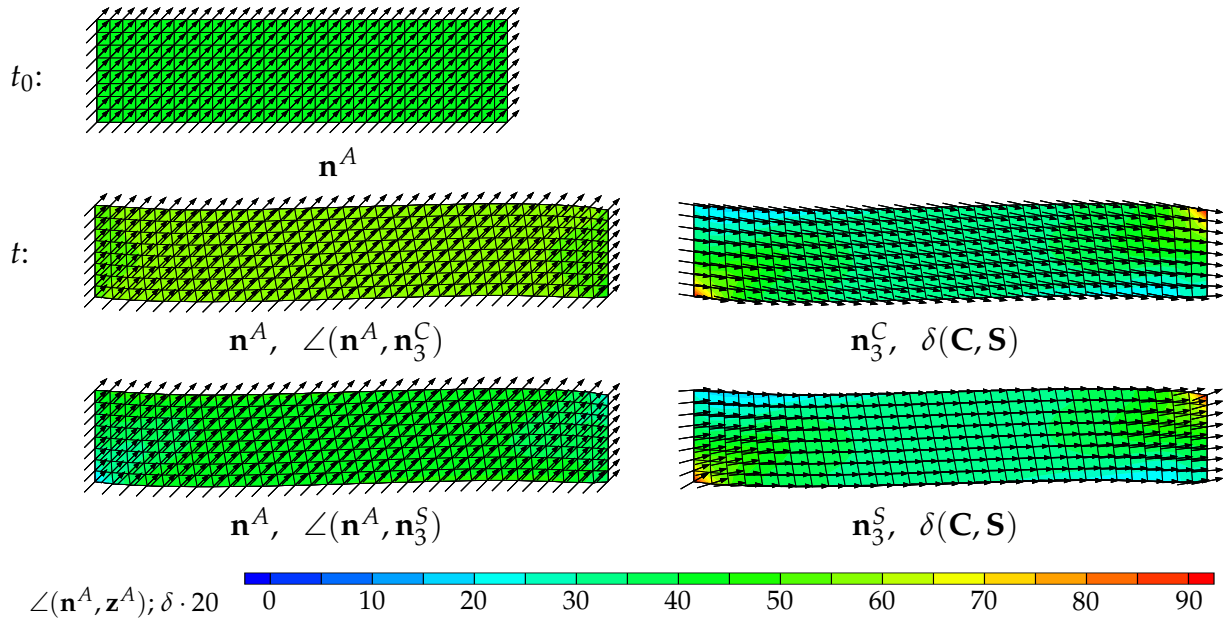


Figure 5.12: Deformation and some characteristic quantities of the transversely isotropic strip with fixed characteristic direction under tension at $t_0 = 0$ and $t > t_0$. The angle between the initial characteristic direction and the loading direction is $\theta_0 = -45^\circ$.

rotate until in the final equilibrium state the angle between \mathbf{n}^A and \mathbf{z}^A is zero. Both for strain and stress driven reorientation, the characteristic direction and the principal strain and stress direction are aligned with the loading direction. Consequently, for both types of reorientation, the deformation of the strip changes from the s-shape to an almost homogeneous elongation of the strip, and the stresses and strains are coaxial in the final equilibrium state. Although the relaxation time parameter for strain driven reorientation is chosen twice as large as the one for stress driven reorientation, namely $t_C^* = 2.0t_S^*$, in the latter case it needs more time steps to reach the the final equilibrium state. The numerical convergence is quadratic both on the global and on the local level, as exemplary depicted in tables 5.2 and 5.3. Therein the left tables, in each case, show the global convergence for the first three loading steps. In the right tables the local convergence in a point of the left bearing is depicted for the global iterations marked gray on the left. In the other loading steps a similar convergence can be observed.

To show the independence of the final state on the initial fiber direction, we next additionally study a fiber orientation according to the angle $\theta_0 = -120^\circ$. Further on, as described in remark 5.1, the material behavior depends only on the orientation of \mathbf{n}^A , but not on the direction. To verify this, an initial fiber angle of $\theta_0 = 60^\circ$ is considered so that the fiber points opposite to the direction represented by $\theta_0 = -120^\circ$. As one can see in figures 5.14 and 5.15 both the independence on the initial configuration and the independence on the direction of the fiber vector, is maintained for strain and stress driven reorientation.

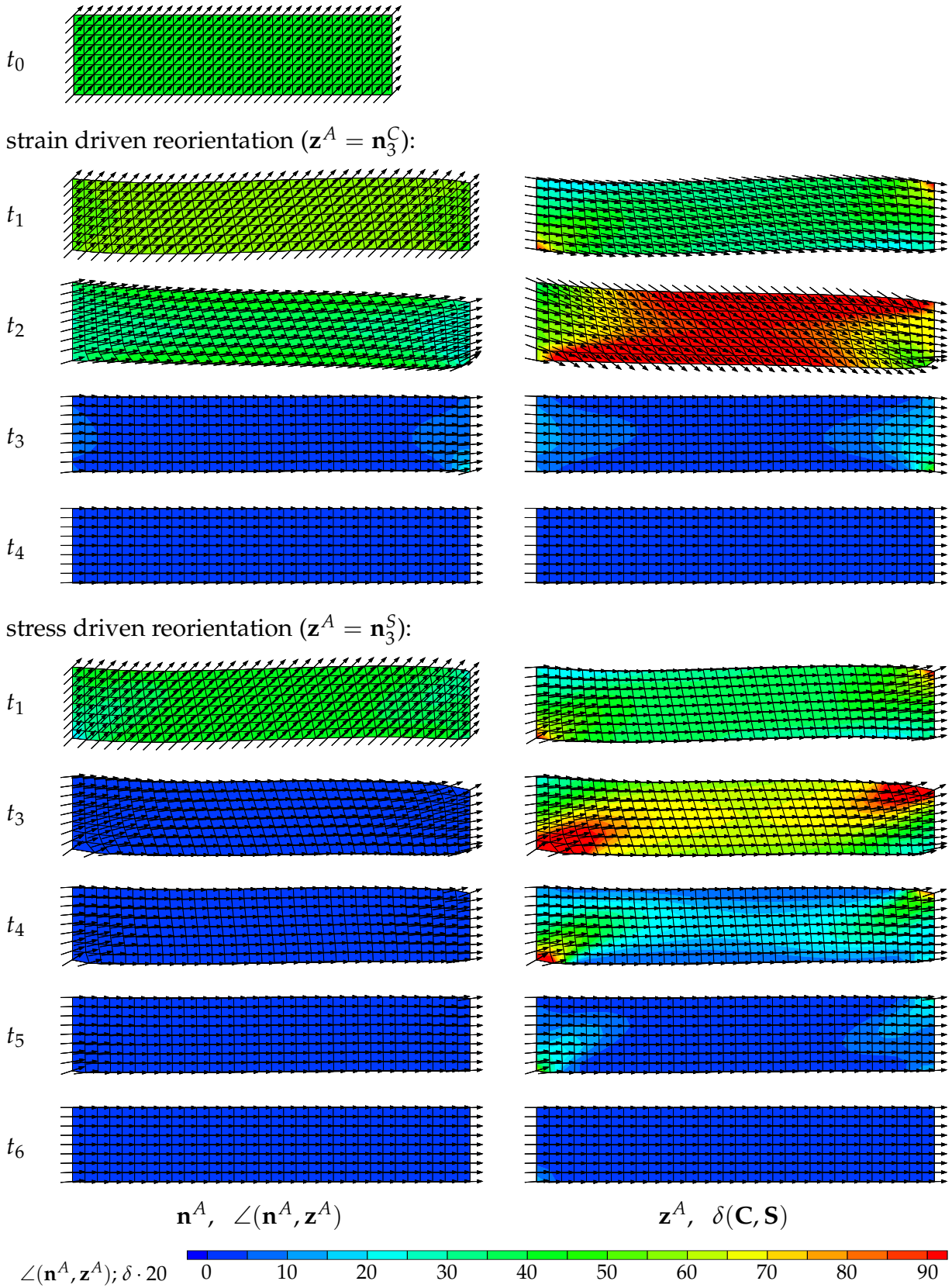


Figure 5.13: Deformation and some characteristic quantities of the transversely isotropic strip under tension at $t_0 = 0$, $t_1 = \Delta t$, $t_2 = 50 \Delta t$, $t_3 = 100 \Delta t$, $t_4 = 200 \Delta t$, $t_5 = 400 \Delta t$ and $t_6 = 800 \Delta t$. The angle between the initial characteristic direction and the loading direction is $\theta_0 = -45^\circ$.

inc	global it.	global residual
1	0	5.19615E+00
1	1	1.78594E-01
1	2	1.17985E-02
1	3	1.49095E-04
1	4	4.74097E-08
1	5	1.39653E-14
2	0	5.80585E-02
2	1	7.81362E-04
2	2	5.12785E-07
2	3	1.00017E-12
3	0	5.64678E-02
3	1	8.12269E-04
3	2	4.66719E-07
3	3	8.57712E-13

global convergence

inc	global iteration	local iteration	local residual
1	4	1	7.45637075E-03
1	4	2	1.65287778E-05
1	4	3	7.45841642E-11
1	5	1	7.45637209E-03
1	5	2	1.65287901E-05
1	5	3	7.45845562E-11
2	0	1	7.07034309E-03
2	0	2	1.30493897E-05
2	0	3	4.09969550E-11
2	1	1	6.86824077E-03
2	1	2	1.19161426E-05
2	1	3	3.31267290E-11

local convergence

Table 5.2: Quadratic convergence on the global and on the local level for strain driven reorientation

inc	global it.	global residual
1	0	5.19615E+00
1	1	1.76210E-01
1	2	7.68834E-03
1	3	1.42211E-04
1	4	3.46068E-08
1	5	1.59632E-14
2	0	4.24187E-02
2	1	2.85094E-04
2	2	1.63652E-07
2	3	5.42645E-14
3	0	4.22067E-02
3	1	2.81362E-04
3	2	1.52259E-07
3	3	4.88088E-14

global convergence

inc	global iteration	local iteration	local residual
1	4	1	1.25502160E-02
1	4	2	3.23125787E-07
1	4	3	1.11022303E-16
1	5	1	1.25502160E-02
1	5	2	3.23125790E-07
1	5	3	1.11022302E-16
2	0	1	1.24318177E-02
2	0	2	3.13964952E-07
2	0	3	1.11022302E-16
2	1	1	1.24644729E-02
2	1	2	3.16473606E-07
2	1	3	1.35525272E-20

local convergence

Table 5.3: Quadratic convergence on the global and on the local level for stress driven reorientation

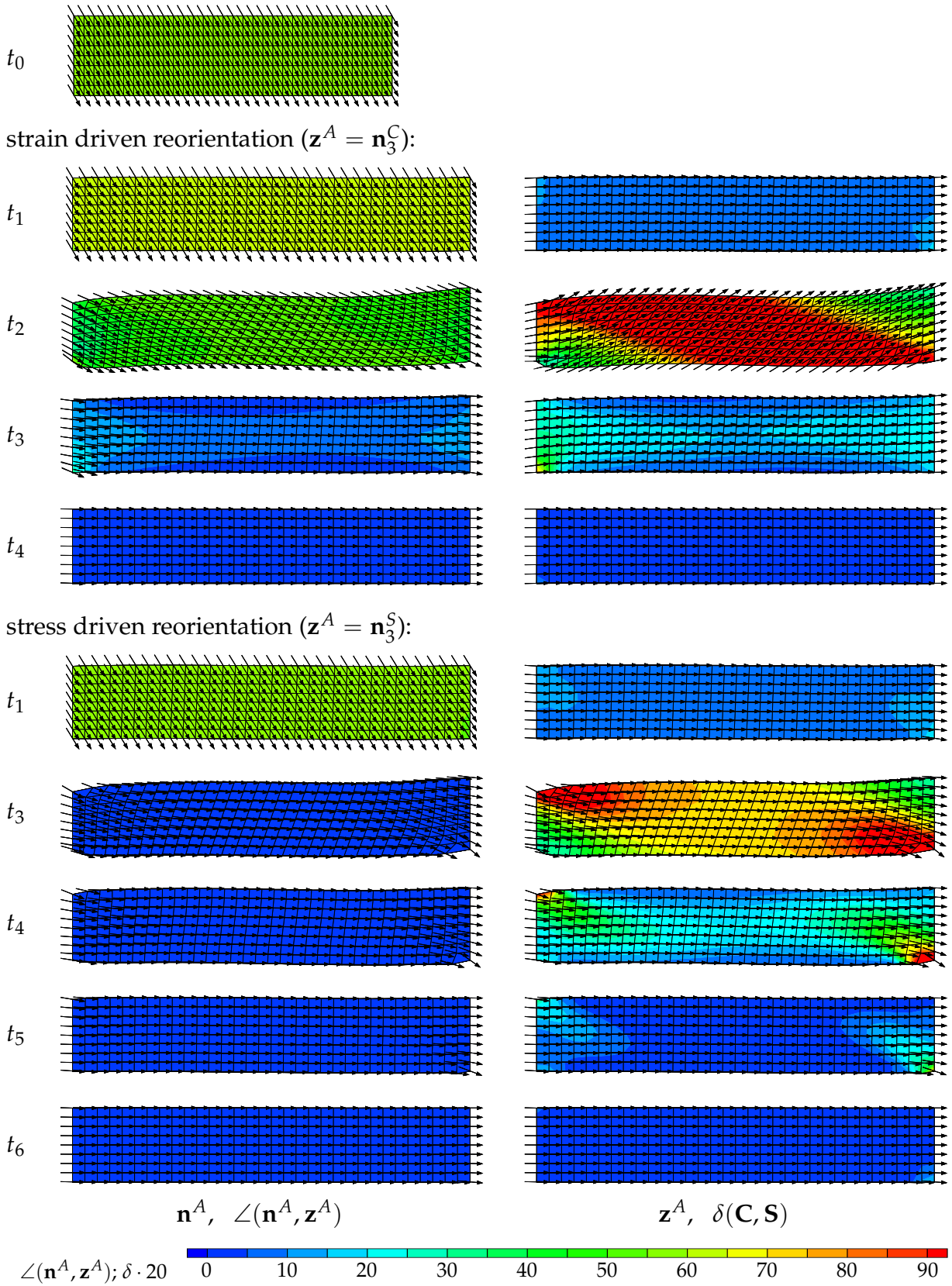


Figure 5.14: Deformation and some characteristic quantities of the transversely isotropic strip under tension at $t_0 = 0, t_1 = \Delta t, t_2 = 50 \Delta t, t_3 = 100 \Delta t, t_4 = 200 \Delta t, t_5 = 400 \Delta t$ and $t_6 = 800 \Delta t$. The angle between the initial characteristic direction and the loading direction is $\theta_0 = 60^\circ$.

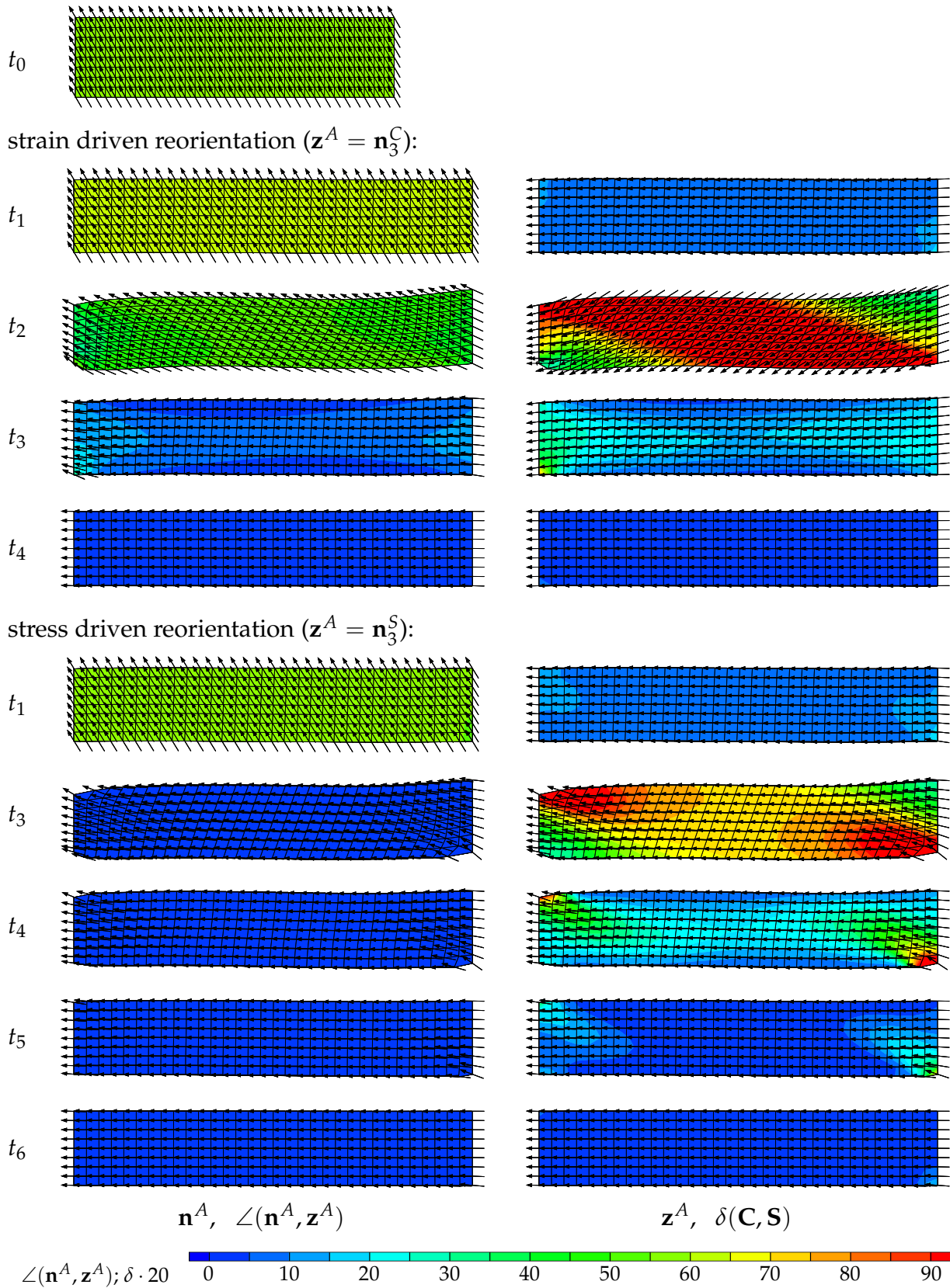


Figure 5.15: Deformation and some characteristic quantities of the transversely isotropic strip under tension at $t_0 = 0, t_1 = \Delta t, t_2 = 50 \Delta t, t_3 = 100 \Delta t, t_4 = 200 \Delta t, t_5 = 400 \Delta t$ and $t_6 = 800 \Delta t$. The angle between the initial characteristic direction and the loading direction is $\theta_0 = -120^\circ$.

5.4.3 Tube under inside radial displacement load

In the previous examples we considered problems with more or less homogeneous deformations in the final state. At this point we consider a non-homogeneous deformation by means of a transversely isotropic tube with a radial displacement load as depicted in figure 5.16. We apply an out-warded sinusoidal displacement load at the

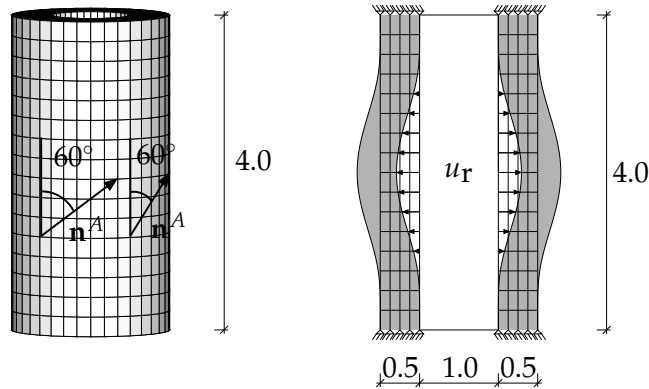


Figure 5.16: Loads and boundary conditions for the inhomogeneously deformed tube.

inside of the tube with a maximum displacement $u_r^{\max} = 0.3$ in the middle of the tube. The upper and lower boundaries of the tube are fixed in space. The characteristic direction is arranged in the tangential plane with an inclination angle of 60° . The material parameters are $E = 3.0\text{N/mm}^2$ and $\nu = 0.4$, related to $\lambda = 4.285\text{N/mm}^2$ and $\mu = 1.071\text{N/mm}^2$, and $\alpha = 2.0\text{N/mm}$. The time step is set to $\Delta t = 0.1$. Once more, materials with fixed and reorienting characteristic directions are compared, as well as strain and stress driven reorientation. The relaxation time parameter for strain and stress driven reorientation is $t_C^* = 10.0$ and $t_S^* = 5.0$, respectively. As one can see in figure 5.17, for fixed fibers, the tube twists at the first time step due to higher stiffness of the fibers. The angle between the characteristic direction and the maximum principal strain or stress direction is distributed inhomogeneously. According to expectations, for a fixed load level, the characteristic direction and the deformation stay constant. In figure 5.18 the deformation, the fiber directions and the angle between \mathbf{n}^A and \mathbf{z}^A as well as the coaxiality measure $\delta(\mathbf{C}, \mathbf{S})$ are depicted for strain driven reorientation. For the first time step, as expected, the deformation and fiber distribution is similar to the case with fixed fibers. For the following time steps, however, the fibers begin to rotate until they are aligned with the maximum principal strain direction. Again the reorientation at the beginning proceeds faster than close to the final equilibrium state. The maximum principal stretch direction is tangential in the middle of the tube and axial at the upper and lower boundary of the tube. Consequently, the final fiber distribution is directed axially in the upper and lower parts and tangentially in the middle part. Due to the reorientation of the fibers, the twist of the tube, indicated at the beginning of the

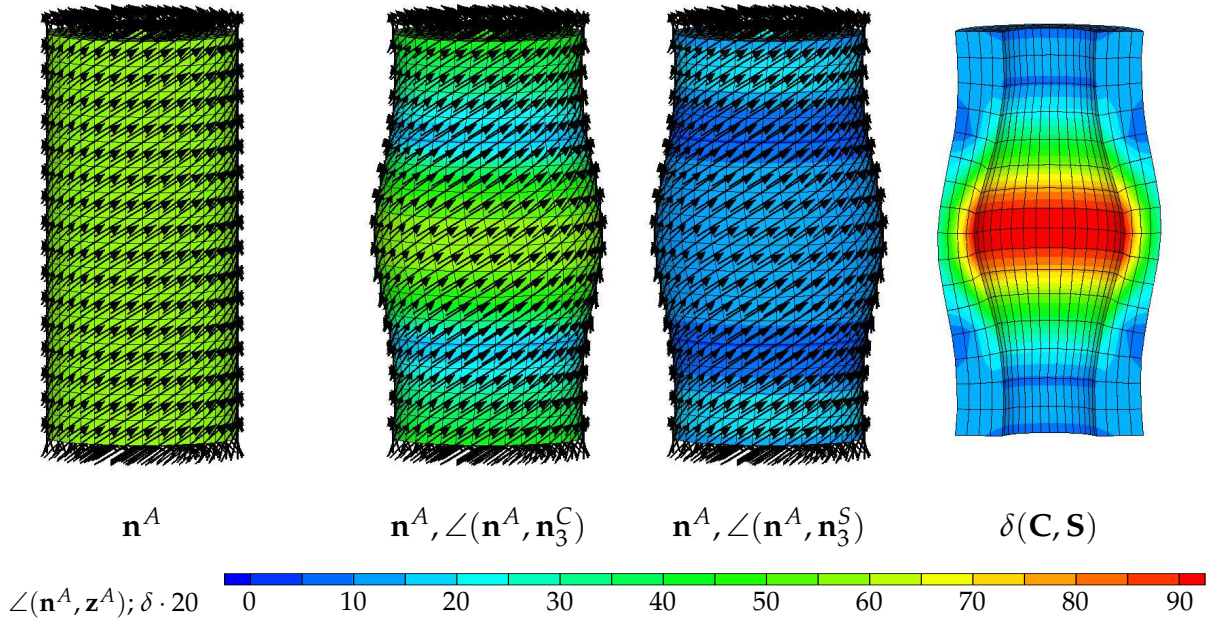


Figure 5.17: Deformation and some characteristic quantities of the transversely isotropic tube with fixed characteristic direction at $t_0 = 0$ (left figure) and $t > t_0$ (three figures on the right).

deformation, recedes over the simulation. Analogous observations can be made for stress driven reorientation, as depicted in figure 5.19. Again, although the relaxation time parameter is half of that for strain driven reorientation, i.e., $t_{\mathcal{S}}^* = 0.5t_{\mathcal{C}}^* = 5.0$, the reorientation occurs much slower than for strain driven reorientation.

5.5 Discussion

In this chapter we focus on reorientation in transversely isotropic elastic materials, i.e., rotation of a single fiber direction. Equivalent to the latter two chapters, we excluded mass changes in any case from the general framework discussed in chapter 2 by an adequate choice of constitutive equations. Based on mathematical and biomechanical observations, we consider both principal strains and principal stresses as stimuli for the reorientation process, and compare these two approaches. Since we restrict ourselves to materials with one family of fibers, it seems reasonable to choose an alignment with maximum principal directions. Further on, in analogy to the theory of shells, we avoided drilling rotations. Nonetheless, due to the general framework, combinations with remodeling and growth are as straightforward realizable as further forms of reorientation. For a geometrically exact update of the characteristic direction we applied an exponential scheme. In contrast to previous contributions, see for instance MENZEL [97], the present work includes consistent linearizations of the rotational update. Since, in contrast to the strains, the stresses depend on the fiber direction and, consequently, vary during the local update procedure, the linearizations for stress driven reorientation are more cumbersome than for strain driven reorientation. Nonetheless,

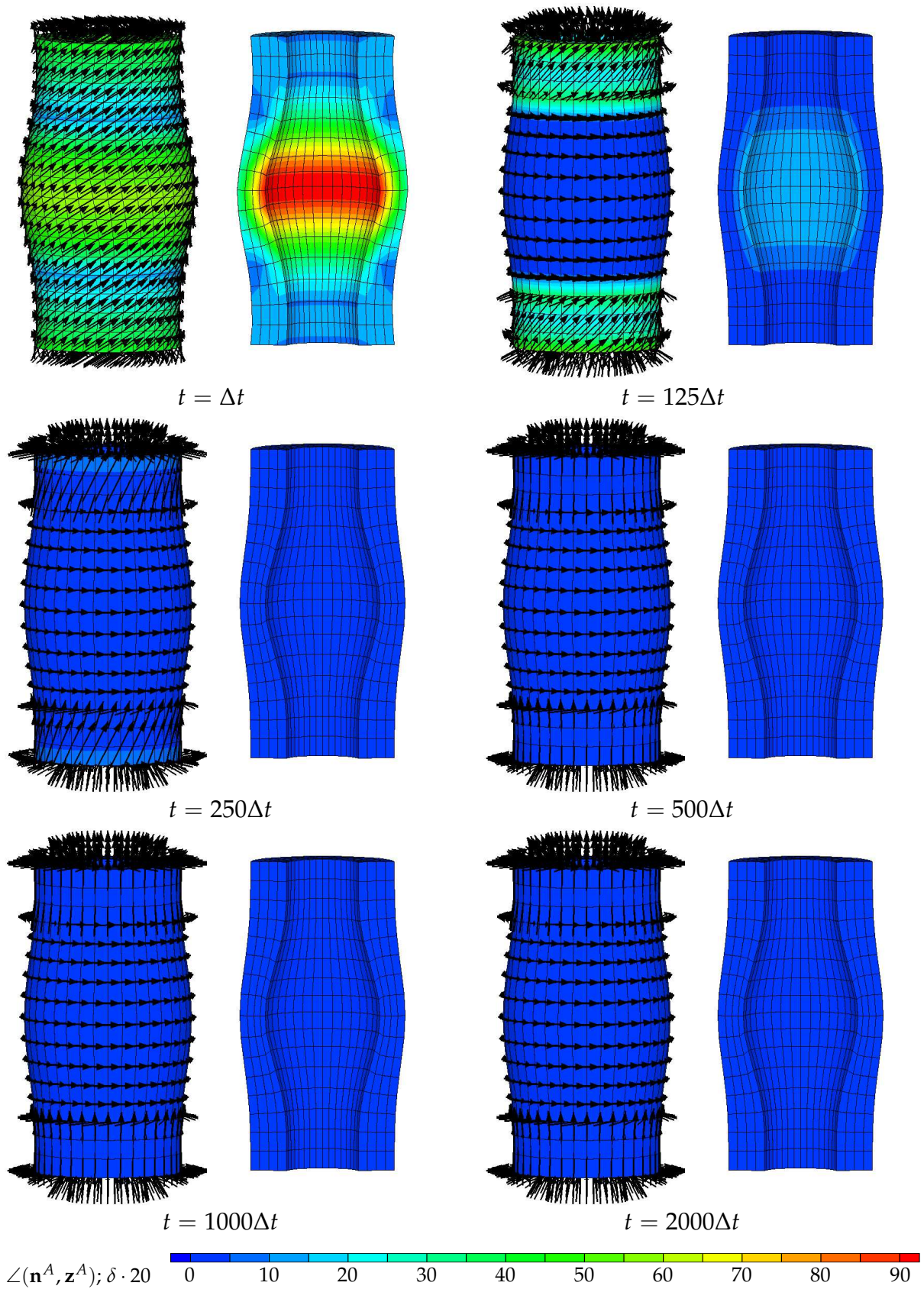


Figure 5.18: Deformation of the transversely isotropic tube for strain driven reorientation. The left figures show the orientation of \mathbf{n}^A and the angle $\angle(\mathbf{n}^A, \mathbf{z}^A)$ and the right figures show the coaxiality measure $\delta(\mathbf{C}, \mathbf{S})$.

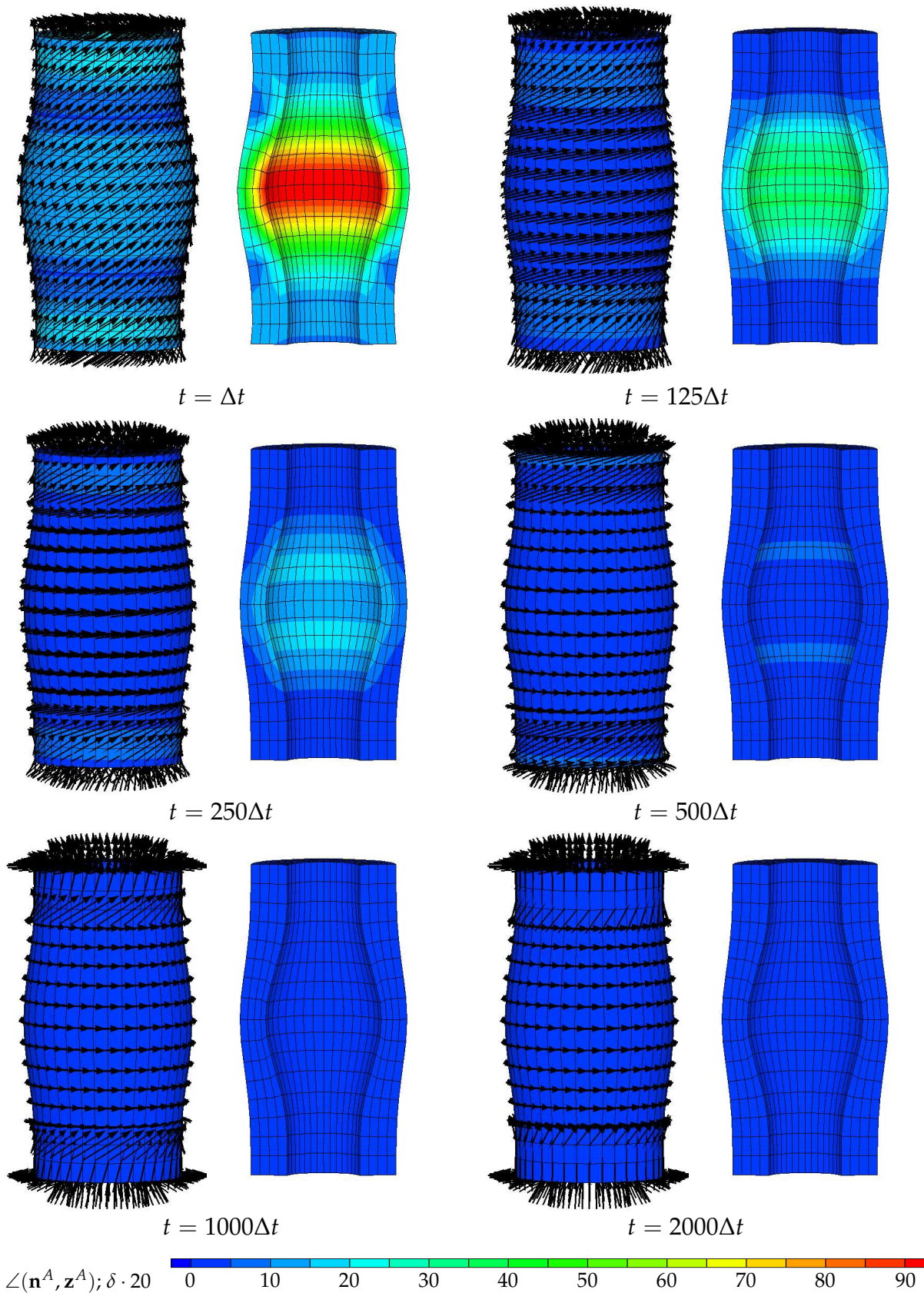


Figure 5.19: Deformation of the transversely isotropic tube for stress driven reorientation. The left figures show the orientation of \mathbf{n}^A and the angle $\angle(\mathbf{n}^A, \mathbf{z}^A)$ and the right figures show the coaxiality measure $\delta(\mathbf{C}, \mathbf{S})$.

the strategies are the same. This can also be observed by means of the update algorithm in schedular form. In the main, the algorithms for strain and stress driven reorientation are equivalent, but for the stress driven case, the alignment direction, namely the principal stress direction, has to be computed in each local iteration step. Thus, the computational costs for stress driven reorientation are higher than for strain driven reorientation. For both types of reorientation, the solution converges quadratically on the local and the global level. Due to choice of the evolution equation for the fiber direction, the reorientation converges over time to a final equilibrium state. For all numerical examples within this work, we observed, that the number of time steps required to reach the final equilibrium state is a multiple higher for stress driven reorientation than for strain driven reorientation. Depending on the boundary conditions, we mostly get same results for both types of reorientation, but not in all computations. It seems, that the stronger the boundary conditions are, i.e. the less free boundaries we assume, the higher are the differences between both types of reorientation. But this is solely a very vague conclusion which needs more experimental conclusiveness. Not for nothing, it is a very extensive topic of current research, to examine how mechanotransduction on cell and tissue level works.

6 Discussion

6.1 Conclusion

The main concern of this contribution is the computational modeling of remodeling, growth and reorientation for transversely isotropic materials. Within this work the term *remodeling* signifies volume preserving mass changes, i.e., pure density changes, whereas density preserving mass changes, i.e., pure volume changes, are denoted as *growth*. For these two phenomena the characteristic direction describing transverse isotropy is assumed to be constant. Inversely, the sole change of the characteristic direction for a constant mass is discussed as *reorientation*.

For a combination of the three above mentioned effects within one framework, the fundamental equations are initially discussed in a general form. This requires the description of the overall kinematics, the balance equations and the constitutive setting. In the course of this, the possibility of volume changes is incorporated within the kinematic framework by a split of the total deformation into a growth part and an elastic part. This includes the introduction of a generally incompatible intermediate configuration as well as a growth deformation tensor and an elastic deformation tensor, see SKALAK ET AL. [125]. An analogous approach is common for the continuummechanical description of finite elastoplasticity, as first introduced by LEE [90]. The ability to describe mass changes, i.e., changes of volume and density, is realized by the introduction of a mass source in the material configuration, which also affects the formulation of the balance equations, or more precisely, of the mass balance. Additionally, the change of density has an influence on the free energy and, thus, on the constitutive equations. This is taken into account within this work by weighting the free energy with a relative density, as recommended by HARRIGAN & HAMILTON [46]. The ability to reorient the characteristic direction is determined on the constitutive level as well. Additional material equations have to be defined specifying the form of reorientation. The quantities describing remodeling, growth and reorientation can be introduced in the continuummechanical setting by using internal variables. For a specific description of the individual effects, concrete approaches must be considered.

To describe remodeling as pure changes of density, the effects of growth and reorientation are suppressed in the general approach. Specifically, to prevent growth, the growth deformation tensor is equated with the identity so that the elastic deformation equals the total deformation. Consequently, the intermediate configuration can be neglected. Further, to prevent reorientation, the characteristic direction is set constant. For the admittance of density changes, the material density is introduced as an

internal variable. Due to the balance of mass, its evolution takes the interpretation of a mass source. Within this work, the mass source is defined based on the arguments of HARRIGAN & HAMILTON [46,47]. For the implementation standard finite elements can be used with an internal variable formulation for the density. To compute the density field from its evolution in time, an implicit Euler backward scheme is applied. To update the density within a local Newton iteration, the appropriate equation is linearized. Equivalently, the computation of the incremental tangent modulus in a finite element setting is realized by consistent linearizations. This requires computation of the change of density with respect to the change of strains. Since solely the evolution of density is specified, the term in demand is computed via the derivative of the discrete residual of the density in the Euler backward scheme. The complete algorithm is summarized in a scheduler manner. Finally, the material behavior is demonstrated in terms of numerical examples. After exemplification of the basic features by an isotropic simple tension test, the more biologically relevant examples of a human femur and a three dimensional cylindrical tube are considered both isotropically and transversely isotropically.

Analogously, to describe growth as pure volume changes, the other two effects are suppressed in the material model by appropriate specifications. For this, analogous to remodeling, the characteristic direction is constant for pure growth. Further on, density preservation from the initial to the intermediate configuration is prescribed. Consequently the mass source follows directly from the growth deformation tensor. Within the determination of transversely isotropic growth, we claim that the characteristic direction does not change during the growth process. Consequently the characteristic direction is the principal direction of the growth deformation tensor, which is characterized by two values: the stretch ratio in the fiber direction and that perpendicular to the fiber. These stretch ratios are treated as internal variables. For the specification of their evolution in time, stress driven growth is applied distinguishing between tension and compression, as recommended by LUBARDA & HOGER [93]. In contrast to these authors, we assume a dependence of the stretch ratios on the Mandel stresses rather than on the elastic Piola-Kirchhoff stresses. Analogous to remodeling, for the implementation into a finite element code, the algorithmic evolution of the stretch ratios as well as the incremental tangent modulus are derived based on an implicit Euler backward scheme. The theory is discussed by numerical examples. At first the sensitivity of the material parameters is shown by an isotropic simple tension test. Finally a cylindrical tube under homogeneous and inhomogeneous deformation is discussed within a finite element setting both for isotropy and transverse isotropy.

For the description of sole fiber reorientation, a constant mass is presumed, including constant density and volume. Consequently the mass source is equal to zero and the intermediate configuration is identical to the material configuration and, thus, dispensable. The evolution of the characteristic direction in time is, based on the rigid body motion of a line element, specified by a time dependent rotation. To describe the

rotation axis, we assume an alignment with a direction to be specified in more detail. Analogous to the theory of shells, drilling rotations are excluded in the reorientation process, see also MENZEL [99]. For the specification of the alignment direction, different approaches are conceivable. For anisotropic elasticity the free energy reaches a critical state for coaxial stresses and strains, see for instance VIANELLO [136]. For transverse isotropy such a coaxiality can be achieved if the structural tensor and the strain tensor are coaxial. Accordingly, a reorientation of fibers along the maximum principal stretch directions seems a natural choice. Strain driven reorientations are reasonable from the biological point of view as well. As PAUWELS [108] stated, collagen fibrils in cartilage tissue are oriented along principal strain directions. On the other hand the trajectorial hypothesis of WOLFF [142] says, that the trabeculae in bone are aligned with the principal stress direction. Thus, in this work, both an alignment with the maximum principal strain direction and an alignment with the maximum principal stress direction are considered. The incorporation of other criteria, such as reorientation along averaged principal directions, is straightforward and would require only minor modifications of the numerical treatment. The implementation for both approaches has been realized by an implicit exponential map for the characteristic direction and application of the Rodriguez formula. Again, consistent linearizations have been demonstrated on the local reorientation level as well as on the global finite element level. The complete algorithm is equivalent for strain and stress driven reorientation, instead of the update of the principal directions. Since the stresses in the local Newton iteration, in contrast to the strains, depend on the characteristic direction, the principal stress directions have to be updated in each local iteration step. The theory has been discussed by numerical examples. After a demonstration of the general material behavior in terms of a uniaxial stress test and a uniaxial tension test, a deformation with a homogeneous as well as an inhomogeneous final state has been considered within a finite element setting, wherein we compared materials with fixed and reorienting fiber directions.

In contrast to previous works related to remodeling, growth and reorientation individually, the formulation proposed in this contribution includes these three effects in a combined manner. Consequently, the similarities and differences of the three models are very well conspicuous, with respect to the continuummechanical modeling as well as concerning the numerical implementation. The different effects are included in the material model on different levels, each via internal variables. In this contribution we discussed the pure forms of remodeling, growth and reorientation by adequate choice of constitutive equations. Nonetheless, the comprehensive format of the material model approves combinations of the individual effects by solely minor amendments. For an implicit update of the internal variables within a finite element formulation we use an Euler update scheme for remodeling and growth and an exponential update scheme for reorientation. Besides this slight difference, the numerical implementation is equivalent for each effect. As distinct from existing explicit algorithms suggested in the literature, in this work we consistently linearized the nonlinear equa-

tions for computing the residuals on the local and the global level. Although this is cumbersome on paper, the effort pays off immediately as it results in quadratic convergence and the need of a low storage capacity. Moreover, with the suggested computational schemes, an implementation into any finite element program is straightforward. This will not only be useful for the modeling of biological tissue adaptation but rather can be applied for applications in the wide field of optimization processes in material and structural design.

6.2 Future work

In this work we focused on the algorithmic implementation of remodeling, growth and reorientation in transversely isotropic materials. This is applicable for a wide range of materials. Admittedly, in the context of hard tissues, it can be shown that, depending on the area from which a sample is taken, bone may be orthotropic, see, for instance, COWIN & MEHRABADI [24] and MILLER, FUCHS & ARCAN [103]. Also in soft tissues, for instance, in the arterial wall two families of fibers can be observed, see HOLZAPFEL [56]. Thus, it seems reasonable to consider materials with two families of fibers, which may not necessarily be perpendicular, see, for instance, LUBARDA & HOGER [93] in the context of orthotropic growth and MENZEL [100] for a combined model of orthotropic growth and reorientation. Further on, it is conceivable, to include a typically distributed orientation of the characteristic direction, as discussed in GASSER, OGDEN & HOLZAPFEL [42].

The model considered here has been implemented in an in-house finite element program. To consider more complex boundary conditions and patient specific simulations, it is reasonable to implement the model in a commercial finite element program. As discussed in MAAS [94] and KUHL ET AL. [77], a patient specific model can be generated from computer tomography data. The material model commonly has to be introduced via a user subroutine into the finite element program.

Since this work focused solely on the numerical implementation, we used common parameters from the literature, as available. A fundamental point for further development of the model would be parameter identification based on experimental work.

A Notation

Throughout this work scalar quantities are denoted by standard (non-bold) symbols, e.g., c . Vectors and second order tensors are denoted by bold symbols. Unless otherwise stated, lower case letters characterize vectors, e.g., \mathbf{a} and \mathbf{b} , and capital letters stand for second-order tensors, e.g., \mathbf{A} and \mathbf{B} . Fourth-order tensors are denoted by blackboard bold symbols, e.g., \mathbb{C} . To distinguish between material and spatial quantities, if applicable, we use the subscripts 0 and t , respectively. The push-forward of a material quantity to the intermediate configuration is denoted by a hat. For example, the material density is denoted by ρ_0 , its counterpart in the intermediate configuration is characterized by $\hat{\rho}_0$, and ρ_t is the spatial analog. For the sake of clarity and consistency with other authors, material vectors and their spatial counterparts are denoted by lower case and capital letters, e.g., \mathbf{x} and \mathbf{X} , respectively. The analog in the intermediate is, accordingly, $\hat{\mathbf{X}}$. The rules for frequently used calculations are summarized in the following.

single contraction	$c = \mathbf{a} \cdot \mathbf{b}$	$c = a_i b_i$
	$\mathbf{a} = \mathbf{A} \cdot \mathbf{b}$	$a_i = A_{ij} b_j$
	$\mathbf{A} = \mathbf{B} \cdot \mathbf{C}$	$A_{ij} = B_{ik} C_{kj}$
	$\mathbb{d} = \mathbb{C} \cdot \mathbf{a}$	$d_{ijk} = C_{ijkl} a_l$
	$\mathbb{D} = \mathbb{C} \cdot \mathbf{A}$	$D_{ijkl} = C_{ijkm} A_{ml}$
double contraction	$c = \mathbf{A} : \mathbf{B}$	$c = A_{ij} B_{ij}$
	$\mathbf{A} = \mathbb{C} : \mathbf{B}$	$A_{ij} = C_{ijkl} B_{kl}$
dyadic product	$\mathbf{A} = \mathbf{a} \otimes \mathbf{b}$	$A_{ij} = a_i b_j$
	$\mathbb{d} = \mathbf{a} \otimes \mathbf{B}$	$d_{ijk} = a_i B_{jk}$
	$\mathbb{d} = \mathbf{A} \otimes \mathbf{b}$	$d_{ijk} = A_{ij} b_k$
	$\mathbb{C} = \mathbf{A} \otimes \mathbf{B}$	$C_{ijkl} = A_{ij} B_{kl}$
varied dyadic products	$\mathbb{d} = \mathbf{A} \overline{\otimes} \mathbf{b}$	$d_{ijk} = A_{ik} b_j$
	$\mathbb{C} = \mathbf{A} \overline{\otimes} \mathbf{B}$	$C_{ijkl} = A_{ik} B_{jl}$
	$\mathbb{C} = \mathbf{A} \underline{\otimes} \mathbf{B}$	$C_{ijkl} = A_{il} B_{jk}$
outer product	$\mathbf{c} = \mathbf{a} \times \mathbf{b}$	$c_k = \varepsilon_{ijk} a_i b_j$
	$\mathbf{c} = \mathbf{A} \times \mathbf{B}$	$c_k = \varepsilon_{ijk} A_{il} B_{jl}$
	$\mathbf{A} = \mathbf{a} \times \mathbf{B}$	$A_{kl} = \varepsilon_{ijk} a_i B_{jl}$

For the index notation we used cartesian coordinates and the Einstein sum convention as well as the permutation symbol

$$\varepsilon_{ijk} = \begin{cases} +1 & \text{if } \{i, j, k\} \text{ is an even permutation of } \{1, 2, 3\} \\ -1 & \text{if } \{i, j, k\} \text{ is an odd permutation of } \{1, 2, 3\} \\ 0 & \text{if any index is repeated} \end{cases}$$

Further on, the second-order tensor $\mathbf{1}$ characterizes the identity $1_{ij} = \delta_{ij}$ and the fourth-order tensor \mathbb{I} takes the component representation $I_{ijkl} = \frac{1}{2}[\delta_{ik}\delta_{jl} + \delta_{il}\delta_{jk}]$. The transposed and inverse of a second-order tensor \mathbf{A} are denoted as \mathbf{A}^t and \mathbf{A}^{-1} , respectively. The transposition of a column vector \mathbf{a} yields a row vector \mathbf{a}^t . The symmetric part of a second-order tensor \mathbf{B} is denoted by $[\mathbf{B}]^{sym} = \frac{1}{2}[\mathbf{B} + \mathbf{B}^t]$. Analogously the symmetric part of a fourth-order tensor \mathbb{C} can be represented in index notation as $[C_{ijkl}]^{sym} = \frac{1}{4}[C_{ijkl} + C_{ijlk} + C_{jilk} + C_{jikl}]$.

B Some matrix identities

B.1 Matrix determinant lemma

The matrix determinant lemma, see for instance HARVILLE [48], specifies the determinant of a matrix,

$$\det(\mathbf{A} + \mathbf{u} \otimes \mathbf{v}) = \left[1 + \mathbf{v} \cdot \mathbf{A}^{-1} \cdot \mathbf{u}\right] \det \mathbf{A}, \quad (\text{B.1})$$

in which the matrix itself is the sum of an invertible matrix $\mathbf{A} \in \mathbb{R}^{n \times n}$ and the dyadic product of two vectors $\mathbf{u}, \mathbf{v} \in \mathbb{R}^n$. In case of the transversely isotropic growth deformation tensor

$$\mathbf{F}_g = \vartheta \mathbf{1} + [\eta - \vartheta] \mathbf{n}^A \otimes \mathbf{n}^A \quad (\text{B.2})$$

we identify

$$\mathbf{A} = \vartheta \mathbf{1}, \quad \mathbf{u} = [\eta - \vartheta] \mathbf{n}^A \quad \text{and} \quad \mathbf{v} = \mathbf{n}^A, \quad (\text{B.3})$$

so that its determinant results in

$$\begin{aligned} \det \mathbf{F}_g &= \det \left(\vartheta \mathbf{1} + [\eta - \vartheta] \mathbf{n}^A \otimes \mathbf{n}^A \right) \\ &= \left[1 + \mathbf{n}^A \cdot (\vartheta \mathbf{1})^{-1} \cdot [\eta - \vartheta] \mathbf{n}^A \right] \det(\vartheta \mathbf{1}) = \eta \vartheta^2. \end{aligned} \quad (\text{B.4})$$

B.2 Sherman-Morrison formula

To compute the inverse of a matrix, which is defined as the sum of an invertible matrix $\mathbf{A} \in \mathbb{R}^{n \times n}$ and the dyadic product of two vectors $\mathbf{u}, \mathbf{v} \in \mathbb{R}^n$, the Sherman-Morrison formula

$$(\mathbf{A} + \mathbf{u} \otimes \mathbf{v})^{-1} = \mathbf{A}^{-1} - \frac{\mathbf{A}^{-1} \cdot \mathbf{u} \otimes \mathbf{v} \cdot \mathbf{A}^{-1}}{1 + \mathbf{v} \cdot \mathbf{A}^{-1} \cdot \mathbf{u}} \quad (\text{B.5})$$

can be applied. In this it must be required that $(1 + \mathbf{v} \cdot \mathbf{A}^{-1} \cdot \mathbf{u})$ is non-zero. With the identifications depicted in equation (B.3) the inverse of the growth deformation tensor

(B.2) can be computed as

$$\begin{aligned}
 \mathbf{F}_g^{-1} &= \left(\vartheta \mathbf{1} + (\eta - \vartheta) \mathbf{n}^A \otimes \mathbf{n}^A \right)^{-1} \\
 &= (\vartheta \mathbf{1})^{-1} - \frac{(\vartheta \mathbf{1})^{-1} \cdot [\eta - \vartheta] \mathbf{n}^A \otimes \mathbf{n}^A \cdot (\vartheta \mathbf{1})^{-1}}{1 + \mathbf{n}^A \cdot (\vartheta \mathbf{1})^{-1} \cdot [\eta - \vartheta] \mathbf{n}^A} = \frac{1}{\vartheta} \mathbf{1} + \left[\frac{1}{\eta} - \frac{1}{\vartheta} \right] \mathbf{n}^A \otimes \mathbf{n}^A. \tag{B.6}
 \end{aligned}$$

The Sherman-Morrison formula is a special case of the Sherman-Morrison-Woodbury formula, see for instance RAO [111] and GOLUB & VAN LOAN [43].

C Derivatives

C.1 Exponent of a skew symmetric tensor

The derivative of the exponent of a skew symmetric tensor $\hat{\mathbf{v}}$ with respect to the corresponding axial vector \mathbf{v} can be determined by application of the Rodriguez formula

$$\exp(\hat{\mathbf{v}}) = \cos(v)\mathbf{1} + [1 - \cos(v)] \mathbf{n} \otimes \mathbf{n} + \sin(v)\hat{\mathbf{n}}, \quad (\text{C.1})$$

with the norm $v = \|\mathbf{v}\|$ and the normal vector $\mathbf{n} = \mathbf{v}/\|\mathbf{v}\|$ of the axial vector $\mathbf{v} = -\frac{1}{2}\hat{\mathbf{v}} : \boldsymbol{\varepsilon}$ as well as the according skew symmetric tensor $\hat{\mathbf{n}} = -\boldsymbol{\varepsilon} \cdot \mathbf{n}$. Based on this the derivative of the exponent of a skew symmetric tensor with respect to the according axial vector is

$$\begin{aligned} \frac{\partial \exp(\hat{\mathbf{v}})}{\partial \mathbf{v}} = & -\sin(v) \mathbf{1} \otimes \mathbf{n} + \frac{1 - \cos(v)}{v} [\mathbf{1} \otimes \mathbf{n} + \mathbf{n} \otimes \mathbf{1}] \\ & - \frac{\sin(v)}{v} \boldsymbol{\varepsilon} + \left[\sin(v) - 2 \frac{1 - \cos(v)}{v} \right] \mathbf{n} \otimes \mathbf{n} \otimes \mathbf{n} \\ & + \left[\frac{\sin(v)}{v} - \cos(v) \right] \boldsymbol{\varepsilon} \cdot [\mathbf{n} \otimes \mathbf{n}]. \end{aligned} \quad (\text{C.2})$$

Since this derivative includes terms depending on the inverse of the norm of the axial vector, the limit must be determined by means of l'Hospital's rule if the norm of the axial vector tends to zero

$$\lim_{v \rightarrow 0} \frac{\partial \exp(\hat{\mathbf{v}})}{\partial \mathbf{v}} = -\boldsymbol{\varepsilon}. \quad (\text{C.3})$$

C.2 Eigenvectors and eigenvalues

The eigenvalue problem of the symmetric second-order tensor $\mathbf{C} \in \mathbb{R}^{3 \times 3}$

$$[\mathbf{C} - \lambda^{\mathbf{C}} \mathbf{1}] \cdot \mathbf{n}^{\mathbf{C}} = \mathbf{0} \quad (\text{C.4})$$

yields the eigenvalues $\lambda_{I=1,2,3}^{\mathbf{C}} \in \mathbb{R}$ and the eigenvectors $\mathbf{n}_{I=1,2,3}^{\mathbf{C}} \in \mathbb{R}^3$ of \mathbf{C} . To obtain the derivative of the eigenvector $\mathbf{n}_I^{\mathbf{C}}$ and eigenvalue $\lambda_I^{\mathbf{C}}$ with respect to the tensor \mathbf{C} itself, we follow the lines of derivation highlighted in MOSLER & MESCHKE [104]. We combine the derivative of the eigenvalue problem (C.4) with respect to the individual

component $T_{\alpha\beta}$

$$\left[\frac{\partial \mathbf{C}}{\partial T_{\alpha\beta}} - \frac{\partial \lambda_I^C}{\partial T_{\alpha\beta}} \mathbf{1} \right] \cdot \mathbf{n}_I^C + \left[\mathbf{C} - \lambda_I^C \mathbf{1} \right] \cdot \frac{\partial \mathbf{n}_I^C}{\partial T_{\alpha\beta}} = \mathbf{0} \quad (\text{C.5})$$

with the derivative of the constraint that \mathbf{n}_I^C is a normal vector with respect to $T_{\alpha\beta}$

$$\mathbf{n}_I^C \cdot \mathbf{n}_I^C = 1 \quad \Rightarrow \quad \mathbf{n}_I^C \cdot \frac{\partial \mathbf{n}_I^C}{\partial T_{\alpha\beta}} = 0 \quad (\text{C.6})$$

in a linear system of equations

$$\underbrace{\begin{bmatrix} \mathbf{C} - \lambda_I^C \mathbf{1} & -\mathbf{n}_I^C \\ \mathbf{n}_I^{Ct} & 0 \end{bmatrix}}_{\mathbf{K}^+} \cdot \begin{bmatrix} \frac{\partial \mathbf{n}_I^C}{\partial T_{\alpha\beta}} \\ \frac{\partial \lambda_I^C}{\partial T_{\alpha\beta}} \end{bmatrix} = \begin{bmatrix} -\frac{\partial \mathbf{C}}{\partial T_{\alpha\beta}} \cdot \mathbf{n}_I^C \\ 0 \end{bmatrix} \quad (\text{C.7})$$

The derivative of the eigenvector and eigenvalue with respect to one individual component $T_{\alpha\beta}$ can be obtained by solving this linear system of equations (C.7) for the vector $[[\partial \mathbf{n}_I^C / \partial T_{\alpha\beta}]^t, \partial \lambda_I^C / \partial T_{\alpha\beta}]^t$, for instance by inverting \mathbf{K}^+ . Application of this procedure to each component of the tensor \mathbf{C} generates nine vectors $\partial \mathbf{n}_I^C / \partial T_{\alpha\beta} \in \mathbb{R}^3$ which can be combined in the quantity $\partial \mathbf{n}_I^C / \partial \mathbf{C} \in \mathbb{R}^{3 \times 3 \times 3}$. Concurrently, we obtain nine scalars $\partial \lambda_I^C / \partial T_{\alpha\beta} \in \mathbb{R}$ which can be combined in $\partial \lambda_I^C / \partial \mathbf{C} \in \mathbb{R}^{3 \times 3}$.

Analogously, the derivative of the negative eigenvector with respect to the corresponding tensor can be computed via

$$\underbrace{\begin{bmatrix} \mathbf{C} - \lambda_I^C \mathbf{1} & \mathbf{n}_I^C \\ \mathbf{n}_I^{Ct} & 0 \end{bmatrix}}_{\mathbf{K}^-} \cdot \begin{bmatrix} \frac{\partial (-\mathbf{n}_I^C)}{\partial T_{\alpha\beta}} \\ \frac{\partial \lambda_I^C}{\partial T_{\alpha\beta}} \end{bmatrix} = \begin{bmatrix} \frac{\partial \mathbf{C}}{\partial T_{\alpha\beta}} \cdot \mathbf{n}_I^C \\ 0 \end{bmatrix}. \quad (\text{C.8})$$

For identical eigenvalues λ_I^C of \mathbf{C} the matrix \mathbf{K}^\pm becomes singular. In that case small perturbations $\delta \ll 1$ can be applied to the eigenvalues, namely

$$\text{IF } \frac{|\lambda_I - \lambda_J|}{\max(|\lambda_I|, |\lambda_J|, |\lambda_K|)} < \text{tol}_\delta \quad \text{THEN} \quad \begin{cases} \lambda_I = \lambda_I [1 + \delta] \\ \lambda_J = \lambda_J [1 - \delta] \\ \lambda_K = \lambda_K / [(1 + \delta) [1 - \delta]] \end{cases} \quad (\text{C.9})$$

see, for instance, MIEHE [102].

C.3 Invariants

The stresses \mathbf{S} and the tangent moduli \mathbb{C}^e and \mathbb{C}^n can be determined by means of the invariant-based version of the free energy function

$$\psi_0 = \psi_0(I_1, I_2, I_3, I_4, I_5) \quad \text{with } I_{i=1,2,3} = \text{tr}(\mathbf{C}^i) \text{ and } I_{i=4,5} = \text{tr}(\mathbf{C}^{i-3} \cdot \mathbf{A}) \quad (\text{C.10})$$

by application of the chain rule

$$\begin{aligned} \mathbf{S} &= 2 \frac{\partial \psi_0}{\partial \mathbf{C}} = 2 \sum_{i=1}^5 \frac{\partial \psi_0}{\partial I_i} \frac{\partial I_i}{\partial \mathbf{C}}, \\ \mathbb{C}^e &= 4 \frac{\partial^2 \psi_0}{\partial \mathbf{C} \partial \mathbf{C}} = 4 \sum_{i=1}^5 \left[\sum_{j=1}^5 \left[\frac{\partial^2 \psi_0}{\partial I_i \partial I_j} \frac{\partial I_i}{\partial \mathbf{C}} \otimes \frac{\partial I_j}{\partial \mathbf{C}} \right] + \frac{\partial \psi_0}{\partial I_i} \frac{\partial^2 I_i}{\partial \mathbf{C} \partial \mathbf{C}} \right], \\ \mathbb{C}^n &= 4 \frac{\partial^2 \psi_0}{\partial \mathbf{C} \partial \mathbf{A}} = 4 \sum_{i=1}^5 \left[\sum_{j=4}^5 \left[\frac{\partial^2 \psi_0}{\partial I_i \partial I_j} \frac{\partial I_i}{\partial \mathbf{C}} \otimes \frac{\partial I_j}{\partial \mathbf{A}} \right] + 4 \sum_{i=4}^5 \left[\frac{\partial \psi_0}{\partial I_i} \frac{\partial^2 I_i}{\partial \mathbf{C} \partial \mathbf{A}} \right] \right]. \end{aligned} \quad (\text{C.11})$$

The invariants as defined in equation (C.10)₂ are called basic invariants. Alternatively, principal invariants can be defined. One of them is the determinant $\det \mathbf{C} = \frac{1}{6} I_1^3 - \frac{1}{2} I_1 I_2 + \frac{1}{3} I_3$. The additional invariants for transverse isotropy as defined in equation (C.10)₃ are called mixed invariants. For more details about invariants see APEL [4] and references cited therein. The derivatives of the invariants can be summarized as depicted in the following tabular.

	I_i	$\frac{\partial I_i}{\partial \mathbf{C}}$	$\frac{\partial^2 I_i}{\partial \mathbf{C} \partial \mathbf{C}}$	$\frac{\partial I_i}{\partial \mathbf{A}}$	$\frac{\partial^2 I_i}{\partial \mathbf{C} \partial \mathbf{A}}$
1	$\text{tr } \mathbf{C}$	$\mathbf{1}$	$\mathbf{0}$	$\mathbf{0}$	$\mathbf{0}$
2	$\text{tr}(\mathbf{C}^2)$	$2\mathbf{C}$	$2\mathbb{I}$	$\mathbf{0}$	$\mathbf{0}$
3	$\text{tr}(\mathbf{C}^3)$	$3\mathbf{C}^3$	$6(\mathbf{C} \otimes \mathbf{1})^{sym}$	$\mathbf{0}$	$\mathbf{0}$
4	$\text{tr}(\mathbf{C} \cdot \mathbf{A})$	\mathbf{A}	$\mathbf{0}$	\mathbf{C}	\mathbb{I}
5	$\text{tr}(\mathbf{C}^2 \cdot \mathbf{A})$	$2(\mathbf{C} \cdot \mathbf{A})^{sym}$	$2(\mathbf{A} \otimes \mathbf{1})^{sym}$	\mathbf{C}^2	$2(\mathbf{C} \otimes \mathbf{1})^{sym}$
	$\det \mathbf{C}$	$\det(\mathbf{C})\mathbf{C}^{-1}$	$\det(\mathbf{C}) \left[\mathbf{C}^{-1} \otimes \mathbf{C}^{-1} - (\mathbf{C}^{-1} \otimes \mathbf{C}^{-1})^{sym} \right]$	$\mathbf{0}$	$\mathbf{0}$

Bibliography

- [1] ABÉ, H.; HAYASHI, K.; SATO, M. [1997]: *Data book on mechanical properties of living cells, tissues, and organs*, Springer
- [2] AMBROSI, D.; MOLLIKA, F. [2002]: "On the mechanics of a growing tumor", *International Journal of Engineering Science*, Vol. 40, 1297–1316
- [3] ANVERSA, P.; VITALI-MAZZA, L.; VISIOLI, O.; MARCHETTI, G. [1971]: "Experimental cardiac hypertrophy: A quantitative ultrastructural study in the compensatory stage", *Journal of Molecular and Cellular Cardiology*, Vol. 3, 213–227
- [4] APEL, N. [2004]: *Approaches to the description of anisotropic material behaviour at finite elastic and plastic deformations*, Dissertation, Institut für Mechanik (Bauwesen), Lehrstuhl I, Universität Stuttgart, Bericht Nr. I-12
- [5] AROCKIARAJAN, A.; DELIBAS, B.; MENZEL, A.; SEEMANN, W. [2006]: "Studies on rate-dependent switching effects of piezoelectric materials using a finite element model", *Computational Materials Science*, Vol. 37, 306–317
- [6] AROCKIARAJAN, A.; MENZEL, A.; DELIBAS, B.; SEEMANN, W. [2006]: "Computational modeling of rate-dependent domain switching in piezoelectric materials", *European Journal of Mechanics, A/Solids*, Vol. 25(6), 950–964
- [7] AROCKIARAJAN, A.; MENZEL, A.; DELIBAS, B.; SEEMANN, W. [2007]: "Micromechanical modeling of switching effects in piezoelectric materials - A robust coupled finite element approach", *Journal of Intelligent Material Systems and Structures*, available online, DOI 10.1177/1045389X06074117
- [8] BAŞAR, Y.; WEICHERT, D. [2000]: *Nonlinear continuum mechanics of solids*, Springer-Verlag, Berlin
- [9] BALLE, F. [2004]: *Biomechanische Untersuchungen zur Knochen-Implantat-Interaktion mit Hilfe der Methode der finiten Elemente*, Diplomarbeit, Lehrstuhl für technische Mechanik, TU Kaiserslautern, U04-02
- [10] BEAUPRÉ, G. S.; ORR, T. E.; CARTER, D. R. [1990]: "An approach for time-dependent bone modeling and remodeling - Application: A preliminary remodeling simulation", *Journal of Orthopaedic Research*, Vol. 8, 662–670
- [11] BEAUPRÉ, G. S.; ORR, T. E.; CARTER, D. R. [1990]: "An approach for time-dependent bone modeling and remodeling - Theoretical development", *Journal of Orthopaedic Research*, Vol. 8, 651–661

- [12] BETSCH, P.; MENZEL, A.; STEIN, E. [1998]: "On the parametrisation of finite rotations in computational mechanics - A classification of concepts with application to smooth shells", *Computer Methods in Applied Mechanics and Engineering*, Vol. 155, 273–305
- [13] BOEHLER, J.-P. [1979]: "A simple derivation of representations for non-polynomial constitutive equations in some cases of anisotropy", *Zeitschrift für angewandte Mathematik und Mechanik*, Vol. 59, 157–167
- [14] BORCHARDT-OTT, W. [1997]: *Kristallographie*, Springer
- [15] CARTER, D. R.; BEAUPRÉ, G. S. [2001]: *Skeletal function and form: Mechanobiology of skeletal development, aging, and regeneration*, Cambridge University Press
- [16] CARTER, D. R.; HAYES, W. C. [1977]: "The compressive behavior of bone as a two-phase porous structure", *Journal of Bone and Joint Surgery*, Vol. 59-A(7), 954–962
- [17] CHADWICK, P. [1976]: *Continuum mechanics. Concise theory and problems*, Allen & Unwin Ltd. London
- [18] CHEN, Y.-C.; HOGER, A. [2000]: "Constitutive functions of elastic materials in finite growth and deformation", *Journal of Elasticity*, Vol. 59, 175–193
- [19] COLLINGS, P. J. [1990]: *Liquid crystals: Nature's delicate phase of matter*, Princeton University Press
- [20] COWIN, S. C. [1984]: "Mechanical modeling of the stress adaptation process in bone", *Calcified Tissue International*, Vol. 36, 98–103
- [21] COWIN, S. C. [1986]: "Wolff's law of trabecular architecture at remodeling equilibrium", *Transactions of the ASME*, Vol. 108, 83–88
- [22] COWIN, S. C. [1994]: "Optimization of the strain energy density in linear anisotropic elasticity", *Journal of Elasticity*, Vol. 34, 45–68
- [23] COWIN, S. C.; HEGEDUS, D. H. [1976]: "Bone remodeling I: Theory of adaptive elasticity", *Journal of Elasticity*, Vol. 6(3), 313–326
- [24] COWIN, S. C.; MEHRABADI, M. [1989]: "Identification of the elastic symmetry of bone and other materials", *Journal of Biomechanics*, Vol. 22(6/7), 503–515
- [25] CULMANN, C. [1866]: *Die graphische Statik*, Meyer & Zeller, Zürich
- [26] DE BOER, R. [1982]: *Vektor- und Tensorrechnung für Ingenieure*, Springer-Verlag
- [27] DE BOER, R. [1991]: *Theorie poröser Medien*, Gesamthochschule Essen
- [28] DRIESSEN, N. J. B.; BOERBOOM, R. A.; HUYGHE, J. M.; BOUTEN, C. V. C.; BAAIJENS, F. P. T. [2003]: "Computational analyses of mechanically induced collagen fiber remodeling in the aortic heart valve", *Journal of Biomechanical Engineering*, Vol. 125, 549–557

- [29] DRIESSEN, N. J. B.; BOUTEN, C. V. C.; BAAIJENS, F. P. T. [2005]: "Improved prediction of the collagen fiber architecture in the aortic heart valve", *Journal of Biomechanical Engineering*, Vol. 127, 329–336
- [30] DRIESSEN, N. J. B.; COX, M. A.; BOUTEN, C. V. C.; BAAIJENS, F. P. T. [2007]: "Remodelling of the angular collagen fiber distribution in cardiovascular tissues", *Biomechanics and Modeling in Mechanobiology*, available online, DOI 10.1007/s10237-007-0078-x
- [31] DRIESSEN, N. J. B.; PETERS, G. W. M.; HUYGHE, J. M.; BOUTEN, C. V. C.; BAAIJENS, F. P. T. [2003]: "Remodelling of continuously distributed collagen fibres in soft connective tissues", *Journal of Biomechanics*, Vol. 36, 1151–1158
- [32] DRIESSEN, N. J. B.; WILSON, W.; BOUTEN, C. V. C.; BAAIJENS, F. P. T. [2004]: "A computational model for collagen fibre remodelling in the arterial wall", *Journal of Theoretical Biology*, Vol. 226, 53–64
- [33] EPSTEIN, M.; MAUGIN, G. A. [2000]: "Material evolution in plasticity and growth", *Continuum Thermomechanics*, 153–162
- [34] EPSTEIN, M.; MAUGIN, G. A. [2000]: "Thermomechanics of volumetric growth in uniform bodies", *International Journal of Plasticity*, Vol. 16, 951–978
- [35] ERICKSEN, J. L. [1991]: *Introduction to the thermodynamics of solids*, 1st ed., Vol. Vol.131 of *Applied Mathematical Sciences*, Chapman & Hall
- [36] EVANS, F. G. [1973]: *Mechanical properties of bone*, Charles C. Thomas
- [37] FUNG, Y.-C. [1981]: *Biomechanics: Mechanical properties of living tissue*, Springer
- [38] FUNG, Y.-C. [1990]: *Biomechanics: Motion, flow, stress, and growth*, Springer
- [39] GARDEN, R. S. [1961]: "The structure and function of the proximal end of the femur", *The Journal of Bone and Joint Surgery*, Vol. 43-B(3), 576–589
- [40] GARIKIPATI, K.; NARAYANAN, H.; ARRUDA, E. M.; GROSH, K.; CALVE, S. [2004]: "Material forces in the context of biotissue remodelling", in P. Steinmann; G. A. Maugin (Editors), "Mechanics of Material Forces", 77–84, *Euromech Colloquium 445*
- [41] GARIKIPATI, K.; OLBERDING, J. E.; NARAYANAN, H.; ARRUDA, E. M.; GROSH, K.; CALVE, S. [2006]: "Biological remodelling: Stationary energy, configurational change, internal variables and dissipation", *Journal of the Mechanics and Physics of Solids*, Vol. 54, 1493–1515
- [42] GASSER, T. C.; OGDEN, R. W.; HOLZAPFEL, G. A. [2006]: "Hyperelastic modelling of arterial layers with distributed collagen fibre orientations", *Journal of the Royal Society Interface*, Vol. 3(6), 15–35
- [43] GOLUB, G. H.; VAN LOAN, C. F. [1996]: *Matrix computations*, 3rd ed., Johns Hopkins University Press

- [44] GURTIN, M. E. [1981]: *An introduction to continuum mechanics*, Vol. 158 of *Mathematics in Science and Engineering*, Academic Press
- [45] HARITON, I.; DEBOTTON, G.; GASSER, T. C.; HOLZAPFEL, G. A. [2007]: "Stress-driven collagen fiber remodeling in arterial walls", *Biomechanics and Modeling in Mechanobiology*, Vol. 6(3), 163–175
- [46] HARRIGAN, T. P.; HAMILTON, J. J. [1992]: "Optimality conditions for finite element simulation of adaptive bone remodeling", *International Journal of Solids and Structures*, Vol. 29(23), 2897–2906
- [47] HARRIGAN, T. P.; HAMILTON, J. J. [1993]: "Finite element simulation of adaptive bone remodeling: A stability criterion and time stepping method", *International Journal for Numerical Methods in Engineering*, Vol. 36, 837–854
- [48] HARVILLE, D. A. [1997]: *Matrix algebra from a statistician's perspective*, Springer
- [49] HAUPT, P. [2000]: *Continuum mechanics and theory of materials*, Springer-Verlag, Berlin
- [50] HIMPEL, G. [2003]: *On the modeling of material growth in anisotropic solids. Internal variable approach and numerical implementation*, Diplomarbeit, Institut für Mechanik (Bauwesen), Lehrstuhl I, Universität Stuttgart, Report/Preprint No. 03-I-08
- [51] HIMPEL, G.; KUHL, E.; MENZEL, A.; STEINMANN, P. [2005]: "Anisotropic Growth based on a Multiplicative Decomposition of the Deformation Gradient", in W. Ehlers; B. Markert (Editors), "Proceedings of the 1st GAMM Seminar on Continuum Biomechanics", 69–78, Report No. II-14
- [52] HIMPEL, G.; KUHL, E.; MENZEL, A.; STEINMANN, P. [2005]: "Computational modelling of isotropic multiplicative growth", *Computer Modeling in Engineering & Sciences*, Vol. 8(2), 119–134
- [53] HIMPEL, G.; MENZEL, A.; KUHL, E.; STEINMANN, P. [2007]: "Time-dependent fibre re-orientation of transversely isotropic continua - Finite element formulation and consistent linearisation", *International Journal for Numerical Methods in Engineering*, available online, DOI 10.1002/nme.2124
- [54] HOGER, A. [1997]: "Virtual Configurations and Constitutive Equations for Residually Stressed", *Journal of Elasticity*, Vol. 48, 125–144
- [55] HOLZAPFEL, G. A. [2000]: *Nonlinear solid mechanics, a continuum approach for engineering*, John Wiley & Sons
- [56] HOLZAPFEL, G. A. [2004]: *Computational Biomechanics of Soft Biological Tissue*, Vol. 2 of *Encyclopedia of Computational Mechanics (Solids and Structures)*, Ch. 18, John Wiley & Sons
- [57] HOLZAPFEL, G. A.; GASSER, T. C.; OGDEN, R. W. [2000]: "A new constitutive framework for arterial wall mechanics and a comparative study of material models", *Journal of Elasticity*, Vol. 61, 1–48

- [58] HOLZAPFEL, G. A.; STADLER, M.; SCHULZE-BAUER, C. A. J. [2002]: "A layer-specific three-dimensional model for the simulation of balloon angioplasty using magnetic resonance imaging and mechanical testing", *Annals of Biomedical Engineering*, Vol. 30(6), 753–767
- [59] HU, J.-J.; FOSSUM, T. W.; MILLER, M. W.; XU, H.; LIU, J.-C.; HUMPHREY, J. D. [2007]: "Biomechanics of the Porcine Basilar Artery in Hypertension", *Annals of Biomedical Engineering*, Vol. 35(1), 19–29
- [60] HUGHES, T. J. R.; WINGET, J. [1980]: "Finite rotation effects in numerical integration of rate constitutive equations arising in large-deformation analysis", *International Journal for Numerical Methods in Engineering*, Vol. 15, 1862–1867
- [61] HUISKES, R.; RUIMERMAN, R.; VAN LENTHE, G. H.; JANSSEN, J. D. [2000]: "Effects of mechanical forces on maintenance and adaption of form in trabecular bone", *Nature*, Vol. 405, 704–706
- [62] HUISKES, R.; WEINANS, H.; GROOTENBOER, H. J.; DALSTRA, M.; FUDALA, B.; SLOOFF, T. J. [1987]: "Adaptive bone-remodelling theory applied to prosthetic-design analysis", *Journal of Biomechanics*, Vol. 20(11-12), 1135–1150
- [63] HUMPHREY, J. D. [2002]: *Cardiovascular solid mechanics. Cells, tissues, and organs*, Springer
- [64] HUMPHREY, J. D.; DELANGE, S. L. [2004]: *An introduction to biomechanics*, Springer
- [65] HUMPHREY, J. D.; RAJAGOPAL, K. R. [2002]: "A constrained mixture model for growth and remodeling of soft tissues", *Mathematical Models and Methods in Applied Sciences*, Vol. 12, 407–430
- [66] IMATANI, S.; MAUGIN, G. A. [2002]: "A constitutive model for material growth and its application to three-dimensional finite element analysis", *Mechanics Research Communications*, Vol. 29, 477–483
- [67] JOHANSSON, G.; MENZEL, A.; RUNESSON, K. [2005]: "Modeling of anisotropic inelasticity in pearlitic steel at large strains due to deformation induced substructure evolution", *European Journal of Mechanics, A/Solids*, Vol. 24(6), 899–918
- [68] JOHNSON, B. E.; HOGER, A. [1995]: "The Use of a Virtual Configuration in Formulating Constitutive Equations for Residually Stressed Elastic Materials", *Journal of Elasticity*, Vol. 41, 177–215
- [69] KAMLAH, M. [2001]: "Ferroelectric and ferroelastic piezoceramics - Modeling of electromechanical hysteresis phenomena", *Continuum Mechanics and Thermodynamics*, Vol. 13, 219–268
- [70] KLISCH, S. M.; VAN DYKE, T. J.; HOGER, A. [2001]: "A theory of volumetric growth for compressible elastic biological materials", *Mathematics and Mechanics of Solids*, Vol. 6, 551–575

- [71] KNAUSS, P. [1980]: *Materialkennwerte und Festigkeitsverhalten des spongiösen und kompakten Knochengewebes am coxalen Human-Femur*, Dissertation, Institut für Flugzeugbau, Universität Stuttgart
- [72] KOCKS, U.; TOMÉ, C.; WENK, H.-R. (Editors) [2000]: *Texture and Anisotropy – Preferred Orientations in Polycrystals and their Effect on Material Properties*, Cambridge University Press
- [73] KRSTIN, N.; NACKENHORST, U.; LAMMERING, R. [2000]: “Zur konstitutiven Beschreibung des anisotropen beanspruchungsadaptiven Knochenbaus”, *Technische Mechanik*, Vol. 20(1), 31–40
- [74] KUHL, E. [2004]: “Theory and numerics of open system continuum thermodynamics - Spatial and material settings”, Habilitation, Lehrstuhl für Technische Mechanik, Technische Universität Kaiserslautern, UKL/LTM T 04-02
- [75] KUHL, E.; BALLE, F. [2005]: “Computational modeling of hip replacement surgery: Total hip replacement vs. hip resurfacing”, *Technische Mechanik*, Vol. 25(2), 107–114
- [76] KUHL, E.; GARIKIPATI, K.; ARRUDA, E. M.; GROSH, K. [2005]: “Remodeling of biological tissue: Mechanically induced reorientation of a transversely isotropic chain network”, *Journal of the Mechanics and Physics of Solids*, Vol. 53, 1552–1573
- [77] KUHL, E.; MAAS, R.; HIMPEL, G.; MENZEL, A. [2007]: “Computational modeling of arterial wall growth - Attempts towards a patient specific simulation based on computer tomography”, *Biomechanics and Modeling in Mechanobiology*, Vol. 6(5), 321–331, DOI 10.1007/s10237-006-0062-x
- [78] KUHL, E.; MENZEL, A.; STEINMANN, P. [2003]: “Computational modeling of growth - A critical review, a classification of concepts and two new consistent approaches”, *Computational Mechanics*, Vol. 32(1-2), 71–88
- [79] KUHL, E.; STEINMANN, P. [2002]: “Geometrically nonlinear functional adaption of biological microstructures”, in H. Mang; F. Rammerstorfer; J. Eberhardsteiner (Editors), “WCCM V, Fifth World Congress on Computational Mechanics”, Vienna, Austria
- [80] KUHL, E.; STEINMANN, P. [2003]: “On spatial and material settings of thermo-hyperelastodynamics for open systems”, *Acta Mechanica*, Vol. 160, 179–217
- [81] KUHL, E.; STEINMANN, P. [2003]: “Theory and numerics of geometrically nonlinear open system mechanics”, *International Journal for Numerical Methods in Engineering*, Vol. 58, 1593–1615
- [82] KUHL, E.; STEINMANN, P. [2003b]: “Mass- and volume specific views on thermodynamics for open systems”, *Proceedings of the Royal Society of London A*, Vol. 459, 2547–2568
- [83] KUHL, E.; STEINMANN, P. [2004]: “Computational modeling of healing: An application of the material force method”, *Biomechanics and Modeling in Mechanobiology*, Vol. 2, 187–203

- [84] LANGER, K. [1861/62]: "Zur Anatomie und Physiologie der Haut.", *Sitzungsbericht der mathematisch-naturwissenschaftlichen Classe der Kaiserlichen Academie der Wissenschaft*, Vol. 44/45
- [85] LANGER, K. [1978]: "On the anatomy and physiology of the skin. Conclusions", *British Journal of Plastic Surgery*, Vol. 31(4), 277–278
- [86] LANGER, K. [1978]: "On the anatomy and physiology of the skin. I. The cleavability of the cutis", *British Journal of Plastic Surgery*, Vol. 31(1), 3–8
- [87] LANGER, K. [1978]: "On the anatomy and physiology of the skin. II. Skin tension", *British Journal of Plastic Surgery*, Vol. 31(2), 93–106
- [88] LANGER, K. [1978]: "On the anatomy and physiology of the skin. III. The elasticity of the cutis", *British Journal of Plastic Surgery*, Vol. 31(3), 185–199
- [89] LANGER, K. [1978]: "On the anatomy and physiology of the skin. IV. The swelling capabilities of skin", *British Journal of Plastic Surgery*, Vol. 31(4), 273–276
- [90] LEE, E. H. [1969]: "Elastic-plastic deformation at finite strains", *Journal of Applied Mechanics*, Vol. 36, 1–6
- [91] LOKHIN, V. V.; SEDOV, L. I. [1963]: "Nonlinear tensor functions of several tensor arguments", *Journal of Applied Mathematics and Mechanics*, Vol. 27(3), 393–417
- [92] LUBARDA, V. A. [2004]: "Constitutive theories based on the multiplicative decomposition of deformation gradient: Thermoelasticity, elastoplasticity, and biomechanics", *Applied Mechanics Reviews*, Vol. 57(2), 95–108
- [93] LUBARDA, V. A.; HOGER, A. [2002]: "On the mechanics of solids with a growing mass", *International Journal of Solids and Structures*, Vol. 39, 4627–4664
- [94] MAAS, R. [2005]: *On the Implementation of Material Growth into the Commercial Finite Element System ABAQUS*, Diplomarbeit, Lehrstuhl für technische Mechanik, Technische Universität Kaiserslautern
- [95] MARSDEN, J. E.; HUGHES, T. J. R. [1983]: *Mathematical foundation of elasticity*, Dover
- [96] MARSDEN, J. E.; RATIU, T. S. [1994]: *Introduction to mechanics and symmetry*, Springer
- [97] MENZEL, A. [2005]: "Modelling of anisotropic growth in biological tissues - A new approach and computational aspects", *Biomechanics and Modeling in Mechanobiology*, Vol. 3(3), 147–171, DOI: 10.1007/s10237-004-0047-6
- [98] MENZEL, A. [2006]: "Adaption of biological tissues - A fibre reorientation model for orthotropic multiplicative growth", in C. A. M. Soares (Editor), "III European Conference on Computational Mechanics",
- [99] MENZEL, A. [2006]: "Anisotropic remodelling of biological tissues", in G. A. Holzapfel; R. W. Ogden (Editors), "Mechanics of Biological Tissue", IUTAM Symposium, 91–104, Springer

- [100] MENZEL, A. [2007]: "A fibre reorientation model for orthotropic multiplicative growth", *Biomechanics and Modeling in Mechanobiology*, Vol. 6(5), 303–320
- [101] MIEHE, C. [1988]: *Zur numerischen Behandlung thermomechanischer Prozesse*, Dissertation, Institut für Baumechanik und Numerische Mechanik, Universität Hannover, Bericht Nr. F88/6
- [102] MIEHE, C. [1993]: "Computation of isotropic tensor functions", *Communications in Numerical Methods in Engineering*, Vol. 9, 889–896
- [103] MILLER, Z.; FUCHS, M. B.; ARCAN, M. [2002]: "Trabecular bone adaption with an orthotropic material model", *Journal of Biomechanics*, Vol. 35(2), 247–256
- [104] MOSLER, J.; MESCHKE, G. [2003]: "3D modeling of strong discontinuities in elastoplastic solids: Fixed and rotating localization formulations", *International Journal for Numerical Methods in Engineering*, Vol. 57, 1553–1576
- [105] NACKENHORST, U. [1997]: "Numerical simulation of stress stimulated bone remodeling", *Technische Mechanik*, Vol. 17(1), 31–40
- [106] OGDEN, R. W. [1997]: *Non-linear elastic deformations*, Dover
- [107] ORR, T. E.; BEAUPRÉ, G. S.; CARTER, D. R.; SCHURMAN, D. J. [1990]: "Computer predictions of bone remodeling around porous-coated implants", *Journal of Arthroplasty*, Vol. 5(3), 191–200
- [108] PAUWELS, F. [1965]: *Gesammelte Abhandlungen zur funktionellen Anatomie des Bewegungsapparates*, Springer
- [109] PAUWELS, F. [1973]: *Atlas zur Biomechanik der gesunden und kranken Hüfte*, Springer
- [110] PEDERSEN, N. L. [2006]: "On design of fiber-nets and orientation for eigenfrequency optimization of plates", *Computational Mechanics*, Vol. 39(1), 1–13
- [111] RAO, C. R. [1973]: *Linear statistical inference and its applications*, 2nd ed., John Wiley & Sons
- [112] RAO, I. J.; HUMPHREY, J. D.; RAJAGOPAL, K. R. [2003]: "Biological growth and remodeling: A uniaxial example with possible application to tendons and ligaments", *Computer Methods in Engineering and Sciences*, Vol. 4(3/4), 439–455
- [113] REILLY, D. T.; BURSTEIN, A. H. [1975]: "The elastic and ultimate properties of compact bone tissue", *Journal of Biomechanics*, Vol. 8, 393–405
- [114] RICHTER, G. W.; KELLNER, A. [1963]: "Hypertrophy of the human heart at the level of fine structure", *Journal of Cell Biology*, Vol. 18, 195–206
- [115] RICKEN, T.; SCHWARZ, A.; BLUHM, J. [2006]: "A triphasic theory for growth in biological tissue - Basics and applications", *Materialwissenschaft und Werkstofftechnik*, Vol. 37(6), 446–456

-
- [116] RODRIGUEZ, E. K.; HOGER, A.; MCCULLOCH, A. D. [1994]: "Stress-dependent finite growth in soft elastic tissues", *Journal of Biomechanics*, Vol. 27(4), 455–467
- [117] ROUX, W. [1895]: *Gesammelte Abhandlungen über die Entwicklungsmechanik der Organismen*, W. Engelmann, Leipzig
- [118] SCHRÖDER, J. [1996]: *Theoretische und algorithmische Konzepte zur phänomenologischen Beschreibung anisotropen Materialverhaltens*, Ph.D. thesis, Institut für Mechanik und Numerische Mechanik, Universität Hannover, Bericht-Nr. F96/3
- [119] SCHRÖDER, J.; NEFF, P. [2003]: "Invariant formulation of hyperelastic transverse isotropy based on polyconvex free energy functions", *International Journal of Solid and Structures*, Vol. 40, 401–445
- [120] SCHRÖDER, J.; ROMANOWSKI, H. [2005]: "A thermodynamically consistent mesoscopic model for transversely isotropic ferroelectric ceramics in a coordinate-invariant setting", *Archive of Applied Mechanics*, Vol. 74, 863–877
- [121] SGARRA, C.; VIANELLO, M. [1997]: "Directions of coaxiality between pure strain and stress in linear elasticity", *Journal of Elasticity*, Vol. 46, 263–265
- [122] SGARRA, C.; VIANELLO, M. [1997]: "Rotations which make strain and stress coaxial", *Journal of Elasticity*, Vol. 47, 217–224
- [123] SHERRAT, J. A.; MARTIN, P.; MURRAY, J.; LEWIS, J. [1992]: "Mathematical models of wound healing in embryonic and adult epidermis", *Journal of Mathematics Applied in Medicine and Biology*, Vol. 9, 177–196
- [124] SKALAK, R.; DASGUPTA, G.; MOSS, M.; OTTEN, E.; DULLEMEIJER, P.; VILMANN, H. [1982]: "Analytical Description of Growth", *Journal of Theoretical Biology*, Vol. 94, 555–577
- [125] SKALAK, R.; ZARGARYAN, S.; JAIN, R. K.; NETTI, P. A.; HOGER, A. [1996]: "Compatibility and the genesis of residual stress by volumetric growth", *Journal of Mathematical Biology*, Vol. 34, 889–914
- [126] SMITH, R. C. [2005]: *Smart material systems*, Society for Industrial and Applied Mechanics
- [127] SPENCER, A. J. M. [1971]: "Theory of invariants", in C. Eringen (Editor), "Continuum physics", Vol. 1, Academic Press
- [128] STEEB, H.; DIEBELS, S. [2003]: "A thermodynamic-consistent model describing growth and remodeling phenomena", *Computational Materials Science*, Vol. 28(3-4), 597–607
- [129] TABER, L. A. [1995]: "Biomechanics of growth, remodeling, and morphogenesis", *ASME Applied Mechanics Reviews*, Vol. 48(8), 487–545
- [130] TABER, L. A.; EGGERS, D. W. [1996]: "Theoretical Study of Stress-Modulated Growth in the Aorta", *Journal of Theoretical Biology*, Vol. 180, 343–357
- [131] TABER, L. A.; PERUCCHIO, R. [2000]: "Modeling heart development", *Journal of Elasticity*, Vol. 61, 165–197

- [132] TITTEL, K. [2003]: *Beschreibende und funktionelle Anatomie des Menschen*, 14th ed., Urban & Fischer
- [133] TRUESDELL, C.; NOLL, W. [1965]: *The non-linear field theories of mechanics*, Vol. III, 3, Springer
- [134] VAISHNAV, R. N.; VOSSOUGH, J. [1983]: "Estimation of residual strains in aortic segments", in C. W. Hall (Editor), "Biomedical Engineering II: Recent Developments", 330–333, New York: Pergamon Press
- [135] VAN RIETBERGEN, B.; HUISKES, R.; ECKSTEIN, F.; RÜEGSEGG, P. [2003]: "Trabecular bone tissue strains in the healthy and osteoporotic human femur", *Journal of Bone and Mineral Research*, Vol. 18(10), 1781–1788
- [136] VIANELLO, M. [1996]: "Coaxiality of strain and stress in anisotropic linear elasticity", *Journal of Elasticity*, Vol. 42, 283–289
- [137] VIANELLO, M. [1996]: "Optimization of the stored energy and coaxiality of strain and stress in finite elasticity", *Journal of Elasticity*, Vol. 44, 193–202
- [138] VINCENT, L.; CALLOCH, S.; MARQUIS, D. [2004]: "A general cyclic plasticity model taking into account yield surface distortion for multiaxial ratchetting", *International Journal of Plasticity*, Vol. 20, 1817–1850
- [139] VON MEYER, G. H. [1867]: "Die Architektur der Spongiosa", *Archiv für Anatomie, Physiologie und wissenschaftliche Medizin, Reichert und DuBois-Reymonds Archiv*, Vol. 34, 615–628
- [140] WENG, S. [1997]: *Ein Evolutionsmodell zur mechanischen Analyse biologischer Strukturen*, Dissertation, Institut für Mechanik, Ruhr-Universität Bochum
- [141] WOLFF, J. [1870]: "Über die innere Architektur der Knochen und ihre Bedeutung für die Frage vom Knochenwachstum", *Virchows Archiv für Pathologische Anatomie und Physiologie*, Vol. 50(3), 389–450
- [142] WOLFF, J. [1892]: *Das Gesetz der Transformation der Knochen*, Hirschwald, Berlin

List of Figures

2.1	Each element of the body grows or degrades in the growth process	6
2.2	Multiplicative split of the deformation gradient	7
2.3	Metric tensors and deformation tensors	8
2.4	Isolated part \mathcal{P}_t of the body \mathcal{B}_t	9
2.5	Stress tensors and work conjugated deformation tensors	10
2.6	The balanced quantity changes in time	11
2.7	Mass and density expressions	12
2.8	Different cases of mass change	22
3.1	Loads and boundary conditions in the simple tension test.	32
3.2	Simple tension test	33
3.3	Simple tension test - variation of the materials parameters	34
3.4	Simple tension test - tension vs. compression	35
3.5	Loads and boundary conditions of the human femur model.	36
3.6	Isotropic human femur model	37
3.7	Transversely isotropic human femur model	37
3.8	Loads and boundary conditions for the tube under tension	39
3.9	Isotropic tube under tension	40
3.10	Isotropic tube under tension - evolution of density and volume	40
3.11	Transversely isotropic tube under tension.	41
3.12	Loads and boundary conditions for the tube under inside displacement load	41
3.13	Isotropic tube under under inside displacement load	43
3.14	Transversely isotropic tube under under inside displacement load	43
4.1	Loads and boundary conditions in the simple tension test.	56
4.2	Simple tension test	56
4.3	Simple tension test - variation of the limiting stretch ratio	57
4.4	Simple tension test - variation of the material parameters	58
4.5	Simple tension test - tension vs. compression	58
4.6	Loads and boundary conditions for the tube under tension	59
4.7	Isotropic tube under tension	60
4.8	Isotropic tube under tension - radial displacement	60
4.9	Isotropic tube under tension - evolution of density and volume	61
4.10	Transversely isotropic tube under tension - variation of the stretch ratios	61
4.11	Transversely isotropic tube under tension - variation of the orientation of \mathbf{n}^A	62
4.12	Transversely isotropic tube under tension - inclined characteristic direction	63
4.13	Loads and boundary conditions for the tube under inside displacement load	63
4.14	Isotropic tube under under inside displacement load	64
4.15	Transversely isotropic tube under under inside displacement load	64
5.1	Evolution of the characteristic direction amounts to a rotation	71
5.2	Magnitude of the evolution of the characteristic direction	72

5.3	Loads and boundary conditions in the simple tension test	82
5.4	Uniaxial stress test ($\theta_0 = 90^\circ$) - fixed characteristic direction	83
5.5	Uniaxial stress test ($\theta_0 = 0^\circ$) - reorientation	84
5.6	Uniaxial stress test ($\theta_0 = 90^\circ$) - strain driven reorientation	85
5.7	Uniaxial stress test ($\theta_0 = 90^\circ$) - stress driven reorientation	86
5.8	Uniaxial stress test ($\theta_0 = 90^\circ$) - strain vs. stress driven reorientation	87
5.9	Uniaxial tension test ($\theta_0 = 90^\circ$) - strain vs. stress driven reorientation	88
5.10	Uniaxial tension test ($\theta_0 = 30^\circ$) - strain vs. stress driven reorientation	89
5.11	Loads and boundary conditions of the transversely isotropic strip	90
5.12	Transversely isotropic strip ($\theta_0 = -45^\circ$) - fixed fibers	91
5.13	Transversely isotropic strip ($\theta_0 = -45^\circ$) - reorientation	92
5.14	Transversely isotropic strip ($\theta_0 = 60^\circ$) - reorientation	94
5.15	Transversely isotropic strip ($\theta_0 = -120^\circ$) - reorientation	95
5.16	Loads and boundary conditions for the inhomogeneously deformed tube.	96
5.17	Transversely isotropic tube - fixed fibers	97
5.18	Transversely isotropic tube - strain driven reorientation	98
5.19	Transversely isotropic tube - stress driven reorientation	99

List of Tables

3.1	Algorithmic update scheme for remodeling	31
3.2	Quadratic convergence for remodeling	38
4.1	Algorithmic update scheme for growth (part 1)	54
4.1	Algorithmic update scheme for growth (part 2)	55
4.2	Quadratic convergence for growth	65
5.1	Algorithmic update scheme for reorientation (part 1)	80
5.1	Algorithmic update scheme for reorientation (part 2)	81
5.2	Quadratic convergence for strain driven reorientation	93
5.3	Quadratic convergence for stress driven reorientation	93

Curriculum Vitae

Name	Grieta Anna Himpel
Nationality	German
Date of Birth	January 10th, 1978
Place of Birth	Aachen
08/1984 - 07/1987	Grundschule Mahlberg
08/1987 - 07/1989	Grund- und Hauptschule Münchweier
08/1989 - 06/1998	Städtisches Gymnasium Ettenheim
10/1998 - 07/2003	Study of Civil Engineering, University of Stuttgart
since 09/2003	Research Associate, University of Kaiserslautern Department of Mechanical and Process Engineering Chair of Applied Mechanics (Prof. Dr.-Ing. P. Steinmann)

